

IPICYT

---

**INSTITUTO POTOSINO DE INVESTIGACIÓN  
CIENTÍFICA Y TECNOLÓGICA, A.C.**

POSGRADO EN CIENCIAS APLICADAS

**Nitrogen doped carbon nanomaterials for  
biosensing applications**

Tesis que presenta

**Josué Ortiz-Medina**

para obtener el grado de

**Doctor en Ciencias Aplicadas**

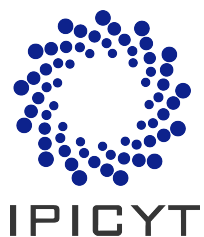
en la opción de

**Nanociencias y Nanotecnología**

Director de Tesis:

**Dr. Fernando J. Rodríguez Macías**

San Luis Potosí, S.L.P., Octubre 2013



## Constancia de aprobación de tesis

La tesis *Nitrogen doped carbon nanomaterials for biosensing applications*, presentada para obtener el grado de Doctor en Ciencias Aplicadas, con opción en Nanociencias y Nanotecnología, fue elaborada por **Josué Ortiz-Medina** y aprobada el **7 de octubre de 2013** por los suscritos, designados por el Colegio de Profesores de la División de Materiales Avanzados del Instituto Potosino de Investigación Científica y Tecnológica, A.C.

**Dr. Fernando J. Rodríguez Macías**  
Director de Tesis

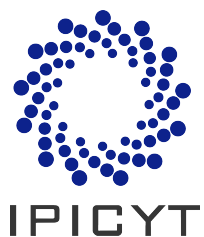
**Dr. Florentino López Urías**  
Miembro del comité tutorial

**Dra. Yadira I. Vega Cantú**  
Miembro del comité tutorial

**Dr. Braulio Gutiérrez Medina**  
Miembro del comité tutorial

**Dr. José Luis Sánchez Llamazares**  
Miembro del comité tutorial

**Dr. Marcelo F. Videá Vargas**  
Miembro del comité tutorial



## **Créditos Institucionales**

Esta tesis fue elaborada en la División de Materiales Avanzados del Instituto Potosino de Investigación Científica y Tecnológica A.C., bajo la dirección del Dr. Fernando J. Rodríguez Macías. Parte importante de la investigación que sustenta la presente tesis fue realizada en el Departamento de Física de la Universidad Estatal de Pennsylvania, EE.UU., bajo la dirección externa del Dr. Mauricio Terrones Maldonado.

Durante la realización del presente trabajo de investigación doctoral, el autor recibió una beca académica por parte del Consejo Nacional de Ciencia y Tecnología (registro 223807) y del Instituto Potosino de Investigación Científica y Tecnológica. Adicionalmente, el autor recibió el apoyo de la Dirección General de Relaciones Internacionales de la Secretaría de Educación Pública, dentro del programa de Becas Complemento para estudiantes de posgrado.



# Instituto Potosino de Investigación Científica y Tecnológica, A.C.

## Acta de Examen de Grado

El Secretario Académico del Instituto Potosino de Investigación Científica y Tecnológica, A.C., certifica que en el Acta 041 del Libro Primero de Actas de Exámenes de Grado del Programa de Doctorado en Ciencias Aplicadas en la opción de Nanociencias y Nanotecnología está asentado lo siguiente:

En la ciudad de San Luis Potosí a los 7 días del mes de octubre del año 2013, se reunió a las 16:30 horas en las instalaciones del Instituto Potosino de Investigación Científica y Tecnológica, A.C., el Jurado integrado por:

<b>Dr. Florentino López Urías</b>	<b>Presidente</b>	<b>IPICYT</b>
<b>Dr. José Luis Sánchez Llamazares</b>	<b>Secretario</b>	<b>IPICYT</b>
<b>Dr. Braulio Gutiérrez Medina</b>	<b>Sinodal</b>	<b>IPICYT</b>
<b>Dr. Fernando Jaime Rodríguez Macías</b>	<b>Sinodal</b>	<b>IPICYT</b>
<b>Dra. Yadira Itzel Vega Cantú</b>	<b>Sinodal</b>	<b>IPICYT</b>

a fin de efectuar el examen, que para obtener el Grado de:

DOCTOR EN CIENCIAS APLICADAS  
EN LA OPCIÓN DE NANOCIENCIAS Y NANOTECNOLOGÍA

sustentó el C.

**Josué Ortiz Medina**

sobre la Tesis intitulada:

*Nitrogen doped carbon nanomaterials for biosensing applications*

que se desarrolló bajo la dirección de

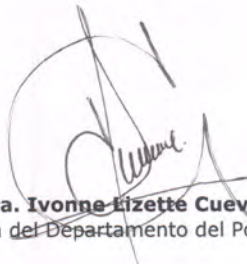
**Dr. Fernando Jaime Rodríguez Macías**

El Jurado, después de deliberar, determinó

APROBARLO

Dándose por terminado el acto a las 19:00 horas, procediendo a la firma del Acta los integrantes del Jurado. Dando fe el Secretario Académico del Instituto.

A petición del interesado y para los fines que al mismo convengan, se extiende el presente documento en la ciudad de San Luis Potosí, S.L.P., México, a los 7 días del mes de octubre de 2013.

  
**Mtra. Ivonne Lizette Cuevas Vélez**  
Jefa del Departamento del Posgrado

  
**Dr. Marcial Bonilla Marín**  
Secretario Académico



*Para Miriam, mi amada esposa, quien estuvo a mi lado todo este tiempo apoyándome con su mejor esfuerzo, y compartiendo los muchos ratos buenos y malos que trajo esta aventura...  
Sin ti no habría sido tan divertido y aleccionador...*

# Acknowledgements

This thesis work would have been impossible to complete without the help and intervention of so many people. First at all, I must recognize early collaborations and discussions with my fellow graduate students: Maria Luisa García, Blanca Gómez, Julio Chacón, Miguel Pelagio, David Rubín and Rafael Martínez, when the first ideas of this research started to appear. I am profoundly indebted with technicians and professors within the IPICYT Advanced Materials Division: Daniel Ramírez, Hugo Martínez, Beatriz Rivera, Gladis Labrada, Karla Gómez, Emilio Muñoz, Yadira Vega, Florentino López and Humberto Terrones, who shared with me part of their knowledge.

I would also to thank all the people who supported me during my research stay at the Pennsylvania State University: Ana Laura Elías, Nestor Perea, Humberto Gutiérrez, Ruitao Lv and all the rest of the staff who helped me with all the small but necessary things when one is far from home.

I want to specially thank to my main research advisors: Dr. Fernando J. Rodríguez and Dr. Mauricio Terrones, for all their help, guidance and support during this time.

Finally, I must recognize all the help, love, confidence and support from my family: Miriam my wife, my parents and brothers. A great part of the good things that I have achieved are because of their influence.

Thanks to all.

Josué Ortiz-Medina

# Contents

## Preliminary Section

Thesis approval certificate .....	iii
Institutional acknowledgements .....	v
Thesis defense certificate .....	vii
Dedication .....	ix
Acknowledgements .....	xi
Contents .....	xiii
Tables list .....	xvii
Figures list .....	xvii
Summary .....	xxv
Abstract .....	xxvii

## Main Section

<b>Introduction .....</b>	<b>1</b>
<b>Chapter 1. An overview of carbon nanomaterials</b>	
1.1 The carbon atom .....	5
1.2 Fullerenes .....	7
1.2.1 Synthesis methods .....	8
1.2.2 Properties .....	9
1.3 Carbon nanotubes .....	10
1.3.1 Undoped carbon nanotubes .....	11
1.3.1.1 Synthesis methods .....	13
1.3.1.2 Properties .....	15
1.3.2 Nitrogen doped carbon nanotubes .....	19
1.3.2.1 Synthesis methods .....	20
1.3.2.2 Properties .....	21

1.4 Graphene .....	24
1.4.1 Undoped graphene .....	25
1.4.1.1 Synthesis methods .....	25
1.4.1.2 Properties .....	28
1.4.2 Nitrogen doped graphene .....	30
1.4.2.1 Synthesis methods .....	31
1.4.2.2 Properties .....	32
Conclusions .....	34
Bibliography .....	35

**Chapter 2. Interaction between nanomaterials and biosystems:  
nanobiotechnology**

2.1 Nanobiotechnology: a brief introduction .....	47
2.1.1 Background: first explorations on the use of nanomaterials in bioapplications .....	48
2.1.1.1 Non-carbon materials .....	49
2.1.1.1.1 Metallic nanoparticles .....	49
2.1.1.1.2 Nanowires .....	50
2.1.1.1.3 Nanostructured polymers .....	51
2.1.1.1.4 Peptide and nucleic acid nanostructures .....	52
2.1.2 Functionalization of carbon nanomaterials for nanobiotechnology .....	54
2.1.2.1 Covalent functionalization .....	54
2.1.2.2 Non-covalent functionalization .....	57
2.1.3 Toxicity concerns and studies .....	59
2.2 Carbon nanomaterials in biomedical technology .....	61
2.2.1 Drug and gene delivery .....	61
2.2.2 Biosensing .....	64
2.2.2.1 Field-effect transistor based biosensing .....	64
2.2.2.2 Optical based biosensing .....	67
2.2.3 Bioelectronic interfaces .....	72
Conclusions .....	77
Bibliography .....	79



### **Chapter 3. Nitrogen-doped graphitic nanoribbons synthesis and characterization**

3.1 Graphitic nanoribbons .....	91
3.2 Background: undoped graphitic nanoribbons .....	92
3.2.1 Synthesis methods .....	92
3.2.2 Properties .....	93
3.3 New nanomaterials: nitrogen-doped graphitic nanoribbons .....	95
3.3.1 Synthesis of $N_x$ -GNR.....	95
3.3.2 Morphology of $N_x$ -GNR .....	96
3.3.3 Spectroscopy of $N_x$ -GNR .....	100
3.3.4 Thermogravimetry .....	103
3.3.5 Electrical properties of $N_x$ -GNR .....	105
3.3.6 Theoretical modeling of the electrical properties of $N_x$ -GNR and comparison to experimental results .....	106
Conclusions .....	110
Bibliography .....	111

### **Chapter 4. Theoretical study on nanomaterials and biomolecules interactions: graphene and dopamine**

4.1 Introduction to theoretical analysis of biosystems .....	115
4.2 Studying graphene and dopamine interaction .....	121
4.3 Research contribution: theoretical model .....	122
4.4 Results and discussions .....	124
Conclusions .....	134
Bibliography .....	135

### **Chapter 5. Biosensing properties of nanomaterials based devices**

5.1 Introduction to biosensing devices .....	141
5.1.1 Carbon nanomaterials based bioelectronics .....	144
5.1.2 Using doped carbon nanomaterials for bioelectronic devices .....	146
5.2 Experimental comparison between pure and N-doped CNTs based biosensor .....	149

5.2.1 Results .....	152
Conclusions .....	157
Bibliography .....	157
<b>Conclusions and perspectives .....</b>	<b>159</b>
<b>Appendix A. Brief description of some nanomaterials characterization techniques</b>	
A.1 Scanning Electron Microscopy (SEM) .....	165
A.2 Transmission Electron Microscopy (TEM) .....	166
A.3 Scanning Probe Microscopy (SPM) .....	168
A.4 Raman Spectroscopy .....	169
A.5 X-ray Photoelectron Spectroscopy (XPS) .....	170
A.6 InfraRed Spectroscopy (IR) .....	171
A.7 Thermogravimetric Analysis (TGA) .....	173
Bibliography .....	174
<b>Appendix B. Overview of Density Functional Theory as approach for carbon nanomaterials simulations</b>	
B.1 Basics of Density Functional Theory (DFT) .....	175
B.2 DFT for carbon nanostructures electronic properties determination .....	177
Bibliography .....	180

# Tables list

## Chapter 1

<b>Table 1.1</b>	Carbon nanotubes synthesis methods.....	13
------------------	---	----

## Chapter 4

<b>Table 4.1</b>	Change in energy gap for dopamine (DA) adsorbed in graphene.....	134
------------------	--	-----

# Figures list

## Chapter 1

<b>Figure 1.1</b>	Orbital hybridizations for carbon atoms.....	6
<b>Figure 1.2</b>	Some allotropes of carbon.....	7
<b>Figure 1.3</b>	Electric arc-discharge setup for fullerenes synthesis.....	8
<b>Figure 1.4</b>	C <sub>60</sub> molecule model, Hückel orbitals and possible addition chemical reactions.....	9
<b>Figure 1.5</b>	Single- and multi-wall carbon nanotubes.....	11
<b>Figure 1.6</b>	Carbon nanotubes chirality.....	12
<b>Figure 1.7</b>	Carbon nanotubes synthesis.....	14
<b>Figure 1.8</b>	Electronic structure of armchair and zigzag carbon nanotubes.....	16

<b>Figure 1.9</b>	Raman spectrum for multi-wall carbon nanotubes (MWNTs)....	17
<b>Figure 1.10</b>	Carbon nanotubes based field-effect transistor (CNT-FET).....	18
<b>Figure 1.11</b>	Molecular models of CNT doping.....	19
<b>Figure 1.12</b>	Nitrogen-doped CNTs (CN <sub>x</sub> ).....	21
<b>Figure 1.13</b>	Electronic structure of CN <sub>x</sub> .....	22
<b>Figure 1.14</b>	Systematic changes in micro-Raman spectra of N-doped SWNTs.....	23
<b>Figure 1.15</b>	Graphene as the “mother” material for other carbon nanostructures.....	24
<b>Figure 1.16</b>	Graphene synthesis methods.....	26
<b>Figure 1.17</b>	Graphene nanoribbons production from MWNTs exfoliation....	27
<b>Figure 1.18</b>	Electronic properties of graphene.....	28
<b>Figure 1.19</b>	Raman spectra of graphene samples.....	29
<b>Figure 1.20</b>	Graphene based field-effect transistor (graphene-FET).....	30
<b>Figure 1.21</b>	Nitrogen-doping in graphene.....	32
<b>Figure 1.22</b>	Characterization of N-doped graphene sample.....	33

## Chapter 2

<b>Figure 2.1</b>	Nanostructured materials for biotechnological applications.....	48
<b>Figure 2.2</b>	Magnetic nanoparticles in nanobiotechnology applications.....	49
<b>Figure 2.3</b>	Nanowires arrays in nanobiotechnology.....	50
<b>Figure 2.4</b>	Nanostructured polymers in biotechnological applications.....	52
<b>Figure 2.5</b>	Peptide nanotubes and nucleic acid based nanostructures.....	53
<b>Figure 2.6</b>	Chemical approaches for CNT functionalization.....	55

<b>Figure 2.7</b>	CNT functionalization with biomolecules.....	56
<b>Figure 2.8</b>	Non-covalent functionalization of carbon nanostructures.....	58
<b>Figure 2.9</b>	CNT size and surface chemistry dependent toxicity.....	60
<b>Figure 2.10</b>	CNT doping dependent toxicity.....	61
<b>Figure 2.11</b>	Drug delivery applications of CNTs.....	63
<b>Figure 2.12</b>	Suggested strategies for cellular delivery of nucleic acids by CNTs.....	65
<b>Figure 2.13</b>	Graphene based drug delivery example.....	66
<b>Figure 2.14</b>	CNT-FET based electronic biosensing.....	68
<b>Figure 2.15</b>	SWNTs substrate for cellular activity detection.....	69
<b>Figure 2.16</b>	Thermally reduced graphene oxide based FET for specific protein detection.....	70
<b>Figure 2.17</b>	Experimental setup for graphene-FET based biosensing.....	71
<b>Figure 2.18</b>	Current/time curve comparison for undoped and N-doped CNTs in glassy carbon electrodes used for H <sub>2</sub> O <sub>2</sub> detection.....	72
<b>Figure 2.19</b>	Use of CNTs' optical properties for fluorescence based biodetection.....	73
<b>Figure 2.20</b>	Setup and response example of a graphene modified surface-plasmon-resonance (SPR) biosensor.....	74
<b>Figure 2.21</b>	Graphene used as substrate for surface-enhanced-Raman- spectroscopy (SERS).....	75
<b>Figure 2.22</b>	Enhanced Raman scattering effect of N-doped graphene sheets for probing Rhodamine B molecules.....	76
<b>Figure 2.23</b>	CNTs in conventional neuroelectrodes.....	77
<b>Figure 2.24</b>	CNTs in neurochips.....	78

### Chapter 3

<b>Figure 3.1</b>	SEM images and elemental EDX line-scan of graphitic nanoribbons.....	93
<b>Figure 3.2</b>	I-V characteristics of individual GNRs, and TEM images of GNRs' edges.....	94
<b>Figure 3.3</b>	SEM images of N <sub>x</sub> -GNRs synthesized using benzylamine .....	96
<b>Figure 3.4</b>	Morphological characterization of N <sub>x</sub> -GNRs.....	97
<b>Figure 3.5</b>	N <sub>x</sub> -GNRs width distribution .....	98
<b>Figure 3.6</b>	High resolution TEM images of N <sub>x</sub> -GNRs .....	99
<b>Figure 3.7</b>	Raman spectroscopy of Nx-GNRs synthesized with low amounts of pyrazine .....	100
<b>Figure 3.8</b>	Raman spectroscopy characterization of N <sub>x</sub> -GNRs.....	102
<b>Figure 3.9</b>	X-ray photoelectron spectroscopy (XPS) of N <sub>x</sub> -GNRs.....	103
<b>Figure 3.10</b>	Thermogravimetric analysis (TGA) of N <sub>x</sub> -GNRs.....	104
<b>Figure 3.11</b>	Electric characterization of individual N <sub>x</sub> -GNRs.....	106
<b>Figure 3.12</b>	Calculated density of states (DOS), quantum conductance and molecular models of N-doped graphene NRs (low concentrations).....	108
<b>Figure 3.13</b>	Calculated density of states (DOS), quantum conductance and molecular models of N-doped graphene NRs (high concentrations).....	109
<b>Figure 3.8</b>	Calculated I-V curves for N-doped and undoped zigzag graphene NRs.....	110

### Chapter 4

<b>Figure 4.1</b>	Anticancer drug docetaxel (DXT) simulated using molecular dynamics (MD) methodologies.....	116
<b>Figure 4.2</b>	MD for drug research.....	117

<b>Figure 4.3</b>	MD for proteins and DNA fragments.....	118
<b>Figure 4.4</b>	Conjugate gradient (CG) simulation of CNT and phospholipid bilayer membrane.....	119
<b>Figure 4.5</b>	Isosurface plots of a SWNT molecular orbitals, calculated by Density Functional Theory (DFT) methods.....	120
<b>Figure 4.6</b>	Chemical representations and molecular model of the dopamine (DA) and graphene system setup for analysis.....	123
<b>Figure 4.7</b>	Electronic states energy distribution for an isolated DA molecule.....	125
<b>Figure 4.8</b>	Energetic stability comparison for all the calculated systems...	126
<b>Figure 4.9</b>	Band structure, DOS and electronic density isosurface plot for pure graphene and DA systems.....	127
<b>Figure 4.10</b>	Band structure, DOS and electronic density isosurface plot for B-doped graphene and DA systems.....	129
<b>Figure 4.11</b>	Band structure, DOS and electronic density isosurface plot for N-doped graphene and DA systems.....	130
<b>Figure 4.12</b>	Band structure, DOS and electronic density isosurface plot for vacancy-defected graphene and DA systems.....	132
<b>Figure 4.13</b>	Band structure, DOS and electronic density isosurface plot for SW-defected graphene and DA systems.....	133

## Chapter 5

<b>Figure 5.1</b>	Scale comparison of common nanomaterials and biosystems, and example bioapplications of 1D nanostructures.....	143
<b>Figure 5.2</b>	Common approaches for neural interface electrodes.....	144
<b>Figure 5.3</b>	Cortical neurons growing on patterned substrates.....	145
<b>Figure 5.4</b>	Example of nanomaterials for improvement of existing biotechnologies.....	146

<b>Figure 5.5</b>	Bioelectronic optical implants and graphene based bioelectronics.....	147
<b>Figure 5.6</b>	Calculated electronic density plot of a dopamine molecule interacting with undoped and B-doped graphene.....	148
<b>Figure 5.7</b>	Setup for experimental comparison between undoped and N-doped CNTs based biosensor.....	150
<b>Figure 5.8</b>	Scanning electron micrographs of undoped and N-doped CNTs conductive networks.....	151
<b>Figure 5.9</b>	Current vs voltage (I-V) curves from measurements on CNTs thin films substrates.....	152
<b>Figure 5.10</b>	Comparison in resistivity changes of undoped and N-doped CNTs with different chemical treatment, produced by the presence of phosphate buffered saline (PBS).....	154
<b>Figure 5.11</b>	Comparison in resistivity changes of undoped and N-doped CNTs with different chemical treatment, produced by the presence of bovine serum albumin (BSA).....	156

## Appendix A

<b>Figure A.1</b>	Scheme of a scanning electron microscope (SEM).....	166
<b>Figure A.2</b>	Scheme of a transmission electron microscope (TEM).....	167
<b>Figure A.3</b>	Basic schematic of a scanning probe microscopy (SPM) system.....	168
<b>Figure A.4</b>	Inelastic photon scattering events related with the Raman effect, and physical origin of graphene's Raman typical modes.....	169
<b>Figure A.5</b>	Physical principle of X-ray photoelectron spectroscopy (XPS).....	171
<b>Figure A.6</b>	Typical atomic bonds vibrations with their correspondent wavelengths, and infrared (IR) example spectra.....	172



**Figure A.7** Schematic of a basic thermogravimetric analysis (TGA) system, and a typical TGA run plot..... 173

**Appendix B**

**Figure B.1** Electronic properties of N-doped and B-doped SWNTs..... 178

**Figure B.2** Results of DFT calculations over graphene nanoribbons..... 179

# Summary

This doctoral thesis work has been devoted to exploring in different ways this hypothesis: “*Carbon nanostructures, undoped and doped with elements such as nitrogen, can be used for the development of new biodetection and biosensing devices. Alternatively, they can be used for improving existing biotechnology applications*”. The results of the experimental and theoretical research work performed, are described in this thesis.

An important part of this thesis is focused in carbon based nanostructures, such as carbon nanotubes, graphene and graphitic nanoribbons. Their basic morphological, physical, and chemical characteristics from experimental and theoretical standpoints are described in chapter 1. One main topic which is recurrently addressed is the doping of these carbon nanomaterials with elements such as boron and nitrogen, and the comparison of their characteristics for specific applications.

Another crucial part of this research work is the report of the synthesis and characterization of a new carbon based nanomaterial: nitrogen-doped graphitic nanoribbons, which is the main contribution of this doctoral research. Chapter 3 includes experimental and theoretical findings that show specific nanoribbons' characteristics attributable to the nitrogen-doping and that could be potentially useful for nanoelectronic applications.

Complementary to the focus on the doping of carbon nanostructures, this thesis addresses the exploration of carbon nanotechnology for biotechnology applications. This topic is explored widely, including a substantial review, in chapter 2, of current research and potential novel devices based in nanomaterials. Two contributions are reported in this regard: A theoretical analysis of interactions between doped graphene and dopamine in chapter 4, and experimental tests of nitrogen-doped carbon nanotubes for biosensing in chapter 5. The results included here demonstrate that the potential of doped carbon nanostructures for biotechnology applications is considerable.

The results shown throughout this thesis work demonstrate the feasibility of using doped carbon nanomaterials for developing bioelectronic devices applicable in biotechnology, given the characteristics reported, such as increased sensitivity and biocompatibility when compared with other undoped nanostructures. This opens new possibilities for novel nanobioelectronics research and development.

# Abstract

The doping of carbon nanostructures with elements such as nitrogen and boron adds useful characteristics to the already remarkable features exhibited by nanocarbons. These new properties can be used for tackling several obstacles encountered for nanotechnology based applications, specially in biotechnology, where biocompatibility and sensitivity are crucial parameters for biosensing applications development. In this thesis work, we report the synthesis of nitrogen-doped graphitic nanoribbons, along with their characterization by SEM and TEM. Raman and XPS spectroscopy results are also shown, and electrical characterization results are presented as well. Our results demonstrate how the presence of nitrogen produces novel morphologic, chemical and physical properties on graphitic nanoribbons, which in turn make the nanomaterial a promising candidate for bioelectronics research.

Additionally, we present results of theoretical and experimental research on interactions of doped carbon nanomaterials and biomolecules. Our theoretical findings suggest strong effects of doping on the stability of interactions between graphene and dopamine, whereas our experimental results suggest improved electrical properties for nitrogen-doped carbon nanotubes based biodevices when compared with undoped ones.

This thesis shows, from theoretical and experimental studies, that doping of carbon nanostructures can be useful for sensing of biomolecules.

**Keywords:** doped carbon nanostructures, nanoribbons, bionanotechnology.

# Introduction

Among all the scientific and technological advances that are revolutionizing the way that the people communicate each other, work, play and live, the manipulation of matter at the *nanoscale* is one of the most innovative ways the science is exploring and finding new fascinating and useful materials. Nanoscale refers to dimensions in the order of nanometers; 1 nanometer (nm) is equal to one billionth of a meter ( $1 \times 10^{-9}$  m), and it is at this scale where quantum phenomena exerts its influence over nanostructures, and produces most of the novel and extraordinary properties these type of materials exhibit.

Carbon nanotechnology has been fueling top research in nanofields for many years, because the continuous and striking advancements that have been achieved throughout this period; from the discovery of carbon nanotubes (CNTs), including theoretical and experimental studies that established their electronic and mechanical properties, to the early theoretical electronic models for graphene, which were confirmed by the extraordinary characteristics measured over experimentally produced graphene samples. In fact, nowadays graphene is a star nanomaterial for a multiple real-world applications, which are promising to revolutionize nanoelectronics.

This doctoral research work is oriented towards the study of applied carbon nanotechnology, within the context of life sciences and bioengineering, where ongoing research efforts attempt to take advantage of nanomaterials characteristics, in order to create novel solutions or improving existent technologies based on new nanomaterials. This thesis presents an in-depth study of the synthesis, characterization and analysis of carbon

---

based nanostructures, and their properties, which could be useful for bioelectronic devices. Special attention is given to the description of doping carbon nanostructures, and their potential advantages over undoped ones for biotechnology and other types of applications. This work is structured in five chapters, describing the background and research work, plus two appendixes where some nanomaterials characterization techniques and theoretical models for nanomaterials study are addressed briefly.

In [Chapter 1](#), an overview of carbon nanomaterials is addressed as a general background, including descriptions of fullerenes, CNTs and graphene. CNTs and graphene are explored more abundantly, given their importance and copious literature regarding their properties and potential use in real-world applications. Also, the concept of carbon nanomaterials doping is introduced, along with information about how it changes some of the fundamental properties of CNTs and graphene, from a theoretical and experimental point of view.

[Chapter 2](#) presents background information about the use of carbon nanomaterials for bioscience and bioengineering applications. Additionally, a comparison with non-carbon nanostructures in biosciences is also presented. Throughout the chapter, topics as chemical treatment of carbon nanomaterials (such as functionalization), toxicity and biocompatibility assessments are addressed, as well as an extensive review of biodevices concepts based on CNTs and graphene. The effects of carbon nanostructures doping on biosystems is also reviewed based in current reports, with a special focus in issues as biocompatibility and sensitivity for potential new bioelectronics design.

[Chapter 3](#) starts with the contributions of this research work. It presents background information about undoped (pristine) graphitic nanoribbons (GNRs), with a brief description of some of their key morphological and physical features. Based on this, experimental results on the synthesis and characterization of nitrogen-doped GNRs (Nx-GNRs) are presented, including morphological features determination, spectroscopic analysis and electrical measurements. Additionally, theoretical calculations of equivalent systems are presented as well, in order to provide a comparative model for the observed characteristics.

In [Chapter 4](#), a theoretical evaluation of graphene interacting with a biomolecule is presented. The theoretical approach is based in Density Functional Theory (DFT) calculations, and variations in the simulated graphene (in form of vacancy and Stone-Wales defects, and boron- and nitrogen-doping) were considered. The simulated biomolecule was

dopamine (DA), which is a neurotransmitter molecule, and the interactions were calculated in presence of an electric field, in order to simulate and detect potential useful features for graphene based field-effect transistors (FETs) biosensors development. The results reported include the description of energetic stabilities, as well as the main electronic properties for each system.

Finally, in [Chapter 5](#) are presented preliminar experimental results of electrical measurements over substrates made of percolating networks of undoped and nitrogen-doped CNTs, in pure (untreated) state and treated with a surfactant and a polysaccharide commonly used for CNTs dispersions. The measurements were intended for evaluation of the effect of adsorbed molecules over CNTs' walls, potentially increasing the resistivity of percolating networks, and contrasting the results between undoped and N-doped tubes. Additionally, measurements of substrates conductivity in presence of model biofluids were also performed, in order to assess the electrical sensitivity of devices made of different type of nanostructures.

The research about the synthesis and characterization of  $N_x$ -GNRs has been already published (article hardcopy included in this work), being one of the two main contributions of this research. The theoretical analysis described in [Chapter 4](#) is the second main contribution, and the results are in the process of being submitted for publication.



# Chapter 1

## An overview on carbon nanomaterials

### 1.1 The carbon atom

Since the first observations of fullerenes [1, 2] and carbon nanotubes [3], the attention they attracted was significant due to their unique molecular structure and the resulting properties. The grounding of these exceptional characteristics lies precisely on the carbon atom nature, which is the lightest element having four valence electrons within its  $1s^2 2s^2 2p^2$  electronic configuration. This valence shell configuration allows the carbon atom to combine and bind in many ways which turn out on only carbon based materials exhibiting very different properties, such as the graphite with its softness commonly used for lubrication purposes, or diamond, one of the hardest materials with a wide variety of applications. This special conformation of the valence shell on the carbon atom and, more precisely, the way the atomic orbitals combine or hybridize are responsible for the carbon-carbon bonding flexibility and strength. In [figure 1.1](#) are depicted the three possible orbital hybridizations for carbon atoms;  $sp$ ,  $sp^2$  and  $sp^3$ . Each hybridization has its specific spatial distribution of electron probability cloud, forcing the molecular geometry to adopt characteristic arrangements;  $sp$  hybridizations are produced by the combination of one  $s$  with one  $p$  orbital, resulting in two  $sp$  orbitals separated by  $180^\circ$ . This is a more reactive configuration and is less common on carbon nanostructures, but can be found in organic



chemistry substances, and its reactivity is useful in chemical reactions, and in achieving high temperatures in processes such as acetylene welding. The three  $sp^2$  hybrid orbitals are formed by the mixing of the  $s$  orbital plus two  $p$  orbitals, resulting on three coplanar orbitals separated by  $120^\circ$  (trigonal planar geometry). The  $sp^2$  orbitals are the most common found on nanocarbons such as fullerenes, carbon nanotubes and graphene, based on the flexibility and strength exhibited by the honeycomb atomic arrangement, which is in turn a direct consequence of this particular carbon hybridization. Finally, the four  $sp^3$  orbitals are the result of the combination of the  $s$  orbital plus the three available  $p$  orbitals, adopting a tetrahedral geometry ( $109.5^\circ$  between each one). This hybridization is very important in organic chemistry and biochemistry, but in most nanocarbons is mostly seen when chemical functionalization is used.

Representative models of the rich diversity of nanocarbons can be observed on [figure 1.2](#), where fullerenes and nanotubes are shown. It is important to point out to the fact that the most interesting pure carbon nanomaterials, at least from the electronic and chemical point of view, are those ones with carbon atoms bonded by  $sp^2$  hybrid orbitals. The  $sp^2$  orbital hybridizations have two main characteristics which are responsible for the outstanding properties; as previously mentioned, it produces flat honeycomb-like carbonaceous lattices where carbon atoms are strongly bonded to three other carbons, conserving a high degree of flexibility that is related with complex structures like carbon nanotubes or fullerenes. The second key characteristic of carbon  $sp^2$  hybrid orbitals is that they produce  $\pi$  (pi-bonding) and  $\pi^*$  (pi-antibonding) orbitals, due to the existence of one pure and unoccupied  $p_z$  orbital per atom, which in turn are conforming the conduction band on perfect monolayer graphene. These two inherent characteristics, together with the

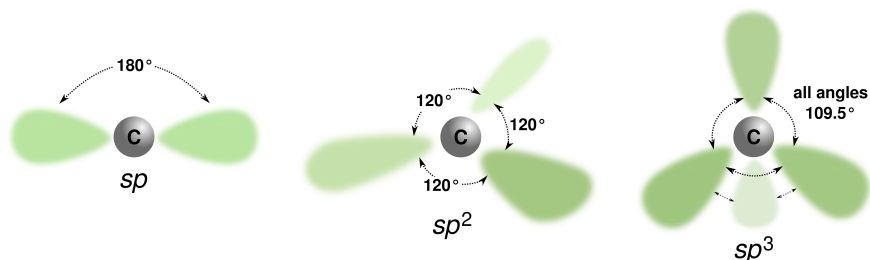


**Figure 1.1.** Orbital hybridizations for carbon atoms. All the hybrid orbitals conformations are produced by the combination of the  $s$  orbital with one, two or three  $p$  orbitals ( $sp$ ,  $sp^2$  and  $sp^3$  respectively) from the carbon valence shell (figure based on molecular geometry models).

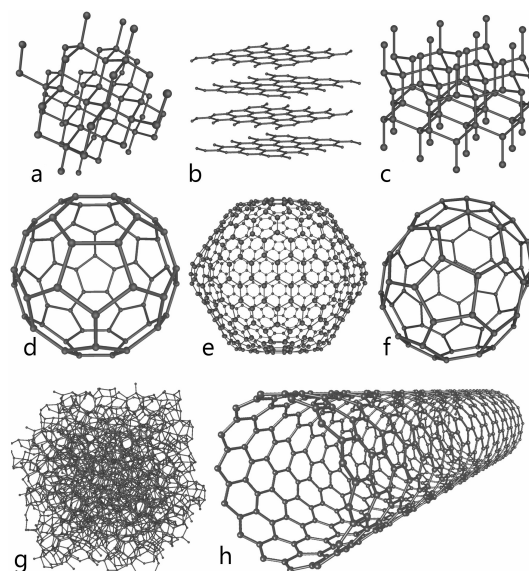


**Figure 1.2.** Some allotropes of carbon: **a)** diamond; **b)** graphite; **c)** lonsdaleite (diamond with an hexagonal crystal lattice); **d–f)** fullerenes ( $C_{60}$ ,  $C_{540}$ ,  $C_{70}$ ); **g)** amorphous carbon; **h)** carbon nanotube.

modifications made possible by doping or with chemical treatments on carbon nanomaterials, are responsible for the wide diversity of topics currently being explored on carbon nanotechnology.

Having considered the general characteristics that make carbon nanomaterials so remarkable, distinguishing characteristics of different nanocarbons will now be presented, considering how nanostructure geometry, size and purity are key factors for their mechanical, electronic and chemical properties.

## 1.2 Fullerenes

Fullerenes or buckyballs are the names given to all carbon nanostructures with closed-cage like morphology, with  $C_{60}$  (buckminsterfullerene) being the most representative one since it was the first to be identified and characterized [1, 2]. The discovery of fullerenes was one of the starting points for the carbon nanotechnology development, since it proved the stability and feasibility of producing  $sp^2$  carbon nanostructures. It also fueled new efforts on carbon-based nanomaterials research, which is now well established and also provided strong contributions to the knowledge and methods for chemical modifications of nanocarbons, now used in nanotubes and graphene research.

Nowadays, the momentum seen on fullerenes research has been refocused on other types of nanocarbons, but their discovery and synthesis established many important approaches for the current carbon nanoscience.

### 1.2.1 Synthesis methods

The first buckyballs synthesis was reported by H. Kroto and collaborators in their famous Nobel prize winning work [1]. The setup used was a pulsed laser vaporizing a graphite target, under vacuum with a helium flow, and using a mass spectrometer as detector. This setup was originally intended for metal clusters production and study, and it was these experiments that first produced reliably the fullerenes, of which  $C_{60}$ , being most stable, was most abundant. Nevertheless, this method produced only very small quantities of the nanomaterial, and was inadequate for extensive research on physico-chemical properties. The breakthrough that overcame this limitation was developed by Krätschmer and collaborators [2], who were looking specifically for a fullerene synthesis method that yielded “bulk” quantities. The result was the electric arc setup depicted on figure 1.3, which under controlled helium pressure conditions allowed to collect gram-quantities of soot containing up to 75% of  $C_{60}$ . Due to its high efficiency, the arc-discharge method has remained in use with few changes, among them: the use of alternate (AC) instead of direct

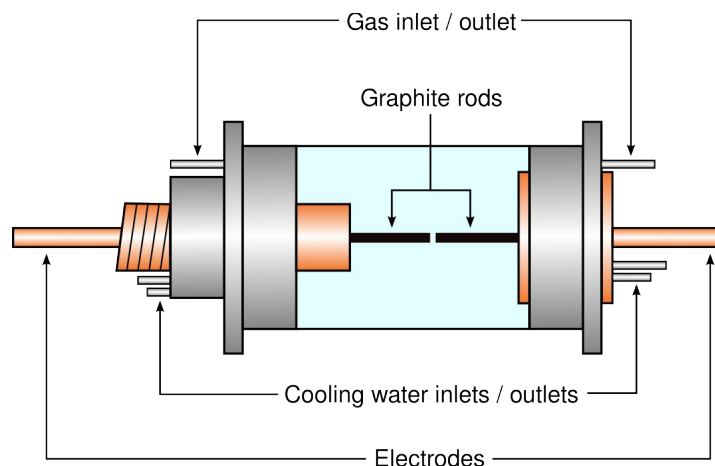


**Figure 1.3.** Electric arc-discharge setup used for fullerenes synthesis. The device is composed by a pyrex chamber and two independent electrodes. The synthesis process is based on pure graphite rods evaporation through the electric arc between them induced by a DC potential applied to the metallic electrodes (figure based on a classical arc-discharge device).

(DC) current for the electric arc generation [4], the inclusion of non-carbon precursors for the synthesis of doped (*i.e.* substitution of one or more carbon atoms for non-carbons, being boron and nitrogen the most common dopants) buckyballs [5], or endohedral trapping of metal atoms (metallofullerenes) [6].

### 1.2.2 Properties

Buckyballs present a structural feature that is key for much of their chemical and physical properties; they are formed by a combination of hexagons and pentagons as polyhedral faces (with the carbon atoms located at the vertex) that fit a mathematical rule known as Euler's theorem. Basically it states that for any closed-cage geometrical structure, including fullerenes, there must be 12 pentagons and a variable number of hexagons. The  $C_{60}$  has exactly 12 pentagons and 20 hexagons (see figure 1.4a), the  $C_{70}$  has 12 pentagons and 25 hexagons. This special geometric distribution allows, specifically in  $C_{60}$ , the even distribution of all bonding electrons, giving the nanostructure its strong stability. Moreover, the presence of pentagons contribute to curvature and high reactivity regions.

Even before experimental characterization was made possible by bulk production of fullerenes, several interesting properties were predicted from the theoretical studies. Figure 1.4b shows the Hückel molecular orbitals model for the  $C_{60}$  molecule, based on tight-binding calculations, considering one free electron per carbon atom. These type of

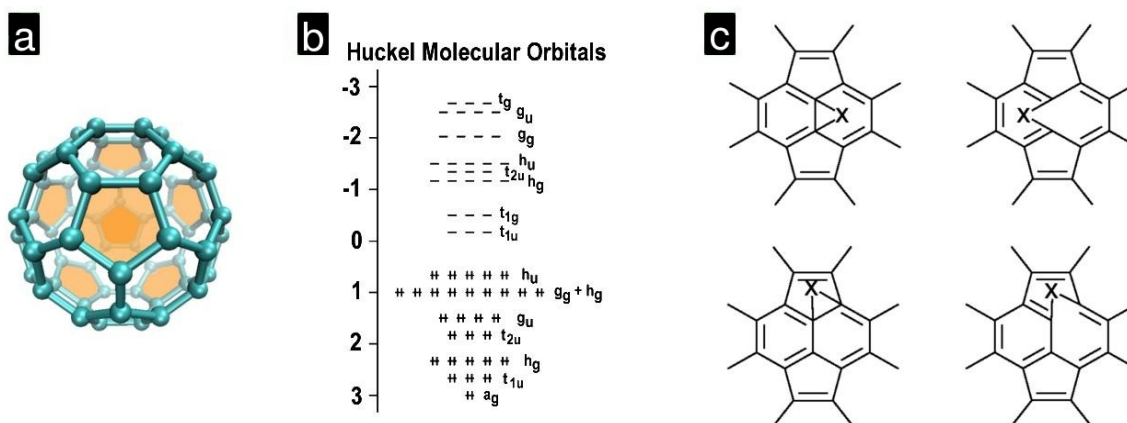


**Figure 1.4.** a)  $C_{60}$  molecular model, with pentagons highlighted by orange shades. b)  $C_{60}$  calculated molecular orbitals according with Hückel ( $\pi$ -atoms) theoretical model. c) Four possible addition reactions for  $C_{60}$  (figure b based on [7], and c based on [9]).

calculations have been fundamental for understanding most of the unique electronic properties exhibited by carbon nanomaterials. The molecular orbitals energy distribution for  $C_{60}$  has obviously a discrete nature given its size (see [figure 1.4b](#)), and shows a completely full valence band and empty electronic states above the Fermi level. This electron distribution accounts for the high inertness displayed by fullerenes without any treatment. On the other hand, it also is responsible for the relevant electronic characteristics arisen from super-molecular arrangements. This was observed since not only the carbon atoms distribution within a fullerene molecule is geometrically interesting. The spatial arrangement of whole  $C_{60}$  molecules in crystalline structures has been studied, alongside with elements as potassium, rubidium and thallium for superconductive structures building [\[7\]](#).

The chemistry of fullerenes has been as well abundantly explored, with a numerous reports addressing different approaches for conjugation and functionalization of fullerenes with metallic atoms, polymers and biomolecules, including drugs [\[8, 9\]](#). [Figure 1.4c](#) shows the bonding configurations for chemical addition in fullerenes, and the way it modifies the pure  $sp^2$  network. Some of these approaches take advantage of the particular shape of fullerenes for their use as a “nucleation” sites for dendritic polymers synthesis or multi-branched systems. In any case, the fullerene chemistry research, alongside to other semiconducting investigations, are still under development, even though the focus nanocarbons research has largely shifted to nanotubes and more recently, graphene.

### **1.3 Carbon nanotubes**

Carbon nanotubes (commonly abbreviated as CNTs) can be considered simply as rolled sheets of hexagonally arranged carbon atoms, in a honeycomb-like pattern. This flat carbonaceous structure is called graphene (which will be described in more detail below), and most of the interesting characteristics they have originate on the elemental properties of graphene. CNTs exhibit a high aspect ratio, with diameters from few nanometers for single-walled nanotubes, up to around 200 nm for thick multi-walled nanotubes, and lengths of several microns or even centimeters [\[10\]](#). There are variations on the number of concentric layers or tubes, giving rise to the two distinct type of nanotubes: single-wall carbon nanotubes (SWNTs), obviously composed of only one rolled graphene sheet; and multi-wall carbon nanotubes (MWNTs) which can be formed from even two up to hundreds of concentric tubes (see [figure 1.5a-b](#)).

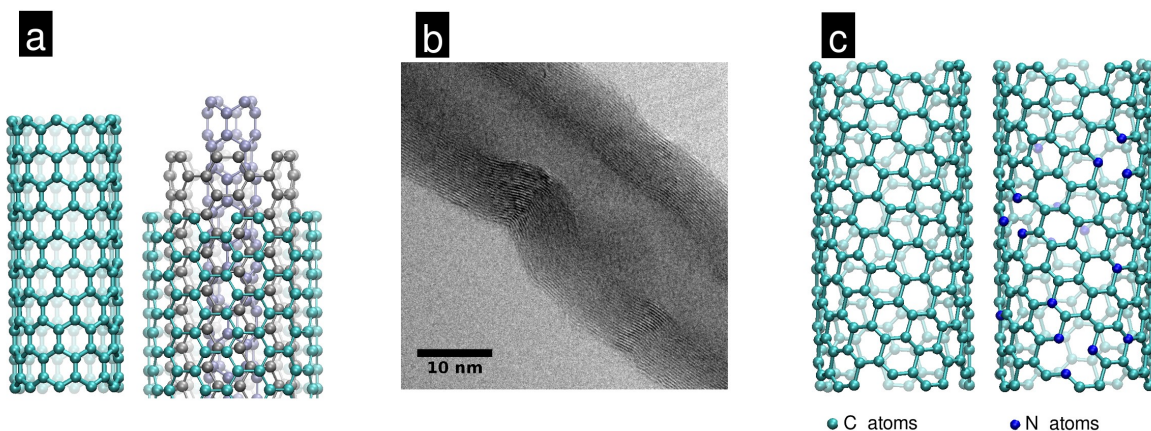


**Figure 1.5.** **a)** Models of single-wall (SWNT) and multi-wall (MWNT) carbon nanotubes. **b)** Transmission electron microscopy (TEM) image of a MWNT. **c)** Models for pure (undoped) SWNT and substitutional nitrogen-doped SWNT (also known as SWNT-CN<sub>x</sub>).

The discovery of CNTs is normally attributed to Iijima [3], even though some previous evidence of their observation can be found [11]. The exciting properties that were predicted, and later measured for them promoted the intense research on CNTs that is still going nowadays, specially for applications development.

From the chemical point of view, two types of CNTs can be produced: pure (or undoped) CNTs, which are the CNTs completely composed by carbon atoms, and doped CNTs, which are the result of the introduction of non-carbon atoms such as nitrogen, boron, silicon or phosphorous into the graphitic lattice (substitutional doping, see figure 1.5c), around CNTs (exohedral doping) or inside the hollow regions of CNTs (endohedral doping). Both present characteristics that make them interesting for different types of applications.

### 1.3.1 Undoped carbon nanotubes

Carbon nanotubes are similar to carbon fibers, in composition, aspect-ratio, and some production methods. Due to this, pure CNTs were first actually seen in 1976 in a carbon fiber sample [11]. This report, where a CNTs were an oddity, did not result in further studies. After MWNTs were properly identified and produced systematically in 1993, the research on understanding their properties boomed. The first theoretical studies on SWNTs showed clearly that they can be classified according to the way the hexagonal carbonaceous

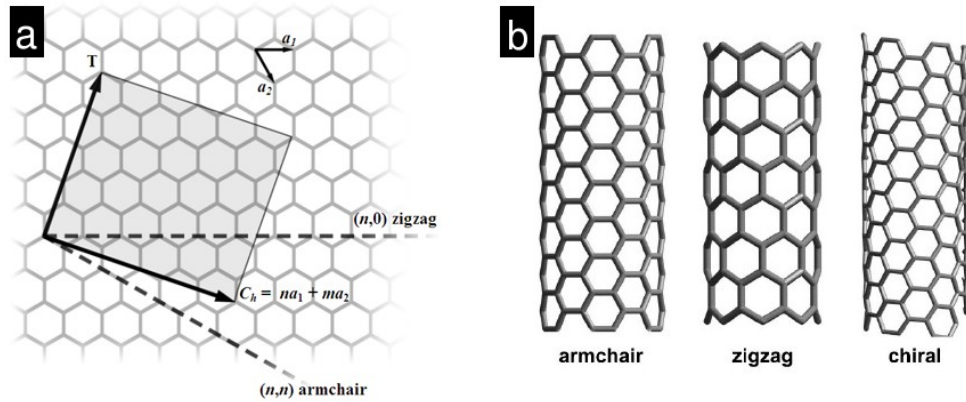


**Figure 1.6.** **a)** Geometrical configuration of CNTs depicted in function of the circumferential vector, with the three possible nanotube construction: armchair, zigzag and chiral. **b)** Example models of the different CNTs types.

lattice is aligned with respect to the nanotube main axis, resulting in three types of CNTs exhibiting different properties [12]. The classification can be visualized as if it was the way the graphene sheet is rolled up to form the nanotube. Figure 1.6a shows the vectors that define the possible alignments of the nanotube ends. This vector is described by a pair of integers  $(n, m)$  representing the relative position of equivalent atoms in the formed CNT, *i.e.*

$$\mathbf{c} = n\mathbf{a}_1 + m\mathbf{a}_2$$

Thus, these two integers precisely define the geometry of CNTs, and their values differentiate three CNT types: armchair (for all the tubes with  $n = m$ ), zig-zag (for all tubes with  $m = 0$ ), and chiral nanotubes (for all other  $n, m$  combinations), and they present distinctive electronic features which will be described below. See figure 1.6b for models of the three types of SWNTs.

Regarding undoped MWNTs, they are actually an ensemble of SWNTs with increasing diameters concentrically arranged (see figure 1.5a). The individual layers have different geometries, and can be counted from as few as two (double-wall CNTs) to several tens of concentric tubes. Thus, the electrical properties of MWNTs are not defined by a single chirality, and due to the layered structure they have different properties in comparison to SWNTs.

### 1.3.1.1 Synthesis methods

There are several synthesis methods for CNTs that produce specific types of nanotubes. Some of them are based on the catalytic conversion (by transition metal nanoparticles) of vapors of organic precursors, whereas others are based on plasma decomposition of graphite in reactors with conditions such as gas content and pressure tightly controlled. Some of the key reports on CNTs synthesis methods are summarized in [table 1.1](#).

**Table 1.1.** Carbon nanotubes synthesis methods (some information taken from [\[13\]](#)).

Year	Method	Remarks	Reference
1991	Arc-discharge	Carbon nanotubes discovery	[3]
1992	Arc-discharge	One of the first bulk production of MWNTs	[14]
1993	Arc-discharge	First confirmed SWNT production	[15, 16]
1996	Laser ablation	Laser ablation, high yield	[17]
1996	CVD	First SWNT CVD growth	[18]
1998	CVD	First patterned-substrate growth	[19, 20]
1999	CVD	CVD production in gram scale of SWNTs	[21]
1999	CVD (HiPco)	Demonstration of HiPco SWNTs	[22]
2000	Flame	First flame synthesis of SWNTs	[23]
2000	CVD	Demonstration of diameter control in bulk catalyst	[24, 25]
2001	CVD	Diameter-selective substrate synthesis from predefined nanoparticles	[26]
2001	CVD	First aligned SWNTs growth: E-field alignment	[27, 28]
2002	CVD	First growth from alcohol; low temperature	[29]
2002	CVD	First ultralong SWNTs (>400 $\mu\text{m}$ )	[30]
2003	CVD	Aligned SWNTs from gas flow utilizing fast heating and tip growth (>1 mm)	[31]
2003	PECVD	First plasma-enhanced CVD (PECVD) of SWNTs	[32]
2004	PECVD	Preferential low T growth of semiconducting SWNTs	[33]
2004	CVD	First vertical SWNTs films (<15 $\mu\text{m}$ tall)	[34]
2004	CVD	SWNTs “super-growth”, water assisted ultrahigh yield	[35]

CVD = Chemical Vapor Deposition

HiPco = High Pressure carbon monoxide (CO)

PECVD = Plasma-enhanced Chemical Vapor Deposition



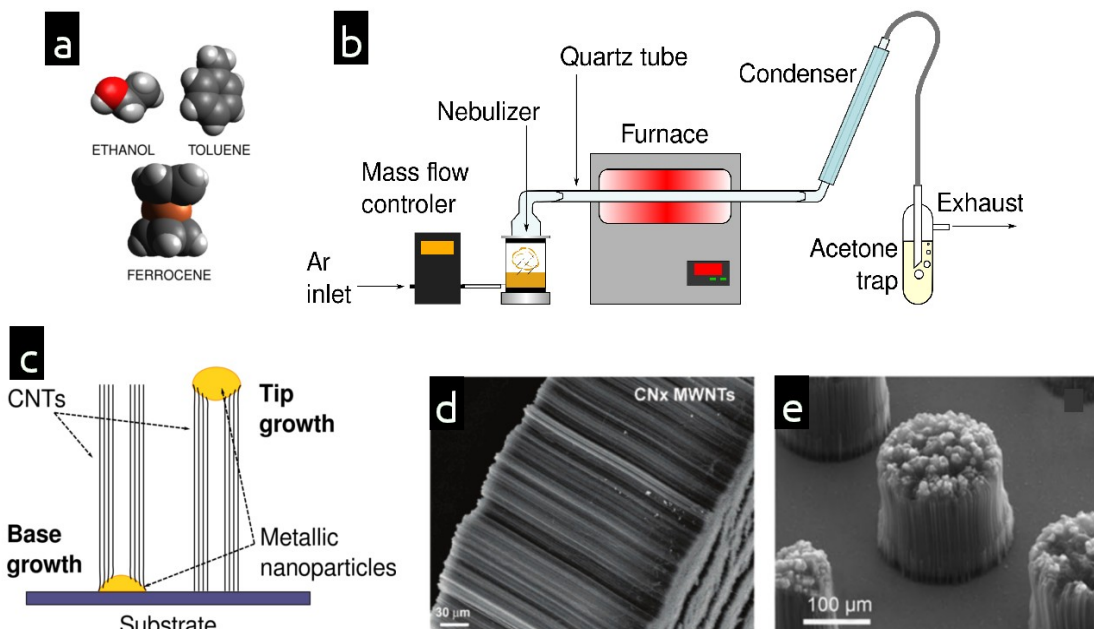


**Figure 1.7.** **a)** Molecular models for common precursors in CNTs synthesis by CVD: ethanol, toluene and ferrocene. **b)** Typical CVD scheme for carbon nanomaterials synthesis. **c)** CNTs base and tip growth mechanisms representation, depicting the catalytic metal particle position with respect to the substrate. **d-e)** Scanning electron micrography (SEM) images of a carpet of aligned nitrogen-doped carbon nanotubes (CN<sub>x</sub>-MWNTs) and CNTs pillars grown from patterned catalyst (images taken from [36] and [37] respectively).

CVD is a versatile and very popular synthesis method for CNTs, and it was used for the production of the material studied in this project. CVD occurs through decomposition of organic vapors by metallic catalyst nanoparticles, either formed in situ from mixtures of organic precursors (e.g. ethanol or toluene) and an organometallic compound (e.g. ferrocene) directly dissolved in the organic solvent (see figure 1.7a), or by prior deposition of catalytic nanoparticles on substrates, the latter method having interesting applications such as patterned growth. On figure 1.7b can be observed the basic configuration for the CVD setup used in this thesis, consisting basically in an ultrasonic nebulizer, which is used to produce an aerosol of the precursors solution, a furnace with a quartz tube and a controlled mass flux system for injecting the nebulized precursors carried by inert gases. The CNTs grow in the hot regions of the tube inside the furnace, where the organic molecules are decomposed and the metal nanoparticles reassemble the carbon atoms into nanotubes, usually deposited on SiO<sub>2</sub> substrates. The growth mechanism has been studied

and explained [38] as occurring by the diffusion of carbon atoms in the surface of metallic particles, or even the dissolution of carbon inside the metallic particles in liquid state (high temperatures). In any case, the result is that CNTs are “extruded” from the metallic particles, which either remain placed at the surface (base growth), or are displaced along with the growing edge of the nanotube (tip growth) while the other end of the CNT is attached to the substrate. Both possible mechanisms are shown in figure 1.7c. On figure 1.7d-e are observed “carpets” of aligned CNTs, with the catalyst dissolved on the precursors solution and with the patterned catalyst on the substrate, respectively.

### 1.3.1.2 Properties

The mechanical and electrical characteristics of CNTs make them an attractive material for composites, electronic, sensing and biological applications. These properties arise from the high stability of C–C bonds, and from the way the electrons are distributed over the  $sp^2$  lattice. By dimensional comparisons, CNTs are one of the strongest and stiffest materials in terms of tensile strength and elastic modulus. For instance, CNTs have been reported to exhibit Young's modulus as high as 4.15 TPa [39], which is around 20 times higher than steel. This resistance and lightness of CNTs make them an ideal candidate for applications involving composites for high performance materials.

Another key characteristic of CNTs is their electronic properties, which were predicted from theoretical explorations on hexagonal  $sp^2$  carbon lattices which revealed many features that stem from fundamental quantum phenomena, showing electronic behaviors strongly correlated to the structure's symmetry [40, 41]. These studies established that for all armchair nanotube configurations (chiral indexes  $n = m$ ), their electronic nature will be always metallic, whereas for zig-zag ones (chiral indexes in  $(n,0)$  form) some are metallic and some semiconducting (see figure 1.8 for CNTs examples, including their electronic band structure and density of states). This behavior is explained considering that the band gap, *i.e.* the energetic difference between the valence band and conduction band in a semiconductor, can be roughly evaluated by the CNT chiral indexes; if  $n - m$  is a multiple of 3, including the case of  $(3n,0)$  for zig-zag tubes, then the nanotube's band gap is close to zero, and the CNT behaves as a metallic conductor. Otherwise, the CNT is a semiconductor with a moderate band gap. Figure 1.8 shows two examples: a  $(7,7)$  metallic nanotube which has states at the Fermi level with overlapping of conduction and valence bands at  $\Gamma$  (center of the Brillouin zone), and a  $(10,0)$  semiconducting tube with a band gap of 1.08 eV at  $\Gamma$ .

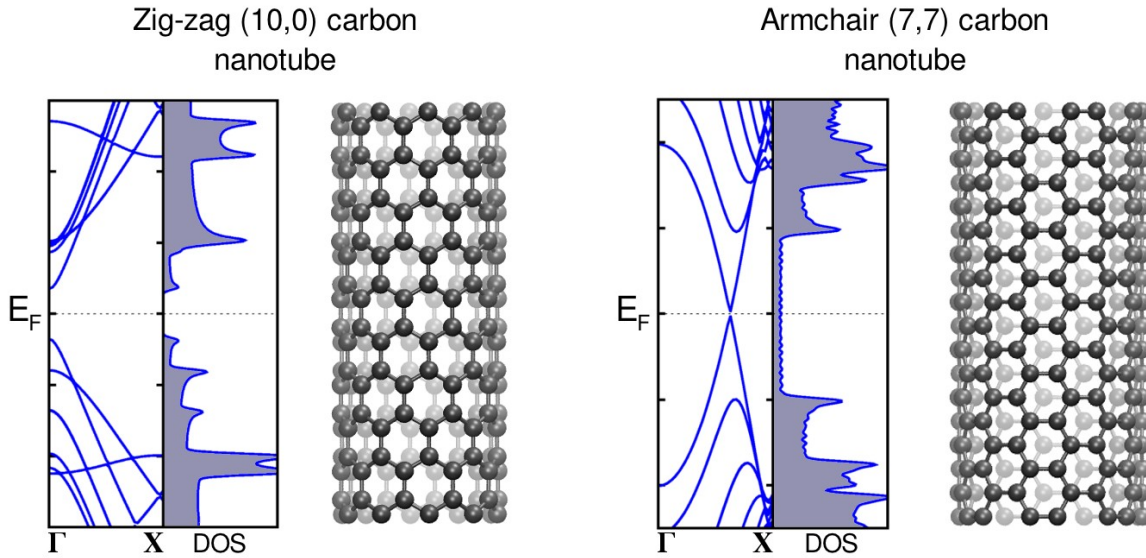


**Figure 1.8.** Calculated electronic structure for two example carbon nanotubes; zig-zag (10,0) and armchair (7,7) chirality. The plots depict the electronic band structure (from  $\Gamma$  to X within the first Brillouin zone) and the correspondent density of states (DOS). Note the band gap between conductive and valence states (top and bottom states with respect to the Fermi energy  $E_F$ ) for the zig-zag nanotube, characteristic of semiconducting behavior. The armchair nanotubes exhibit a metallic (no band gap) behavior (figures from calculations made with SIESTA, using DFT methods, and plotted with *gnuplot*. Molecular models made using *VMD*).

The gap magnitude is directly related with the nanotube chirality, and can span from 0.25 to almost 3.0 eV.

Another important peculiarity of the electronic states on CNTs is that they present special features (*Van Hove singularities*), observables as sharp peaks in the density of states (DOS) plots. The presence of Van Hove singularities in carbon nanotubes gives rise to electronic transitions mainly in the regions close to the Fermi level, with energies within the range of optical phenomena (1.65 to 3.27 eV) [42]. These electronic transitions confer to CNTs specific absorption and photoluminescent characteristics, which have been used for instance for nanotubes chirality characterization. Moreover, the electronic nature of carbon nano-structures in combination with their vibrational features produce electronic scattering effects that can be optically detected and assigned to specific characteristics, such as diameter, structural defects or semiconducting type. These effects can be seen in characterization by Raman scattering spectroscopy, which has been extensively applied to carbon and other nanostructures research [43]. Figure 1.9 shows an example of a Raman

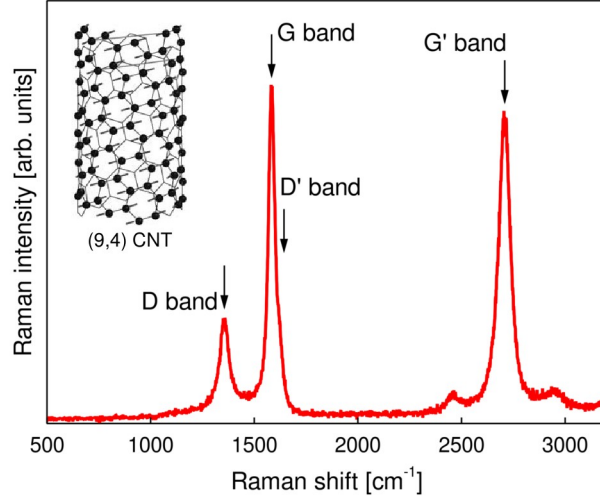


**Figure 1.9.** Raman spectrum for MWNTs obtained using an excitation laser of 514 nm wavelength. Note the typical Raman modes; D (1353  $\text{cm}^{-1}$ ), G (1590  $\text{cm}^{-1}$ ), D' (1619  $\text{cm}^{-1}$ ) and G' (2704  $\text{cm}^{-1}$ ). The D band intensity ratio against G band intensity ( $I_D/I_G$  ratio) is commonly related with defects (non  $sp^2$  carbon) in the carbon nanostructure. **Inset:** Example of one of the active Raman vibrational modes ( $A_1$ ) for a (9,4) CNT (spectrum from CNTs synthesized by CVD as described in section 1.3.1.1, and acquired with a Renishaw inVia microRaman using a 514 nm laser. Inset adapted from [43]).

spectrum of MWNTs, where the typical Raman modes are indicated; the G band is a mode arising from the in-plane resonant vibrations of the carbonaceous  $sp^2$  lattice (the G comes from *graphitic*), the D band originates from non- $sp^2$  carbons, which can be considered as “defects” with respect to a perfect honeycomb lattice, the D' mode is normally a weak feature, and shows shiftings in its central value that are related to changes in electronic properties (as changes towards p- or n-type semiconductor), particularly for SWNTs [44]. The G' band is related as well with the electronic nature of CNTs, as it reflects features as electron transfers from doping through changes in the peak frequency. In addition, there are important relationships between the intensities of some of the Raman modes; for instance, the ratio between the D and G bands intensities (commonly known as  $I_D/I_G$  ratio), is used as a “signature” for lattice defects within the CNT's walls, which can be product, for example, of chemical treatments like oxidation or other types of functionalization (see section 2.1.2 for an overview of functionalization), or of doping with atoms or vacancies.

Several approaches for technological developments based on CNTs most relevant properties have been explored, among them CNT based electronic devices have been studied the most. Figure 1.10 shows both a stylized model and an atomic force microscopy

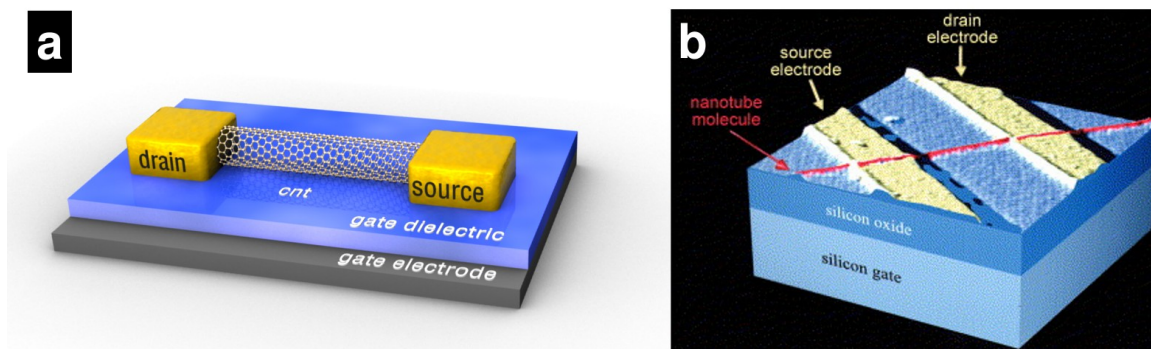


**Figure 1.10.** (a) Model representation of a CNT based field effect transistor (CNT-FET), depicting the drain and source electrodes in a back gate configuration. (b) AFM image of a CNT-FET, where the CNT and electrodes have been false-colored (image taken from [45]).

(AFM) image of an actual individual CNT based field effect transistor (CNT-FET), which consists in two main electrodes connected directly to the CNT ends, and a back gate electrode electrically isolated from the nanotube channel. The working principle for the CNT-FET is essentially the same for conventional FETs, with an electric field produced between the gate and source electrodes controlling the availability of free charge carriers along the semiconducting CNT. Several reports have observed promising results, highlighting key advantages of CNT-FETs over conventional FETs based on silicon, such as high carrier mobility from ballistic instead of scattered electron transport [46] and higher ON/OFF current ratios [47], among others.

Finally, from the chemical point of view, CNTs exhibit an intrinsic inertness given the stability of the  $sp^2$  bondings. To introduce functional groups capable of chemical interactions with other molecules, CNTs commonly require strong treatments such as acidic oxidation, fluorination or plasma activation, and other relatively aggressive chemical reactions capable of attaching specific groups or molecules to the CNTs' sides, increasing their usability in applications such as polymer grafting or pharmacology. Nevertheless, these harsh chemical treatments can affect the structural integrity of nanotubes, affecting their electronic properties. Alternative methods of non-covalent functionalization of CNTs based on  $\pi$ - $\pi$  stacking of aromatic molecules such as pyrene, allow the conservation of the CNTs' electronic and mechanical properties (see the extensive review on [48] for in deep information regarding the chemistry of CNTs).

### 1.3.2 Nitrogen doped carbon nanotubes

Pure CNTs are chemically inert, which is desirable for applications where interactions with surrounding species could affect their performance. However, when interaction with the medium is desirable, CNTs and other nanocarbons require different chemical attributes while preserving as much as possible their mechanical and electronic properties. Doping of CNTs is one of the most explored alternatives for tailoring their electronic and chemical characteristics, with important implications already reported for applications such as composites [49], sensing [50] and devices for solar energy harvesting [51]. Additionally, doped CNTs have revealed promising results when interacting with biosystems in nanobiotechnology research [36, 52].

The doping of CNTs can occur in different ways, in terms of where the dopant atoms are located in the carbon nanostructure. In analogy with the process for conventional semiconductors as silicon, doping refers to the addition of free charge carriers (either electrons or holes) to the CNT molecular structure, in order to unbalance the electrons-holes ratio and promote a n- or p-type semiconducting material behavior. This charge addition is done by the incorporation small amounts of dopant atoms with an extra electron or with one less valence electron with respect to the number of valence electrons of the material to be doped (e.g., arsenic, boron or phosphorous for silicon). For CNTs, this can be carried out in three ways, which are represented schematically for double-wall CNTs (DWNTs) in [figure 1.11](#); the first two cases rely on charge transfers between CNTs and

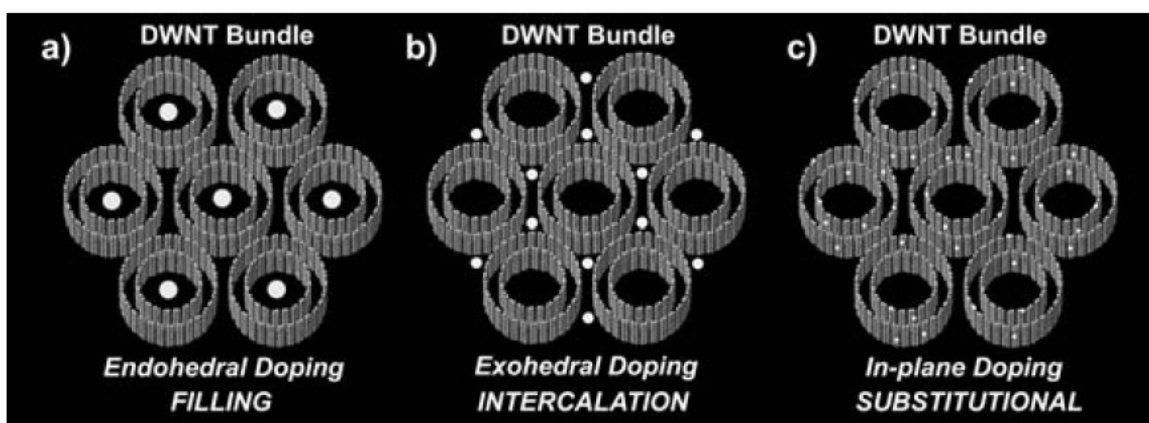


**Figure 1.11.** Molecular models representing schematically (a) endohedral doping; (b) exohedral doping or intercalation, and (c) in-plane (substitutional) doping in double-wall CNTs bundles. (Image taken from [53]).

external atoms or clusters, either internally to the CNTs structure (endohedral doping), or externally, in the gaps between adjacent CNTs (exohedral doping). Both cases can occur with clusters of atoms of a wide variety of elements [53], since the size of the dopant is relatively unrestricted when compared with in-plane or substitutional doping. This in-plane doping implies the replacement of carbon for other type of atoms, such as nitrogen, boron, phosphorous or silicon, which are comparable in size to carbon atoms and hence compatible with the  $sp^2$  honeycomb-like lattice of CNTs.

Most of the studies about doping of CNTs are devoted to substitutionally doped CNTs, either theoretically (since they are easier to analyze compared to exohedral or endohedral doping) or experimentally (due to the abundant reports on the synthesis of doped nanomaterials). Moreover, nitrogen doping (N-doping) is among the most observed type in scientific reports, due to the well established synthesis methods and the similarities existing between nitrogen and carbon atoms that further facilitate theoretical calculations. Henceforth, in this work the term “doping” for nanocarbons will refer to in-plane substitution of carbon for nitrogen atoms, unless otherwise stated.

### 1.3.2.1 Synthesis methods

The synthesis methods for nitrogen doped (N-doped) CNTs (also known as  $CN_x$ ), are in most cases similar to the methods for undoped ones. The differences reside in the precursors utilized during the synthesis processes. For instance, when synthesizing doped CNTs by the arc-discharge method, small amounts of boron nitride are encapsulated into the graphite electrodes, resulting in boron-nitrogen doped CNTs [54, 55]. Also, techniques for substitutionally doping pure synthesized CNTs by physico-chemical means (as thermo-chemical treatments of pure CNTs bundles) have been reported as well, yielding comparatively low doping levels with respect to the ones with the doping at the production stage [56].

CVD synthesis methods for doped CNTs only require the addition of adequate precursors, together with small changes in process parameters such as synthesis temperatures, pressure and mass flow [57]. In figure 1.12a-c are depicted three common substances used as carbon and nitrogen precursors for  $CN_x$  fabrication by CVD; acetonitrile, benzylamine and melamine.

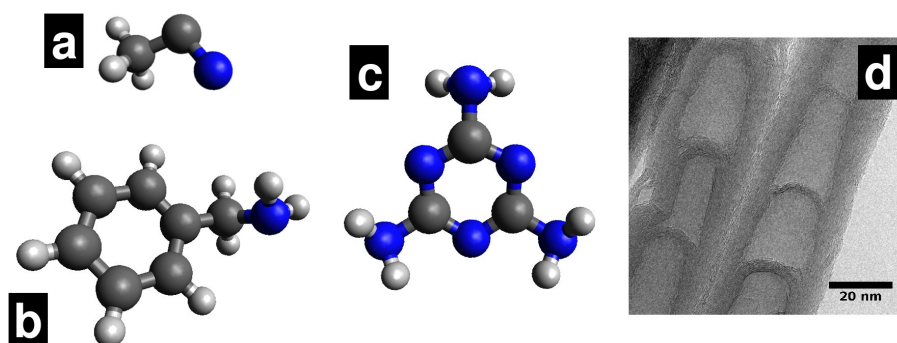


**Figure 1.12.** Molecular representations of (a) acetonitrile, (b) benzylamine and (c) melamine, which are common organic precursors for nitrogen-doped CNTs (or  $CN_x$ ) synthesis. (d) TEM image of a couple of  $CN_x$ , where their typical bamboo-like compartmentalization is observed.

### 1.3.2.2 Properties

One of the morphological features that differentiates N-doped CNTs from their undoped counterparts is the compartmentalization of the inner shells of  $CN_x$ -MWNTs (see [figure 1.12d](#)). This effect has been unequivocally associated with nitrogen presence in carbonaceous lattices, as it induces structural curvature regions [58]. Theoretical studies have shown that the presence of nitrogen atoms in the carbon lattices introduces structural stress, which in turn forces the nanostructure to curve in specific sections, in a similar way to how pentagons or heptagons produce curvature (note for example the necessity of pentagons for closing nanostructures such as fullerenes). The curvature formation in CNTs have important effects not only in morphological characteristics, but also in electronic and chemical properties.

Changes on electronic properties of CNTs are the most significant consequences of N-doping. Several studies have revealed clearly an introduction of quasi-bound or very localized electronic states associated to nitrogen atoms within the CNT [59, 60]. [Figure 1.13a](#) shows the band structure and density of states (DOS) of a  $CN_x$ -SWNT, substitutionally doped with one nitrogen atom, as well as the electron density isosurface correspondent to the states close to  $E_F$ . Note that, comparing with the electronic properties for undoped CNT (see [figure 1.8](#)), the symmetry of the electronic states for the valence and conduction bands is broken, shifting the overall CNT behavior towards a n-type material. This is due to the fact that nitrogen has one more electron than a carbon atom, thus giving to the nanostructure an excess of negative charges. The electron density plot on a nanotube model also reveals the higher electron density near the N-doping site (see the arrow and



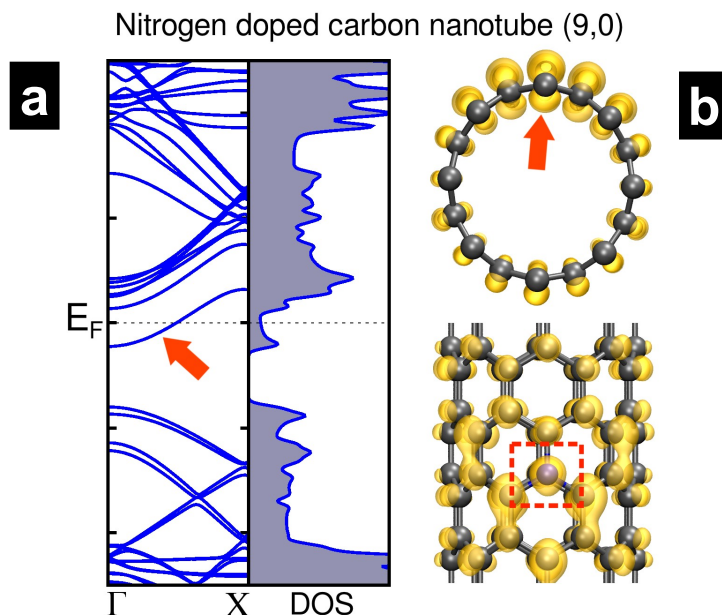


**Figure 1.13.** Calculated electronic structure for a  $CN_x$  (9,0). The band structure and correspondent density of states (DOS) show the effect of one N atom substitutionally placed into the CNT lattice (atom position highlighted by the arrow and square in the molecular model). Nitrogen introduces states at the Fermi level  $E_F$  (the N-induced band is pointed by an arrow in the band structure) which makes the nanotube metallic, by a n-type semiconductor shifting. The isosurface depicted over the molecular model corresponds to the electron density for states close to  $E_F$ .

square in [figure 1.13b](#)). This unbalanced electron density along the nanostructure has important effects in the vibrational modes of CNTs, significantly altering their electronic transport and optical properties [44, 61]. [Figure 1.14](#) shows a set of Raman spectra related to  $CN_x$ -SWNTs which have been doped using different concentrations of nitrogen precursor (0-33% at. N, in a xylene solution of acetonitrile). Increased nitrogen amounts produce changes in the intensity of two important modes; radial breathing modes (RBM), which are related to synchronous out-of-plane SWNT vibrations, and D-band mode, which is related to the non- $sp^2$  bonding within a carbon lattice. Another notable change in Raman spectra is the down-shifting occurring in D-bands wavelength, indicative of specific n-type doping according to extensive studies in phononic dispersion studies [44].

Regarding the chemical properties of  $CN_x$ , it has been proved that their reactivity is considerably higher than the correspondent to the undoped CNTs [62]. The strong chemical stability of undoped CNTs arises from the uniform distribution of the electronic density

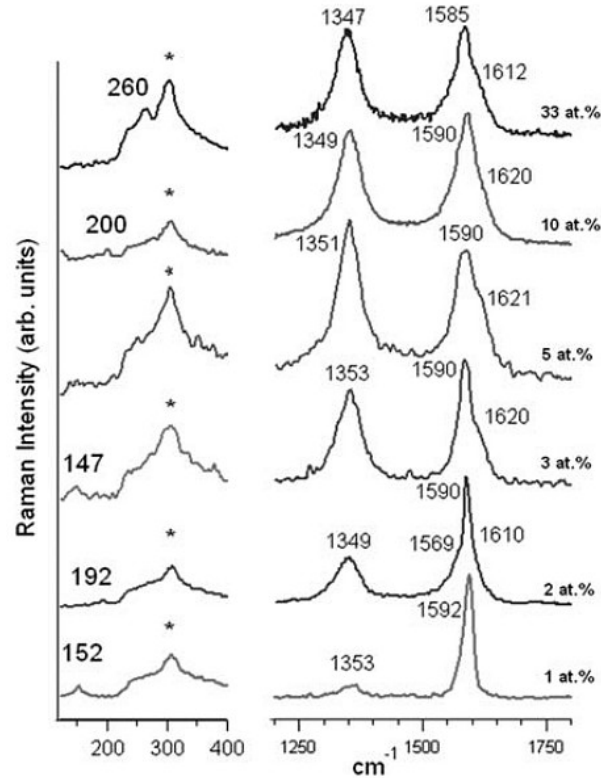


**Figure 1.14.** Systematic changes in micro-Raman spectra of isolated SWNTs synthesized from precursors with varying nitrogen concentration (1-33% label refers to nominal concentrations in the precursor solutions, not to actual doping level in the SWNT). Note the changes occurring at RBM (around  $300\text{ cm}^{-1}$ ) and D-band (around  $1350\text{ cm}^{-1}$ ) intensities with respect to the nitrogen precursor concentration. (Image taken from [61]).

along the structure, without localized charge regions. By contrast, N-doping produces local charge unbalancing, conferring to the surrounding carbon atoms a partial negative charge, making them prone to chemical interactions with surrounding moieties [59]. This increased reactivity can be an advantage in applications where the interaction between  $\text{CN}_x$  and external entity is desired. For instance, it has been demonstrated that the interface of  $\text{CN}_x$  with polymeric matrices can be stronger than with undoped CNTs [63]. Moreover, increased reactivity can allow higher sensibility to analytes in sensing applications [50].

## 1.4 Graphene

Graphene has been called the primordial carbon nanomaterial since it can be seen as the base for fullerenes, carbon nanotubes and other derived nanostructures (see [figure 1.15](#)). Recently, it has attracted an enormous amount of attention after the experimental discovery of monolayer graphene [\[64\]](#), and from that point, a copious number of reports on synthesis methods and applications for graphene and related structures has been published. Similarly to carbon nanotubes, graphene has been explored as a potential new material for a wide range of applications, with most efforts devoted to nanoelectronics [\[65-67\]](#), given the exceptional electronic characteristics of this bidimensional nanostructure. Moreover, the new properties and exciting results that have appeared up to date are promising in several multidisciplinary fields, such as energy generation [\[68\]](#) and storage [\[69\]](#) and nanobiotechnology [\[70-72\]](#).

From the synthesis point of view, the methods for graphene production vary

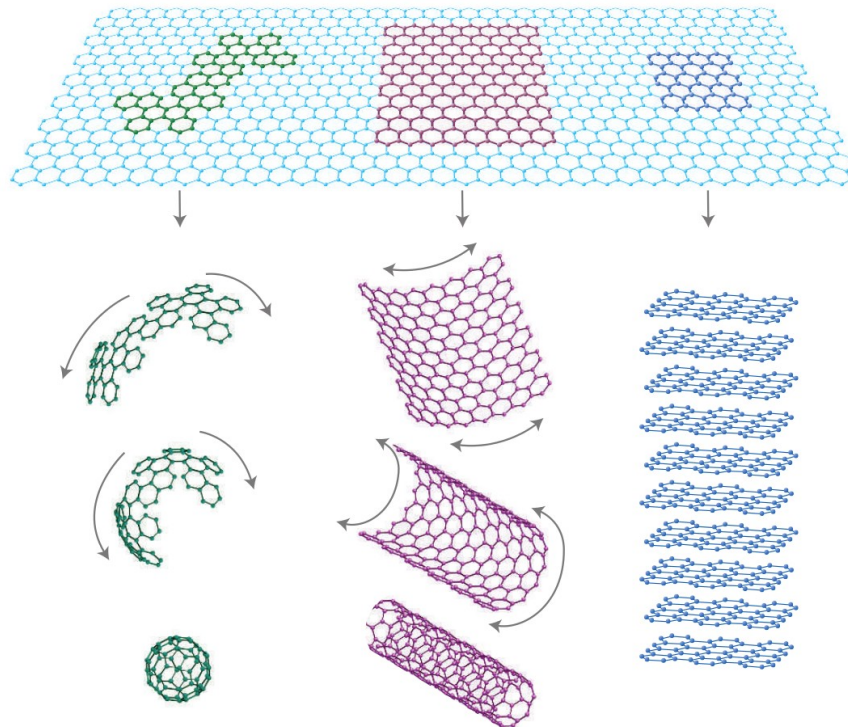


**Figure 1.15.** Graphene as the “mother” material for other carbon nanostructures as fullerenes and CNTs, and for common graphite, which is basically stacked graphene pieces (image taken from [\[64\]](#)).

significantly from CNTs synthesis methods; as can be seen below in section 1.4.1.1. It is important to note that graphene synthesis requires considerably more control than the processes for other nanocarbons [73], the production of monolayer graphene has been particularly difficult to standardize.

Graphene, as other nanocarbons, is susceptible to be doped, which alters its electronic and chemical properties in a similar way. Graphene doping is explained in more detail below in section 1.4.2.

### 1.4.1 Undoped graphene

Graphene is essentially a pure  $sp^2$  carbon hexagonal lattice, conformed by two sublattices of equivalent carbon atoms [74]. From the morphological point of view, it is a 2D material, even though it can be obtained as bi- or multi-layer graphene depending on the number of stacked monolayers. The properties of these “few layer graphenes” are different from that of graphene (a name corresponding only to the monolayer), and change with the number of layers. When the number of layers reaches ten, most of the properties are essentially those of bulk graphite.

Interestingly, most of the graphene's characteristics started to be revealed theoretically decades ago, in the mid 20th century [75, 76], when highlights of the novel and striking electronic properties of the  $sp^2$  carbonaceous lattice were first reported. The actual existence of graphene, however, was in fact predicted as unlikely, from the supposed instability of one-atom layers [64]. Nevertheless, the demonstration of stable graphene samples produced by a Nobel prize winner research group proved this theoretical notion wrong [77], paving the way for the graphene research boom currently observed.

#### 1.4.1.1 Synthesis methods

Graphene's synthesis can be achieved by different approaches, as it occurs for CNTs synthesis; the first reports involve mechanical exfoliation of graphite flakes (using the scotch tape method), and the commonly used CVD process for CNTs has substantial differences when utilized for graphene production [73]. Other initial results were obtained from the separation of graphene layers from graphite by intercalation and exfoliation means (see figure 1.16a), which commonly resulted in other types of 3D compounds [78, 79]. Such

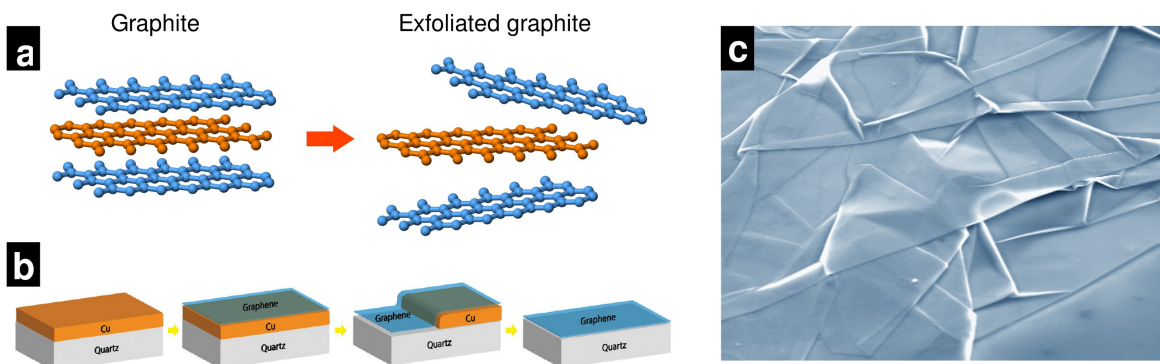


**Figure 1.16.** (a) Graphene from graphite exfoliation model, e.i., the separation of individual graphene layers from graphite using chemical or mechanical means. (b) Schematic model of graphene synthesis by CVD using a copper film (image taken from [87]). (c) Scanning electron microscopy (SEM) image of several graphene sheets (taken from [88]).

graphite intercalation compounds (GIC) had been known since the 19th century and studied extensively since then. Exfoliation of graphite has been in use for extended graphite commercial products (e.g. gaskets). After the discovery of graphene, such methods were adapted as routes for monolayer and few-layer graphenes. The process consists in the intercalation of non-carbon atoms between the graphitic planes, then forcing an abrupt disassembling of the graphite stacking by strong chemical and/or thermal process. The main drawback of these methods is the relative small size and irregular shape of the resulting graphene pieces, since they come from polycrystalline graphite.

With the progress on graphene research, CVD has become considerably popular for graphene sheets synthesis [80]. The process involves the growth of graphene from a metallic flat substrate, normally copper or nickel, where carbon atoms coming from vaporized or gaseous organic precursors (e.g.  $\text{CH}_4$ ) are diffused into and rearranged as an hexagonal lattice (see figure 1.16b) [81, 82]. One of the most important advantages of this method is that the size of the synthesized graphene sheet depends basically on the size of the metallic substrate, being able to produce graphene in a wide range of sizes (see figure 1.16c). In fact, much of the progress made in graphene research has been done using CVD grown graphene, since it makes it feasible to build electronic devices and other applications.

An additional approach for graphene production comes from the opening or “unzipping” of carbon nanotubes walls, which produces in fact graphene nanoribbons [84, 85]. In figure 1.17 are shown transmission electron microscopy (TEM) images of partially opened CNTs,

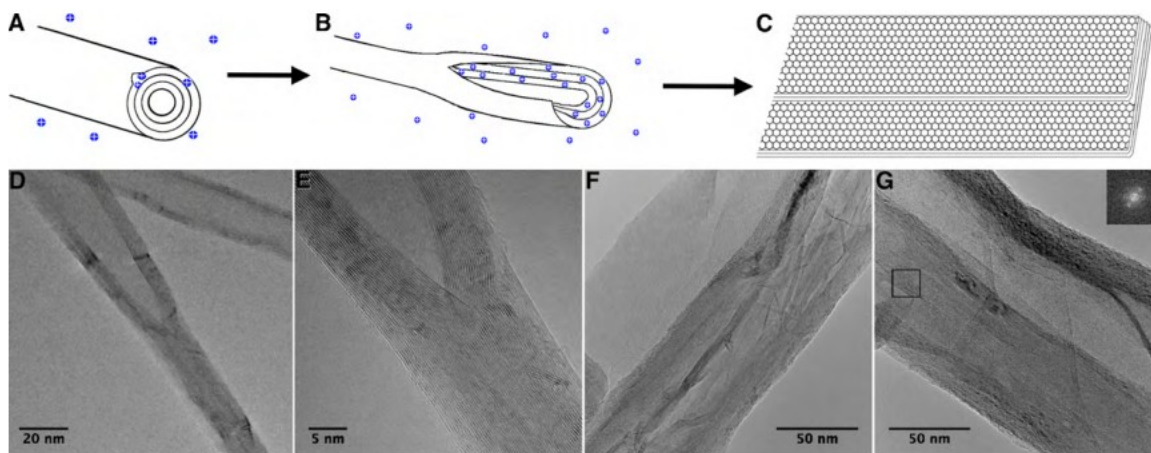


**Figure 1.17.** Graphene nanoribbons (GNRs) production by CNT exfoliation. The process involves lithium intercalation of MWNTs and a strong thermal treatment to “unzip” the CNT walls (image taken from [84]).

where the resulting nanoribbons can be seen. These nanoribbons retain the high aspect-ratio of CNTs, since the unzipping occurs through the main CNT axis. The scheme in [figure 1.17](#) depicts a proposed model for CNTs unzipping, based on the co-intercalation of lithium atoms and ammonia molecules in between CNT walls, and posterior exfoliation through chemical and thermal treatments that forces the abrupt escape of the intercalants from the CNTs interwalls spaces. For more information on methods to obtain GNRs from CNTs, as well as other synthesis methods, see reference [84].

The graphene nanoribbons produced by these means can be considered as 1D nanostructures [85], given the considerably smaller width (below a hundred of nanometers) compared against their length (up to micrometers range).

It is worth to mention interesting findings regarding the synthesis of specific shaped graphene nanoribbons by chemical coupling of aromatic molecules [86]. This kind of processes can produce uniform graphene morphologies, which could be tuned within certain limits by selecting appropriate organic molecules as “bricks”. The main disadvantage for this methods resides in the relatively low yield compared with other synthesis methods, and consequently its high cost. Nevertheless, this approach opens up alternatives for specific graphene's edges design, which are crucial for graphene's electronic properties determination.

## 1.4.1.2 Properties

In essence, all the outstanding characteristics exhibited by CNTs, fullerenes and other related nanostructures are derived from the physical properties of graphene [64]. The nature of the  $sp^2$  carbon bondings in the monoatomic carbon lattice is the root cause for the exceptional mechanical stability of graphene, and also the cause of graphene's particular electronic properties, which come from the electronic density arrangement caused by the  $sp^2$  hybridization of the atomic orbitals. The honeycomb-like lattice of carbon atoms in graphene can be considered as two sublattices of equivalent carbon atoms, with symmetric distribution of their valence and conduction bands for energies close to the Fermi level (see figure 1.18a-b) [41, 74]. The outstanding electronic phenomena occurring at graphene precisely comes from this symmetric band system, which allows a zero-band-gap semiconductor (or zero-band-overlap semimetal) behavior [87]. The absence of a band-gap and the delocalized nature of the band structure for states near the Fermi level (see figure 1.18c-d) also allow ballistic electron transport (i.e., electrons traveling along a conductive material without scattering) phenomena, which is potentially useful for high-frequency and low-dissipation nanoelectronic devices [88, 89].

Another direct consequence of graphene electronic characteristics is that most of the

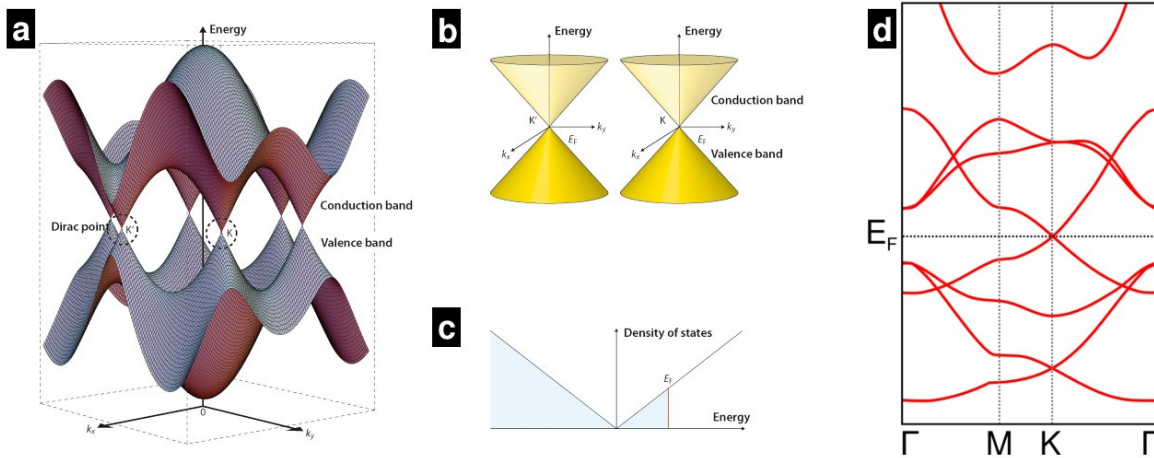


**Figure 1.18.** Electronic properties of graphene. **(a)** 3D representation of graphene electronic structure within the Brillouin zone, depicting the valence and conduction bands, and the zero band-gap regions at the K and K' points. **(b)** Representation of valence and conduction bands in graphene in  $k$ -space and **(c)** the density of states (DOS) typical plot. **(d)** Graphene electronic band structure between its high symmetry points in  $k$ -space. (Figures a-c taken from [92]).

electronic transitions fall into an energetic region where optical phenomena occurs [90], and those transitions can be utilized not only for graphene samples characterization, but also for applications where the electronic dispersion within the graphene lattice is slightly altered, such as doping caused by foreign atoms (see next section) or by external molecules or clusters, a situation that is exploited in graphene-based sensors research, for example [91, 92]. The optical sensitivity of graphene to slight changes in its electronic dispersion is evident for instance in Raman spectroscopy. As it can be seen in figure 1.19, the Raman spectra for monolayer graphene has a clear peak intensity ratio for the G- and 2D-modes ( $I_{2D}/I_G$ ), which is always close to 2, whereas for multi-layered graphene, the ratio decreases drastically, even though graphene layers interact through a relatively weak  $\pi$ - $\pi$  coupling. This is a substantial evidence of graphene's high sensitivity to external molecules, which is fueling extensive research in sensors development [91].

It is important to consider that graphene's electronic properties are normally calculated from a perfect and infinite sheet perspective, without considering the arrangement of the carbon atoms at the lattice limits or *edges*. When a graphene piece is limited in width, the nanostructure is considered a 1D-graphene nanoribbon, and the morphology of the edges are a determinant factor for the electronic behavior of the whole structure [94, 95]. It can be compared to the chirality-dependent metallicity of CNTs, as nanoribbons edges can be classified in armchair or zigzag configurations. Interestingly, the metallicity of graphene nanoribbons appears inverted with respect to the CNTs classification, since nanoribbons

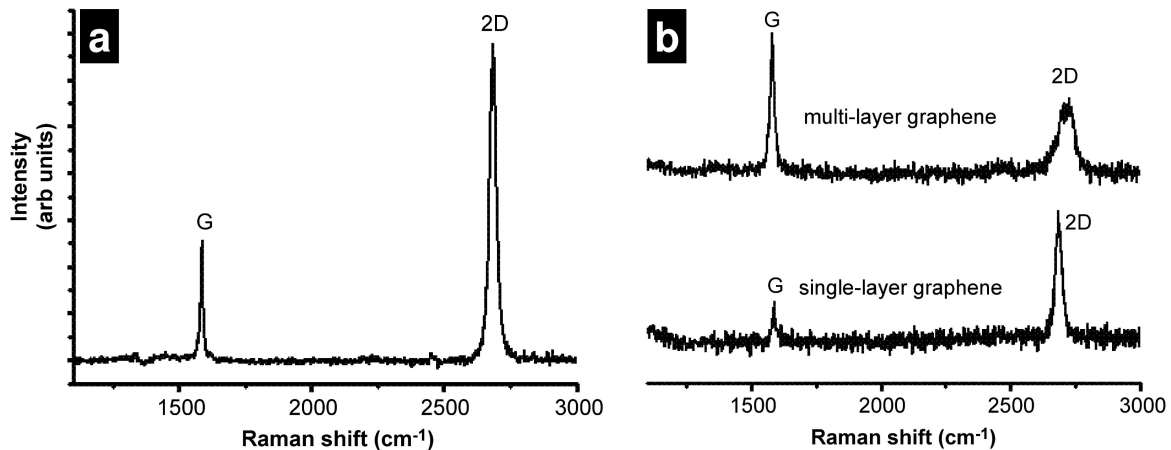


**Figure 1.19.** Raman spectra of graphene samples. **(a)** Characteristic spectrum of monolayer graphene. **(b)** Contrast between G- and 2D-Raman modes intensities in function of number of graphene layers (Image taken from [98]).



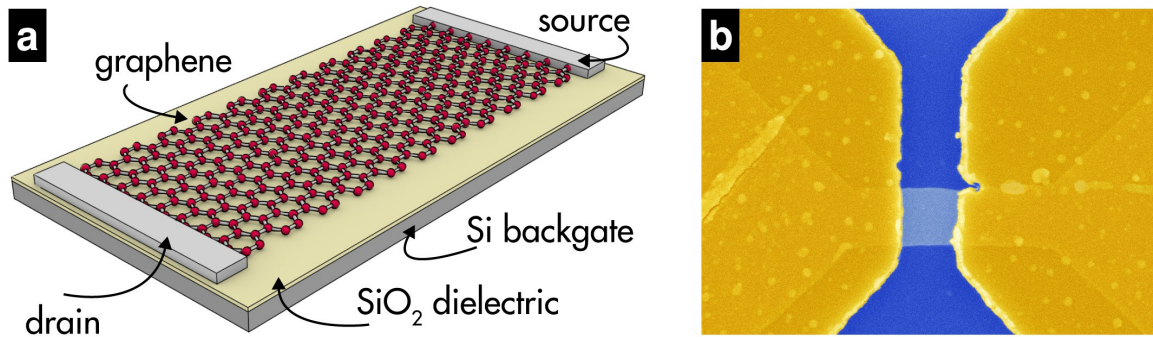


**Figure 1.20.** (a) Model of a graphene-based FET, indicating all the typical components, including a graphene nanoribbon as a FET channel. (b) SEM image (false-colored) of a graphene-FET (metallic electrodes in yellow, Si/SiO<sub>2</sub> substrate in blue and graphene channel in light blue). (Images taken from [102] and [88] respectively).

with armchair edges behave as semiconductors or metals as a nanoribbon width function, whereas the ones with zigzag edges exhibit always a metallic nature [96]. In the practice, most of the graphene devices reported so far for field-effect devices consist of flakes large enough to neglect the edges effects in some extent. Nevertheless, as nanofabrication techniques become more precise, and the ability to produce graphene with features designed within few nanometers range, the quantum effects of graphene edges will significantly affect the electronic characteristics of graphene-based nanodevices. This could actually be an advantage, since semiconducting GNRs have an intrinsic bandgap, while in most graphene devices a bandgap has to be induced by an electric field or by chemical modifications. For instance, in figure 1.20a is shown a model for a graphene-based field effect transistor (graphene-FET), where the typical components as main and gate electrodes, dielectric layer and graphene as channel are depicted, and figure 1.20b shows a false-colored SEM image of an actual graphene-FET experimental device. As it can be observed, the goal for devices miniaturization involves uniform and small pieces of graphene, where the edges morphology determination is crucial.

#### 1.4.2 Nitrogen doped graphene

Doping of graphene is an appealing way to tailor its electronic properties, and it can be achieved by several ways. Graphene doping can be achieved by using organic precursors containing the dopant element (as occurs for CN<sub>x</sub> for example) in the CVD growth process

[98], and by physico-chemical methods such as electrothermal reactions or graphite exfoliation in presence of ammonia (for N-doping) [99], for instance. The doping of graphene has been extensively explored as an alternative for developing new nanoelectronics and derived applications, like ultrasensitive gas sensors [100] or high-specificity and high-sensitivity biosensors [101]. Electric fields have the capability of tuning the charge carrier concentration within the graphene electronic structure, being either electrons or holes, at the conduction/valence band regions which are close to the Fermi level. Consequently, the physical doping of graphene can be done by the application of electric fields over graphene-based devices (e.g. FETs), which avoids the disruption of the lattice structure [77, 102]. On the other hand, the chemical doping of graphene involves the non-covalent adsorption of molecules or clusters of metallic atoms [103, 104], or more frequently, the introduction of non-carbon atoms such as nitrogen [98], boron [105], phosphorous, sulfur [106] and silicon [107] within the  $sp^2$  honeycomb lattice. The introduction of heteroatoms within the graphene structure implies the substitution of carbons, thus producing permanent charge imbalance effects. Additionally, the replacement of carbon for dopant atoms confers special chemical properties to graphene and other carbon nanostructures, which are beneficial in most cases for the development of sensing applications.

Currently, N-doping of carbon nanostructures, and specially graphene, is being intensively explored, given its relative easy synthesis and extensive theoretical analysis reported. For these reasons and other that will be mentioned later, nitrogen chemical doping will be the main focus of this work.

#### 1.4.2.1 Synthesis methods

For doped graphene production, one of two alternatives can be chosen; the incorporation of dopant species at the synthesis phase by the addition of adequate precursors to the synthesis feedstock [98, 105], or by the introduction of heteroatoms (e.g. boron, nitrogen, sulfur or silicon) within graphene by chemical [108], thermal or electric treatments [99].

Focusing on N-doping of graphene, there are works reporting the use of CVD for its synthesis, by the addition of nitrogen-containing substances such as  $NH_3$  to the conventional gaseous precursors [109], with final N-doping concentrations ranging from around 1.2% to 9% of atomic weight, depending on the  $CH_4:NH_3$  ratio, for instance [98].

The nature of the synthesis process is essentially the same that the one occurring for undoped graphene, with carbon atoms diffusing on the metallic substrate and rearranging themselves as  $sp^2$  hexagonal carbon at the surface, having in this case the presence of nitrogen atoms that occasionally sit within the graphene lattice.

Other synthesis methods for N-doped graphene rely on combination of chemical and physical treatments; for instance, Wang et al. described the incorporation of nitrogen atoms into pristine graphene nanoribbons by reactions with gaseous ammonia while applying an electric current (Joule heating) through the nanostructure [99], leading to a n-type semiconducting behavior. Also, boron- and nitrogen-doped graphene by the arc-discharge synthesis method has been reported [105], by the addition of diborane ( $B_2H_6$ ) and pyridine ( $C_5H_5N$ ) or ammonia ( $NH_3$ ) as boron and nitrogen precursors respectively.

#### 1.4.2.2 Properties

The N-doping on graphene can occur in different ways, in terms of how the dopant atoms are arranged within the carbon  $sp^2$  lattice. The varieties of nitrogen-doping commonly produced are shown in figure 1.21a; the substitutional doping implies a direct replacement of a carbon for a dopant (nitrogen in this case) atom, without disrupting the overall hexagonal lattice morphology. Experimentally, the preferred type of N-doping observed is the substitutional case (see XPS spectrum in figure 1.22d), nevertheless, pyridine- and pyrrolic-like doping are also observed [98, 110].

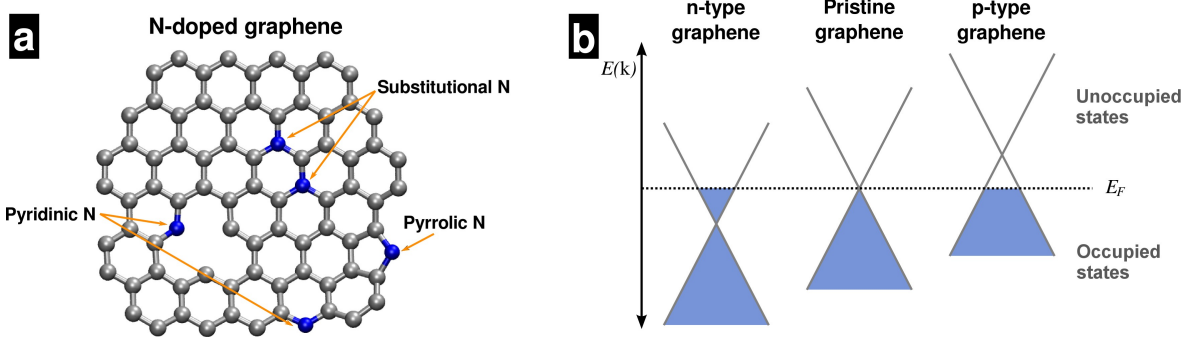


**Figure 1.21.** (a) Models of N-doping in graphene: substitutional, pyridinic and pyrrolic. (b) Diagram of occupied (electrons) and unoccupied (holes) states in graphene, near the Fermi level  $E_F$ . The diagram depicts the  $E_F$  shifting from pristine to negative (n-) and positive (p-) type semiconductor as a consequence of doping.

The main effect of the nitrogen and other types of graphene chemical doping is consequence of the imbalance of the charge carriers on graphene's valence and conduction bands [111]. Nitrogen, which has one more electron than carbon in its valence band, induces naturally an excess of negative charges on the valence band, up-shifting the Fermi level towards the conduction band and thus producing a n-type material (see figure 1.21b).

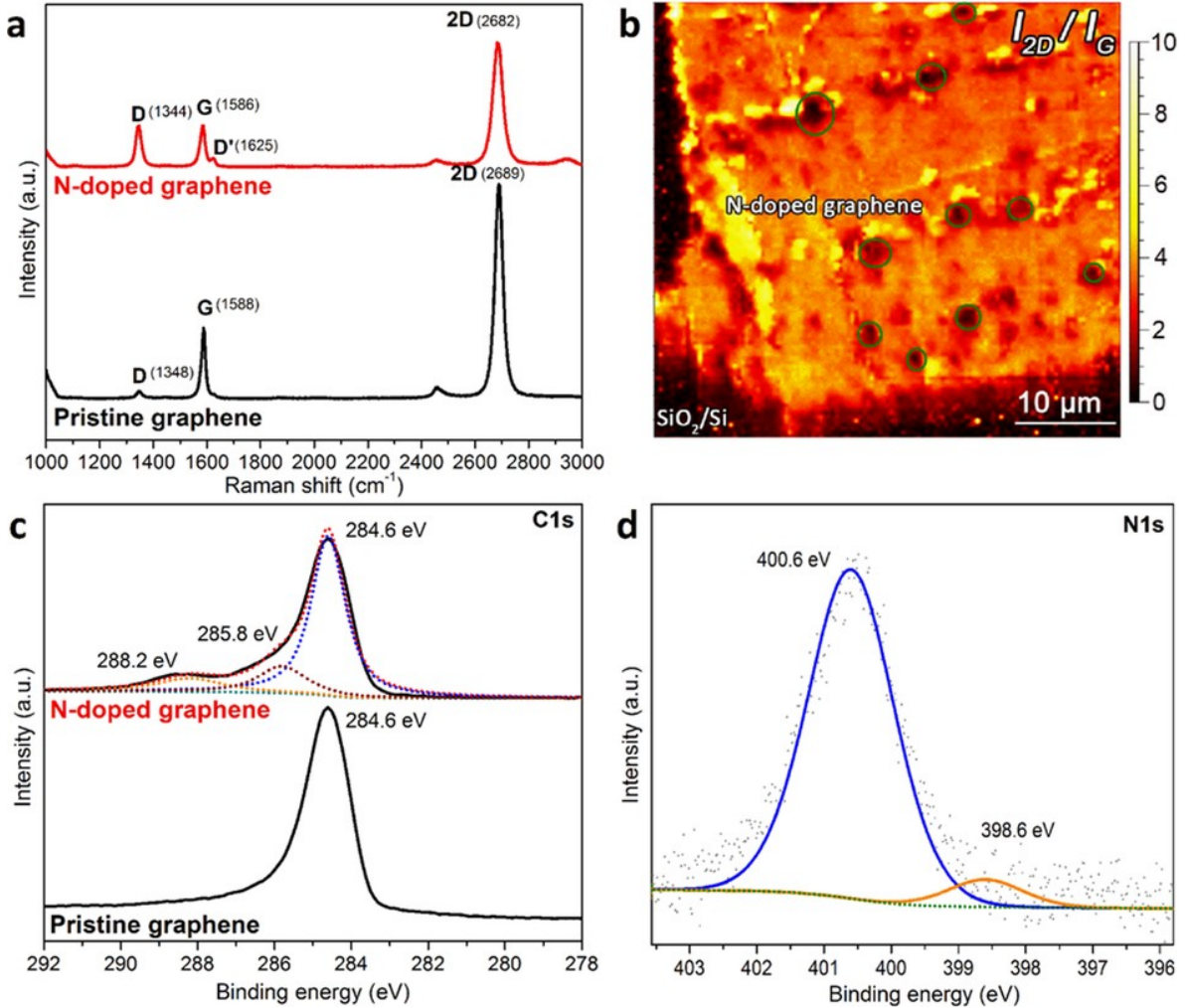


**Figure 1.22.** (a) Raman spectra for monolayer pristine (bottom plot) and N-doped (top plot) graphene on SiO<sub>2</sub>/Si substrate. (b) Raman 2D-band to G-band intensity ratio ( $I_{2D}/I_G$ ) mapping over N-doped graphene sample. (c) X-ray photoelectron spectroscopy (XPS) spectra for C1s in pristine (bottom plot) and N-doped (top plot) graphene, where the distribution of carbon hybridizations is observed. (d) XPS spectra for N1s in N-doped graphene, indicating strong components from substitutional N-doping (400.6 eV) contrasted to pyridine-like N-doping (398.6 eV). Image taken from [110].

These changes in the electronic nature of graphene by N-doping have clear effects in their optical absorption, which can be used as “fingerprints” in spectroscopic characterization, specially Raman spectroscopy [112, 113]. Figure 1.22a shows Raman spectra for undoped (pristine) and N-doped graphene. One of the most notable features is the increase in the D-band intensity, which is produced by the non  $sp^2$  carbon resonant scattering introduced by N-doping sites. Moreover, changes in electronic structure towards n- or p-type semiconductor are reflected in by down- and up-shiftings respectively, on the G-band and 2D-band frequencies, which are observed as well for the N-doped graphene spectrum.

The nitrogen incorporation into graphene can be also detected and characterized by X-ray photoelectron spectroscopy (XPS), which additionally provides information about the type of N-doping present at the samples. Figure 1.22c-d shows reported XPS spectra for carbon (C1s) and nitrogen (N1s) binding energies scans, in pristine and N-doped graphene [110].

The chemical properties of graphene also change with the extra electrons that N-doping introduces to the graphene structure, which are kept in quasi-bound states, which localizes charges around the doping sites [114]. This increased charge density points present higher chemical reactivity than the  $sp^2$  carbon lattice, thus altering interactions of graphene with external molecules, clusters or electro-magnetic fields [115, 116]. In fact, these enhanced interactions with external systems are being explored for applications such as sensing, since the graphene conductivity becomes highly sensitive to changes through N-doping sites [110]. Energy related applications are also under intensive studies since N-doped graphene exhibits interesting hydrogen storage properties, for instance [117]. Moreover, it shows promising characteristics as electro-catalytic material for fuel cells and other type of energy harvesting systems [118].

## Conclusions

Carbon nanotechnology has seen many important advances in the last two decades which make it one of the most important sub-fields in nanotechnology research. The outstanding physical properties of carbon give rise to plenty of possibilities on carbon based structures. The  $sp^2$  hexagonal carbon network of graphene revealed surprising electronic, mechanical and chemical properties, which are inherited in variable extents by all the graphene-related

materials, i.e., mono- and multi-layer graphene, fullerenes, nanotubes, nanocones, nanoribbons, etc.

The advances on carbon nanomaterials research has been extensive, specially in the synthesis of new types on structures and in the theoretical prediction of their electronic and other physical properties. Nevertheless, the real world applications development based on carbon nanomaterials is still limited with respect to having precise, repeatable control of their size and other properties. The doping of carbon structures with elements such as nitrogen, boron, phosphorous, silicon and others, is a plausible alternative to overcome some of the challenges of carbon nanotechnology. For example, N-doping can contribute to the applicability of graphene, carbon nanotubes and nanoribbons in new electronic and sensing developments. Moreover, it confers characteristics that make some nanomaterials (carbon nanotubes) more biocompatible, thus enabling their use for biomedical applications research. Taking this into account, we can safely say that many novel technologies based on carbon nanotechnology are just starting to reveal themselves.

## Bibliography

- [1] H. W. Kroto, J. R. Heath, S. C. O'Brien, R. F. Curl, and R. E. Smalley, "C<sub>60</sub>: Buckminsterfullerene," *Nature*, vol. 318, no. 6042, pp. 162–163, 1985.
- [2] W. Krätschmer, L. D. Lamb, K. Fostiropoulos, and D. R. Huffman, "Solid C<sub>60</sub>: a new form of carbon," *Nature*, vol. 347, no. 6291, pp. 354–358, 1990.
- [3] S. Iijima, "Helical microtubules of graphitic carbon," *Nature*, vol. 354, no. 6348, pp. 56–58, 1991.
- [4] L. Fulcheri, Y. Schwob, F. Fabry, G. Flamant, L. F. P. Chibante, and D. Laplaze, "Fullerene production in a 3-phase AC plasma process," *Carbon*, vol. 38, no. 6, pp. 797–803, 2000.
- [5] R. Yu, M. Zhan, D. Cheng, S. Yang, Z. Liu, and L. Zheng, "Simultaneous Synthesis of Carbon Nanotubes and Nitrogen-Doped Fullerenes in Nitrogen Atmosphere," *Journal of Physical Chemistry*, vol. 99, no. 7, pp. 1818–1819, 1995.
- [6] B. Xu, J. Guo, X. Wang, X. Liu, and H. Ichinose, "Synthesis of carbon nanocapsules containing Fe, Ni or Co by arc-discharge in aqueous solution," *Carbon*, vol. 44, no. 13, pp. 2631–2634, 2006.

- [7] S. Margadonna and K. Prassides, "Recent Advances in Fullerene Superconductivity," *Journal of Solid State Chemistry*, vol. 168, no. 2, pp. 639–652, 2002.
- [8] K. E. Geckeler and S. Samal, "Syntheses and properties of macromolecular fullerenes, a review," *Polymer International*, vol. 48, no. 9, pp. 743–757, 1999.
- [9] A. Montellano López, A. Mateo-Alonso, and M. Prato, "Materials chemistry of fullerene C<sub>60</sub> derivatives," *Journal of Materials Chemistry*, vol. 21, no. 5, p. 1305, 2011.
- [10] X. Wang, Q. Li, J. Xie, Z. Jin, J. Wang, Y. Li, K. Jiang, and S. Fan, "Fabrication of ultralong and electrically uniform single-walled carbon nanotubes on clean substrates.," *Nano Letters*, vol. 9, no. 9, pp. 3137–41, 2009.
- [11] A. Oberlin, M. Endo, and T. Koyama, "Filamentous growth of carbon through benzene decomposition," *Journal of Crystal Growth*, vol. 32, no. 3, pp. 335–349, 1976.
- [12] M. Dresselhaus, G. Dresselhaus, and R. Saito, "Carbon fibers based on C<sub>60</sub> and their symmetry," *Physical Review B*, vol. 45, no. 11, pp. 6234–6242, 1992.
- [13] D. Mann, "Synthesis of carbon nanotubes" in *Carbon nanotubes: Properties and Applications*, M. J. O'Connell, Ed. Taylor & Francis, 2006, pp. 19–49.
- [14] T. W. Ebbesen and P. M. Ajayan, "Large-scale synthesis of carbon nanotubes," *Nature*, vol. 358, no. 6383, pp. 220–222, 1992.
- [15] S. Iijima and T. Ichihashi, "Single-shell carbon nanotubes of 1-nm diameter," *Nature*, vol. 363, no. 6430, pp. 603–605, 1993.
- [16] D. S. Bethune, C. H. Klang, M. S. de Vries, G. Gorman, R. Savoy, J. Vazquez, and R. Beyers, "Cobalt-catalysed growth of carbon nanotubes with single-atomic-layer walls," *Nature*, vol. 363, no. 6430, pp. 605–607, 1993.
- [17] A. Thess, R. Lee, P. Nikolaev, H. Dai, P. Petit, J. Robert, C. Xu, Y. H. Lee, S. G. Kim, A. G. Rinzler, D. T. Colbert, G. E. Scuseria, D. Tomanek, J. E. Fischer, and R. E. Smalley, "Crystalline Ropes of Metallic Carbon Nanotubes," *Science*, vol. 273, no. 5274, pp. 483–487, 1996.
- [18] H. Dai, A. G. Rinzler, P. Nikolaev, A. Thess, D. T. Colbert, and R. E. Smalley, "Single-wall nanotubes produced by metal-catalyzed disproportionation of carbon monoxide," *Chemical Physics Letters*, vol. 260, no. 3–4, pp. 471–475, 1996.
- [19] J. Kong, H. T. Soh, A. M. Cassell, C. F. Quate, and H. Dai, "Synthesis of individual single-walled carbon nanotubes on patterned silicon wafers," *Nature*, vol. 395, no.

- 6705, pp. 878–881, 1998.
- [20] J. Kong, A. M. Cassell, and H. Dai, “Chemical vapor deposition of methane for single-walled carbon nanotubes,” *Chemical Physics Letters*, vol. 292, no. 4–6, pp. 567–574, 1998.
- [21] A. M. Cassell, J. A. Raymakers, J. Kong, and H. Dai, “Large Scale CVD Synthesis of Single-Walled Carbon Nanotubes,” *Journal of Physical Chemistry B*, vol. 103, no. 31, pp. 6484–6492, 1999.
- [22] P. Nikolaev, M. J. Bronikowski, R. K. Bradley, F. Rohmund, D. T. Colbert, K. . Smith, and R. E. Smalley, “Gas-phase catalytic growth of single-walled carbon nanotubes from carbon monoxide,” *Chemical Physics Letters*, vol. 313, no. 1–2, pp. 91–97, 1999.
- [23] R. L. Vander Wal, T. M. Tichich, and V. E. Curtis, “Diffusion flame synthesis of single-walled carbon nanotubes,” *Chemical Physics Letters*, vol. 323, no. 3–4, pp. 217–223, 2000.
- [24] B. Kitiyanan, W. E. Alvarez, J. H. Harwell, and D. E. Resasco, “Controlled production of single-wall carbon nanotubes by catalytic decomposition of CO on bimetallic Co–Mo catalysts,” *Chemical Physics Letters*, vol. 317, no. 3–5, pp. 497–503, 2000.
- [25] S. M. Bachilo, L. Balzano, J. E. Herrera, F. Pompeo, D. E. Resasco, and R. B. Weisman, “Narrow (n,m)-distribution of single-walled carbon nanotubes grown using a solid supported catalyst.,” *Journal of the American Chemical Society*, vol. 125, no. 37, pp. 11186–7, 2003.
- [26] Y. Li, W. Kim, Y. Zhang, M. Rolandi, D. Wang, and H. Dai, “Growth of Single-Walled Carbon Nanotubes from Discrete Catalytic Nanoparticles of Various Sizes,” *Journal of Physical Chemistry B*, vol. 105, no. 46, pp. 11424–11431, 2001.
- [27] Y. Zhang, A. Chang, J. Cao, Q. Wang, W. Kim, Y. Li, N. Morris, E. Yenilmez, J. Kong, and H. Dai, “Electric-field-directed growth of aligned single-walled carbon nanotubes,” *Applied Physics Letters*, vol. 79, no. 19, p. 3155, 2001.
- [28] A. Ural, Y. Li, and H. Dai, “Electric-field-aligned growth of single-walled carbon nanotubes on surfaces,” *Applied Physics Letters*, vol. 81, no. 18, p. 3464, 2002.
- [29] S. Maruyama, R. Kojima, Y. Miyauchi, S. Chiashi, and M. Kohno, “Low-temperature synthesis of high-purity single-walled carbon nanotubes from alcohol,” *Chemical Physics Letters*, vol. 360, no. 3–4, pp. 229–234, 2002.
- [30] W. Kim, H. C. Choi, M. Shim, Y. Li, D. Wang, and H. Dai, “Synthesis of Ultralong and



- High Percentage of Semiconducting Single-walled Carbon Nanotubes,” *Nano Letters*, vol. 2, no. 7, pp. 703–708, 2002.
- [31] S. Huang, X. Cai, and J. Liu, “Growth of millimeter-long and horizontally aligned single-walled carbon nanotubes on flat substrates.,” *Journal of the American Chemical Society*, vol. 125, no. 19, pp. 5636–7, 2003.
- [32] T. Kato, G.-H. Jeong, T. Hirata, R. Hatakeyama, K. Tohji, and K. Motomiya, “Single-walled carbon nanotubes produced by plasma-enhanced chemical vapor deposition,” *Chemical Physics Letters*, vol. 381, no. 3–4, pp. 422–426, 2003.
- [33] Y. Li, D. Mann, M. Rolandi, W. Kim, A. Ural, S. Hung, A. Javey, J. Cao, D. Wang, E. Yenilmez, Q. Wang, J. F. Gibbons, Y. Nishi, and H. Dai, “Preferential Growth of Semiconducting Single-Walled Carbon Nanotubes by a Plasma Enhanced CVD Method,” *Nano Letters*, vol. 4, no. 2, pp. 317–321, 2004.
- [34] Y. Murakami, “Growth of vertically aligned single-walled carbon nanotube films on quartz substrates and their optical anisotropy,” *Chemical Physics Letters*, vol. 385, no. 3–4, pp. 298–303, 2004.
- [35] K. Hata, D. N. Futaba, K. Mizuno, T. Namai, M. Yumura, and S. Iijima, “Water-assisted highly efficient synthesis of impurity-free single-walled carbon nanotubes.,” *Science*, vol. 306, no. 5700, pp. 1362–4, 2004.
- [36] J. C. Carrero-Sanchez, A. L. Elías, R. Mancilla, G. Arrellín, H. Terrones, J. P. Laclette, and M. Terrones, “Biocompatibility and toxicological studies of carbon nanotubes doped with nitrogen.,” *Nano Letters*, vol. 6, no. 8, pp. 1609–16, 2006.
- [37] E. Muñoz-Sandoval, V. Agarwal, J. Escorcía-García, D. Ramírez-González, M. M. Martínez-Mondragón, E. Cruz-Silva, D. Meneses-Rodríguez, J. A. Rodríguez-Manzo, H. Terrones, and M. Terrones, “Architectures from aligned nanotubes using controlled micropatterning of silicon substrates and electrochemical methods.,” *Small*, vol. 3, no. 7, pp. 1157–63, 2007.
- [38] Y. Saito, M. Okuda, M. Tomita, and T. Hayashi, “Extrusion of single-wall carbon nanotubes via formation of small particles condensed near an arc evaporation source,” *Chemical Physics Letters*, vol. 236, no. 4–5, pp. 419–426, 1995.
- [39] J.-P. Salvetat, J.-M. Bonard, N. H. Thomson, A. J. Kulik, L. Forró, W. Benoit, and L. Zuppiroli, “Mechanical properties of carbon nanotubes,” *Applied Physics A: Materials Science & Processing*, vol. 69, no. 3, pp. 255–260, 1999.
- [40] R. Jishi, M. Dresselhaus, and G. Dresselhaus, “Symmetry properties of chiral carbon nanotubes,” *Physical Review B*, vol. 47, no. 24, pp. 16671–16674, 1993.

- [41] M. S. Dresselhaus, G. Dresselhaus, and R. Saito, "Physics of carbon nanotubes," *Carbon*, vol. 33, no. 7, pp. 883–891, 1995.
- [42] H. Kataura, Y. Kumazawa, Y. Maniwa, I. Umezu, S. Suzuki, Y. Ohtsuka, and Y. Achiba, "Optical properties of single-wall carbon nanotubes," *Synthetic Metals*, vol. 103, no. 1–3, pp. 2555–2558, 1999.
- [43] C. Thomsen and S. Reich, "Raman Scattering in Carbon Nanotubes," in *Light Scattering in Solid IX*, R. Cardona M;Merlin, Ed. Springer-Verlag Berlin Heidelberg, 2007, pp. 115–232.
- [44] M. Dresselhaus, G. Dresselhaus, R. Saito, and A. Jorio, "Raman spectroscopy of carbon nanotubes," *Physics Reports*, vol. 409, no. 2, pp. 47–99, 2005.
- [45] W. Hoenlein, F. Kreupl, G. S. Duesberg, A. P. Graham, M. Liebau, R. Seidel, and E. Unger, "Carbon nanotubes for microelectronics: status and future prospects," *Materials Science and Engineering: C*, vol. 23, no. 6–8, pp. 663–669, 2003.
- [46] J. Guo, S. Datta, M. Lundstrom, M. Brink, P. McEuen, A. Javey, H. Dai, H. Kim and P. McIntyre, "Assessment of silicon MOS and carbon nanotube FET performance limits using a general theory of ballistic transistors," in *IEDM'02 Digest International, International Electron Devices Meeting*, no. 12, pp. 711–714, 2002.
- [47] H. Dai, A. Javey, E. Pop, D. Mann, W. Kim, and Y. Lu, "Electrical transport properties and field effect transistors of carbon nanotubes," *Nano*, vol. 01, no. 01, pp. 1–13, 2006.
- [48] D. Tasis, N. Tagmatarchis, A. Bianco, and M. Prato, "Chemistry of Carbon Nanotubes," *Chemical Reviews*, vol. 106, no. 3, pp. 1105–1136, 2006.
- [49] P. C. P. Watts, W. K. Hsu, G. Z. Chen, D. J. Fray, H. W. Kroto, and D. R. M. Walton, "A low resistance boron-doped carbon nanotube–polystyrene composite," *Journal of Materials Chemistry*, vol. 11, no. 10, pp. 2482–2488, 2001.
- [50] F. Villalpando-Páez, A. H. Romero, E. Muñoz-Sandoval, L. M. Martinez, H. Terrones, and M. Terrones, "Fabrication of vapor and gas sensors using films of aligned CN<sub>x</sub> nanotubes," *Chemical Physics Letters*, vol. 386, no. 1–3, pp. 137–143, 2004.
- [51] V. Saini, Z. Li, S. Bourdo, V. P. Kunets, S. Trigwell, A. Couraud, J. Rioux, C. Boyer, V. Nteziyaremye, E. Dervishi, A. R. Biris, G. J. Salamo, T. Viswanathan, and A. S. Biris, "Photovoltaic devices based on high density boron-doped single-walled carbon nanotube/n-Si heterojunctions," *Journal of Applied Physics*, vol. 109, no. 1, p. 014321, 2011.
- [52] S. Y. Deng, G. Q. Jian, J. P. Lei, Z. Hu, and H. X. Ju, "A glucose biosensor based on

- direct electrochemistry of glucose oxidase immobilized on nitrogen-doped carbon nanotubes,” *Biosensors & Bioelectronics*, vol. 25, no. 2, pp. 373–377, 2009.
- [53] M. Terrones, A. Filho, and A. Rao, “Doped Carbon Nanotubes: Synthesis, Characterization and Applications,” vol. 111, Springer Berlin / Heidelberg, 2008, pp. 531–566.
- [54] M. Terrones, W. K. Hsu, S. Ramos, R. Castillo, and H. Terrenes, “The Role of Boron Nitride in Graphite Plasma Arcs,” *Fullerene Science and Technology*, vol. 6, no. 5, pp. 787–800, 1998.
- [55] M. Glerup, J. Steinmetz, D. Samaille, O. Stéphan, S. Enouz, A. Loiseau, S. Roth, and P. Bernier, “Synthesis of N-doped SWNT using the arc-discharge procedure,” *Chemical Physics Letters*, vol. 387, no. 1–3, pp. 193–197, 2004.
- [56] D. Golberg, Y. Bando, L. Bourgeois, K. Kurashima, and T. Sato, “Large-scale synthesis and HRTEM analysis of single-walled B- and N-doped carbon nanotube bundles,” *Carbon*, vol. 38, no. 14, pp. 2017–2027, 2000.
- [57] E. Cruz-Silva, D. A. Cullen, L. Gu, J. M. Romo-Herrera, E. Muñoz-Sandoval, F. López-Urías, B. G. Sumpter, V. Meunier, J.-C. Charlier, D. J. Smith, H. Terrones, and M. Terrones, “Heterodoped nanotubes: theory, synthesis, and characterization of phosphorus-nitrogen doped multiwalled carbon nanotubes,” *ACS Nano*, vol. 2, no. 3, pp. 441–8, 2008.
- [58] M. Terrones, P. M. Ajayan, F. Banhart, X. Blase, D. L. Carroll, J. C. Charlier, R. Czerw, B. Foley, N. Grobert, R. Kamalakaran, P. Kohler-Redlich, M. Rühle, T. Seeger, and H. Terrones, “N-doping and coalescence of carbon nanotubes: synthesis and electronic properties,” *Applied Physics A: Materials Science & Processing*, vol. 74, no. 3, pp. 355–361, 2002.
- [59] A. Nevidomskyy, G. Csányi, and M. Payne, “Chemically Active Substitutional Nitrogen Impurity in Carbon Nanotubes,” *Physical Review Letters*, vol. 91, no. 10, 2003.
- [60] R. Czerw, M. Terrones, J.-C. Charlier, X. Blase, B. Foley, R. Kamalakaran, N. Grobert, H. Terrones, D. Tekleab, P. M. Ajayan, W. Blau, M. Rühle, and D. L. Carroll, “Identification of Electron Donor States in N-Doped Carbon Nanotubes,” *Nano Letters*, vol. 1, no. 9, pp. 457–460, 2001.
- [61] G. Keskar, R. Rao, J. Luo, J. Hudson, J. Chen, and A. M. Rao, “Growth, nitrogen doping and characterization of isolated single-wall carbon nanotubes using liquid precursors,” *Chemical Physics Letters*, vol. 412, no. 4–6, pp. 269–273, 2005.
- [62] S. Maldonado, S. Morin, and K. J. Stevenson, “Structure, composition, and chemical

- reactivity of carbon nanotubes by selective nitrogen doping,” *Carbon*, vol. 44, no. 8, pp. 1429–1437, 2006.
- [63] B. Fragneaud, K. Masenelli-Varlot, A. Gonzalez-Montiel, M. Terrones, and J.-Y. Cavaillé, “Efficient coating of N-doped carbon nanotubes with polystyrene using atomic transfer radical polymerization,” *Chemical Physics Letters*, vol. 419, no. 4–6, pp. 567–573, 2006.
- [64] A. K. Geim and K. S. Novoselov, “The rise of graphene,” *Nature Materials*, vol. 6, pp. 183–191, 2007.
- [65] F. Schwierz, “Graphene transistors,” *Nature Nanotechnology*, vol. 5, no. 7, pp. 487–496, 2010.
- [66] E. W. Hill, A. Vijayaraghavan, and K. Novoselov, “Graphene Sensors,” *IEEE Sensors Journal*, vol. 11, no. 12, pp. 3161–3170, 2011.
- [67] Y. Zhang, T.-T. Tang, C. Girit, Z. Hao, M. C. Martin, A. Zettl, M. F. Crommie, Y. R. Shen, and F. Wang, “Direct observation of a widely tunable bandgap in bilayer graphene,” *Nature*, vol. 459, no. 7248, pp. 820–3, 2009.
- [68] C. X. Guo, G. H. Guai, and C. M. Li, “Graphene Based Materials: Enhancing Solar Energy Harvesting,” *Advanced Energy Materials*, vol. 1, no. 3, pp. 448–452, 2011.
- [69] M. D. Stoller, S. Park, Y. Zhu, J. An, and R. S. Ruoff, “Graphene-based ultracapacitors,” *Nano Letters*, vol. 8, no. 10, pp. 3498–502, 2008.
- [70] N. Mohanty and V. Berry, “Graphene-Based Single-Bacterium Resolution Biodevice and DNA Transistor: Interfacing Graphene Derivatives with Nanoscale and Microscale Biocomponents,” *Nano Letters*, vol. 8, no. 12, pp. 4469–4476, 2008.
- [71] S. Y. Park, J. Park, S. H. Sim, M. G. Sung, K. S. Kim, B. H. Hong, and S. Hong, “Enhanced Differentiation of Human Neural Stem Cells into Neurons on Graphene,” *Advanced Materials*, vol. 23, no. 36, pp. H263–H267, 2011.
- [72] Y. Wang, Z. Li, J. Wang, J. Li, and Y. Lin, “Graphene and graphene oxide: biofunctionalization and applications in biotechnology,” *Trends in Biotechnology*, vol. 29, no. 5, pp. 205–212, 2011.
- [73] X. Li, C. W. Magnuson, A. Venugopal, J. An, J. W. Suk, B. Han, M. Borysiak, W. Cai, A. Velamakanni, Y. Zhu, L. Fu, E. M. Vogel, E. Voelkl, L. Colombo, and R. S. Ruoff, “Graphene films with large domain size by a two-step chemical vapor deposition process,” *Nano Letters*, vol. 10, no. 11, pp. 4328–34, 2010.
- [74] A. H. Castro Neto, N. M. R. Peres, K. S. Novoselov, and A. K. Geim, “The electronic properties of graphene,” *Reviews of Modern Physics*, vol. 81, no. 1, pp. 109–162,

Jan. 2009.

- [75] P. Wallace, "The Band Theory of Graphite," *Physical Review*, vol. 71, no. 9, pp. 622–634, 1947.
- [76] J. Slonczewski and P. Weiss, "Band Structure of Graphite," *Physical Review*, vol. 109, no. 2, pp. 272–279, 1958.
- [77] K. S. Novoselov, A. K. Geim, S. V. Morozov, S. V. Dubonos, Y. Zhang, and D. Jiang, "Room-temperature electric field effect and carrier-type inversion in graphene films," *Science*, vol. 306, no. 5696, pp. 660–662, 2004.
- [78] J. E. Fischer and T. E. Thompson, "Graphite intercalation compounds," *Physics Today*, vol. 31, no. 7, p. 36, 1978.
- [79] M. S. Dresselhaus and G. Dresselhaus, "Intercalation compounds of graphite," *Advances in Physics*, vol. 30, no. 2, pp. 139–326, 1981.
- [80] A. Reina, X. Jia, J. Ho, D. Nezich, H. Son, V. Bulovic, M. S. Dresselhaus, and J. Kong, "Large area, few-layer graphene films on arbitrary substrates by chemical vapor deposition.," *Nano Letters*, vol. 9, no. 1, pp. 30–5, 2009.
- [81] X. Li, W. Cai, L. Colombo, and R. S. Ruoff, "Evolution of graphene growth on Ni and Cu by carbon isotope labeling.," *Nano Letters*, vol. 9, no. 12, pp. 4268–72, 2009.
- [82] A. Ismach, C. Druzgalski, S. Penwell, A. Schwartzberg, M. Zheng, A. Javey, J. Bokor, and Y. Zhang, "Direct Chemical Vapor Deposition of Graphene on Dielectric Surfaces," *Nano Letters*, vol. 10, no. 5, pp. 1542–1548, 2010.
- [83] "Condensed Matter Physics Group - The University of Manchester." [Online]. Available: <http://www.condmat.physics.manchester.ac.uk/pictures/>.
- [84] A. G. Cano-Márquez, F. J. Rodríguez-Macías, J. Campos-Delgado, C. G. Espinosa-González, F. Tristán-López, D. Ramírez-González, D. A. Cullen, D. J. Smith, M. Terrones, Y. I. Vega-Cantú, and A. G. Cano-Márquez, "Ex-MWNTs: Graphene Sheets and Ribbons Produced by Lithium Intercalation and Exfoliation of Carbon Nanotubes," *Nano Letters*, vol. 9, no. 4, pp. 1527–1533, 2009.
- [85] M. Terrones, A. R. Botello-Méndez, J. Campos-Delgado, F. López-Urías, Y. I. Vega-Cantú, F. J. Rodríguez-Macías, A. L. Elías, E. Muñoz-Sandoval, A. G. Cano-Márquez, and J.-C. Charlier, "Graphene and graphite nanoribbons: Morphology, properties, synthesis, defects and applications," *Nano Today*, vol. 5, no. 4, pp. 351–372, 2010.
- [86] J. Cai, P. Ruffieux, R. Jaafar, M. Bieri, T. Braun, S. Blankenburg, M. Muoth, A. P. Seitsonen, M. Saleh, X. Feng, K. Mullen, and R. Fasel, "Atomically precise bottom-

- up fabrication of graphene nanoribbons,” *Nature*, vol. 466, no. 7305, pp. 470–473, 2010.
- [87] T. Ando, “The electronic properties of graphene and carbon nanotubes,” *NPG Asia Materials*, vol. 1, pp. 17–21, 2009.
- [88] G. Liang, N. Neophytou, D. E. Nikonov, and M. S. Lundstrom, “Performance projections for ballistic graphene nanoribbon field-effect transistors,” *IEEE Transactions on Electronic Devices*, vol. 54, pp. 677–682, 2007.
- [89] S. O. Koswatta, A. Valdes-Garcia, M. B. Steiner, Y.-M. Lin, and P. Avouris, “Ultimate RF Performance Potential of Carbon Electronics,” *IEEE Transactions on Microwave Theory and Techniques*, vol. 59, no. 10, pp. 2739–2750, 2011.
- [90] F. Bonaccorso, Z. Sun, T. Hasan, and A. C. Ferrari, “Graphene photonics and optoelectronics,” *Nature Photonics*, vol. 4, no. 9, pp. 611–622, 2010.
- [91] X. Ling, L. Xie, Y. Fang, H. Xu, H. Zhang, J. Kong, M. S. Dresselhaus, J. Zhang, and Z. Liu, “Can graphene be used as a substrate for Raman enhancement?,” *Nano Letters*, vol. 10, no. 2, pp. 553–61, 2010.
- [92] H. Zhang, A. Kulkarni, H. Kim, D. Woo, Y.-J. Kim, B. H. Hong, J.-B. Choi, and T. Kim, “Detection of Acetone Vapor Using Graphene on Polymer Optical Fiber,” *Journal of Nanoscience and Nanotechnology*, vol. 11, no. 7, pp. 5939–5943, 2011.
- [93] M. A. Pimenta, G. Dresselhaus, M. S. Dresselhaus, L. G. Cançado, A. Jorio, and R. Saito, “Studying disorder in graphite-based systems by Raman spectroscopy,” *Physical Chemistry Chemical Physics*, vol. 9, no. 11, pp. 1276–91, 2007.
- [94] K. Nakada, M. Fujita, G. Dresselhaus, and M. S. Dresselhaus, “Edge state in graphene ribbons: nanometer size effect and edge shape dependence,” *Physical Review B*, vol. 54, pp. 17954–17961, 1996.
- [95] V. Barone, O. Hod, and G. E. Scuseria, “Electronic Structure and Stability of Semiconducting Graphene Nanoribbons,” *Nano Letters*, vol. 6, no. 12, pp. 2748–2754, 2006.
- [96] Y.-W. Y.-W. Son, M. L. Cohen, and S. G. Louie, “Energy Gaps in Graphene Nanoribbons,” *Physical Review Letters*, vol. 97, no. 21, p. 216803, 2006.
- [97] J. Hedberg, “Image of graphene transistor cartoon (labeled) by James Hedberg.” [Online]. Available: <http://www.jameshedberg.com/scienceGraphics.php?sort=nano&id=graphene-transistor-labeled-cartoon>. [Accessed: 02-Oct-2012].
- [98] D. Wei, Y. Liu, Y. Wang, H. Zhang, L. Huang, and G. Yu, “Synthesis of N-Doped Graphene by Chemical Vapor Deposition and Its Electrical Properties,” *Nano*

- Letters*, vol. 9, no. 5, pp. 1752–1758, 2009.
- [99] X. Wang, X. Li, L. Zhang, Y. Yoon, P. K. Weber, H. Wang, J. Guo, and H. Dai, “N-doping of graphene through electrothermal reactions with ammonia,” *Science*, vol. 324, no. 5928, pp. 768–71, 2009.
- [100] X.-L. Wei, Y.-P. Chen, W.-L. Liu, and J.-X. Zhong, “Enhanced gas sensor based on nitrogen-vacancy graphene nanoribbons,” *Physics Letters A*, vol. 376, no. 4, pp. 559–562, 2012.
- [101] S. Alwarappan, C. Liu, A. Kumar, and C.-Z. Li, “Enzyme-Doped Graphene Nanosheets for Enhanced Glucose Biosensing,” *Journal of Physical Chemistry C*, vol. 114, no. 30, pp. 12920–12924, 2010.
- [102] K. S. Novoselov, “Electric field effect in atomically thin carbon films,” *Science*, vol. 306, pp. 666–669, 2004.
- [103] B. N. Szafranek, D. Schall, M. Otto, D. Neumaier, and H. Kurz, “High On/Off Ratios in Bilayer Graphene Field Effect Transistors Realized by Surface Dopants,” *Nano Letters*, vol. 11, no. 7, pp. 2640–2643, 2011.
- [104] Z. X. Zhang, H. S. Jia, F. Ma, P. D. Han, X. G. Liu, and B. S. Xu, “First principle study of cysteine molecule on intrinsic and Au-doped graphene surface as a chemosensor device,” *Journal of Molecular Modeling*, vol. 17, no. 4, pp. 649–655, 2011.
- [105] L. S. Panchakarla, K. S. Subrahmanyam, S. K. Saha, A. Govindaraj, H. R. Krishnamurthy, U. V. Waghmare, and C. N. R. Rao, “Synthesis, Structure, and Properties of Boron- and Nitrogen-Doped Graphene,” *Advanced Materials*, vol. 21, pp. 4726–4730, 2009.
- [106] A. G. Garcia, S. E. Baltazar, A. H. R. Castro, J. F. P. Robles, and A. Rubio, “Influence of S and P Doping in a Graphene Sheet,” *Journal of Computational and Theoretical Nanoscience*, vol. 5, no. 11, pp. 2221–2229, 2008.
- [107] P. A. Denis, “Band gap opening of monolayer and bilayer graphene doped with aluminium, silicon, phosphorus, and sulfur,” *Chemical Physics Letters*, vol. 492, no. 4–6, pp. 251–257, 2010.
- [108] K. Brenner and R. Murali, “In situ doping of graphene by exfoliation in a nitrogen ambient,” *Applied Physics Letters*, vol. 98, no. 11, p. 113115, 2011.
- [109] L. Zhao, R. He, K. T. Rim, T. Schiros, K. S. Kim, H. Zhou, C. Gutiérrez, S. P. Chockalingam, C. J. Arguello, L. Pálová, D. Nordlund, M. S. Hybertsen, D. R. Reichman, T. F. Heinz, P. Kim, A. Pinczuk, G. W. Flynn, and A. N. Pasupathy,

- “Visualizing individual nitrogen dopants in monolayer graphene.” *Science*, vol. 333, no. 6045, pp. 999–1003, 2011.
- [110] R. Lv, Q. Li, A. R. Botello-Méndez, T. Hayashi, B. Wang, A. Berkdemir, Q. Hao, A. L. Elías, R. Cruz-Silva, H. R. Gutiérrez, Y. A. Kim, H. Muramatsu, J. Zhu, M. Endo, H. Terrones, J.-C. Charlier, M. Pan, and M. Terrones, “Nitrogen-doped graphene: beyond single substitution and enhanced molecular sensing.” *Scientific Reports*, vol. 2, p. 586, 2012.
- [111] E. Cruz-Silva, Z. M. Barnett, B. G. Sumpter, and V. Meunier, “Structural, magnetic, and transport properties of substitutionally doped graphene nanoribbons from first principles”, *Physical Review B*, vol. 83, p. 155445, 2011.
- [112] M. W. Iqbal, A. K. Singh, M. Z. Iqbal, and J. Eom, “Raman fingerprint of doping due to metal adsorbates on graphene.”, *Journal of Physics: Condensed Matter*, vol. 24, no. 33, p. 335301, 2012.
- [113] B. Tang, H. Guoxin, and H. Gao, “Raman Spectroscopic Characterization of Graphene,” *Applied Spectroscopy Reviews*, vol. 45, no. 5, pp. 369–407, 2010.
- [114] F. Joucken, Y. Tison, J. Lagoute, J. Dumont, D. Cabosart, B. Zheng, V. Repain, C. Chacon, Y. Girard, A. R. Botello-Méndez, S. Rousset, R. Sporken, J.-C. Charlier, and L. Henrard, “Localized state and charge transfer in nitrogen-doped graphene,” *Physical Review B*, vol. 85, no. 16, p. 161408, 2012.
- [115] J. Russell and P. Kral, “Configuration-sensitive molecular sensing on doped graphene sheets,” *Nano Research*, vol. 3, no. 7, pp. 472–480, 2010.
- [116] Z. M. Ao and F. M. Peeters, “Electric Field Activated Hydrogen Dissociative Adsorption to Nitrogen-Doped Graphene,” *The Journal of Physical Chemistry C*, vol. 114, no. 34, pp. 14503–14509, 2010.
- [117] Z. M. Ao, A. D. Hernandez-Nieves, F. M. Peeters, and S. Li, “The electric field as a novel switch for uptake/release of hydrogen for storage in nitrogen doped graphene,” *Physical Chemistry Chemical Physics*, vol. 14, no. 4, pp. 1463–1467, 2012.
- [118] M.-Y. Yen, C.-K. Hsieh, C.-C. Teng, M.-C. Hsiao, P.-I. Liu, C.-C. M. Ma, M.-C. Tsai, C.-H. Tsai, Y.-R. Lin, and T.-Y. Chou, “Metal-free, nitrogen-doped graphene used as a novel catalyst for dye-sensitized solar cell counter electrodes,” *RSC Advances*, vol. 2, no. 7, p. 2725, 2012.





# Chapter 2

## Interaction between nanomaterials and biosystems: nanobiotechnology

### 2.1 Nanobiotechnology: a brief introduction

The development of nanotechnology through the discovery and characterization of new materials opens up novel possibilities in a wide range of fields. In fact, it has already achieved notable successes in applications development based on nanotechnology, from new composites for high-tech uses such as aerospace industry [1], new electronic devices [2, 3], energy generation [4] and storage [5], and even as a value-additive for relative low-tech textile [6] and cosmetic [7] products. One of the areas where nano-technology is expected to have a significant impact is the field of life sciences. *Nanobiotechnology*, a general term used for this multidisciplinary area where nanostructured materials interact with biological sciences for a broad spectrum of potential applications, is starting to play an increasingly important role in biotechnological research. In this sense, different types of nanoparticles, peptide nanotubes, fullerenes, carbon nanotubes and graphene are among the most popular nanomaterials being used for explorations in bioimaging, pharmacology, genetic research and bioengineering, among others, promising innovative and effective alternatives to current technologies.

### 2.1.1 Background: first explorations on the use of nanomaterials in bio-applications

Since the discovery of carbon nanomaterials, their use in nanobiotechnology related research has been incremental, with an enormous amount of reports on the use of the most important carbon nanostructures: fullerenes, CNTs and graphene. Nevertheless, many other nanostructured materials, such as silver nanoparticles, silicon and silver nanowires, peptide nanotubes, DNA complex nanostructures and nanostructured polymers as PEDOT nanotubes or complex dendrimers have been explored similarly, with interesting results that can help to build an adequate contrast framework for carbon nanomaterials in nanobiotechnology (see [figure 2.1](#) for a few examples). [8]

From our point of view, it is convenient to divide the nanomaterials used in nanobiotechnology in two groups: carbon and non-carbon nanomaterials. This classification stands only for the proper differentiation between research done with pure nanocarbons

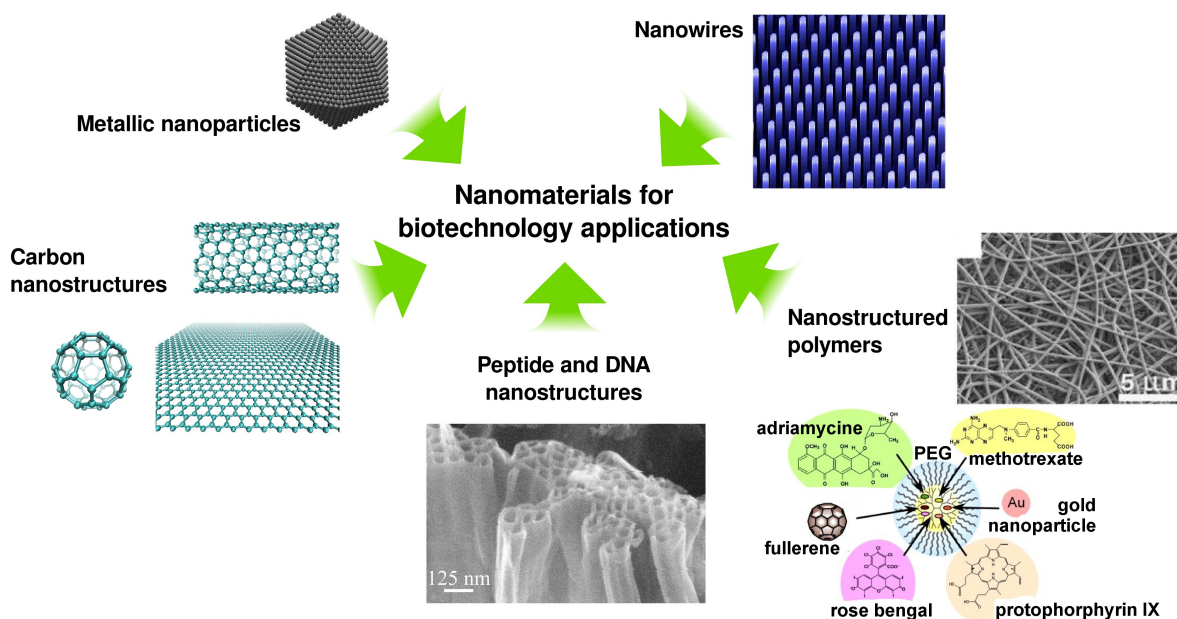


**Figure 2.1.** Nanostructured materials for biotechnological applications, ranging from metallic nanoparticles to nanowires, nanostructured polymers, peptide and DNA nanostructures, and carbon nanomaterials, including fullerenes, carbon nanotubes and graphene (*Metallic nanoparticles* figure taken from [8], *Nanowires* figure taken from [9], *Peptide and DNA* figure taken from [10], and *Nanostructured polymers* scheme adapted from [11]. All the other figures were prepared from results of this thesis work).

(fullerenes, CNTs and graphene) and other nanostructures that can indeed have carbon as a main constituent (like polymers or peptide and DNA structures), but are not part of the “pure” carbon-nanotechnology.

### 2.1.1.1 Non-carbon nanomaterials

#### 2.1.1.1.1 Metallic nanoparticles

The use of metallic nanoparticles (m-NPs) in nanobiotechnology has been objective of several studies towards applications in areas such as bioimaging [12], antibacterial composites [13], hyperthermia for cancer treatment [14] and sensing [15]. These applications take advantage of m-NPs' attributes such as magnetic and optical excitability, high degree of size control at the synthesis time and variety on the raw materials (e.g. Fe, Co, Pt, Ag) utilized for their production. For instance, it has been proposed that m-NPs with magnetic properties can exhibit high multimodal functionality by their coating with biofunctional molecules such as antibodies, DNA and specific ligands or receptors for smart targeting (see figure 2.2) [16]. Additionally, the synthesis of complex m-NPs, using different kinds of metals and structures, can expand their applicability for a variety of imaging and other therapeutic techniques.

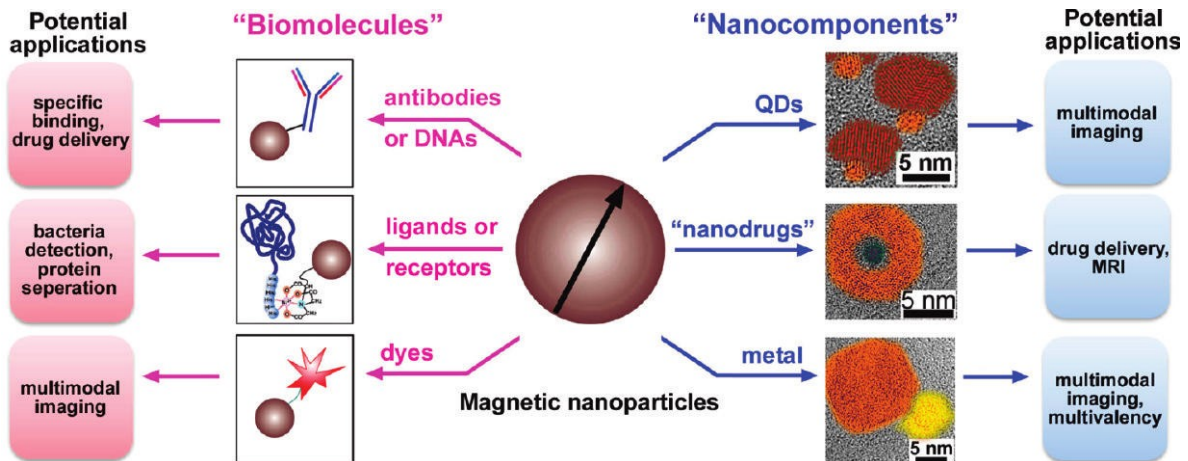


**Figure 2.2.** Explorations of magnetic m-NPs in nanobiotechnology applications. The m-NPs can be functionalized with biomolecules such as antibodies or specific receptors (left panels) or can be part of complex nanosystems for imaging applications (right panel). Image extracted from [16].

The attractive characteristics m-NPs exhibit are founded in the physical phenomena occurring at the nanoscale, which is directly related with their size and atomic arrangement. This quantum phenomena is currently driving the m-NPs research towards promising optical-based biodetection techniques as well (i.e. plasmonics) [17, 18], with initial efforts in conjunction with carbon nanostructures like graphene being also explored [19].

#### 2.1.1.1.2 Nanowires

Nanowires (NWs) are nanostructures which exhibit a characteristic high aspect ratio (diameters in the nanometers scale and lengths up to several microns), similarly to CNTs, but with the difference that NWs are commonly formed by solid blocks of elements such as Si [20], Bi [21], Pt [22] or Ni [23], or from semiconducting compounds like ZnO [24], GaN [25] and InP [26], for example. The two-dimensional limited size of NWs imposes quantum phenomena to the electronic properties, resulting in clearly different optical, thermal and conductive characteristics when compared with their bulk crystalline counterparts. NWs can be produced mainly by two general approaches: top-down, which means that they are nanofabricated from pieces of bulk crystalline material by techniques such as lithography and etching or template casting, for example (see figure 2.3a) [25]. Bottom-top approaches imply the self arrangement of nanosized blocks or even atoms into NWs driven by catalyzers such as metallic nanoparticles, in a very similar way CNTs grow by CVD techniques (see chapter 1).

NWs use in nanobiotechnology research is oriented mainly to biosensing applications.

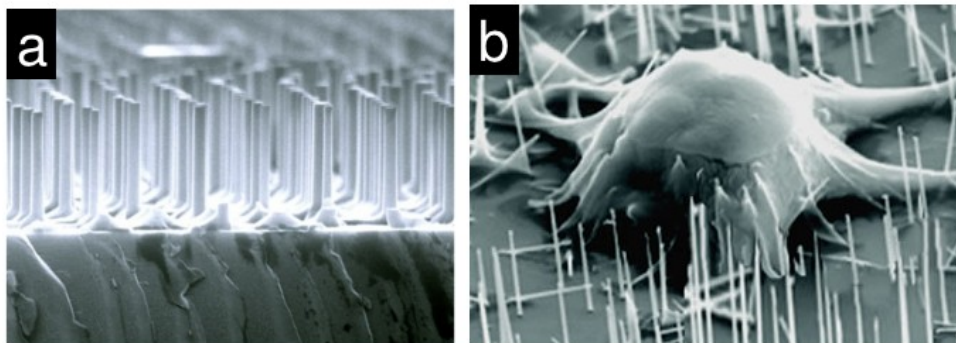


**Figure 2.3.** SEM images of (a) GaN nanowires array, grown by top-down fabrication (taken from [25]), and (b) Mouse embryonic stem cell (mES) grown and interfaced with Si-NWs (taken from [27]).

For instance, ZnO- and Si-NWs have been reported for ion and cholesterol biosensing [24], enzymes as cortisol [28] or cytokines [29], and even for DNA detection [30]. Interestingly, NWs can be functionalized for specific biodetection as well [28, 31]. Moreover, several groups have reported research where direct interfaces between NWs and cells like mouse embryonic stem cells (mES, see figure 2.3b) for gene delivery [27], and fibroblasts for cell adhesion analysis [32].

#### *2.1.1.1.3 Nanostructured polymers*

Nanotechnology principles are applicable to polymeric structures, conferring to nanostructured polymers properties that are not observable when polymers are used in a “bulk” manner. The enormous diversity of polymeric molecules give rise to many possibilities in terms of nanostructuring, which can produce materials such as nanotubes (see figure 2.4a-b) [33], dendrimers (figure 2.4c) [34, 35], block copolymers [36], Langmuir-Blodgett films [37], and even combinations of these with other kind of nanostructures. For instance, the attachment of polyethylene glycol (PEG) molecules to carbon nanotubes [38] or even drug complexes [39] is a well established method (known as PEGylation) for increasing their solubility and decreasing potential immune responses from the host.

Nanostructured polymers exhibit several key characteristics which make them ideal for certain types of bioengineering research. The polypyrrole (PPy) nanotubes shown in figure 2.4a-b, for example, have been utilized for improving the interface between neural tissue and electrodes for neural activity recording. Thanks to their electrical conductivity and high surface-to-volume ratio, the PPy nanotubes exhibit a improved transduction of bioelectric signals with respect with conventional neural electrodes [33].

Another example are the polymeric dendrimers, which are spherical nanostructures made of repetitive branching chains (see figure 2.4c). This kind of structures present several advantages in terms of drug (and other biomolecules such as DNA for gene delivery) carrying capabilities, since depending on the type of monomer and spatial chains arrangement, they can have hollow regions where hydrophobic drugs can be encapsulated. The external polymeric skin can also be altered high specificity by the attachment of functional groups [35]. For more information on dendrimers see for example [40].

Finally, it is worth to mention that certain type of polymers with hydrophobic and hydrophilic sides (amphiphiles) can be nanostructured in near 2D films (either by

Langmuir-Blodgett or self-assembly over specific substrates), since their thickness can be in the range of nanometers, while having areas much larger than that. It has been demonstrated, for instance, that films of the amphiphilic block copolymer poly(methoxyloxazoline)-polydimethylsiloxane-poly(methoxyloxazoline) (PMOXA-PDMS-PMOXA) can be “loaded” with tethering anti-inflammatory dexamethasone molecules, resulting in a polymeric nanostructured film for biomedical applications [36].

#### 2.1.1.1.4 Peptide and nucleic acids nanostructures

Within all the varieties of biomolecules, proteins and peptides, as well as nucleic acids are of special interest from the point of view of nanostructures research, due to the variety of

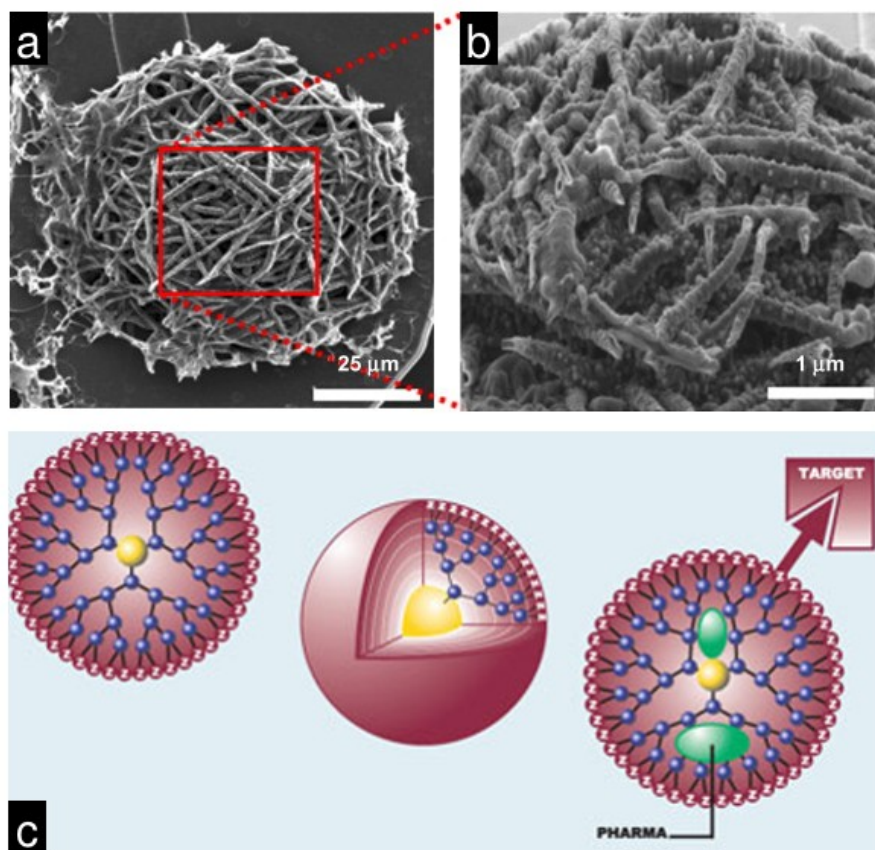


**Figure 2.4.** (a-b) SEM images (at different magnifications) of polypyrrole (PPy) nanotubes, used in neural microelectrodes (image adapted from [33]). (c) Scheme of a polymeric dendrimer for targeted drug delivery, where the charge of the polymeric molecules play an important role in the targeting process (image taken from [35]).

nanostructures possible from a few building blocks. In the case of proteins and peptides, the latter being shorter chains, are formed by the combination of about twenty building blocks, called aminoacids. Aminoacids are very simple molecules, which can be joined in chains through peptide links (amide bonds between the  $\alpha$ -amino and terminal carboxylic acid group). These few building blocks generate an immense amount of possible configurations, with thousands of uses in living organisms, from structural (e.g. collagen and keratin) to functional (e.g. enzymes, hormones, transport proteins).

In addition to the natural proteinic structures, different kinds of nanostructures can be built using the same self-assembling principles. In [figure 2.5a-b](#) are shown high resolution SEM images of peptide nanotubes produced of self-assembled oligopeptides [10]. The applicability of these peptide nanostructures has been proposed and explored mostly for biosensing [41] and drug delivery [42].

In the case of DNA, the conforming unit blocks are nucleotide base pairs, which are formed basically by a sugar and phosphate backbone and one of four possible nucleic bases (guanine, adenine, thymine and cytosine, see [figure 2.5c](#) for adenine example). DNA in its natural state has a distinctive double-stranded helix shape, which is direct consequence of

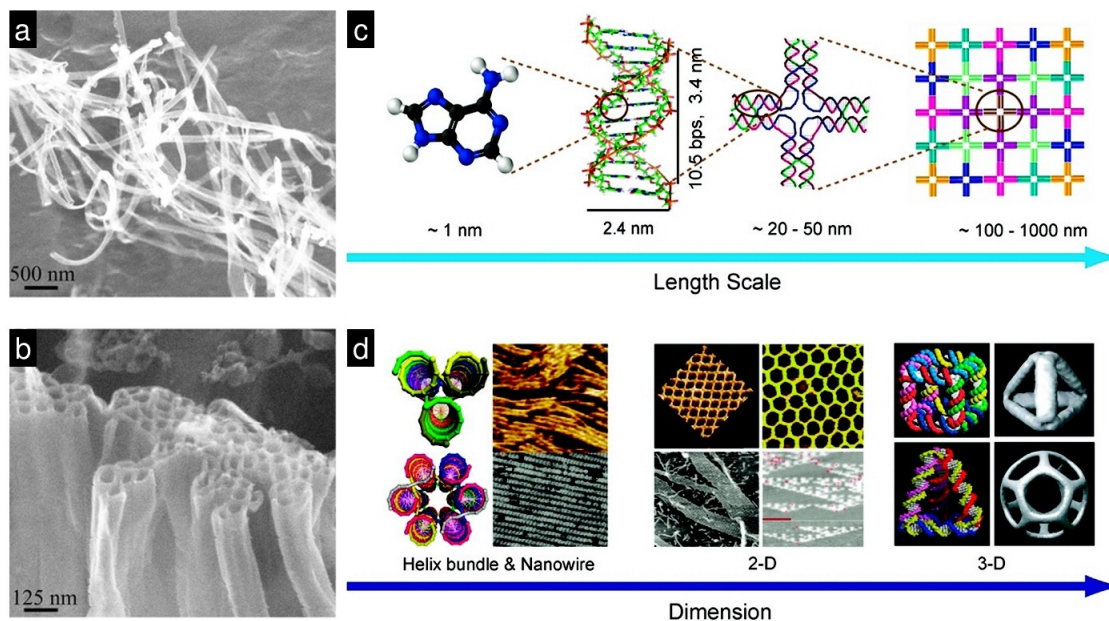


**Figure 2.5.** High resolution SEM images of peptide nanotubes before (a) and after bundling (b) by sulfate salts addition (images taken from [10]). Representation of nanostructured DNA from different scales (c) and dimensionality (d), showing the rich variety of possible morphologies achievable (image adapted from [33]).



the interactions between conforming base pairs. Moreover, the flexibility of the specific interactions between its building blocks enables various types of structural assemblies such as the ones depicted in [figure 2.5c](#) and [d](#) [43]. These self-assembled geometrical DNA structures are being explored for applications such as new data encoding systems [44] and templating for protein and metallic nanostructures [45]. Other potential applications are related to biophysics analysis, biomimetics, and new diagnostic-therapeutic approaches [46].

### 2.1.2 Functionalization of carbon nanomaterials for nanobiotechnology

All the carbon nanomaterials mentioned in the prior chapter have been explored by several groups to some extent for biotechnology applications. From functionalized fullerenes and nanotubes for drug delivery, to new biosensing devices harnessing the exceptional electronic and optical characteristics of graphene, for instance. A deeper description of these and other nanobio-technological advances will be addressed later in this chapter, but first it is necessary to consider common treatments for nanocarbons, in order to make them more compatible with biological environments. In this regard, some toxicological concerns as well as some alternatives for overcoming those issues will be explored.

#### 2.1.2.1 Covalent functionalization

All carbon nanomaterials are formed by  $sp^2$  carbonaceous hexagonal networks, which exhibit exceptional electronic and mechanical properties. Nevertheless, is precisely this high stability of carbon bonds hinders chemical interactions with external molecules. This is specially problematic with water-based systems (as practically all biosystems), given the hydrophobicity displayed by carbon nanostructures.

Among various approaches for overcoming the carbon nanomaterials' inertness, covalent functionalization is probably the most utilized. This type of functionalization frequently implies harsh chemical treatments in order to attach anchoring groups to the carbonaceous lattices. For instance, for CNTs case, several functionalization methodologies have been well established [47, 48]. Some those methods were previously developed from fullerene chemistry, some from graphite chemistry, and some from nanotube research by itself. Those methods involve treating the carbon nanotubes with highly reactive species

such as F, cycloadditive reactions, or most often, strong acid treatments for carboxyl and carbonyl groups attachment (see figure 2.6). The presence of these groups at the CNTs walls enhance their chemical reactivity and hydrophilicity. Moreover, these groups are commonly used as anchoring sites for further chemical reactions with a wide variety of molecules, including biocompatible polymers, small peptides and proteins, and even nucleic acids (see figure 2.7) [49].

Some functionalizations have proven convenient in terms of enhancing solubility of carbon nanostructures while decreasing undesired effects, such as immune response. For

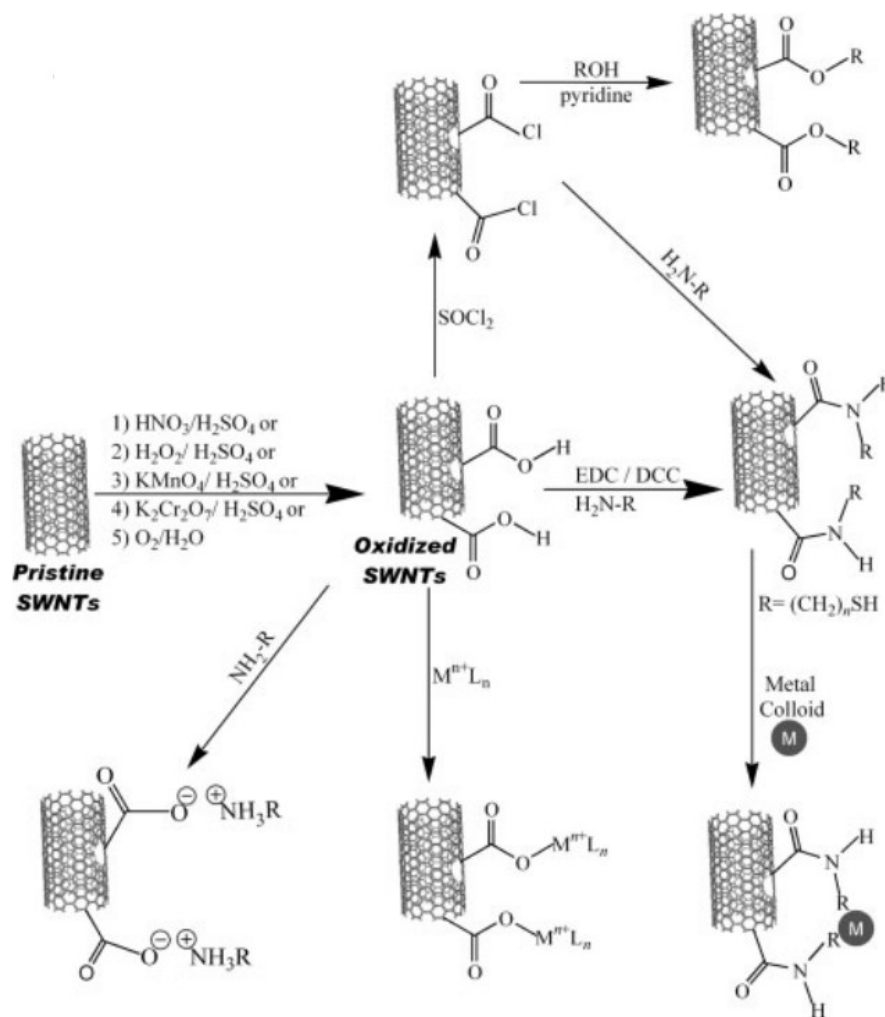


**Figure 2.6.** Chemical approaches for CNTs functionalization. Different type of functional groups, and hence assorted types of chemical interactions are possible by using a variety of initial treatments (figure adapted from [47]).

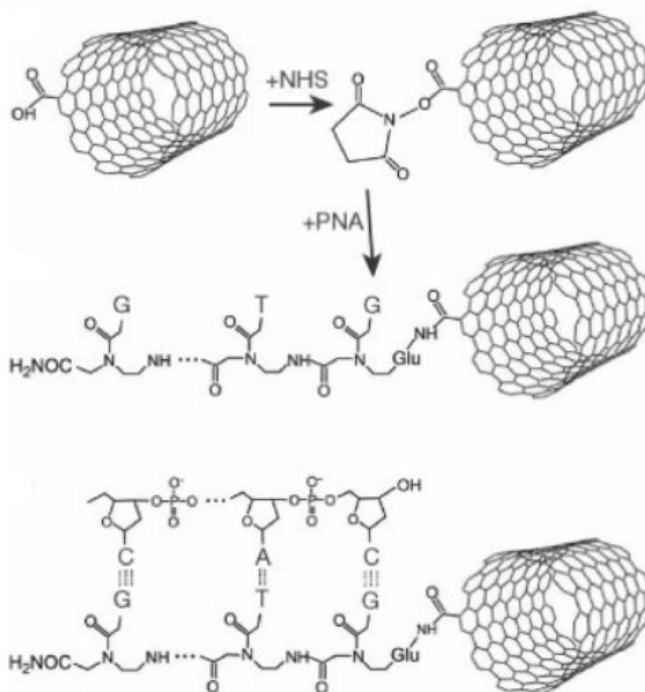


**Figure 2.7.** Chemical approaches for CNTs functionalization. Example of CNT functionalization with nucleic acids molecules based on carboxylic functional groups and peptidic coupling reactions (Image adapted from [47]).

instance, as mentioned above, PEGylation is a common treatment for carbon [50] and other nanomaterials in applications where dispersions are intended to be circulating in the main bloodstream. Another example is the attachment of biotin molecules, which enable specific interactions (through biotin-streptavidin specific binding) useful for biosensing [51].

Covalent functionalization of graphene for bioapplications has been explored as well, but to a lesser extent given the advantages of non-covalent approaches for this planar nanomaterial. A couple of examples are the attachment of peptide chains to graphene for enzymatic detection [52], and the linking of PEG chains in order to improve the dispersability and antibodies attachment [53].

One of the drawbacks of using covalent functionalizations on these carbon nanostructures is the impact that they have on their electronic properties. Disrupting the  $sp^2$  carbon network introduce scattering electronic points which reduces charge mobility and thus the electrical conductance.

### 2.1.2.2 Non-covalent functionalization

Non-covalent functionalization of carbon nanostructures is possible because of the stability of  $\pi$ - $\pi$  interactions between aromatic groups and  $sp^2$  carbon lattices. In this regard, there are numerous reports on different types of molecules that can be used for anchoring of a wide variety of moieties based on a  $\pi$ -stacking section. Many of those functionalizations have proven useful in biotechnological applications. For example, [figure 2.8a](#) shows several aromatic groups used for functionalization of CNTs with inorganic nanoparticles. These groups include pyrene derivatives, porphyrines, phthalocyanines, triphenyl phosphines, and benzyl alcohols [\[54\]](#).

Graphene is naturally an ideal candidate for non-covalent functionalization based on  $\pi$ - $\pi$  interactions. [Figure 2.8b](#) depicts a representative example of two conducting polymers; polystyrene sulfonate (PSS) and polyethylenedioxythiophene (PEDOT), which are formed by aromatic monomers and thus likely to stabilize over the graphene surface [\[55\]](#). These kind of interactions between conducting polymers and graphene can improve the performance of transparent electrodes intended for biomedical and other applications.

Graphene non-covalent functionalization has been explored as well for loading of drug molecules which have the potential of establishing  $\pi$ -stacking interactions, opening possibilities for drug delivery applications. For instance, the anticancer drug doxorubicin has been studied within this context, with results demonstrating that the non-covalent interaction with graphene produces the expected therapeutic effects with smaller dosages, than when doxorubicin is used in a free state [\[53\]](#).

Another important advantage of non-covalent functionalization of carbon nanomaterials is the fact that it does not affect their structural integrity, and thus avoids negative impacts in the electronic properties of CNTs and graphene. Moreover,  $\pi$ -stacking based functionalizations allow consistent charge interactions between the adsorbed molecule and the nanostructure, as shown by several reports on experimental biosensing applications. For instance, the non-covalent interaction of CNTs with modified Tween-20 molecules allowed the biodetection of specific ligands, along with non-specific protein binding prevention [\[56\]](#). [Figure 2.8c](#) shows another example for graphene; non-covalent functionalization with pyrene based groups enabled the optical detection (through fluorescence resonance energy transfer) of concanavalin A proteins [\[57\]](#).

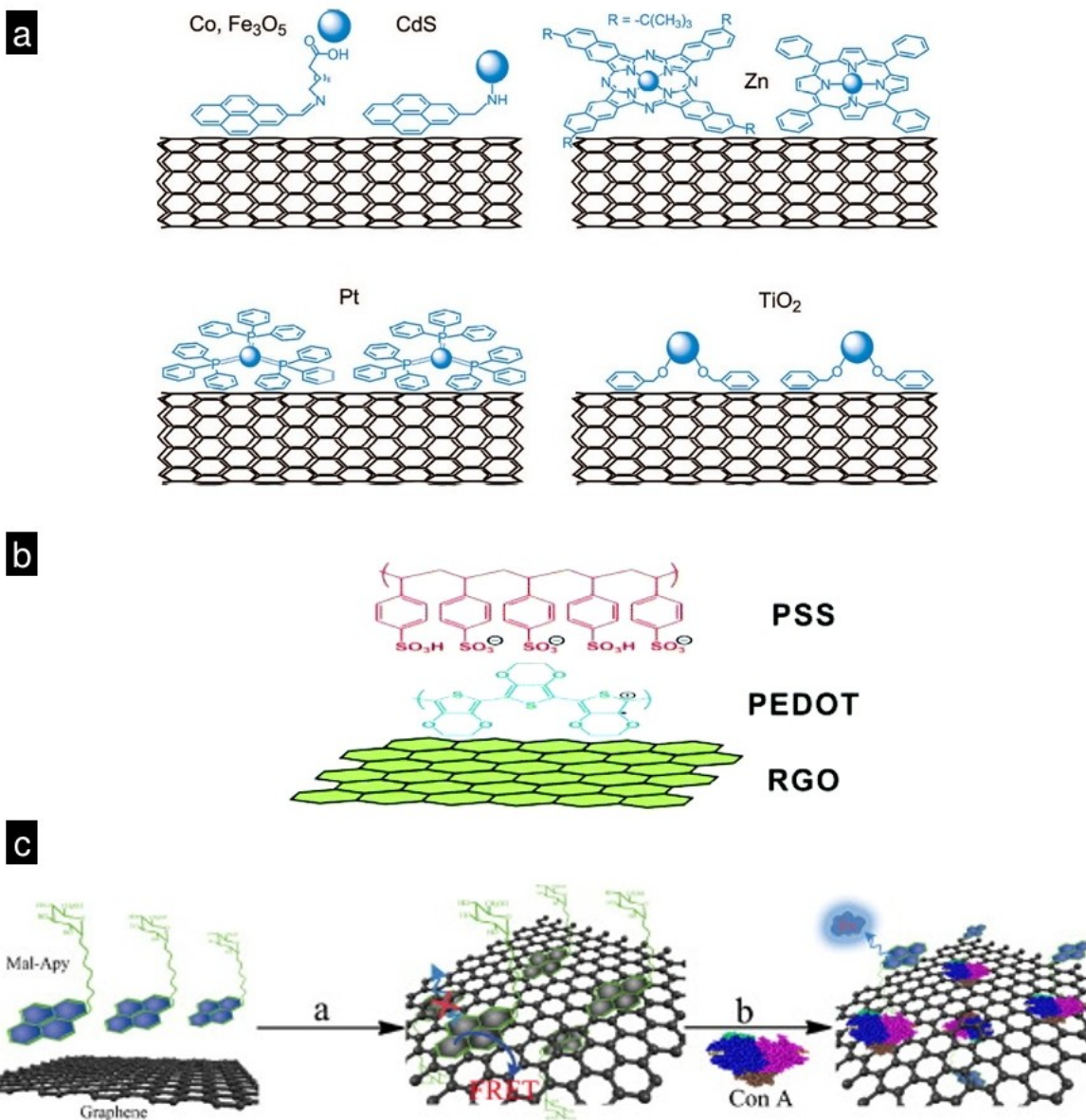


**Figure 2.8.** CNTs and graphene non-covalent functionalization examples. **(a)** Aromatic groups such as pyrene derivatives, porphyrines, phthalocyanines, triphenyl phosphines, and benzyl alcohols for linking inorganic NPs (image taken from [10]). **(b)** Polymers with aromatic monomers such as PSS and PEDOT can be interacted with graphene oxide surfaces (image adapted from [55]). **(c)** Specific graphene-based biosensors can be developed using  $\pi$ -stacking of pyrene-based groups, keeping graphene's electronic properties unaffected (taken from [57]).

### 2.1.3 Toxicity concerns and studies

Along with the incursion of carbon nanotechnology into the life sciences, concerns about potential harmful effects naturally arose, fueling a considerable amount of research regarding toxicity effects of carbon and other nanomaterials. Nevertheless, up to date a full agreement regarding toxicity of nanomaterials has not been achieved: different results suggest variable degrees of toxicity in function of the cell lines assessed and nanomaterials treatments.

Despite several somewhat contradictory reports, a general consensus about key characteristics such as nanomaterials size [58, 59], dispersability [60] and surface charge [61] as a main factors for toxicity is being reached. For instance, [figure 2.9](#) shows two graphical depictions of the effects of CNTs size in the phagocytosis process, which is used by most animals for clearance of foreign and potential damaging particles from the organism. According to one important review [58], large CNTs cannot undergo a proper phagocytosis, triggering abnormal cellular signaling that ultimately may produce inflammatory responses and in worst cases, mutagenesis and other carcinogenic processes (see [fig. 2.9a](#)). The cited review also addresses the dispersability of carbon nanomaterials as a key factor for their biocompatibility (see [fig. 2.9b](#)), highlighting that their functionalization with hydrophilic groups improves their stability in biological fluids, as mentioned earlier.

One important characteristic of carbon nanomaterials (specially CNTs and graphene) is that besides the diversity of possible chemical functionalizations, doping with heteroatoms such as B, N and P, among others, is a feasible alternative for tailoring not only electronic but chemical properties as well (see chapter 1.3.2 and 1.4.2). The use of doped nanocarbons for biological applications is still relatively unexplored, nevertheless a few studies have shown that they present better biocompatibility characteristics compared with undoped ones. For instance, [figure 2.10](#) shows comparative images of mice pulmonary tissue after exposure (intratracheal administration) to undoped MWNTs and nitrogen-doped MWNTs (CN<sub>x</sub>-MWNTs). The former produced lesions on the pulmonary tissue, which were strongly dependent on the dosage, whereas for CN<sub>x</sub>-MWNTs, the administration of different doses did not cause any damage to the analyzed tissues [62].

Given the promising results of such studies on the use of doped carbon nanostructures for biomedical applications, it is worth it to continue further analysis on potential effects when interacting with biosystems, since some of the key properties that differentiate them

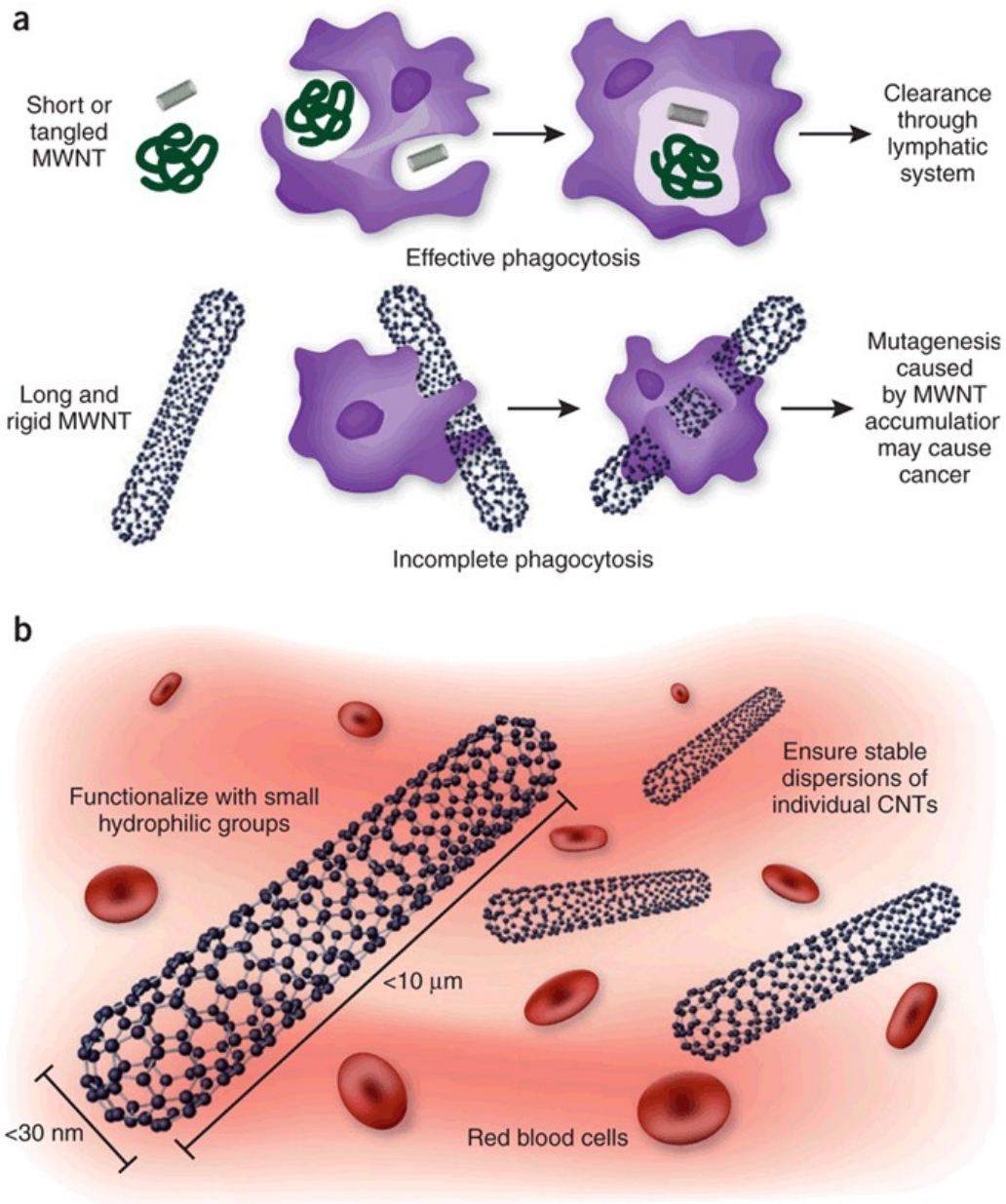


**Figure 2.9.** CNT size and surface chemistry dependent toxicity. **(a)** High aspect ratio CNTs commonly produce failed phagocytosis, triggering a series of immune responses or other abnormal cell signaling that ultimately may cause illnesses like cancer. **(b)** CNT surface functionalization with hydrophilic groups contribute to decrease potential damaging effects and abnormal signaling within cellular environments (image taken from [58]).

from undoped ones (surface charge distribution and chemical reactivity, for instance) are crucial factors for toxicological issues.

## 2.2 Carbon nanomaterials in biomedical technology

Many improvements on biomedical technology will be possible with an increased ability for nanoscale manipulation and with the use of nanostructures in biomedical applications. In the context of biomedical technology, carbon nanomaterials are starting to play an increasingly important role for efficient and low-cost devices, given their outstanding electronic and chemical properties. Here is a summary of relevant applications of nanocarbons that exemplify their great potential in life sciences fields.

### 2.2.1 Drug and gene delivery

Efficient drug delivery systems (DDS) are a basic requirement for the advancement of biomedical technologies, given the high specificity of most modern drug molecules. The efficiency must be achieved in terms of high load capacity, drug bioactivity protection from harsh conditions during translocation, and targeting, preventing the drug to exert its effects until it is located at the desired site. The same principles apply to gene delivery technology,

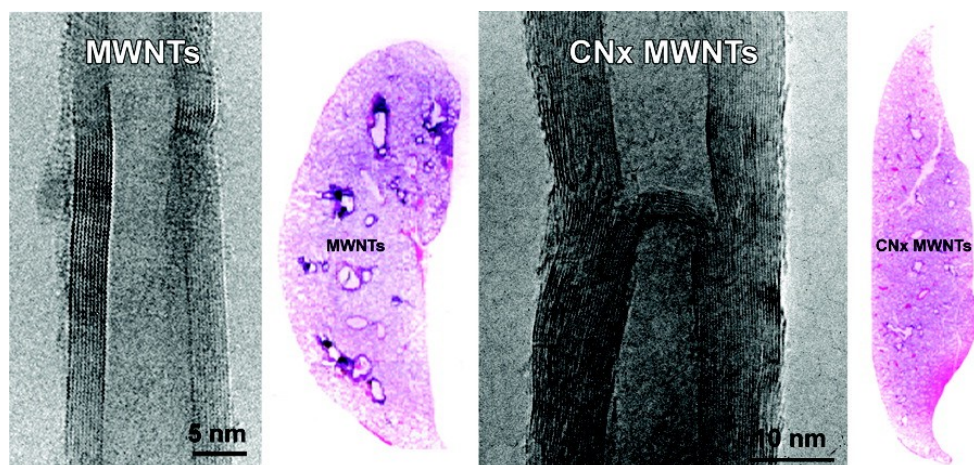


**Figure 2.10.** CNT doping dependant toxicity. Nanotubes accumulation and induced pulmonary lesions in mice was observed for undoped MWNTs (left images), whereas nitrogen-doped MWNTs (right images) did not show toxicological effects at any dose (image taken from [62]).



which consists on the introduction of foreign genetic material into a cell or group of cells. Currently, it is possible to find several nanostructures being used for DDS, such as liposomes [63], dendrimers [35], polymers [64], virus-based systems [65] and nanocarbons [66], particularly CNTs and graphene.

The flexibility of carbon nanomaterials functionalization, through different types of interactions (covalent or non-covalent) has been harnessed for DDS explorations, with promising results when compared against traditional approaches for drug administration. Additionally, the high surface area exhibited by CNTs and graphene allows to design complex DDS, comprising several type of molecules besides the drug, in order to gain control over specificity and traceability. For example, the multi-functionalization of SWNTs with the anticancer drug doxorubicin (DOX), a monoclonal antibody and a fluorescent marker (see [figure 2.11A](#)) has been reported [67]. The complexes DOX-fluorescein-BSA-antibody-SWNT (DOX-SWNT) were designed for targeting colon cancer cells through their carcinoembryonic antigen. The results showed efficient DOX-SWNT complexes uptake by the cancer cells, and a translocation and release of DOX inside the nuclei, as is clearly observed in [figure 2.11B](#), by the optical tracing of the complexes through the fluorescein and DOX molecules.

CNTs are being explored as well for DNA delivery, for gene therapy applications. Single stranded DNA (ssDNA) chains can be linked to CNTs surfaces in several ways, including CNTs with amino groups [68], polymers such as polyethylenimine [69] or cationic polyelectrolytes [70], or even linking to metallic clusters anchored on CNTs' surface [71].

The structural and physico-chemical nature of CNTs allows a variety of potential gene delivery concepts to be explored. [Figure 2.12](#) depicts different modes of nucleic acids delivery to the cell nucleus, which take advantage of the flexibility of interactions between biomolecules and CNTs. These interactions can lead to the use of CNTs as simple channels through the cell wall, or include covalent or non-covalent functionalizations, which can undergo cleavage under potentially controlled conditions [72].

Regarding graphene use for DDS, most of the research reported up to date is based in graphene oxide (GO), commonly synthesized from the exfoliation of graphite through strong oxidizing treatments. In terms of potential for drug loading, graphene is potentially useful due to its high surface-to-volume ratio and consequent high drug load capacity, which is in turn harnessed for non-covalent interactions between nanocarbons and potent

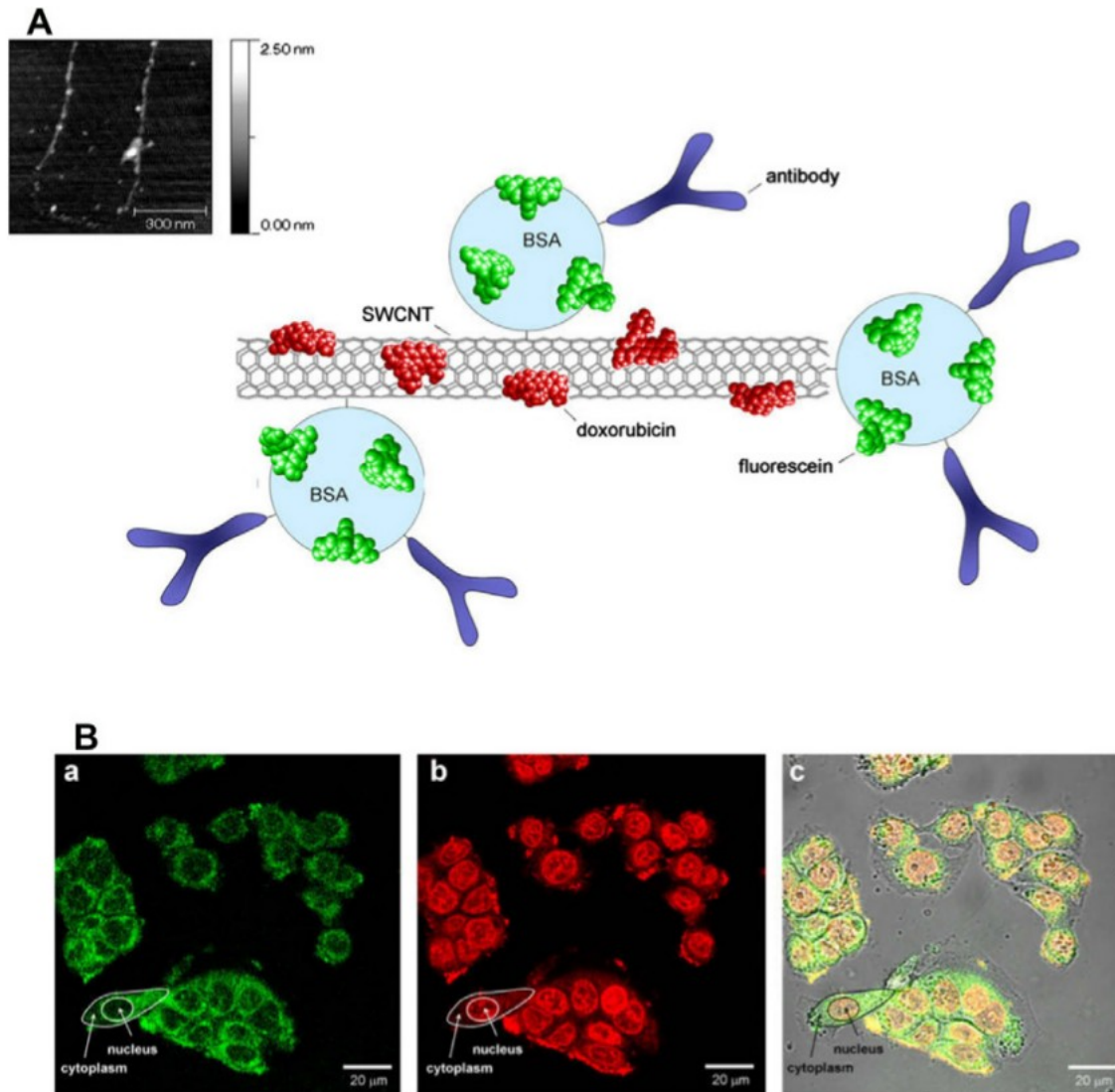


**Figure 2.11.** (A) Schematic illustration of DOX-SWNT complexes. Inset: AFM image of the DOX-SWNT complexes (without antibodies). (B) Confocal images of cancer cells incubated with DOX-SWNT complexes with emission measured at 500-530 nm (fluorescein, **a**) and at 650-710 nm (DOX, **b**). **c** shows all channels (Image taken from [67]).

anticancer drugs such as DOX and camptothecin (CPT) (see [figure 2.13a](#)). One published work reports additional functionalization of nanoscale graphene oxide (NGO) with folic acid molecules (FA) for targeting cells with folate receptors, which are commonly overexpressed in cancerous cells [73]. The proposed DDS demonstrated an increased effectiveness for killing cancerous cells.

Another report on graphene for DDS involves the reduction of exfoliated graphene oxide (EGO) in the presence of gelatin, producing gelatin-graphene nanosheets (GNS) complexes [74]. The cited work reports an absence of cytotoxicity and a high dispersion stability under biological conditions, attributed to the linked gelatin chains. Further non-covalent functionalization with DOX successfully provides an anticancer effect, through its controlled release after the internalization of the complexes into cancer cells (see [figure 2.13b](#)).

Summarizing, the use of carbon nanomaterials for DDS has been promising, at least at the research stage, given the exceptional characteristics they exhibit in terms of drug load capacity, chemical flexibility and mechanical stability, which allow these nanostructures to safely transport their pharmacological cargo, with some key advantages such as traceability, for instance. Nevertheless, most of the studies state that a deep analysis of potential toxicity effects must be addressed before real therapeutics can be developed based on these carbon nanomaterials.

## 2.2.2 Biosensing

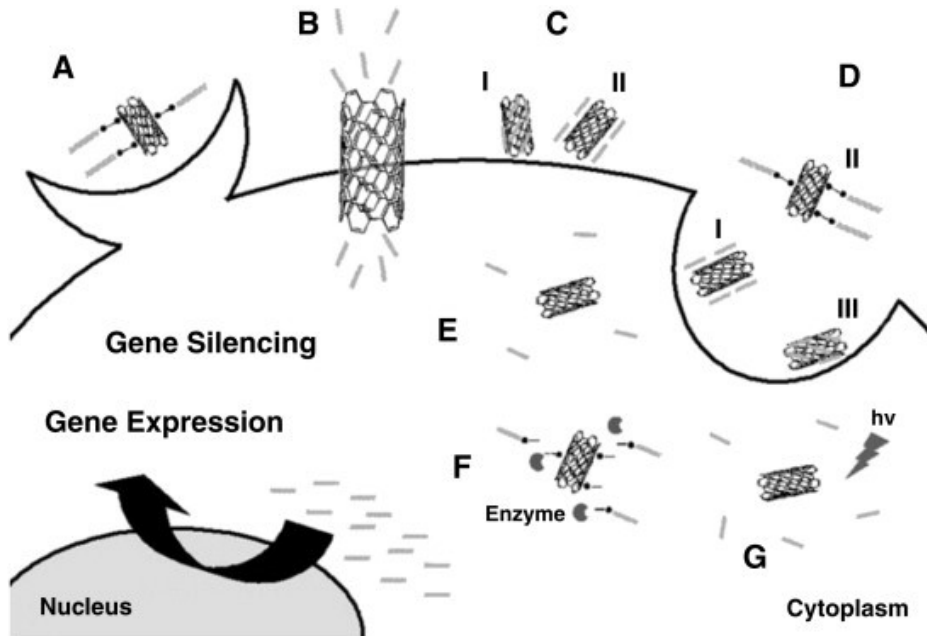
Since the discovery of CNTs and graphene, their electronic properties were object of intense study given the exceptional characteristics they started to reveal. They were immediately the focus for new nanoelectronic devices research and development, and biosensing is in fact one of the field where most of the advancements are expected. Carbon nanomaterials exhibit ideal features for biosensing devices development; their nanoscale dimensions allow to use them directly as field-effect transistors' (FET) channels, which along with their extraordinary electronic and chemical properties, opened novel routes for supersensitive detectors. Moreover, their peculiar electronic structure also permits the detection of slight electronic changes through optical-based techniques.

### 2.2.2.1 Field-effect transistor based biosensing

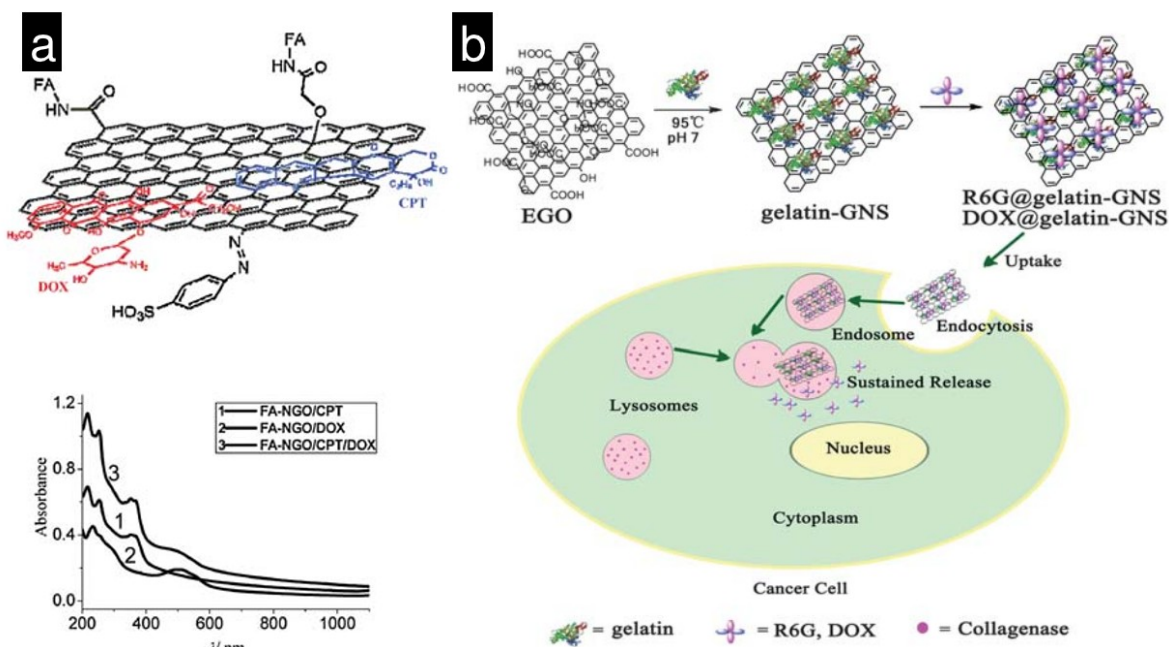
One of the most popular biosensing configuration for CNTs, graphene and graphene-nanoribbons is on FET devices, where the nanostructure is utilized as conducting channel between two metallic electrodes, including a controlling gate that can either be structurally separated from the analyte to be detected (as in back-gating configuration, example in

figure 2.14-top), or directly based on the “gating” effect produced by the interaction between the nanomaterial and the analyte (see figure 2.14-bottom for an example). In any case, the FET biosensing approach depends on changes in channel conductivity caused by alterations in the electric field and available charges at its surroundings.

The chemical flexibility of CNTs, graphene and other nanocarbons plays an important role in the specificity that can be achieved with these nanodevices. For instance, it has been demonstrated that non-covalent interaction of CNTs with modified surfactants such as Tween-20 (see figure 2.14-bottom) can prevent non-specific protein binding to CNT-FETs, which is a potential problem for all biosensors given the nature of biological environments. At the same time, the modified surfactant can work as an anchoring molecule for specific ligand-receptors or specific pairs of biomolecules with high affinity, such as biotin (B) and streptavidin (SA), or protein A (SpA) and immunoglobulin G (IgG) [56]. One important



**Figure 2.12.** Suggested strategies for cellular delivery of nucleic acids by CNT: phagocytosis of nucleic acids covalently linked to CNT (A), injection of nucleic acids through CNT nanochannels (B), penetration of nucleic acids adsorbed on the surface of CNT (C<sub>I</sub>) or complexed with CNT by electrostatic forces (C<sub>II</sub>); and endocytosis of nucleic acids electrostatically complexed (D<sub>I</sub>), covalently linked (D<sub>II</sub>) or adsorbed (D<sub>III</sub>) to CNT. Suggested strategies for intracellular release of the nucleic acid from the CNT: electrostatic dissociation (E), enzymatic cleavage (F) and NIR radiation (G). Image taken from [72].



**Figure 2.13. (a)** Schematic representation of doxorubicin (DOX) and camptothecin (CPT) loading onto folic acid-nanoscale graphene oxide (FA-NGO), along with the UV/Vis spectra of DOX, CPT and both DOX / CPT loaded onto FA-NGO (image taken from [73]). **(b)** Depiction of green synthesis of gelatin-GNS and the possible mechanism of drug delivery as well as gelatin-mediated intracellular sustained release (figure taken from [74]).

advantage of these type of approaches is that non-covalent interactions with carbon nanomaterials tend to keep their structural integrity unaffected, which contributes to maintain their electronic properties.

Real time biosensing of cellular activity is another field where carbon nanomaterials are expected to have an impact, since their wide spectrum of chemical interactions facilitates multiple applications. For example, in figure 2.15 are shown reported results on the growth of PC12 (neuroendocrine) cells over glycosylated CNTs networks working as biosensing FET device for cell chemical signaling [76]. The CNTs glycosylation also conveys full biocompatibility to the network, while simultaneously maintaining the electronic properties. The CNT-FET could detect triggered exocytosis of neurotransmitters (dopamine and norepinephrine), but was insensitive to changes in  $K^+$  ions concentration or culture media pH.

Graphene based FETs are also abundantly reported [77-79], using different types of graphene in function of the synthesis method (CVD grown and reduced graphene oxide

(rGO) being the most popular ones for bioapplications). Moreover, it is possible to find various approaches for functionalization, in order to confer biocompatibility and specificity to the devices. For instance, it has been reported that the incorporation of antigen-functionalized gold nanoparticles (Au-NPs) on thermally-reduced GO (TRGO) surface in FET devices (see [figure 2.16](#)) led to high performance specific sensing of proteins, in concentrations as low as  $0.2 \text{ ng mL}^{-1}$  [80]. Real-time monitoring biosensors have been developed as well using graphene-based FETs; in [figure 2.17](#) are shown images and schematics of a device constructed of rGO patterns over a polymer sheet (polyethylene terephthalate or PET), which can be used as a substrate for cell growth (PC12 cells in this case) and cell activity monitoring simultaneously [81].

Biosensing FET devices based on carbon nanomaterials have been explored as well for cancer biomarkers recognition [82], glucose [78] and DNA [83], for instance, which makes evident the flexibility they can exhibit in terms of analytes diversity. Nevertheless, research towards biosensors development based on nitrogen- or boron-doped CNTs or graphene remains limited, with some examples in theoretical studies between doped nanocarbons and biomolecules [84-86], and few experimental reports, which are mainly based in the analysis of the exceptional electrocatalytic behavior of doped CNTs [87, 88] and graphene [89, 90]. For example, [figure 2.18](#) shows current/time curves for hydrogen peroxide ( $\text{H}_2\text{O}_2$ ) detection through electrochemical reactions, using glassy-carbon (GC) electrodes modified with undoped multi-walled CNTs (MWCNT) and with nitrogen-doped multi-wall CNTs ( $\text{CN}_x$ ). It is clear that the sensitivity of electrodes with  $\text{CN}_x$  is considerably higher than MWCNT, which is attributed to the enhanced catalytic properties of N-doping sites within the doped CNTs [87].

### 2.2.2.2 Optical based biosensing

Another extremely useful feature of carbon nanostructures, is the set of optical phenomena they exhibit. The unique 1D band structure of CNTs gives rise to sharp features in the electronic density of states (DOS), which in turn promotes different types of electronic transitions. These electron or hole energy shiftings are strongly related to absorbed and transmitted photons, giving to CNTs their broad absorbance and fluorescence properties (see [figure 2.19a](#)) [91]. Conveniently for biotechnology applications, the optical characteristics of CNTs do not overlap with optical activity of living matter (see [figure 2.19b](#)) [92],

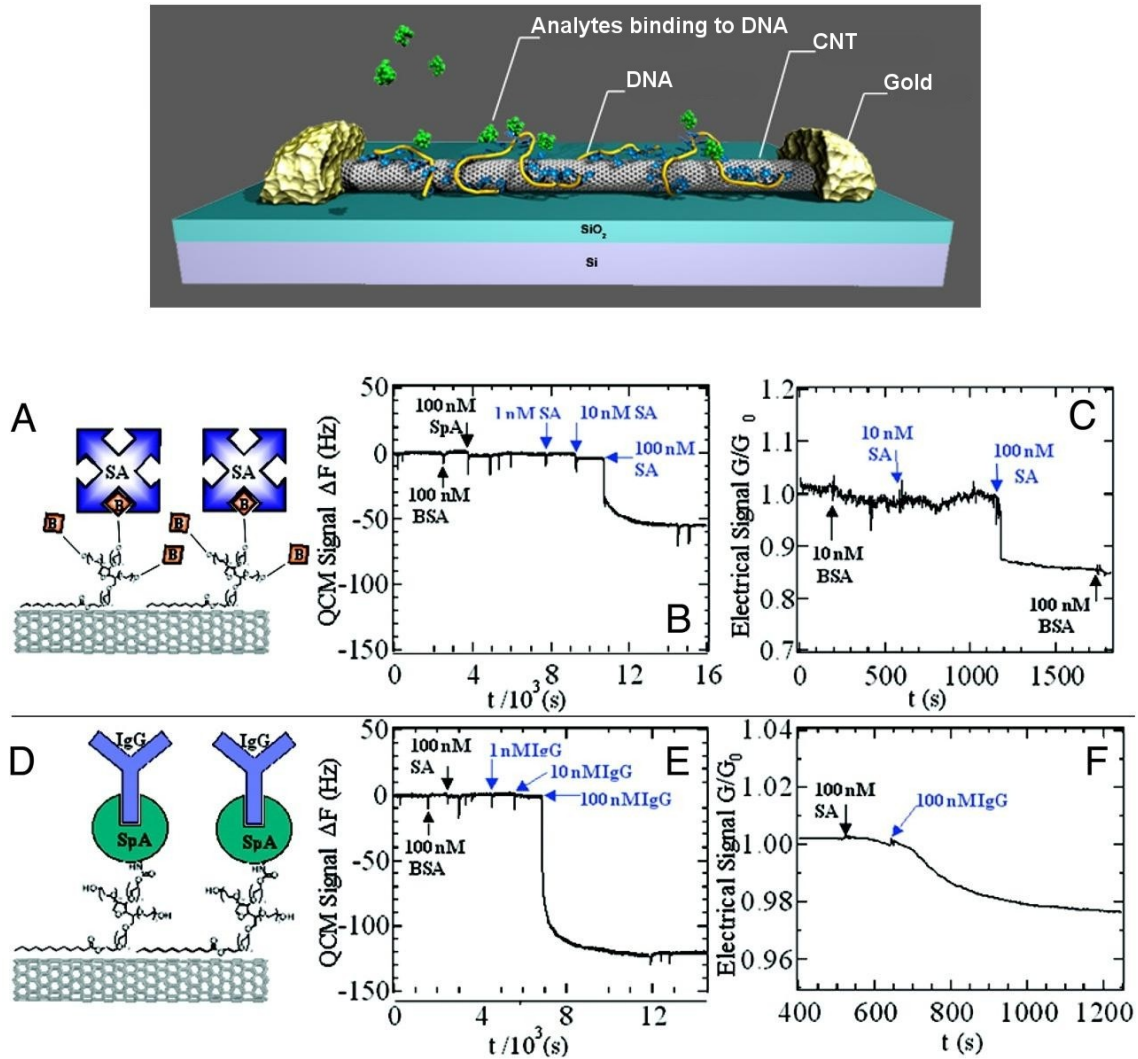


**Figure 2.14. (Top)** Representative model of CNT-FET based biosensor, using single-stranded DNA (ssDNA) for specific analyte binding (taken from [75]). **(Bottom)** Real-time quartz crystal microbalance (QCM) and electronic sensing of specific biological recognition on nanotubes. **(A)** Scheme for streptavidin (SA) recognition with a nanotube coated with biotinylated Tween. **(B)** QCM frequency shift vs. time curve showing that a film of nanotubes coated with biotinylated Tween binds SA specifically but not other proteins. **(C)** Conductance vs. time curve of a device during exposure to various protein solutions. Specific binding of SA is detected electronically. **(D)** Scheme for immunoglobuline G (IgG) recognition with a nanotube coated with a protein A (SpA)–Tween conjugate. **(E)** QCM frequency shift vs. time curve showing a film of nanotubes coated with SpA–Tween binding human IgG specifically but not unrelated proteins. **(F)** Conductance vs. time curve of a device during exposure to various protein solutions. Specific binding of IgG is detected electronically (figure taken from [56]).

enabling CNTs and other carbon nanomaterials for imaging applications (figure 2.19d).

In fact, the electronic structure of CNTs and graphene shows additional useful optical phenomena, which can be utilized in combination with their fluorescent properties. For instance, CNTs and graphene show excellent fluorescence quenching properties [93], which is harnessed for the detection of specific interactions [52, 67, 94]. For instance, figure 2.19c shows SWNTs wrapped with modified dextran molecules, aiming to the detection *in-vivo* of nitric oxide (NO). As can be seen in the optical microscopy images in figure 2.19d, the

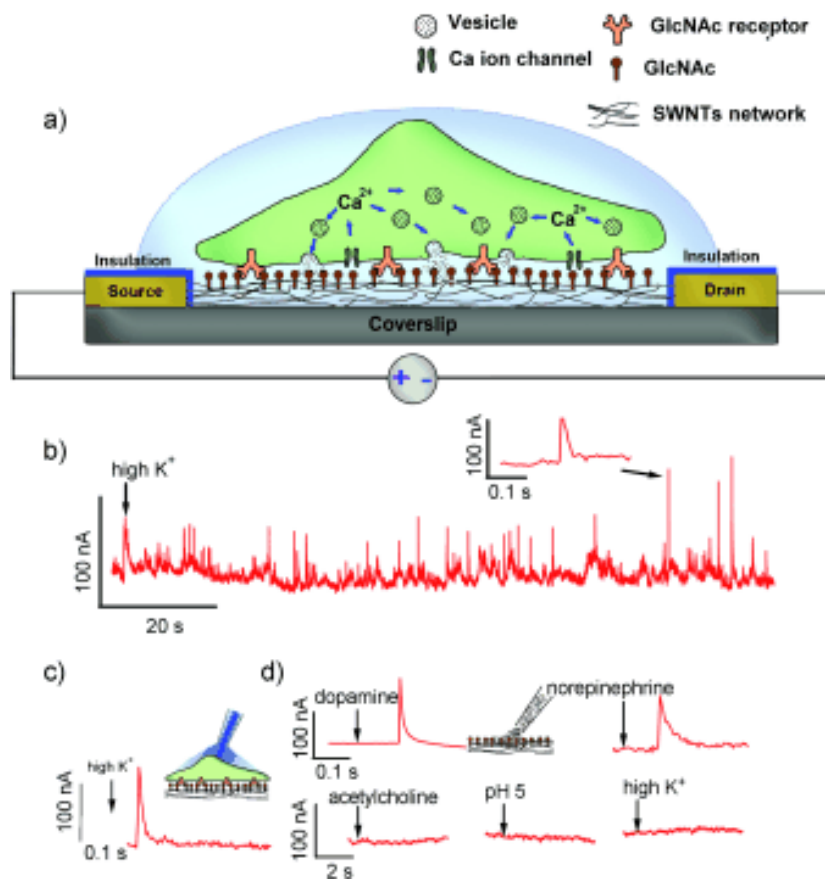


**Figure 2.15.** (a) Triggered exocytosis and SWNT-net detection. (b) Nanotube responses to exocytosis of PC12 cells triggered by high  $K^+$  stimulation. The SWNT-net was biased at  $V_{ds}=0.4$  V. (c) Stimulation of single PC12 cell through micropipette perfusion of high  $K^+$  solution. (d) Transient perfusion of 1 mM dopamine or norepinephrine on glycosylated SWNTs-net results in current spikes, while perfusion of acetylcholine, acidic solution (pH 5.0), and high  $K^+$  did not cause appreciable responses. The arrows in (c) and (d), roughly indicate where the stimulations were applied (figure taken from [76]).



internalization of CNTs complexes by macrophage cells allows to monitor their NO production, based in the SWNT fluorescence quenching at NO presence. The proposed mechanism is based on charge (electron) transfer from SWNT valence band to the unoccupied NO orbitals [95].

Graphene is specially useful as an enhancer for optical-based sensors. For instance, surface plasmon resonance (SPR) biosensors are based in charge transfers occurring at the interface of metallic (normally gold or silver) layers and dielectrics, where the entities to be detected are commonly dissolved [96]. The metallic layer is fixed at one side of a transparent prism, which is used to apply an incident polarized light beam that is reflected with an angle dependent on interactions between the analyte and the metal (see figure 2.20a). The addition of graphene layers contribute to the adsorption and charge transfer capabilities of the metallic films, amplifying the resonance angle changes (see figure 2.20b) [97].

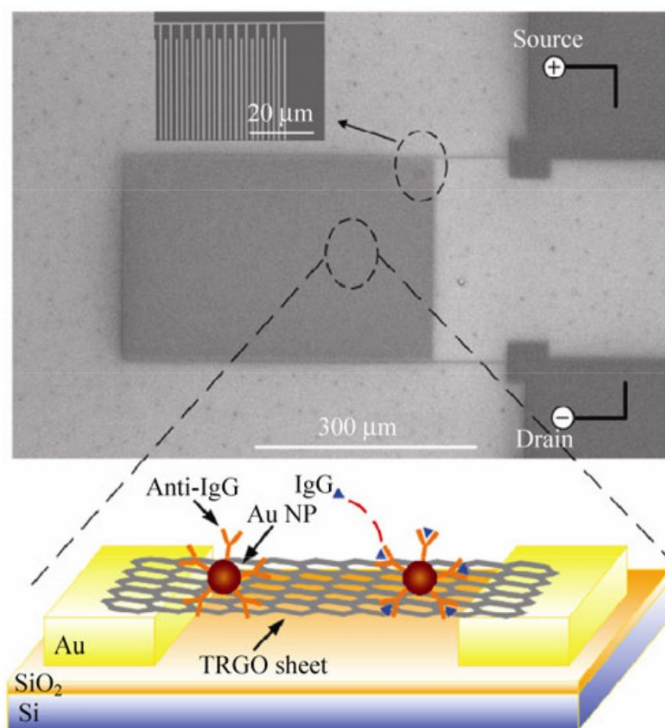


**Figure 2.16.** SEM image and correspondent depiction of thermally-reduced graphene oxide (TRGO) based FET for specific protein detection (IgG). The detection is performed through gold NP-antigen conjugates over the graphene surface (figure taken from [80]).

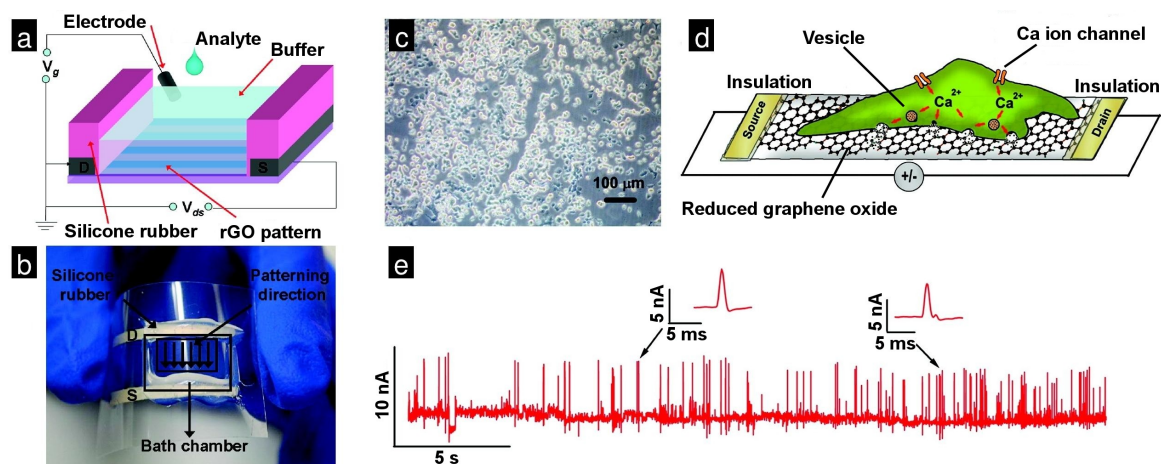


**Figure 2.17.** (a) Schematic illustration of experimental setup of a graphene-FET for biosensing applications. (b) Photograph of a patterned reduced graphene oxide (rGO) sensing device on a polyethylene terephthalate (PET) film. (c) An optical image and (d) schematic illustration of PC12 cells grown on a poly-L-lysine coated rGO-FET fabricated on a PET substrate. (e) The real-time response of the rGO-FET to the vesicular secretion of neurotransmitters from PC12 cells stimulated by a high  $K^+$  concentration solution (figure adapted from [81]).

Another optical enhancement effect which has been intensively explored in the last few years is the use of graphene for surface enhanced Raman scattering (G-SERS). The utility of Raman spectroscopy for multiple fields is well established; in the fields of life sciences and biotechnology research, it is used for the detection of several chemical species by their characteristic spectra, which serve as “fingerprints”; the technique is even capable of detecting important physico-chemical processes related with charge transfer events, for example [98, 99]. Figure 2.21A shows the schematics for the preparation of a proposed G-SERS substrate based in the combination of monolayer graphene (1LG) and a nanostructured metallic film (Au or Ag), which is commonly used for conventional SERS. The resulting spectra depict a cleaner and more stable enhancement effect when a graphene layer is deposited below the metallic nanopatterned layer (see figure 2.21B-C), avoiding undesirable chemical interactions between the analyte (R6G or CuPc) with the metal film, as well as inherent photodegradation of the analyte molecules (figure 2.21D) [100].

Regarding the use of doped nanostructures for optical biodetection, the field is still relatively unexplored. In fact, there are only few reports addressing the use of doped graphene for SERS [101, 102], one of which was published by our group on the use of nitrogen-doped graphene for the detection of Rhodamine B (see figure 2.22). The Raman

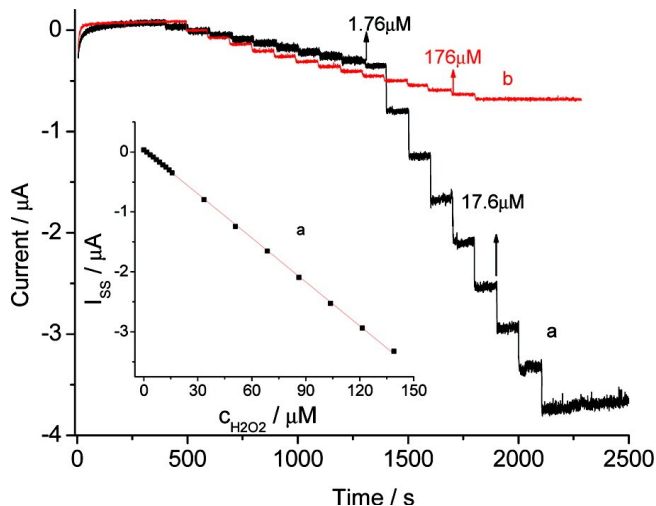


**Figure 2.18.** Current–time curve of (a)  $\text{CN}_x$ /Glassy-carbon electrode and (b) MWCNT/Glassy-carbon electrode with successive addition of  $\text{H}_2\text{O}_2$  (indicated by arrows for marked concentrations) in 0.10 M, pH 7.4, phosphate buffered saline at an applied potential of +0.3 V (vs saturated calomel electrode). Inset: calibration plots illustrating the linear electrode response to  $\text{H}_2\text{O}_2$  addition (figure taken from [87]).

scattering signal was clearly enhanced for N-graphene in comparison to the undoped one, at least for the specific fluorescent molecule analyzed. This improvement is attributed to the enhanced charge transfer capabilities of N-doped graphene, which in turn contributes to higher polarizability of the probe molecules adsorbed over the carbon lattice and an associated increase in vibrational Raman modes intensities [103]. The use of doped graphene for SERS deserves further exploration, as it could be a good substrate, potentially easier and cheaper than noble metal films, for detection of biomolecules.

### 2.2.3 Bioelectronic interfaces

The novel characteristics of carbon nanostructures, specially from the electronic standpoint, are currently fueling an important amount of research towards their incorporation of complex devices for bioelectronic applications. Moreover, their advantages on chemical flexibility and biocompatibility suggest that they can become very important materials for the development of bioelectronic devices that would be usable *in-vivo*, either for real-time monitoring of physiological parameters and/or controlled drug delivery, within an implantable bio-nano/micro-electro-mechanical-system framework, for instance. Research

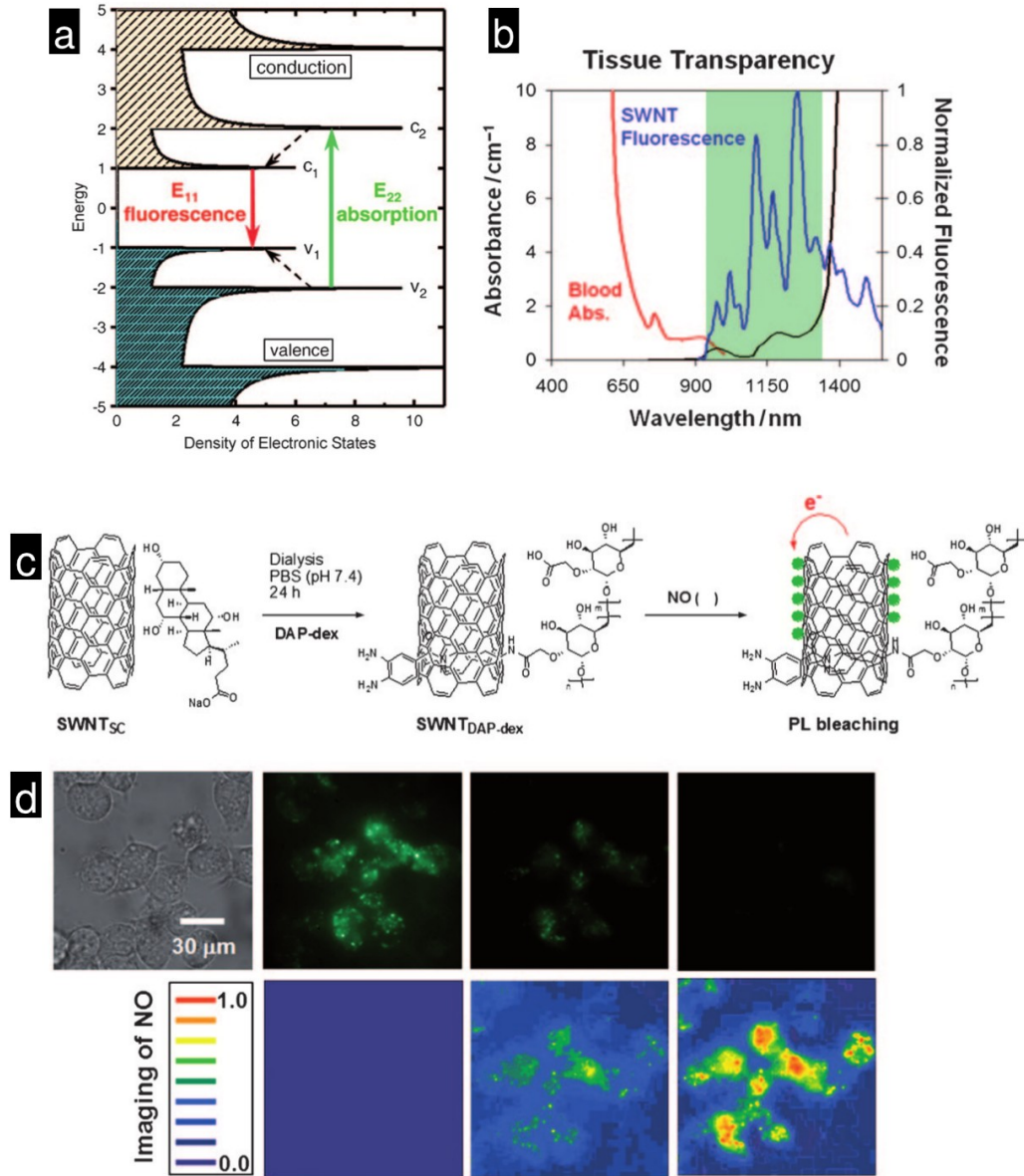


**Figure 2.19.** (a) Schematic DOS for a SWNT. Solid arrows depict the optical excitation and emission transitions; dashed arrows denote non-radiative relaxations of electrons and holes (figure taken from [91]). (b) SWNTs fluoresce primarily in the near-infrared regime (820-1600 nm<sup>-1</sup>). Blood and water absorbance mainly occurs in the visible and infrared regimes, respectively (figure adapted from [92]). (c) Scheme of SWNT wrapping with 3,4-diaminophenyl-functionalized dextran (DAP-dex) for selective optical response to NO presence. The analyte is detected by SWNT fluorescence quenching, produced by electron transfer from SWNT to NO molecules. (d) Detection and imaging of endogenous NO inside macrophage cells, showing the spatio-temporal information of NO production in living cells (figure adapted from [95]).

that can lead to such advanced devices is still scarce. Some examples are reports on the use of CNTs based fuel cells for power generation using circulating glucose redox reactions [104] and skin-like transparent films for pressure and strain sensing [105]. Within this context, carbon nanostructures are natural strong candidates for improvements on current neural interfacing technologies, with several reports suggesting consistent enhancements on impedance magnitudes and charge transfer capabilities for neural electrodes modified with CNTs [106-108]. For instance, figure 2.23a-f shows SEM images of tungsten/stainless steel neural electrodes which have been coated with MWNTs and how this affects their electrical characteristics. Figure 2.23a-c present the results for tungsten implantable electrodes coated only with MWNTs, where a significant increase of charge transfer and decreasing phase angle are observed. The combination of CNTs with conductive polymers such as polypyrrole (PPy) can further enhance the impedance and charge transfer performance of electrodes used in biological environments. Figure 2.23d-f shows an SEM image of stainless steel neural electrode with attached islands of MWNTs/PPy, the electrical characterization shows that the charge transfer capabilities are greatly augmented (1600-fold), with a significant impedance reduction. It is worth noting that such results included *in vivo* tests, either in the motor cortex of anesthetized rats or the visual cortex area V4 of monkey, with

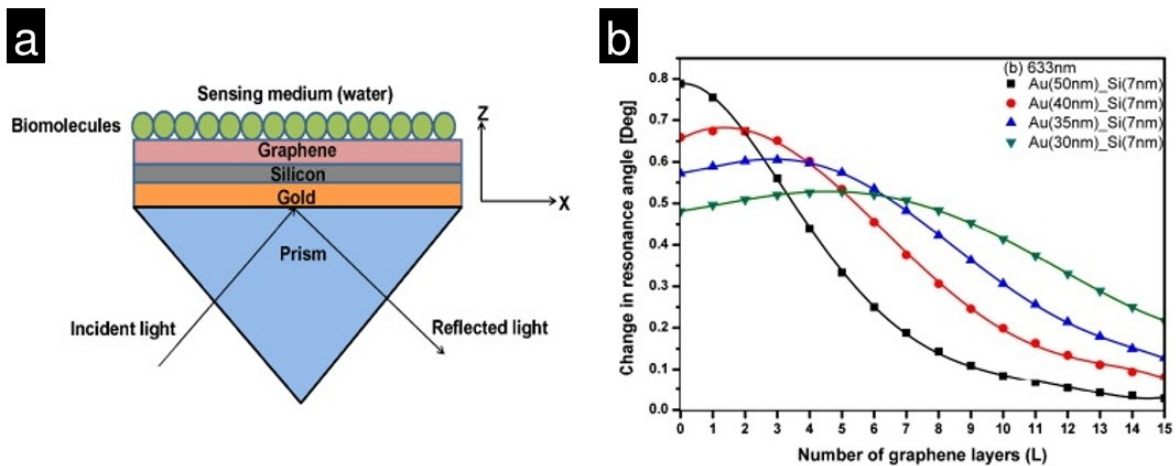


**Figure 2.20.** (a) Schematic diagram of a prism based surface-plasmon-resonance (SPR) biosensor, using graphene, silicon and gold layers. (b) Variation of change in resonance angle due to the adsorption of biomolecules with different layers of graphene for different thicknesses of gold and 7.0 nm silicon layer, using an excitation wavelength of 633 nm. The symbols correspond to the values obtained from the simulated results while the continuous lines are the best fit curves through these symbols (figures adapted from [97]).

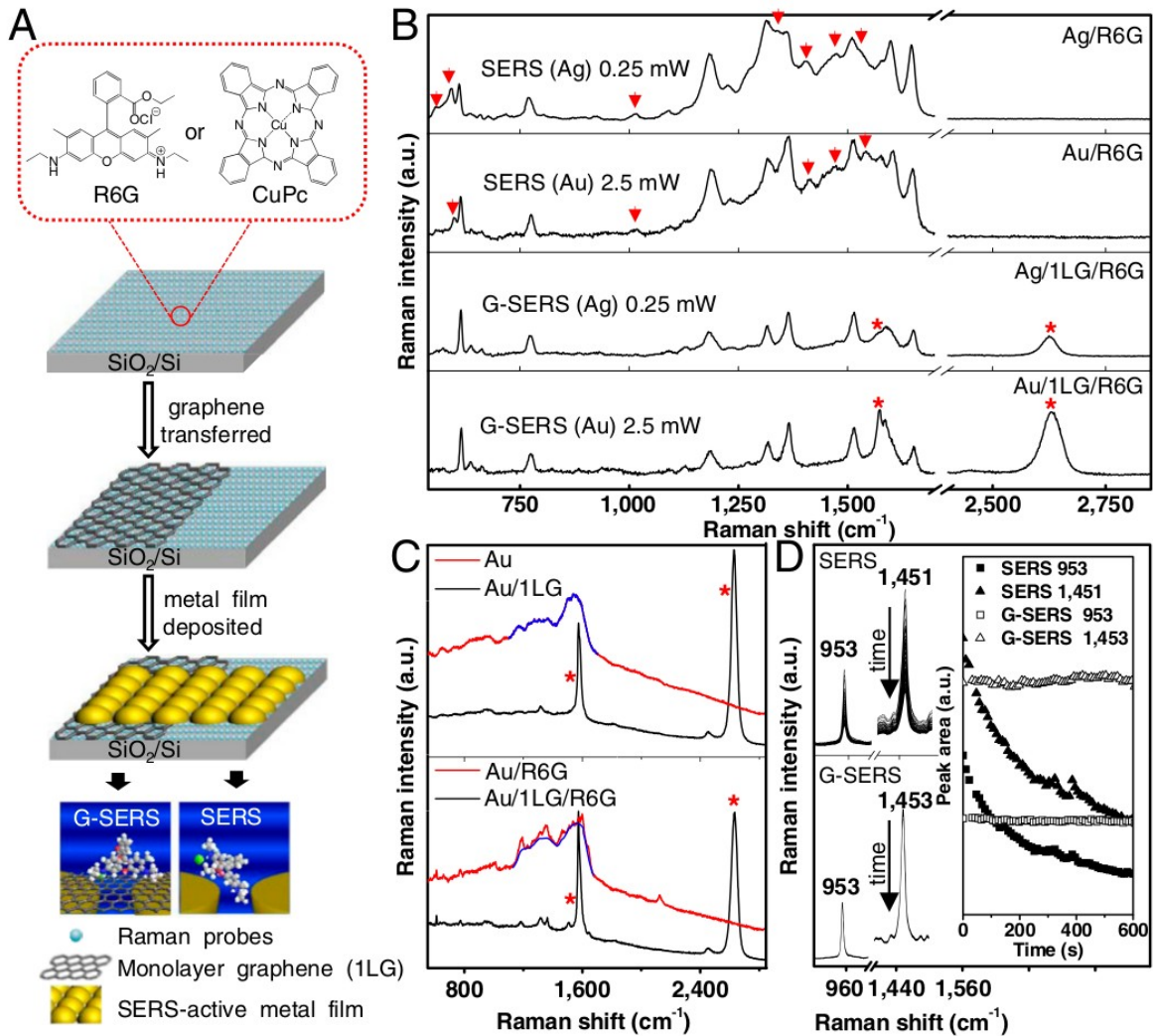


**Figure 2.21.** Comparison of signals from a G-SERS substrate and a normal SERS substrate. **(A)** Schematic for sample preparation with G-SERS and SERS regions on a  $\text{SiO}_2/\text{Si}$  substrate. **(B)** SERS and G-SERS spectra of rhodamine-6g (R6G) with gold and silver nanoislands used as an electromagnetic enhancer, respectively. Red arrows point to additional and non-reproducible peaks in spectra of normal SERS. **(C)** Photocarbonization effect (which causes a background at  $1100 \sim 1700 \text{ cm}^{-1}$ ) in SERS and G-SERS substrates. **(D)** Stability of the SERS (top) and G-SERS (bottom) spectra of CuPc in a time series of 600 s. The inset shows the integrated intensity of the peaks (at  $953;1451 \text{ cm}^{-1}$  for SERS, and  $953;1453 \text{ cm}^{-1}$  for G-SERS, respectively) change with the increased acquisition time. Time sequence: from top to bottom. “\*” in B and C marks the G-band ( $\sim 1570 \text{ cm}^{-1}$ ) and G'-band ( $\sim 2625 \text{ cm}^{-1}$ ) of 1LG (figure taken from [100]).

results clearly indicating an improved electro-chemical and functional performance, which is crucial for efficient neurophysiological recordings [109].

Carbon nanostructures can contribute as well to neural interfaces for the study of nerve networking and stimulation. One example is the microelectrode array shown in figure 2.24, where the main cell-contacting areas are formed by CNTs bundles, with dual capabilities in terms of activity recording and stimulation, and with spatial configuration that allows complex analysis of inter-neural communication [110]. These type of devices can contribute to the elucidation of actual neural processes occurring at the cognitive level, and the enhancements that nanocarbons are offering will impact positively in the efficiency of these technologies.

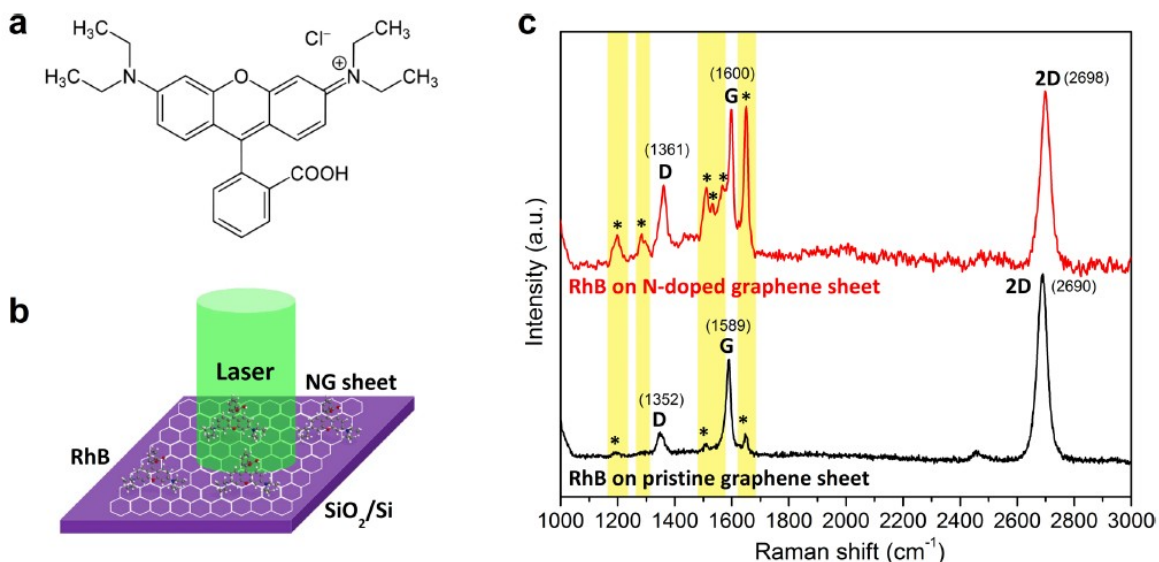


**Figure 2.22.** Enhanced Raman scattering effect of nitrogen doped graphene (NG) sheets for probing Rhodamine B (RhB) molecules. **(a)** Molecular structure of RhB. **(b)** Schematic illustration of experimental setup. RhB molecules are anchored onto NG sheet/SiO<sub>2</sub>/Si substrate. The laser line is 514 nm. **(c)** Raman signals of RhB molecules on pristine and NG sheets. The peaks marked with “\*” are the corresponding signals from RhB molecules. Note that there is a peak of RhB at 1597 cm<sup>-1</sup>, which is overlapped with the G-band of graphene sheets (figure taken from [103]).

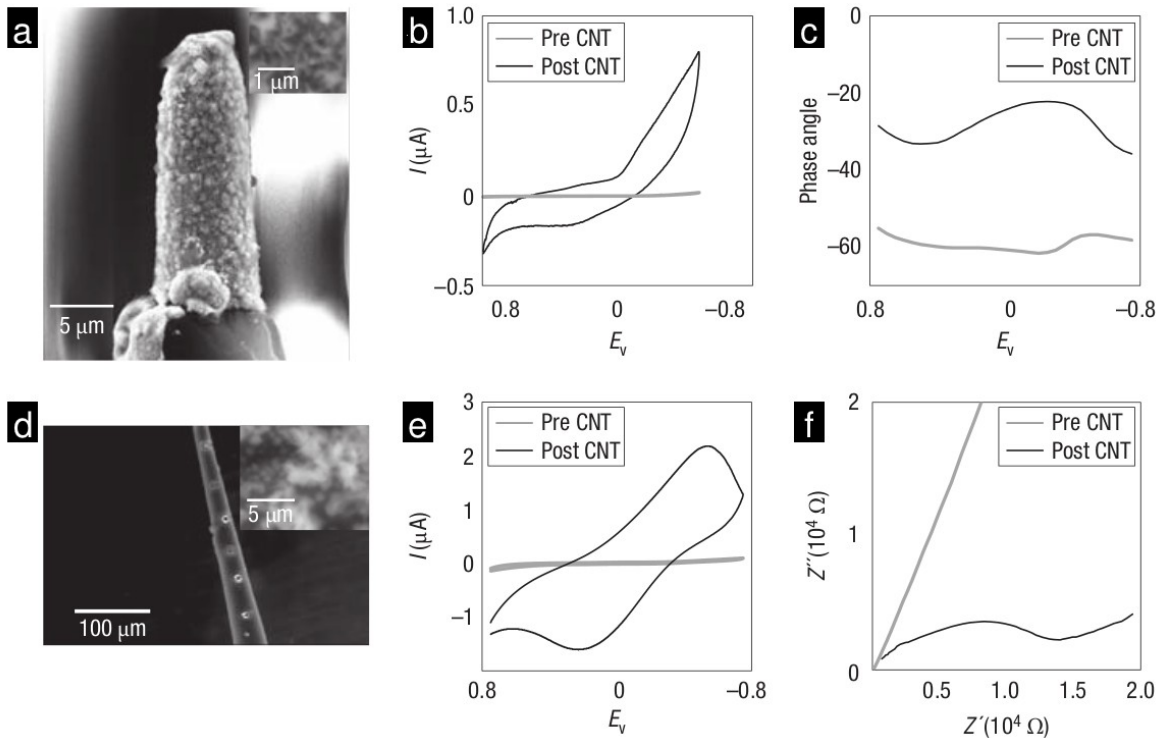


**Figure 2.23.** (a) CNTs covalently attached to a sharp tungsten electrode. Covalent coating of CNTs increased the charge transfer (b) and decreased the phase angle (c). (d) Parylene insulation on the electrode removed by UV laser. The image shows the exposed stainless steel shaft. (e) The CNT–PPy coatings increased charge transfer by a factor of 1,600. (f) Complex-impedance plots show that enhanced charge transfer results from a drop in the real ( $Z'$ ) and imaginary ( $Z''$ ) components of the impedance (taken from [109]).

## Conclusions

The incursion of nanotechnology in life sciences and biotechnological research is underway, and the results so far can be considered exceptionally promising. And even though the application of nanostructures encompasses a wide variety of materials, carbon nanotechnology stands as a very important theme in these research topics.

Among carbon nanostructures, CNTs and graphene are the ones receiving the most attention for the development of nanobiotechnological applications. This is because of their extraordinary electric, mechanical and chemical characteristics, which can be combined with the characteristics of other materials and biomolecules in order to confer specific



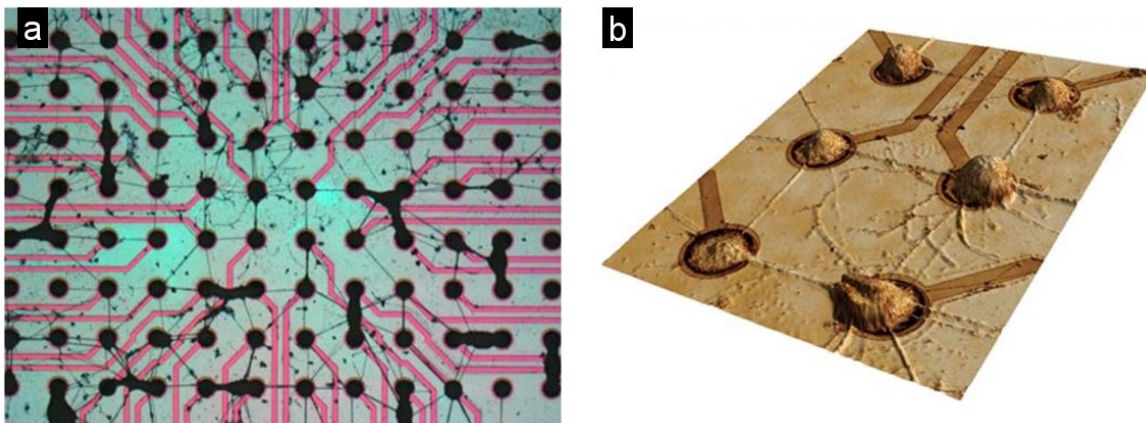


**Figure 2.24.** (a) Neuronal network grown on a CNT neuro-chip for neural activity recording and controlled stimulation. (b) Detail of six interface contacts with neurons growing on top (figures from [110]).

features such as biocompatibility, pharmaceutical activity, specific biosensing capabilities and improved functionality. This flexibility is a unique advantage of carbon nanostructures that has just started to be exploited. Nevertheless, some issues about toxicity concerns and other potential undesirable effects need to be addressed, and are being investigated from diverse standpoints in order to completely establish the feasibility of carbon bionanotechnology.

Finally, another important aspect about carbon nanostructures that has not been explored that much for biological applications, and that can potentially contribute to even more advantages, is the tailoring of nanocarbons through doping. Here, some preliminary works on the use of nitrogen- and boron-doped CNTs have been cited, with results suggesting greater benefits in terms of biocompatibility, chemical activity and charge transfer capabilities contrasted with their undoped counterparts. This in turn could make doped nanostructures a more feasible material for nanobiotechnological developments, considering all the advances that have been achieved by pure carbon nanomaterials.

## **Bibliography**

- [1] R. A. Vaia, "Nanomaterials and future aerospace technologies: opportunities and challenges," On-line information for the Defense Community, [<http://www.dtic.mil/dtic/tr/fulltext/u2/a469619.pdf>], accessed on 9/14/2013.
- [2] W. Lu and C. M. Lieber, "Nanoelectronics from the bottom up.," *Nature Materials*, vol. 6, no. 11, pp. 841–50, 2007.
- [3] M. Haselman and S. Hauck, "The Future of Integrated Circuits: A Survey of Nanoelectronics," *Proceedings of the IEEE*, vol. 98, no. 1, pp. 11–38, 2010.
- [4] T. Umeyama and H. Imahori, "Carbon nanotube-modified electrodes for solar energy conversion," *Energy & Environmental Science*, vol. 1, no. 1, pp. 120-133, 2008.
- [5] C. Liu, F. Li, L.-P. Ma, and H.-M. Cheng, "Advanced materials for energy storage", *Advanced Materials*, vol. 22, no. 8, pp. E28–62, 2010.
- [6] N. Vigneshwaran, S. Kumar, A. A. Kathe, P. V Varadarajan, and V. Prasad, "Functional finishing of cotton fabrics using zinc oxide–soluble starch nanocomposites", *Nanotechnology*, vol. 17, no. 20, pp. 5087–5095, 2006.
- [7] T.-H. Kabri, E. Arab-Tehrany, N. Belhaj, and M. Linder, "Physico-chemical characterization of nano-emulsions in cosmetic matrix enriched on omega-3.," *Journal of Nanobiotechnology*, vol. 9, article no. 41, 2011.
- [8] J. A. Ascencio, M. Pérez, and M. José-Yacamán, "A truncated icosahedral structure observed in gold nanoparticles," *Surface Science*, vol. 447, no. 1–3, pp. 73–80, 2000.
- [9] "Nanowires and Nanowire Devices - Electronic Materials and Devices - Interdisciplinary Research Strengths - Materials Research Institute." [[http://www.mri.psu.edu/research/strengths/electronic\\_materials/nanowires/](http://www.mri.psu.edu/research/strengths/electronic_materials/nanowires/)], accessed on 9/14/2013.
- [10] K. Lu, L. Guo, A. K. Mehta, W. S. Childers, S. N. Dublin, S. Skanthakumar, V. P. Conticello, P. Thiyagarajan, R. P. Apkarian, and D. G. Lynn, "Macroscale assembly of peptide nanotubes", *Chemical Communications*, no. 26, pp. 2729–31, 2007.
- [11] "Kojima laboratory N2RC Osaka Prefecture University Japan." [[http://www.nanosq.21c.osakafu-u.ac.jp/ttsl\\_lab/c\\_kojima/e\\_kojima\\_research2.html](http://www.nanosq.21c.osakafu-u.ac.jp/ttsl_lab/c_kojima/e_kojima_research2.html)], accessed on 9/14/2013.
- [12] R. Bardhan, N. K. Grady, J. R. Cole, A. Joshi, and N. J. Halas, "Fluorescence

- enhancement by Au nanostructures: nanoshells and nanorods.,” *ACS Nano*, vol. 3, no. 3, pp. 744–52, 2009.
- [13] R. Dastjerdi and M. Montazer, “A review on the application of inorganic nanostructured materials in the modification of textiles: focus on anti-microbial properties.,” *Colloids and Surfaces. B, Biointerfaces*, vol. 79, no. 1, pp. 5–18, 2010.
- [14] Y. Xu, M. Mahmood, Z. Li, E. Dervishi, S. Trigwell, V. P. Zharov, N. Ali, V. Saini, A. R. Biris, D. Lupu, D. Boldor, and A. S. Biris, “Cobalt nanoparticles coated with graphitic shells as localized radio frequency absorbers for cancer therapy.,” *Nanotechnology*, vol. 19, no. 43, p. 435102, 2008.
- [15] K. Bosnick, M. Maillard, and L. Brus, “Single Molecule Raman Spectroscopy at the Junctions of Large Ag Nanocrystals,” *The Journal of Physical Chemistry B*, vol. 107, no. 37, pp. 9964–9972, 2003.
- [16] J. Gao, H. Gu, and B. Xu, “Multifunctional magnetic nanoparticles: design, synthesis, and biomedical applications.,” *Accounts of Chemical Research*, vol. 42, no. 8, pp. 1097–107, 2009.
- [17] S. A. Maier and H. A. Atwater, “Plasmonics: Localization and guiding of electromagnetic energy in metal/dielectric structures,” *Journal of Applied Physics*, vol. 98, no. 1, p. 011101, 2005.
- [18] F. Tam, G. P. Goodrich, B. R. Johnson, and N. J. Halas, “Plasmonic enhancement of molecular fluorescence.,” *Nano Letters*, vol. 7, no. 2, pp. 496–501, 2007.
- [19] B. S. Kalanoor, P. B. Bisht, S. A. Ali, T. T. Baby, and S. Ramaprabhu, “Optical nonlinearity of silver-decorated graphene.” *Journal of the Optical Society of America B: Optical Physics*, vol. 29, no. 4, pp. 669-675, 2012.
- [20] N. Misra, J. A. Martinez, S.-C. J. Huang, Y. Wang, P. Stroeve, C. P. Grigoropoulos, and A. Noy, “Bioelectronic silicon nanowire devices using functional membrane proteins.,” *Proceedings of the National Academy of Sciences of the United States of America*, vol. 106, no. 33, pp. 13780–13784, 2009.
- [21] M. Murata, H. Yamamoto, F. Tsunemi, Y. Hasegawa, and T. Komine, “Four-Wire Resistance Measurements of a Bismuth Nanowire Encased in a Quartz Template Utilizing Focused Ion Beam Processing,” *Journal of Electronic Materials*, vol. 41, no. 6, pp. 1442–1449, 2012.
- [22] M. Yang, F. Qu, Y. Lu, Y. He, G. Shen, and R. Yu, “Platinum nanowire nanoelectrode array for the fabrication of biosensors.,” *Biomaterials*, vol. 27, no. 35, pp. 5944–50, 2006.

- [23] X. Hong and Y. Wang, "Partial oxidation of methane to syngas catalyzed by a nickel nanowire catalyst," *Journal of Natural Gas Chemistry*, vol. 18, no. 1, pp. 98–103, 2009.
- [24] M. Willander, O. Nur, M. Fakhar-e-Alam, J. R. Sadaf, M. Q. Israr, K. Sultana, S. M. U. Ali, and M. H. Asif, "Applications of zinc oxide nanowires for bio-photonics and bio-electronics", *SPIE Newsroom*, [[http://spie.org/documents/Newsroom/Imported/003498/003498\\_10.pdf](http://spie.org/documents/Newsroom/Imported/003498/003498_10.pdf)], accessed on 9/14/2013.
- [25] Q. Li, K. R. Westlake, M. H. Crawford, S. R. Lee, D. D. Koleske, J. J. Figiel, K. C. Cross, S. Fatholouloumi, Z. Mi, and G. T. Wang, "Optical performance of top-down fabricated InGaN/GaN nanorod light emitting diode arrays," *Optics Express*, vol. 19, no. 25, p. 25528, 2011.
- [26] T. Chiaramonte, L. H. G. Tizei, D. Ugarte, and M. A. Cotta, "Kinetic effects in InP nanowire growth and stacking fault formation: the role of interface roughening.," *Nano Letters*, vol. 11, no. 5, pp. 1934–40, 2011.
- [27] W. Kim, J. K. Ng, M. E. Kunitake, B. R. Conklin, and P. Yang, "Interfacing silicon nanowires with mammalian cells.," *Journal of the American Chemical Society*, vol. 129, no. 23, pp. 7228–9, 2007.
- [28] A. Kumar, S. Aravamudhan, M. Gordic, S. Bhansali, and S. S. Mohapatra, "Ultrasensitive detection of cortisol with enzyme fragment complementation technology using functionalized nanowire.," *Biosensors & Bioelectronics*, vol. 22, no. 9–10, pp. 2138–44, 2007.
- [29] T.-S. Pui, A. Agarwal, F. Ye, Y. Huang, and P. Chen, "Nanoelectronic detection of triggered secretion of pro-inflammatory cytokines using CMOS compatible silicon nanowires.," *Biosensors & Bioelectronics*, vol. 26, no. 5, pp. 2746–50, 2011.
- [30] C. Baratto, S. Todros, E. Comini, G. Faglia, M. Ferroni, G. Sberveglieri, G. Andreano, L. Cellai, A. Flamini, G. Marrazza, A. Nannini, G. Pennelli, and M. Piotto, "SnO<sub>2</sub> nanowire bio-transistor for electrical DNA sensing", *IEEE Sensors 2007 International Conference*, [DOI: 10.1109/ICSENS.2007.4388606].
- [31] J. A. Streifer, H. Kim, B. M. Nichols, and R. J. Hamers, "Covalent functionalization and biomolecular recognition properties of DNA-modified silicon nanowires," *Nanotechnology*, vol. 16, no. 9, pp. 1868–1873, 2005.
- [32] O. C. Aktas, M. Sander, M. M. Miró, J. Lee, C. K. Akkan, H. Smail, A. Ott, and M. Veith, "Enhanced fibroblast cell adhesion on Al/Al<sub>2</sub>O<sub>3</sub> nanowires," *Applied Surface Science*, vol. 257, no. 8, pp. 3489–3494, 2011.
- [33] M. R. Abidian and D. C. Martin, "Experimental and theoretical characterization of

- implantable neural microelectrodes modified with conducting polymer nanotubes.,” *Biomaterials*, vol. 29, no. 9, pp. 1273–83, 2008.
- [34] “The Ups and Downs of Nanobiotech | The Scientist Magazine”, [<http://www.the-scientist.com/?articles.view/articleNo/15869>], accessed on 9/14/2013.
- [35] C. C. Lee, J. A. MacKay, J. M. J. Fréchet, and F. C. Szoka, “Designing dendrimers for biological applications.,” *Nature Biotechnology*, vol. 23, no. 12, pp. 1517–26, 2005.
- [36] E. K.-H. Chow, E. Pierstorff, G. Cheng, and D. Ho, “Copolymeric Nanofilm Platform for Controlled and Localized Therapeutic Delivery,” *ACS Nano*, vol. 2, no. 1, pp. 33–40, 2008.
- [37] C. Cho, I. Park, J. Nah, and T. Akaike, “Preparation of polymeric self-assembly and its application to biomaterials”, *Macromolecular Research*, vol. 11, no. 1, pp. 2-8, 2003.
- [38] S. Ilbasmiş-Tamer, Ş. Yılmaz, E. Banoğlu, and I. T. Değim, “Carbon Nanotubes to Deliver Drug Molecules,” *Journal of Biomedical Nanotechnology*, vol. 6, no. 1, pp. 20–27, 2010.
- [39] P. Milla, F. Dosio, and L. Cattel, “PEGylation of Proteins and Liposomes: a Powerful and Flexible Strategy to Improve the Drug Delivery”, *Current Drug Metabolism*, vol. 13, no. 1, pp. 105-119, 2012.
- [40] D. Astruc, E. Boisselier, and C. Ornelas, “Dendrimers designed for functions: from physical, photophysical, and supramolecular properties to applications in sensing, catalysis, molecular electronics, photonics, and nanomedicine.,” *Chemical Reviews*, vol. 110, no. 4, pp. 1857–959, 2010.
- [41] J. I. Yeh, A. Lazareck, J. H. Kim, J. Xu, and S. Du, “Peptide nanowires for coordination and signal transduction of peroxidase biosensors to carbon nanotube electrode arrays.,” *Biosensors & Bioelectronics*, vol. 23, no. 4, pp. 568–74, 2007.
- [42] F. Rahmat, N. Thamwattana, and B. J. Cox, “Modelling peptide nanotubes for artificial ion channels.,” *Nanotechnology*, vol. 22, no. 44, p. 445707, 2011.
- [43] J. Fu, M. Liu, Y. Liu, and H. Yan, “Spatially-interactive biomolecular networks organized by nucleic acid nanostructures.,” *Accounts of Chemical Research*, vol. 45, no. 8, pp. 1215–26, 2012.
- [44] K. Halvorsen and W. P. Wong, “Binary DNA nanostructures for data encryption.,” *PLoS One*, vol. 7, no. 9, p. e44212, 2012.
- [45] H. Yan, S. H. Park, G. Finkelstein, J. H. Reif, and T. H. LaBean, “DNA-templated

- self-assembly of protein arrays and highly conductive nanowires.,” *Science*, vol. 301, no. 5641, pp. 1882–4, 2003.
- [46] A. V Pinheiro, D. Han, W. M. Shih, and H. Yan, “Challenges and opportunities for structural DNA nanotechnology.,” *Nature Nanotechnology*, vol. 6, no. 12, pp. 763–72, 2011.
- [47] D. Tasis, N. Tagmatarchis, A. Bianco, and M. Prato, “Chemistry of Carbon Nanotubes,” *Chemical Reviews*, vol. 106, no. 3, pp. 1105–1136, 2006.
- [48] S. Banerjee, T. Hemraj Benny, and S. S. Wong, “Covalent surface chemistry of single walled carbon nanotubes,” *Advanced Materials*, vol. 17, no. 1, pp. 17–29, 2005.
- [49] K. A. Williams, P. T. M. Veenhuizen, B. G. de la Torre, R. Eritja, and C. Dekker, “Nanotechnology: carbon nanotubes with DNA recognition.,” *Nature*, vol. 420, no. 6917, p. 761, 2002.
- [50] E. Heister, C. Lamprecht, V. Neves, C. Tîlmaciu, L. Datas, E. Flahaut, B. Soula, P. Hinterdorfer, H. M. Coley, S. R. P. Silva, and J. McFadden, “Higher dispersion efficacy of functionalized carbon nanotubes in chemical and biological environments.,” *ACS Nano*, vol. 4, no. 5, pp. 2615–2626, 2010.
- [51] Z. Liu, F. Galli, K. G. H. Janssen, L. Jiang, H. J. van der Linden, D. C. de Geus, P. Voskamp, M. E. Kuil, R. C. L. Olsthoorn, T. H. Oosterkamp, T. Hankemeier, and J. P. Abrahams, “Stable Single-Walled Carbon Nanotube–Streptavidin Complex for Biorecognition”, *Journal of Physical Chemistry C*, vol. 114, no. 10, pp. 4345–4352, 2010.
- [52] S. K. Bhunia and N. R. Jana, “Peptide-functionalized colloidal graphene via interdigitated bilayer coating and fluorescence turn-on detection of enzyme.,” *ACS Applied Materials & Interfaces*, vol. 3, no. 9, pp. 3335–3341, 2011.
- [53] X. Sun, Z. Liu, K. Welsher, J. T. Robinson, A. Goodwin, S. Zaric, and H. Dai, “Nano-Graphene Oxide for Cellular Imaging and Drug Delivery.,” *Nano Research*, vol. 1, no. 3, pp. 203–212, 2008.
- [54] D. Eder, “Carbon nanotube-inorganic hybrids.,” *Chemical Reviews*, vol. 110, no. 3, pp. 1348–1385, 2010.
- [55] K. Jo, T. Lee, H. J. Choi, J. H. Park, D. J. Lee, D. W. Lee, and B.-S. Kim, “Stable aqueous dispersion of reduced graphene nanosheets via non-covalent functionalization with conducting polymers and application in transparent electrodes.,” *Langmuir*, vol. 27, no. 5, pp. 2014–2018, 2011.

- [56] R. J. Chen, S. Bangsaruntip, K. A. Drouvalakis, N. W. S. Kam, M. Shim, Y. Li, W. Kim, P. J. Utz, and H. Dai, "Noncovalent functionalization of carbon nanotubes for highly specific electronic biosensors.," *Proceedings of the National Academy of Sciences of the United States of America*, vol. 100, no. 9, pp. 4984–4989, 2003.
- [57] Q. Chen, W. Wei, and J.-M. Lin, "Homogeneous detection of concanavalin A using pyrene-conjugated maltose assembled graphene based on fluorescence resonance energy transfer.," *Biosensors & Bioelectronics*, vol. 26, no. 11, pp. 4497–4502, 2011.
- [58] K. Kostarelos, "The long and short of carbon nanotube toxicity.," *Nature Biotechnology*, vol. 26, no. 7, pp. 774–776, 2008.
- [59] Y. Zhang, S. F. Ali, E. Dervishi, Y. Xu, Z. Li, D. Casciano, and A. S. Biris, "Cytotoxicity effects of graphene and single-wall carbon nanotubes in neural pheochromocytoma-derived PC12 cells.," *ACS Nano*, vol. 4, no. 6, pp. 3181–6, 2010.
- [60] P. Wick, P. Manser, L. K. Limbach, U. Dettlaff-Weglikowska, F. Krumeich, S. Roth, W. J. Stark, and A. Bruinink, "The degree and kind of agglomeration affect carbon nanotube cytotoxicity.," *Toxicology Letters*, vol. 168, no. 2, pp. 121–31, 2007.
- [61] A. S. Karakoti, L. L. Hench, and S. Seal, "The potential toxicity of nanomaterials—The role of surfaces," *JOM*, vol. 58, no. 7, pp. 77–82, 2006.
- [62] J. C. Carrero-Sanchez, A. L. Elías, R. Mancilla, G. Arrellín, H. Terrones, J. P. Laclette, and M. Terrones, "Biocompatibility and toxicological studies of carbon nanotubes doped with nitrogen.," *Nano Letters*, vol. 6, no. 8, pp. 1609–16, 2006.
- [63] V. P. Torchilin, "Recent advances with liposomes as pharmaceutical carriers.," *Nature reviews. Drug Discovery*, vol. 4, no. 2, pp. 145–60, 2005.
- [64] V. P. Torchilin, "Structure and design of polymeric surfactant-based drug delivery systems," *Journal of Controlled Release*, vol. 73, no. 2–3, pp. 137–172, 2001.
- [65] T. B. Lentz, S. J. Gray, and R. J. Samulski, "Viral vectors for gene delivery to the central nervous system.," *Neurobiology of Disease*, vol. 48, no. 2, pp. 179–88, 2012.
- [66] A. Bianco, K. Kostarelos, and M. Prato, "Applications of carbon nanotubes in drug delivery.," *Current Opinion in Chemical Biology*, vol. 9, no. 6, pp. 674–9, 2005.
- [67] E. Heister, V. Neves, C. Tîlmaciu, K. Lipert, V. S. Beltrán, H. M. Coley, S. R. P. Silva, and J. McFadden, "Triple functionalisation of single-walled carbon nanotubes with doxorubicin, a monoclonal antibody, and a fluorescent marker for targeted cancer therapy," *Carbon*, vol. 47, no. 9, pp. 2152–2160, 2009.

- [68] K. Awasthi, D. P. Singh, S. K. Singh, D. Dash, and O. N. Srivastava, "Attachment of biomolecules (protein and DNA) to amino-functionalized carbon nanotubes," *New Carbon Materials*, vol. 24, no. 4, pp. 301–306, 2009.
- [69] Y. Liu, D.-C. Wu, W.-D. Zhang, X. Jiang, C.-B. He, T. S. Chung, S. H. Goh, and K. W. Leong, "Polyethylenimine-grafted multiwalled carbon nanotubes for secure noncovalent immobilization and efficient delivery of DNA.," *Angewandte Chemie*, vol. 44, no. 30, pp. 4782–5, 2005.
- [70] N. Jia, Q. Lian, H. Shen, C. Wang, X. Li, and Z. Yang, "Intracellular delivery of quantum dots tagged antisense oligodeoxynucleotides by functionalized multiwalled carbon nanotubes.," *Nano Letters*, vol. 7, no. 10, pp. 2976–80, 2007.
- [71] D.-H. Jung, B. H. Kim, Y. T. Lim, J. Kim, S. Y. Lee, and H.-T. Jung, "Fabrication of single-walled carbon nanotubes dotted with Au nanocrystals: Potential DNA delivery nanocarriers," *Carbon*, vol. 48, no. 4, pp. 1070–1078, 2010.
- [72] L. Lacerda, A. Bianco, M. Prato, and K. Kostarelos, "Carbon nanotube cell translocation and delivery of nucleic acids in vitro and in vivo," *Journal of Materials Chemistry*, vol. 18, no. 1, p. 17, 2008.
- [73] L. Zhang, J. Xia, Q. Zhao, L. Liu, and Z. Zhang, "Functional graphene oxide as a nanocarrier for controlled loading and targeted delivery of mixed anticancer drugs", *Small*, vol. 6, no. 4, pp. 537–44, 2010.
- [74] K. Liu, J.-J. Zhang, F.-F. Cheng, T.-T. Zheng, C. Wang, and J.-J. Zhu, "Green and facile synthesis of highly biocompatible graphene nanosheets and its application for cellular imaging and drug delivery," *Journal of Materials Chemistry*, vol. 21, no. 32, p. 12034, 2011.
- [75] "Johnson Group: Experimental Nanoscale Physics - Research."  
[<http://www.lrsm.upenn.edu/~nanophys/biosensors.html>], accessed on 9/14/2013.
- [76] H. G. Sudibya, J. Ma, X. Dong, S. Ng, L.-J. Li, X.-W. Liu, and P. Chen, "Interfacing glycosylated carbon-nanotube-network devices with living cells to detect dynamic secretion of biomolecules.," *Angewandte Chemie*, vol. 48, no. 15, pp. 2723–6, 2009.
- [77] Y. Ohno, K. Maehashi, Y. Yamashiro, and K. Matsumoto, "Electrolyte-Gated Graphene Field-Effect Transistors for Detecting pH Protein Adsorption," *Nano Letters*, vol. 9, no. 9, pp. 3318–3322, 2009.
- [78] Y. H. Kwak, D. S. Choi, Y. N. Kim, H. Kim, D. H. Yoon, S.-S. Ahn, J.-W. Yang, W. S. Yang, and S. Seo, "Flexible glucose sensor using CVD-grown graphene-based field effect transistor.," *Biosensors & Bioelectronics*, vol. 37, no. 1, pp. 82–87.



- [79] D. Reddy, L. F. Register, G. D. Carpenter, and S. K. Banerjee, "Graphene field-effect transistors," *Journal of Physics D-Applied Physics*, vol. 44, no. 31, p. 313001, 2011.
- [80] S. Mao, K. Yu, G. Lu, and J. Chen, "Highly sensitive protein sensor based on thermally-reduced graphene oxide field-effect transistor," *Nano Research*, vol. 4, no. 10, pp. 921–930, 2011.
- [81] Q. He, H. G. Sudibya, Z. Yin, S. Wu, H. Li, F. Boey, W. Huang, P. Chen, and H. Zhang, "Centimeter-long and large-scale micropatterns of reduced graphene oxide films: fabrication and sensing applications.," *ACS Nano*, vol. 4, no. 6, pp. 3201–8, 2010.
- [82] S. Myung, A. Solanki, C. Kim, J. Park, K. S. Kim, and K.-B. Lee, "Graphene-encapsulated nanoparticle-based biosensor for the selective detection of cancer biomarkers.," *Advanced Materials*, vol. 23, no. 19, pp. 2221–5, 2011.
- [83] S.-R. Guo, J. Lin, M. Penchev, E. Yengel, M. Ghazinejad, C. S. Ozkan, and M. Ozkan, "Label Free DNA Detection Using Large Area Graphene Based Field Effect Transistor Biosensors," *Journal of Nanoscience and Nanotechnology*, vol. 11, no. 6, pp. 5258–5263, 2011.
- [84] W. Sun, Y. Bu, and Y. Wang, "Interaction between glycine/glycine radicals and intrinsic/boron-doped (8,0) single-walled carbon nanotubes: a density functional theory study.," *Journal of Physical Chemistry. B*, vol. 112, no. 48, pp. 15442–9, 2008.
- [85] C. Cazorla, "Ab initio study of the binding of collagen amino acids to graphene and A-doped (A=H, Ca) graphene," *Thin Solid Films*, vol. 518, no. 23, pp. 6951–6961, 2010.
- [86] R. Chowdhury, S. Adhikari, P. Rees, S. Wilks, and F. Scarpa, "Graphene-based biosensor using transport properties," *Physical Review B*, vol. 83, no. 4, p. 045401, 2011.
- [87] X. Xu, S. Jiang, Z. Hu, and S. Liu, "Nitrogen-doped carbon nanotubes: high electrocatalytic activity toward the oxidation of hydrogen peroxide and its application for biosensing.," *ACS Nano*, vol. 4, no. 7, pp. 4292–8, 2010.
- [88] C. Deng, J. Chen, X. Chen, C. Xiao, L. Nie, and S. Yao, "Direct electrochemistry of glucose oxidase and biosensing for glucose based on boron-doped carbon nanotubes modified electrode.," *Biosensors & Bioelectronics*, vol. 23, no. 8, pp. 1272–7, 2008.
- [89] Z.-H. Sheng, X.-Q. Zheng, J.-Y. Xu, W.-J. Bao, F.-B. Wang, and X.-H. Xia, "Electrochemical sensor based on nitrogen doped graphene: simultaneous

- determination of ascorbic acid, dopamine and uric acid.,” *Biosensors & Bioelectronics*, vol. 34, no. 1, pp. 125–31, 2012.
- [90] Y. Wang, Y. Shao, D. W. Matson, J. Li, and Y. Lin, “Nitrogen-doped graphene and its application in electrochemical biosensing.,” *ACS Nano*, vol. 4, no. 4, pp. 1790–8, 2010.
- [91] S. M. Bachilo, M. S. Strano, C. Kittrell, R. H. Hauge, R. E. Smalley, and R. B. Weisman, “Structure-assigned optical spectra of single-walled carbon nanotubes”, *Science*, vol. 298, no. 5602, pp. 2361–6, 2002.
- [92] A. A. Boghossian, J. Zhang, P. W. Barone, N. F. Reuel, J.-H. Kim, D. A. Heller, J.-H. Ahn, A. J. Hilmer, A. Rwei, J. R. Arkalgud, C. T. Zhang, and M. S. Strano, “Near-infrared fluorescent sensors based on single-walled carbon nanotubes for life sciences applications.,” *ChemSusChem*, vol. 4, no. 7, pp. 848–63, 2011.
- [93] H. Dong, J. Zhang, H. Ju, H. Lu, S. Wang, S. Jin, K. Hao, H. Du, and X. Zhang, “Highly sensitive multiple microRNA detection based on fluorescence quenching of graphene oxide and isothermal strand-displacement polymerase reaction”, *Analytical Chemistry*, vol. 84, no. 10, pp. 4587–93, 2012.
- [94] P. S. Wate, S. S. Banerjee, A. Jalota-Badhwari, R. R. Mascarenhas, K. R. Zope, J. Khandare, and R. D. K. Misra, “Cellular imaging using biocompatible dendrimer-functionalized graphene oxide-based fluorescent probe anchored with magnetic nanoparticles.,” *Nanotechnology*, vol. 23, no. 41, p. 415101, 2012.
- [95] J.-H. Kim, D. A. Heller, H. Jin, P. W. Barone, C. Song, J. Zhang, L. J. Trudel, G. N. Wogan, S. R. Tannenbaum, and M. S. Strano, “The rational design of nitric oxide selectivity in single-walled carbon nanotube near-infrared fluorescence sensors for biological detection”, *Nature Chemistry*, vol. 1, no. 6, pp. 473–81, 2009.
- [96] L. Wang, C. Zhu, L. Han, L. Jin, M. Zhou, and S. Dong, “Label-free, regenerative and sensitive surface plasmon resonance and electrochemical aptasensors based on graphene.,” *Chemical Communications*, vol. 47, no. 27, pp. 7794–6, 2011.
- [97] R. Verma, B. D. Gupta, and R. Jha, “Sensitivity enhancement of a surface plasmon resonance based biomolecules sensor using graphene and silicon layers,” *Sensors and Actuators B: Chemical*, vol. 160, no. 1, pp. 623–631, 2011.
- [98] S. He, K.-K. Liu, S. Su, J. Yan, X. Mao, D. Wang, Y. He, L.-J. Li, S. Song, and C. Fan, “Graphene-based high-efficiency surface-enhanced Raman scattering-active platform for sensitive and multiplex DNA detection.,” *Analytical Chemistry*, vol. 84, no. 10, pp. 4622–7, 2012.
- [99] W. Ren, Y. Fang, and E. Wang, “A binary functional substrate for enrichment and

- ultrasensitive SERS spectroscopic detection of folic acid using graphene oxide/Ag nanoparticle hybrids.,” *ACS Nano*, vol. 5, no. 8, pp. 6425–33, 2011.
- [100] W. Xu, X. Ling, J. Xiao, M. S. Dresselhaus, J. Kong, H. Xu, Z. Liu, and J. Zhang, “Surface enhanced Raman spectroscopy on a flat graphene surface.,” *Proceedings of the National Academy of Sciences of the United States of America*, vol. 109, no. 24, pp. 9281–6, 2012.
- [101] X. Kong, Z. Sun, and Q. Chen, “The positive influence of boron-doped graphene for its supported Au clusters: enhancement of SERS and oxygen molecule adsorption.,” *Physical chemistry chemical physics : Physical Chemistry Chemical Physics*, vol. 14, no. 39, pp. 13564–8, 2012.
- [102] X. Kong and Q. Chen, “The positive influence of boron-doped graphene with pyridine as a probe molecule on SERS: a density functional theory study,” *Journal of Materials Chemistry*, vol. 22, no. 30, p. 15336, 2012.
- [103] R. Lv, Q. Li, A. R. Botello-Méndez, T. Hayashi, B. Wang, A. Berkdemir, Q. Hao, A. L. Elías, R. Cruz-Silva, H. R. Gutiérrez, Y. A. Kim, H. Muramatsu, J. Zhu, M. Endo, H. Terrones, J.-C. Charlier, M. Pan, and M. Terrones, “Nitrogen-doped graphene: beyond single substitution and enhanced molecular sensing.,” *Scientific Reports*, vol. 2, p. 586, 2012.
- [104] B. I. Rapoport, J. T. Kedzierski, and R. Sarpeshkar, “A glucose fuel cell for implantable brain-machine interfaces.,” *PloS One*, vol. 7, no. 6, p. e38436, 2012.
- [105] D. J. Lipomi, M. Vosgueritchian, B. C.-K. Tee, S. L. Hellstrom, J. A. Lee, C. H. Fox, and Z. Bao, “Skin-like pressure and strain sensors based on transparent elastic films of carbon nanotubes.,” *Nature Nanotechnology*, vol. 6, no. 12, pp. 788–792, 2011.
- [106] C. M. Voge and J. P. Stegemann, “Carbon nanotubes in neural interfacing applications.,” *Journal of Neural Engineering*, vol. 8, no. 1, p. 011001, 2011.
- [107] C.-M. Lin, Y.-T. Lee, S.-R. Yeh, and W. Fang, “Flexible carbon nanotubes electrode for neural recording,” *Biosensors and Bioelectronics*, vol. 24, no. 9, pp. 2791–2797, 2009.
- [108] W. M. Tsang, A. L. Stone, D. Otten, Z. N. Aldworth, T. L. Daniel, J. G. Hildebrand, R. B. Levine, and J. Voldman, “Insect-machine interface: a carbon nanotube-enhanced flexible neural probe.,” *Journal of Neuroscience Methods*, vol. 204, no. 2, pp. 355–65, 2012.

- [109] E. W. Keefer, B. R. Botterman, M. I. Romero, A. F. Rossi, and G. W. Gross, "Carbon nanotube coating improves neuronal recordings.," *Nature Nanotechnology*, vol. 3, no. 7, pp. 434–9, 2008.
- [110] M. Shein, A. Greenbaum, T. Gabay, R. Sorkin, M. David-Pur, E. Ben-Jacob, and Y. Hanein, "Engineered neuronal circuits shaped and interfaced with carbon nanotube microelectrode arrays," *Biomedical Microdevices*, vol. 11, no. 2, pp. 495–501, 2008.



# Chapter 3

## Nitrogen-doped graphitic nanoribbons: synthesis and characterization

### 3.1 Graphitic nanoribbons

As shown in the previous chapters, research in nanocarbons has been very extensive and intense. The focus and development have ranged from the fullerenes, zero-dimensional closed cages, passing through the nanotubes, 1D high aspect ratio tubular structures, and more recently into the 2D structures of graphene. As mentioned briefly in [section 1.4](#), the properties of graphene can be modulated, and its applicability extended, by using thin strips of graphene instead of large sheets. Such graphene nanoribbons, when thin enough, can actually behave as 1D nanostructures, where their properties depend on the type of edge, and on the width of the nanoribbon. As mentioned before properly speaking, the term graphene refers only to the monolayer material. By extension we should distinguish between actual graphene nanoribbons, those formed by thin strips of graphene, and graphitic nanoribbons, those formed by multiple layers of graphene but still being thin enough (both in width and number of layers) to be considered quasi-one-dimensional carbon nanostructures. This work will now focus on this latter type of nanomaterials: graphitic nanoribbons (GNR).

As mentioned before, graphitic nanoribbons can be obtained by unzipping carbon nanotubes [1, 2], by exfoliation [3] or lithographic cutting of graphene [4], as well as by bottom-up chemical assembly of aromatic molecules [5]. Such methods have the disadvantage of limitations in yield, or in the number of steps required to obtain GNR, as well as on the reproducibility and uniformity of the dimensions of the GNR.

In this context CVD proved itself again one of the most versatile family of methods for production of nanomaterials, where modifications on the system used for aerosol assisted chemical vapor deposition (AA-CVD) production of multi-walled carbon nanotubes, by Campos-Delgado et al. [6] proved capable of producing a new type of GNR, composed of several layers of stacked graphene planes with very good crystallinity.

This chapter presents a novel contribution which extended that work to achieve for the first time the synthesis of nitrogen-doped graphitic nanoribbons ( $N_x$ -GNR) by AA-CVD. This method has the advantage of making it possible to obtain milligram quantities of  $CN_x$ -GNR, which allowed extensive characterization of these new materials, and our results show that they have promising properties for sensing and electronics applications. Future work should allow further scale-up of the production of  $N_x$ -GNR enabling their use in sensors and other electronic devices.

## **3.2 Background: Undoped graphitic nanoribbons**

Graphitic nanoribbons (GNRs) are nanostructures that have been discovered by small alterations to CVD carbon nanotubes synthesis.

### **3.2.1 Synthesis method**

GNRs are produced by aerosol-assisted CVD as described in reference [6]. The process involves the incorporation of small amounts of thiophene ( $C_4H_4S$ ) to the precursors mixture, which is composed by ethanol ( $C_2H_6O$ ) as the carbon source and ferrocene ( $C_{10}H_{10}Fe$ ) as catalyst. The CVD is run during 30 minutes using  $950^\circ\text{C}$  as pyrolysis temperature, which is around  $100^\circ\text{C}$  higher than the utilized for CNTs. Also, a critical parameter is the flux of inert gas (Ar) used for carrying the chemical vapor, which is  $0.8\text{ L min}^{-1}$ . The produced material is collected as well in a powder form, by scrapping the inner walls of the quartz tube. Each GNRs production run can yield up to several tens of

milligrams, which is higher than other nanoribbons production methods, bearing an important advantage for further research and applications development.

### 3.2.2 Properties

The morphology of GNRs is one of their key characteristics. In [figure 3.1a-c](#) are shown SEM images of GNRs at different magnifications. A clear flat morphology with rippled surface can be clearly observed. [Figure 3.1d](#) exhibits a high angle annular dark field STEM image of a GNR, with a linear EDX scan for elemental detection in [fig. 3.1e](#). Interestingly, even though S is a crucial component for GNRs synthesis, it can not be detected as a part of the nanostructure, suggesting that it could be playing a mayor role over the catalytic particles instead, where the GNRs graphitic planes are generated (it is important to

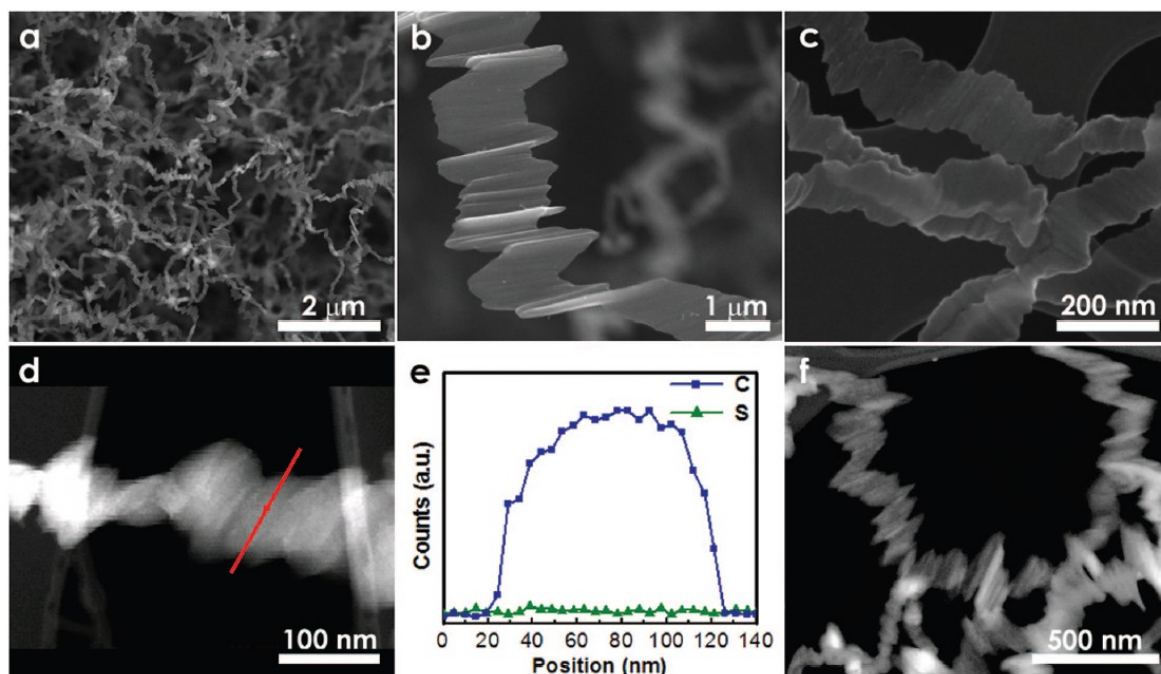


**Figure 3.1.** (a-c) SEM images of graphitic nanoribbons (GNRs) at different magnifications, where a characteristic flat morphology and rippled surface is visible. (d) HAADF image of a nanoribbon and its corresponding elemental EDX line-scan, indicated by the line. The elemental profile (e) shows the absence of S and indicates that the ribbon mainly consists of C; (f) dark field STEM image of bulk nanoribbons displaying rippled regions within the ribbons. Image taken from [\[6\]](#).



consider, however, that the detection limits of EDX are between 0.1 and 0.5% wt., and thiophene was used in the precursors solution at a concentration of 0.12% wt.)

The cited GNRs research includes the electric characterization of individual nanoribbons. The  $I$ - $V$  (current-voltage) curves are shown in [figure 3.2a-b](#), before and after annealing through Joule heating. As it can be observed, the electrical response is purely resistive, from the linear  $I$ - $V$  response. It is noticeable a resistivity magnitude reduction

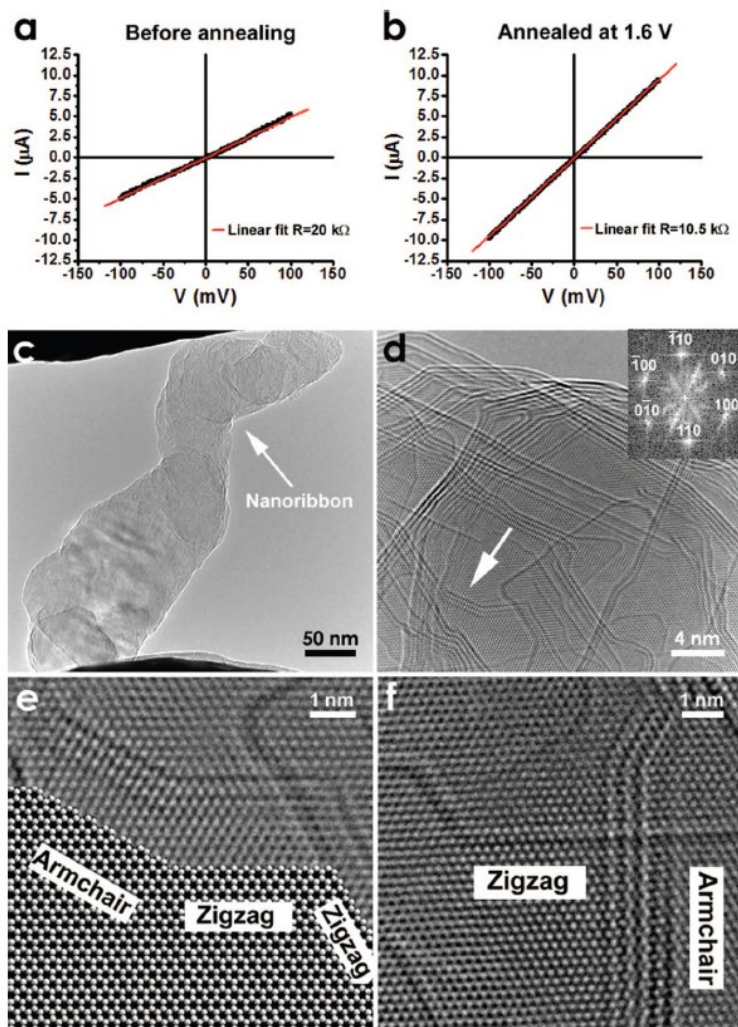


**Figure 3.2.**  $I$ - $V$  characteristic curves for individual GNR, (a) before and (b) after annealing by Joule heating at 1.6 V. (c) shows the GNR attached between the two electrodes used for the electric measurements, inside a HRTEM. (d) depicts the GNR's edge, with well defined shapes after annealing. (e-f) schematic and high magnification HRTEM image of the well defined edges of a GNR. Image taken from [6].

after the annealing process, which is attributed to the “healing” of defects within the  $sp^2$  carbon lattice that affect the electronic flow.

Other key characteristic of undoped GNRs is the morphology present at the edges, which can be either armchair or zigzag for perfect  $sp^2$  hexagonal lattices. [Figure 3.2d-f](#) shows different high magnification HRTEM images where the distinct graphene layers after annealing can be distinguished, from their edges in a sort of “terrace-like” configuration.

The importance of obtaining GNRs with clear defined edges is that many of their potential applications, as well as their electronic properties, are affected by their edges configuration, since these areas are the most sensible ones for possible interactions with external molecules in catalytic or sensing applications, for example.

### **3.3 New nanomaterial: Nitrogen doped graphitic nanoribbons**

The production and characterization of N-doped graphitic nanoribbons ( $N_x$ -GNRs) is a contribution of our group, and has been published very recently [\[7\]](#). This method extends the prior work on GNRs described above. The  $N_x$ -GNRs exhibit several properties that characterize them and in fact possess advantageous properties for new electronic and sensing applications development.

#### **3.3.1 Synthesis of $N_x$ -GNRs**

The production of  $N_x$ -GNRs involves the addition of pyrazine ( $C_4H_4N_2$ ) as a nitrogen precursor to the conventional feedstock mixture for GNRs, which includes ethanol ( $C_2H_6O$ ), ferrocene ( $C_{10}H_{10}Fe$ ) and thiophene ( $C_4H_4S$ ). Here it is important to note that first synthesis experiments were carried out using also benzylamine ( $C_7H_9N$ ) as nitrogen precursor. Nevertheless, the formation of nanoribbons was more consistent using pyrazine instead of benzylamine. For instance, [figure 3.3](#) shows a SEM image of synthesized material using a mixture with 0.2% wt. of benzylamine as N precursor, where a formation of fiber-like structures is observed together with some nanoribbons. The presence of these fibers increased for higher concentrations of benzylamine. This was the reason why pyrazine was chosen over benzylamine as N precursor for N-doped GNRs synthesis.

For a typical synthesis run, 3 g of ferrocene (98%, CAS:102-54-5), 0.283 mL of thiophene (99%, CAS:110-02-1) and amounts between 24 to 72 mg (correspondent to 1 to

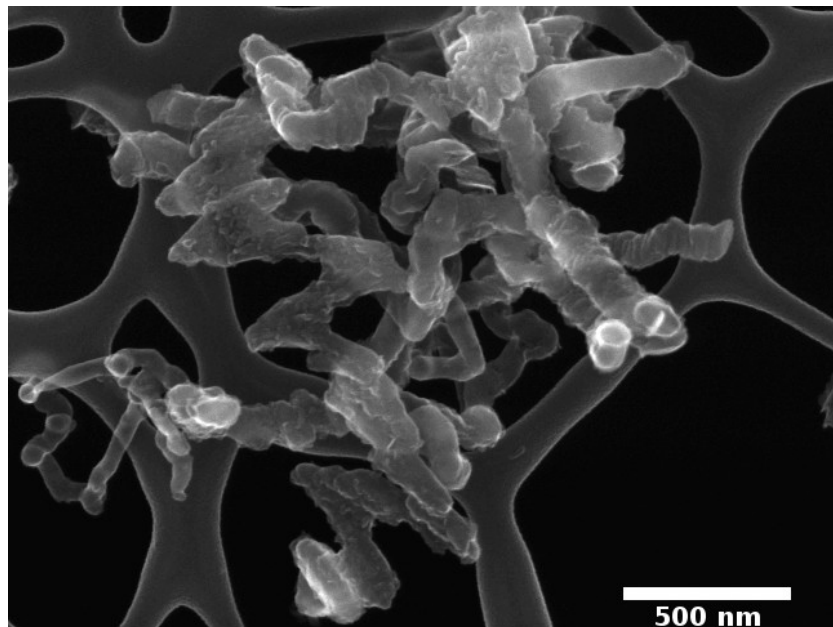


**Figure 3.3.** SEM image of presumably N-doped GNRs synthesized using a precursor solution with 0.2% wt. of benzylamine as N precursor. The preferential formation of nanofibers instead of nanoribbons was observed as benzylamine concentration increased.

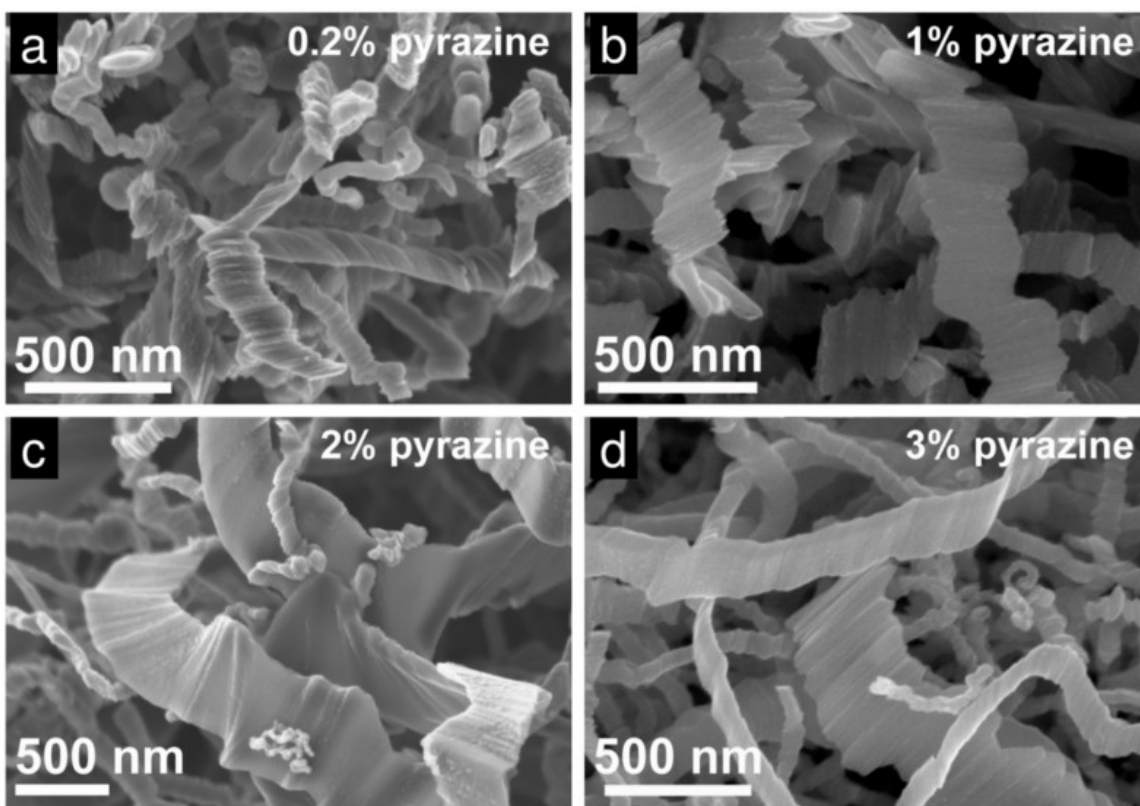
3% wt.) of pyrazine (99%, CAS:290-37-9) are dissolved in 300 mL of ethanol (99.5%, CAS:64-17-5) as precursor solution. This mixture is then used in the aerosol-assisted CVD setup as depicted in [figure 1.7b](#), where it is placed in an aerosol generator and carried with a flow of 0.8 L min<sup>-1</sup> of argon (99%, CAS:7440-37-1), controlled by a mass flow controller into a 1 inch diameter quartz tube. The quartz tube is previously placed and preheated to 950°C in a tubular furnace. The pyrolysis reaction is allowed to run for 30 minutes, then the tube is allowed to cool down (normally for 1 hour) and finally the N<sub>x</sub>-GNRs are collected by scrapping the inner walls of the quartz tube. The typical amounts of produced materials following this procedure are between 50 to 100 mg.

### 3.3.2 Morphology of N<sub>x</sub>-GNRs

Regarding the morphology characteristics of N<sub>x</sub>-GNRs, [figure 3.4](#) shows SEM images of samples produced using different concentrations of pyrazine (i.e., 0.2%, 1.0%, 2.0% and 3.0%). It is clear from the images that all concentrations used in this study yielded N<sub>x</sub>-GNRs exhibiting key characteristics such as high aspect ratio and other morphological

features as nanoribbons width. [Figure 3.5](#) depicts the width distribution of  $N_x$ -GNRs compared to the widths of undoped ones, where a clear feature can be observed: the distribution peak is relatively maintained around 150 nm, whereas the distribution bell shape widens for  $N_x$ -GNRs. This is clear from the presence of ribbons with widths greater than 300 nm in material produced by mixtures pyrazine as N precursor.

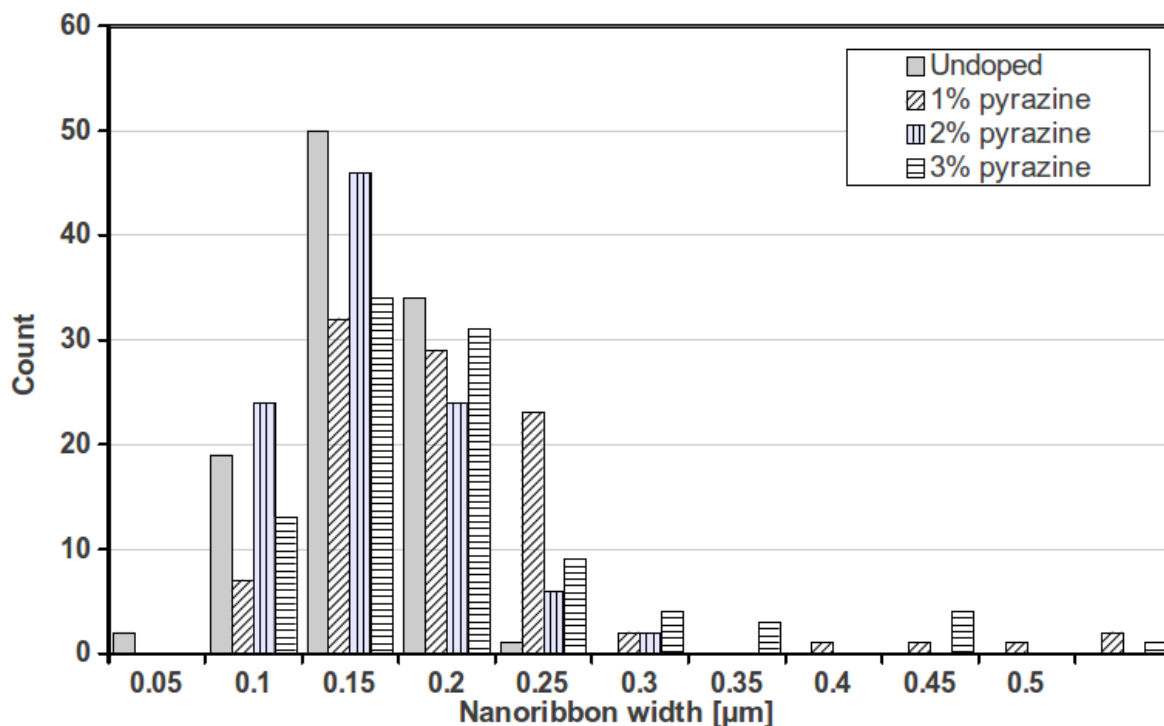
[Figure 3.6](#) shows HRTEM images, where the ribbons' multi-layered nature (ca. 100 graphene layers given the  $N_x$ -GNRs thickness of 30 – 40 nm) is noticeable. It is interesting to mention that  $N_x$ -GNRs exhibit loops (coalesced adjacent graphene edges, see [figure 3.6b, f and h](#)), whereas as-produced undoped GNRs never show these formations. From all the observed loop structures in  $N_x$ -GNRs, it is possible to identify three types of structures: a) “multi-walled” loops, resulting from joining layers' edges in a concentric fashion (see [figures 3.6b and h](#)); b) individual or “single-wall” loops by joining two adjacent graphene edges (see [figure 3.6f](#)); and c) quasi-closed or “open” loops of several bending layers (see



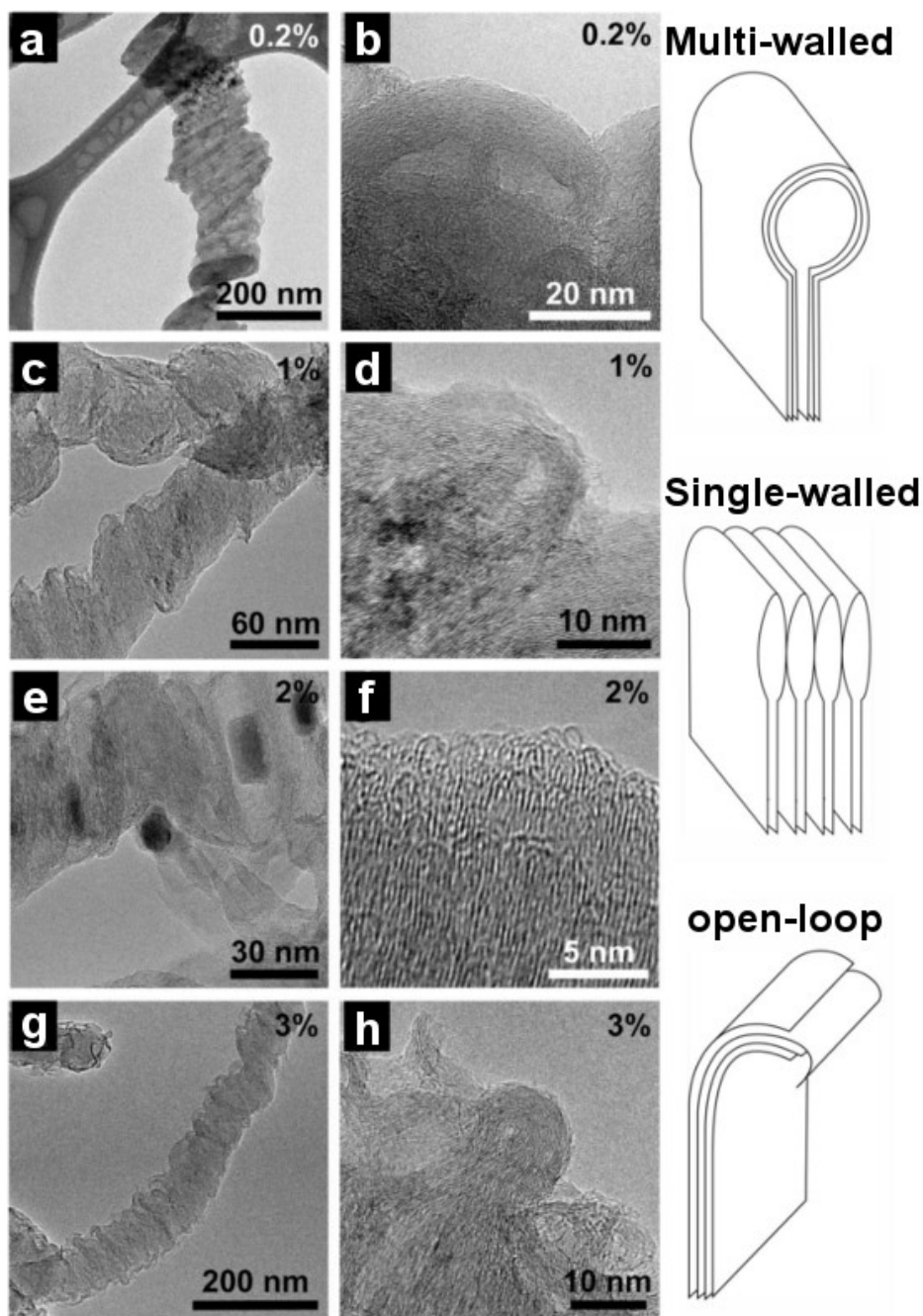
**Figure 3.4.** SEM images of  $N_x$ -GNRs synthesized using different amounts ((**a**) 0.2%, (**b**) 1.0%, (**c**) 2.0% and (**d**) 3.0%) of pyrazine as N precursor, where the flat and rippled surface characteristic is observed for all the samples.

figure 3.6c, g and h). All loop types appear in  $N_x$ -GNRs, but the multi-walled and open loops are seen more frequently with higher concentrations of pyrazine. It is noteworthy that related loop formation has been previously reported on pristine graphitic ribbons after high temperature thermal treatments (above 2000°C) [8].

Even though the described morphological features observed in  $N_x$ -GNRs are clear, their underlying cause still needs further investigations. Nevertheless, given several characteristics identified on other N-doped nanocarbons, such as increased reactivity in N-doping sites and “healing” effects of N over carbon structures [9, 10], it is plausible to propose that nitrogen contributes to keep the ribbons' edges activity towards forming larger networks, resulting in wider nanoribbons. Additionally, the N-doping could also explain the loop formation at the edges, since it has been established that nitrogen easily introduces curvature to carbon  $sp^2$  networks by forming pentagons instead of hexagons [11].



**Figure 3.5.**  $N_x$ -GNR width distribution, compared to the distribution of undoped GNRs. Note that, in general, the N-doping by pyrazine (indicated as %wt. of the precursors mixture) induces a widening in the widths distribution. Ribbons of widths greater than 350nm are only observed for N-doped GNRs.



**Figure 3.6.** HRTEM images of (a-b) 0.2%, (c-d) 1.0%, (e-f) 2.0% and (g-h) 3.0% pyrazine were taken at different magnifications, where it is possible to observe loops formation at the nanoribbons' edges. The drawings depicted at right of HRTEM images represent the different loop formations found in  $N_x$ -GNRs' edges: multi-walled loops (see b and g), single-walled loops (see f) and open loops (see c, g and h).

### 3.3.3 Spectroscopy of $N_x$ -GNRs

As it happens with most of carbon nanostructures, Raman spectroscopy reveals important changes associated with N-doping within  $N_x$ -GNRs. Figure 3.7 displays Raman spectra (acquired with a Renishaw InVia MicroRaman spectrometer, using a 514 nm excitation laser) of  $N_x$ -GNRs synthesized with small amounts (0.05% to 0.3%) of pyrazine in the precursors mixture. The spectra reveals small changes, specially noticeable at the position of the G' band (around  $2660\text{ cm}^{-1}$ ), which could be related to changes in the electronic structure of the ribbons produced by the presence of N atoms. Nevertheless, as it has been explained, higher amounts of pyrazine were preferred due to the morphological features they introduces to the synthesized nanoribbons.

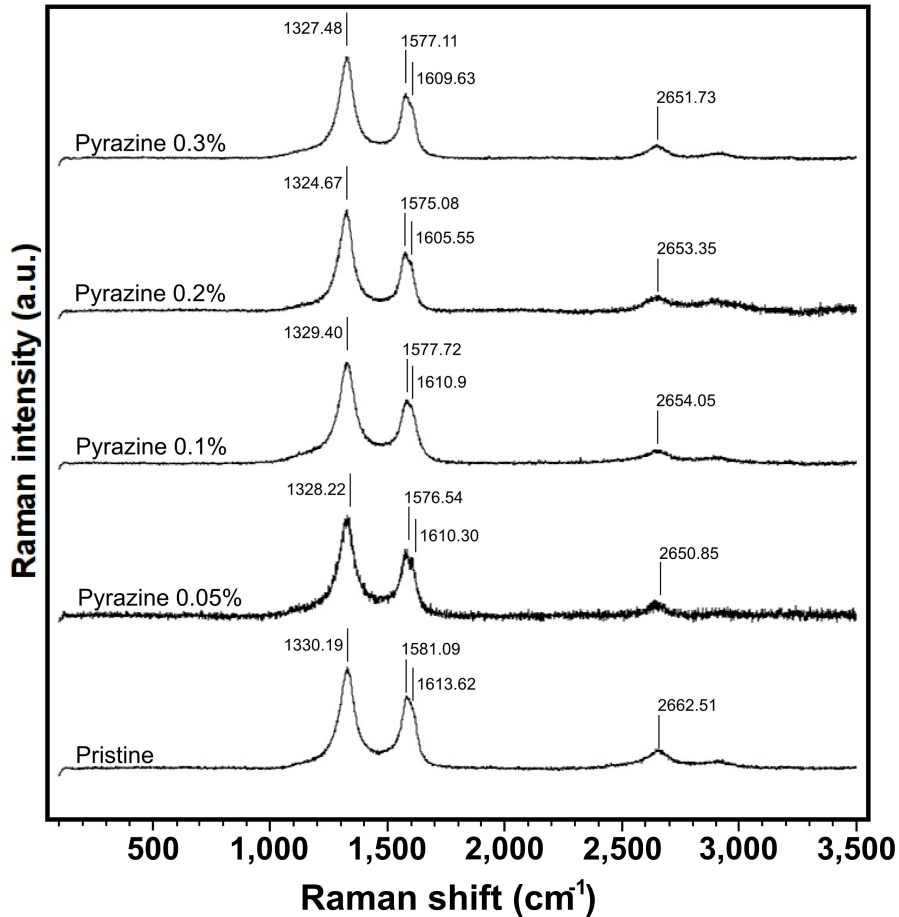


**Figure 3.7.** Raman spectra of  $N_x$ -GNRs synthesized with low pyrazine concentration in the precursors mixture. Note the down-shiftings around  $2660\text{ cm}^{-1}$  (G'-band) for the N-doped GNR produced with pyrazine.

Figures 3.8a and b depict the Raman spectra showing the D-, G-, D'- and G'-bands, corresponding to  $N_x$ -GNRs (synthesized with 0.2% to 3% of pyrazine in the precursors mixture) and undoped GNRs. The D- and G-bands for pure GNRs are localized around  $1351\text{ cm}^{-1}$  and  $1581\text{ cm}^{-1}$ , respectively, and the D- and G-band intensity ratio ( $I_D/I_G$ ) of 1.07 (see figure 3.8e) is similar to the one reported for GNRs [6]. The most significant changes observed are in the intensity ratios for the D-, D'- and G'-bands with respect to the G-band. Specially, the  $I_D/I_G$  increasing ratio with the increasing N concentration is attributable to the presence of more doping sites, which break the  $sp^2$  natural vibrational modes. Moreover, the  $I_{G'}/I_G$  ratio exhibits a clear decreasing trend with increasing in the N-precursor concentration, which indicates as well an increasing in electronic scattering points produced by N atoms within the nanostructure.

X-ray photoelectron spectroscopy (XPS) was done using a Kratos Axis Ultra XPS spectrometer. The results confirms the presence of nitrogen within our  $N_x$ -GNRs. N1s line scans of the samples synthesized with the three higher pyrazine concentrations are shown in figure 3.9; for lower nitrogen precursor concentrations the N1s signal was below the detection limit of the XPS instrument (around 0.1% wt). These XPS analysis revealed nitrogen doping levels of  $0.08\pm 0.024\text{ at\%}$ ,  $0.30\pm 0.09\text{ at\%}$  and  $0.28\pm 0.084\text{ at\%}$ , for samples synthesized using 1%, 2% and 3% of pyrazine. These values are lower than the concentrations reported for other N-doped carbon nanomaterials synthesized by CVD, which report doping levels up to 5% [12-14]. These differences in final concentrations can be attributed to the physical and chemical characteristics of the precursors. The XPS results also reveal that the preponderance of N-doping is substitutional and in adequate quantity to produce electronic scattering events but insufficient to yield a clear n-type doping. Although the amount of nitrogen atoms was close to the equipment's detection limit, broad peaks around 401.4 eV are clearly observed. These are associated with substitutional nitrogen doping (three coordinated nitrogen atoms within the graphene lattice) [13]. For the 2.0% and 3.0% pyrazine samples, there is no significant difference in the measured doping level, possibly indicating a nitrogen saturation within the graphene sheets. A similar trend has been found in N-doped single-walled carbon nanotubes (SWNTs) synthesized with benzilamine as nitrogen source, in which the maximum nitrogen content within the analysed samples was determined as 0.3% of atomic weight [15]. These saturation levels observed for some nanocarbons could be produced, as previously proposed, by the physical and chemical nature of the dopant precursor.



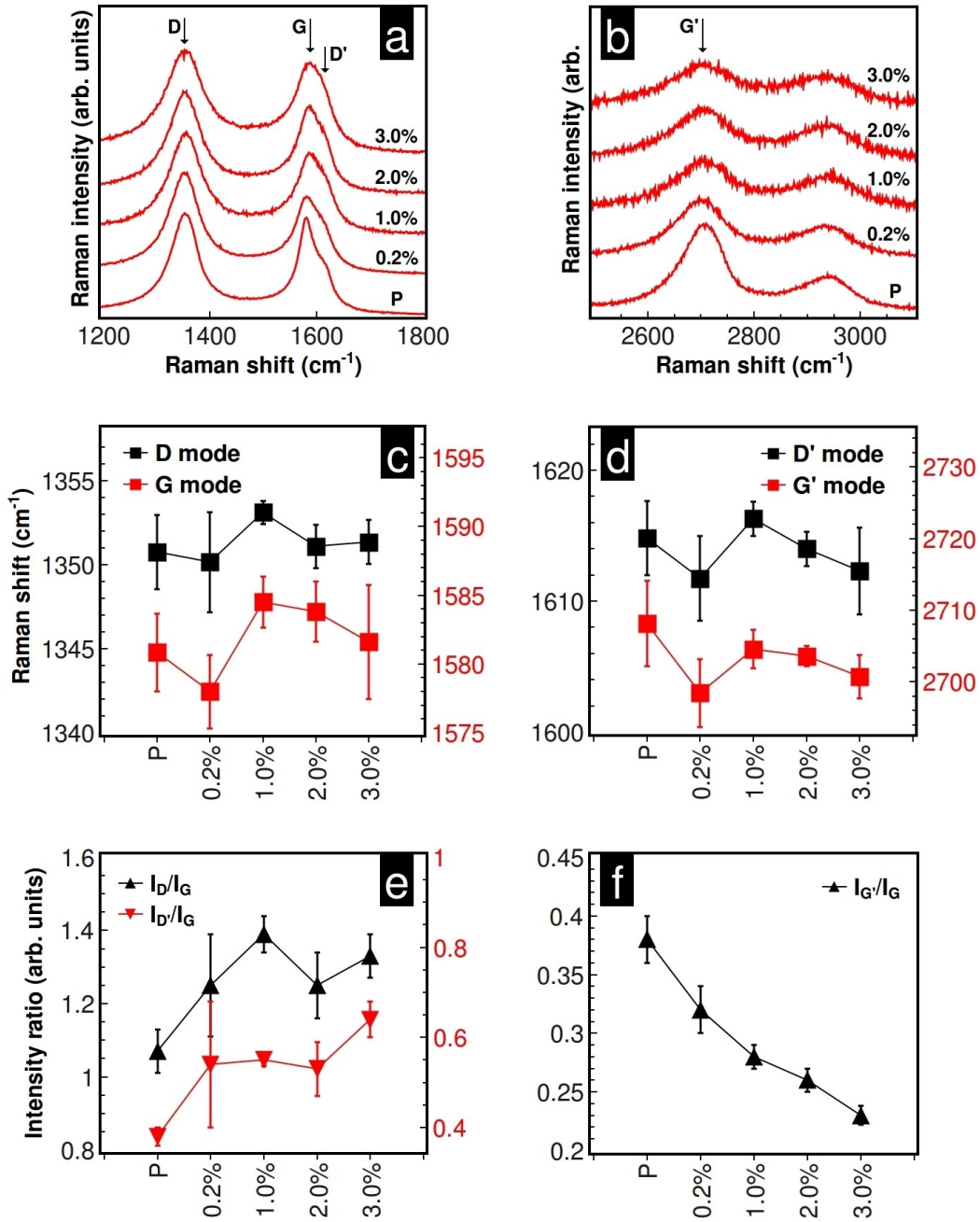


**Figure 3.8.** Raman spectroscopy characterization of  $N_x$ -GNRs. **(a)** Spectra of the D-, G-, D'- and **(b)** G'-bands for different pyrazine concentrations. The **(c-d)** graphs show Raman shifting for the four significant bands. **(e-f)** depict the intensity ratios for D-, D'- and G'-peaks with respect to G-band, revealing an association of  $I_{G'}/I_G$  with the N-doping level (compare with **(b)**).

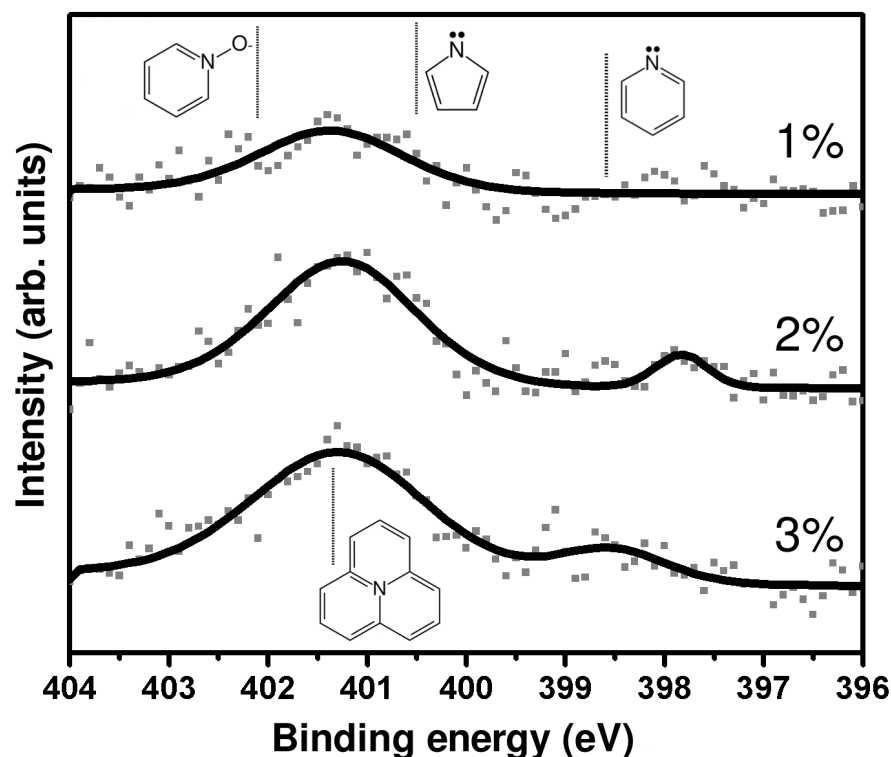


**Figure 3.9.** XPS N(1s) spectra for  $N_x$ -GNRs synthesized with 1.0%, 2.0% and 3.0% of pyrazine in the precursor mixture. The energy positions of the typical N configurations within  $sp^2$  carbon are depicted.

### 3.3.4 Thermogravimetry

Thermogravimetric analysis (TGA) curves and their first derivatives for undoped and  $N_x$ -GNRs are shown in [figure 3.10a](#) and [b](#), respectively. These results indicate that there is a maximum level of doping within  $N_x$ -GNRs, which is reached when using 2% pyrazine. For both 2% and 3% pyrazine  $N_x$ -GNRs, the onset of combustion is 30°C lower than the pristine counterparts, and with a higher burning rate (1.7 and 1.6 times faster, respectively). For 1% pyrazine, the  $N_x$ -GNRs decompose 23°C earlier than the pristine GNRs, and reveal a similar burning rate. The samples obtained using 0.2%wt pyrazine in the solution have the same critical degradation temperature when compared to pristine GNRs, but show a higher burning rate (1.3 times). Such results are explained by increasing the nitrogen concentrations within  $N_x$ -GNRs; nitrogen atoms promote reactions with oxygen. This effect is not only qualitatively similar to  $CN_x$ -MWNTs, but  $CN_x$ -MWNTs and  $N_x$ -GNRs critical degradation temperatures match, according to reported results found in the literature [16].

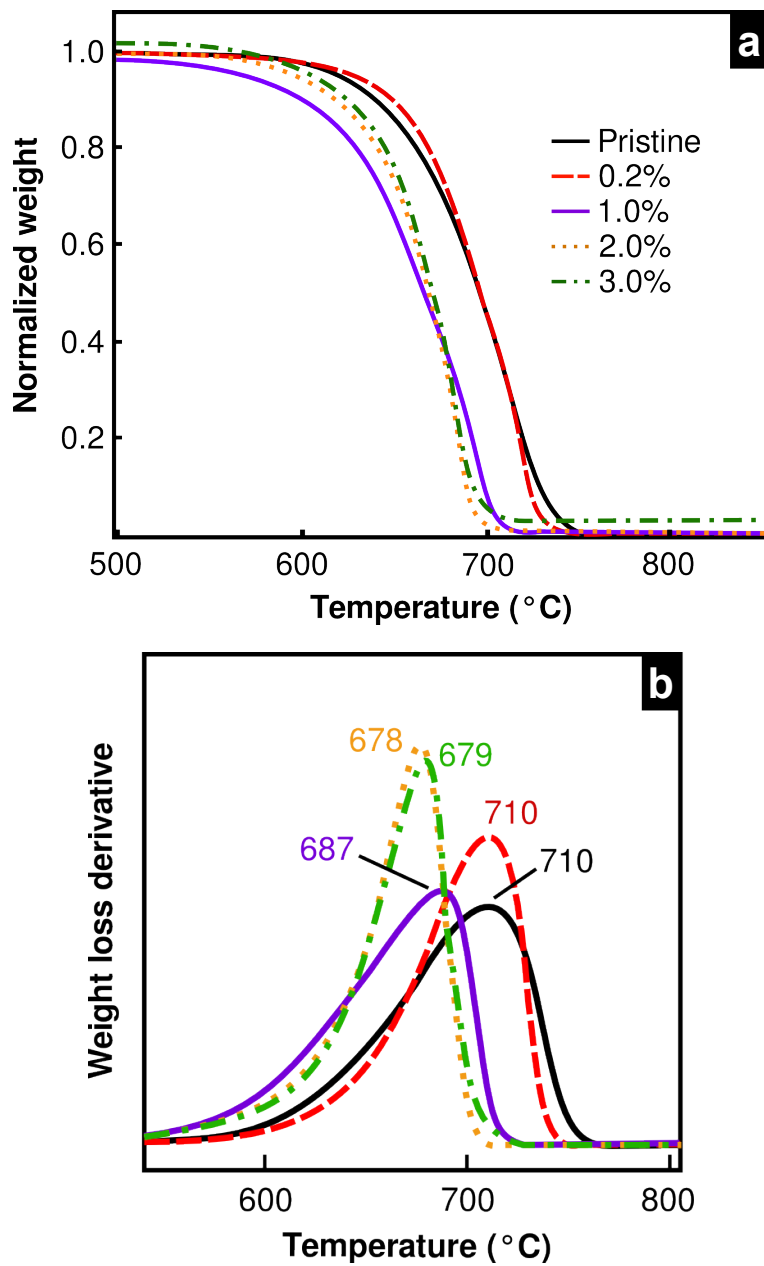


**Figure 3.10.** (a) TGA plots for all the  $\text{N}_x$ -GNR samples compared to the undoped GNRs. (b) Weight loss derivative vs. temperature, showing the respective thermal degradation at critical temperatures.

### 3.3.5 Electrical properties of N<sub>x</sub>-GNRs

The electronic properties were explored from the experimental and the theoretical study is presented in the following section. Experimental results were obtained by assessing the electronic transport at room temperature ( $T=300^{\circ}\text{K}$ ).  $I$ - $V$  (current-voltage) measurements were performed on individual N<sub>x</sub>-GNRs and undoped GNRs for comparison. Individual nanoribbons were connected between metallic electrodes inside a transmission electron microscope, then a sweeping DC voltage (-1.0 to 1.0 V) was applied, and the resulting current was measured. [Figure 3.11a](#) shows the  $I$ - $V$  curves obtained by measurements over an individual undoped GNR, 0.2% pyrazine N<sub>x</sub>-GNR and 3.0% pyrazine N<sub>x</sub>-GNR. The graphical comparison clearly shows a complete different electrical behavior for undoped and N-doped nanoribbons; GNRs exhibit a purely resistive response, from the linear  $I$ - $V$  characteristic. On the other hand, both N<sub>x</sub>-GNRs present a semiconducting-like curve, with a resistance decreasing as the voltage applied increases. It is interesting that even for both N<sub>x</sub>-GNRs the overall semiconducting-like curve shape is the same, the 3.0% pyrazine shows higher resistivities than the 0.2% pyrazine one, which is consistent with the fact that N-doping sites within a carbon structure play as electrons scattering points, thus degrading the overall electrical conductance. [Figure 3.11b](#) reports consecutive  $I$ - $V$  measurements (M1=measurement 1, M2=measurement 2, etc.) over an individual 3.0% pyrazine N<sub>x</sub>-GNR, showing the effects of annealing by the passing currents (Joule heating annealing). It is worth of noting that the semiconducting-like  $I$ - $V$  curve shape is maintained, indicating the persistence of N-doping at conditions where graphitic lattices rearrangements occur [\[8\]](#).

It is necessary to mention that even though N-doping in N<sub>x</sub>-GNRs lowers their electronic transport properties, they increase the chemical activity at the doping sites and the edges produced by them, as occurs with other N-doped carbon nanomaterials. These enhanced chemical reactivity could play a crucial role in further uses of N<sub>x</sub>-GNRs, like applications where strong interactions between carbon nanomaterials and other species is desired for sensing purposes, for example. Moreover, investigation on the use of N<sub>x</sub>-GNRs for biological applications is underway, since it has been demonstrated that N-doping in carbon nanotubes helps to increase their biocompatibility [\[17\]](#) and their interactions with biomolecules such as proteins [\[18\]](#).

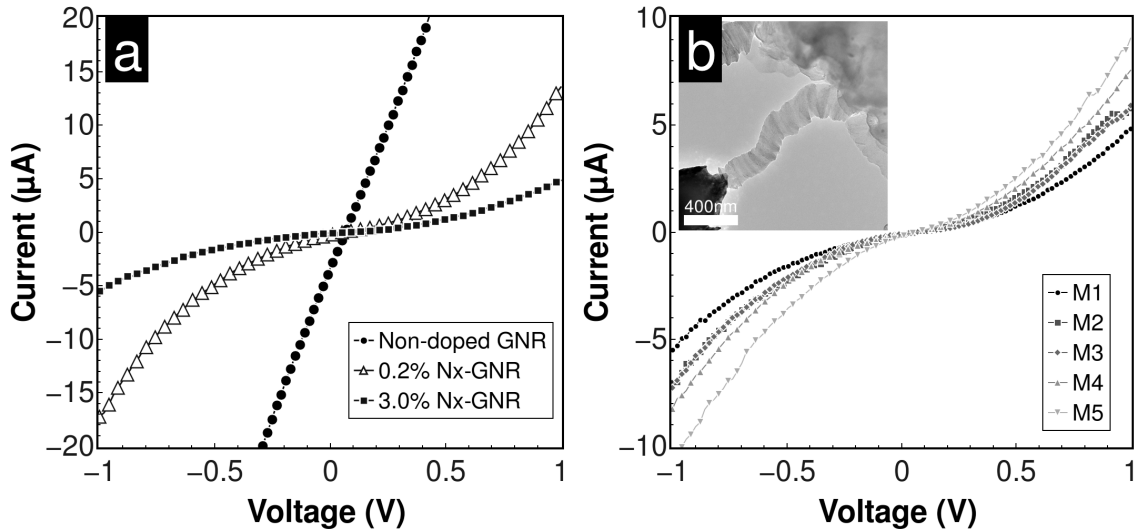


**Figure 3.11.** Electric characterization of  $N_x$ -GNRs. **(a)** Experimental I-V (current-voltage) measurements for individual  $N_x$ -GNRs (undoped and with 0.2% and 3.0% of pyrazine precursor). NRs. **(b)** Consecutive I-V measurements over one  $N_x$ -GNR, showing the annealing effects associated with electrical currents. The inset displays the setup (inside a TEM microscope) for electrical measurements over individual nanoribbons. Image taken from [7].

### 3.3.6 Theoretical modeling of the electrical properties of $N_x$ -GNR and comparison to experimental results

In order to understand the role of nitrogen doping in GNRs, Density Functional Theory (DFT) calculations were performed on zigzag graphene NRs. The electronic calculations were performed using DFT as implemented in the SIESTA code [19]. Generalized gradient approximation (GGA) functionals using the Perdew-Burke-Ernzerhof implementation were used for all calculations [20]. The basis set was made up of double- $\xi$  with single polarization orbitals, with an energy shift of 50 meV. A zigzag graphene-NR with 18 atoms along the width (18-zGNR, width  $w = 1.99$  nm, length  $l = 2.84$  nm) and an armchair GNR (14-aGNR,  $w = 1.79$  nm,  $l = 2.42$  nm) with different amounts and configurations of dopant nitrogen atoms was used to investigate the electron transport as a function of the nitrogen doping. Twelve and six unit cells were considered in the calculations for zGNRs and aGNRs, respectively. A real-space mesh equivalent to a plane-wave cutoff energy of 250 Ry for real-space integrals was used. The Brillouin zone was sampled using a Monkhorst-Pack grid corresponding to four and one k-points, for zGNR and aGNR, respectively, in the

transport direction. Vacuum distances of 18 Å were kept between the graphene nanoribbons in the finite directions. All graphene-NRs were passivated with hydrogen on the edges in order to increase thermodynamic stability [21] and the coordinates of all systems were relaxed using conjugate gradient minimization until the maximum force was less than 0.05 eV Å<sup>-1</sup>.

For zGNRs doping, C atoms in the nanoribbon center were replaced with 1, 3, and 5 (in two different configurations) nitrogen atoms. The aGNRs were doped by the substitution of one (both on the center or edge) and five nitrogen atoms. Starting with the relaxed atomic structure and the converged Hamiltonian and overlap matrices, all obtained from SIESTA, conductance and DOS calculations were performed using our in-house transport code based on the Landauer-Buttiker formalism outlined by Datta [22] and used in previous similar studies [23-25]. In all three doping schemes, the electrodes used were those obtained from the pure SIESTA calculation. An electrode consists of one aGNR or two zGNR unit cells on each end of the system. Results were obtained for both spin-up and spin-down electrons in the doped cases; for the pristine (undoped) structure the electron conductance was invariant between spin-up and spin-down. For energy stability, the nanoribbons are studied in the antiferromagnetic configuration [26]. The *I-V* curves were obtained using simple  $\xi$  orbitals and TRANSIESTA calculations [27].

Figures 3.12 and 3.13 depict spin-up and spin-down density of states (DOS) and quantum conductance for zigzag (18-zGNRs) graphene NRs, including the corresponding molecular models with the doping level expressed as percentage of the substitutional nitrogen atoms with respect to carbon. For these systems, increased nitrogen concentration has a visible effect in the NRs' conduction band, introducing localized states (seen as sharp peaks in DOS plots) that act as electronic scattering points, producing a clear reduction in the number of conductive states above the Fermi level. These results agree with previous theoretical studies of quantum conductivity of nitrogen-doped nanocarbons [28-30], in which the conductivity drop is rationalized as being due to donor- or acceptor-like localized states (seen as flat bands on the NRs' band structures), induced by the extra electron carried by the nitrogen. Most importantly, these results are in good agreement with the experimental results, in which N<sub>x</sub>-GNRs have lower conductivity values when compared to undoped graphene NRs. It is noteworthy that the calculations for DOS and quantum conductance curves were carried out using spin-polarization, which provide the most stable (minimal energy) magnetic ordering structure for undoped and N-doped graphene NRs. The undoped NRs exhibit localized magnetic moments along the edges, with both edges

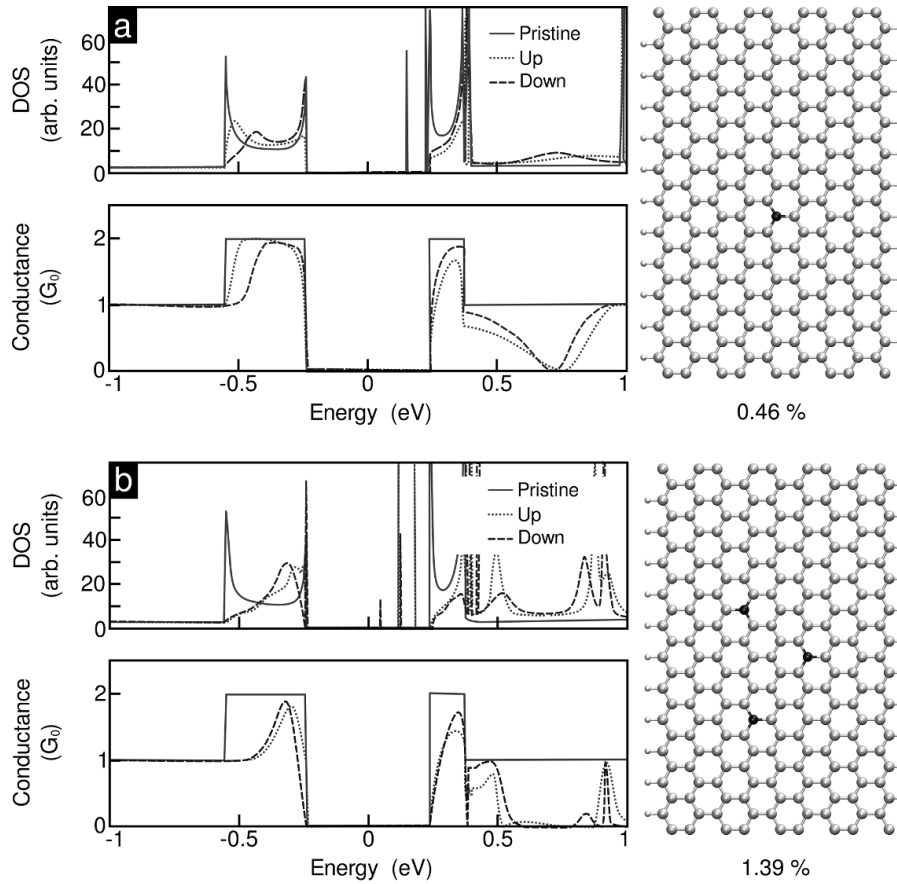


**Figure 3.12.** DOS, conductance (spin-up and spin-down) and visualizations of 18-zGNRs doped with **(a)** one and **(b)** three nitrogen atoms. The solid line represents the DOS and conductance for a pristine (undoped) 18-zGNR for comparison. The spin-up and spin-down DOS are the same for undoped GNRs and only one curve is shown. The percentages represent the number of nitrogen atoms divided by the total atoms (excluding the passivating hydrogens on the edges). The quantum conductance is given in  $G_0$  units ( $G_0 = 2e^2/h$ ).

exhibiting a ferromagnetic order (aligned spins along the edges) with opposite spin directions between edges resulting in a zero total magnetization, thus in the DOS figures there is no noticeable effect of spin-polarization and only one line is shown. Given that there is an electronic band gap for all NRs, the corresponding spin-resolved  $I$ - $V$  curves exhibit a turn-on voltage of  $\approx 0.3$  V for the undoped graphene NR, which contradicts the experimental results. When non spin-polarized calculations are performed, zigzag graphene NRs exhibit a zero electronic band gap. The energy differences between spin-polarized and non spin-polarized calculations fall in the meV range, and decrease with NR's width.

Therefore, it can be expected that at room temperature, the spins do not play an important role in the transport properties of these GNRs.

Figure 3.14 depicts the calculated  $I$ - $V$  curves for the different doped graphene ribbons (non-polarized calculations), where the linear  $I$ - $V$  curve exhibited by undoped graphene NRs qualitatively agrees with the experimental measurements (see figure 3.11a). At any of the considered nitrogen doping cases (both substitutional and pyridine-like), the  $I$ - $V$  curve for N-doped graphene NRs is non-linear, showing a semiconducting-like behavior. Comparing with the experimental results, theoretical results for doped systems also agree

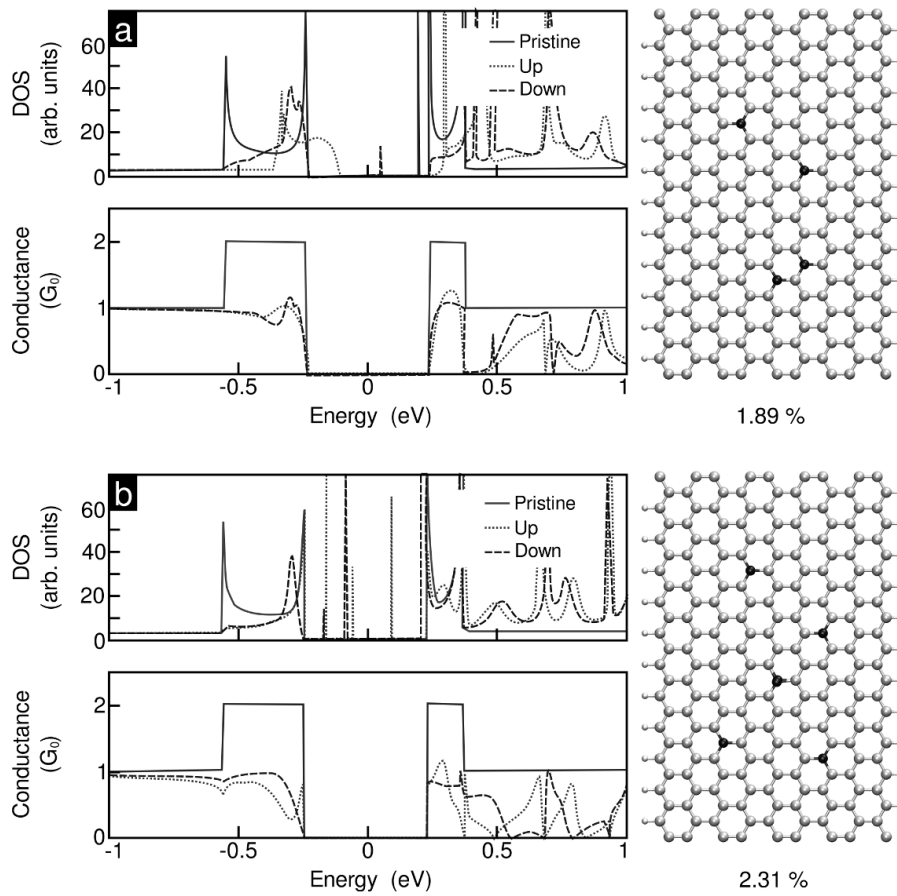


**Figure 3.13.** DOS, conductance (spin-up and spin-down) and visualizations of 18-zGNRs doped with (a) four and (b) five nitrogen atoms. The solid line represents the DOS and conductance for a pristine (undoped) 18-zGNR for comparison. The spin-up and spin-down DOS are the same for undoped GNRs and only one curve is shown. The percentages represent the number of nitrogen atoms divided by the total atoms (excluding the passivating hydrogens on the edges). The quantum conductance is given in  $G_0$  units ( $G_0 = 2e^2/h$ ).



qualitatively, showing a characteristic non-linear  $I$ - $V$  response, with increasing current/voltage rate as voltage raises (semiconducting-like behavior).

## Conclusions

The novel morphological features observed in  $N_x$ -GNRs consist of loops located at the nanoribbons edges, induced by the presence of nitrogen atoms during synthesis; the  $N_x$ -GNRs also possess increased reactivity at high temperatures (as verified by the lower decomposition temperatures in TGA). Therefore, the  $N_x$ -GNRs might be easily functionalized, thus enabling applications related to the fabrication of composite materials, molecular sensors, field emitters, etc. Both TGA and XPS analysis suggest that there is a threshold limit value of nitrogen atoms being capable of being incorporated in doped

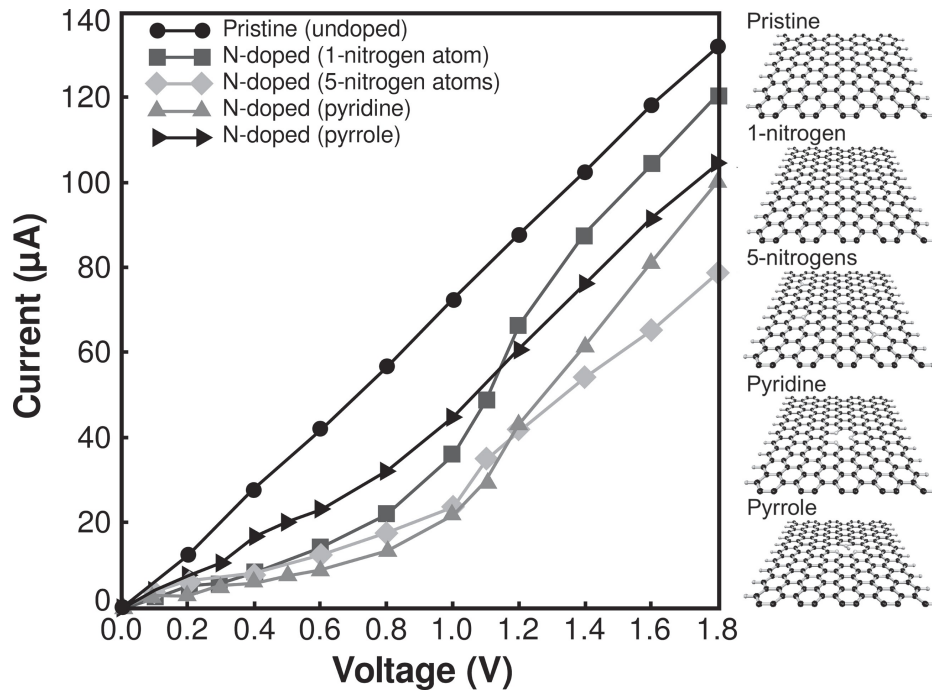


**Figure 3.14.** Electrical current as a function of the applied voltage, for nitrogen-doped and undoped (pristine) zigzag graphene nanoribbons (18-zGNRs). The calculations were carried out with non-spin polarized local density approximation. The nanoribbons were doped in a substitutional, pyridine or pyrrole fashion. In the pyridine and pyrrole doping, one carbon atom is removed (in this case, it was removed from the central part of the nanoribbon) and the carbon atoms around the so created vacancy are replaced by nitrogen atoms. The corresponding structure of the considered cases are shown in the figure's right side.

GNRs. Detailed characterization studies of the  $N_x$ -GNRs by Raman spectroscopy indicate that the intensity ratio between G' and G peaks is correlated to the nitrogen doping concentration. Electrical measurement on individual GNRs showed differences on electronic transport between the N-doped and undoped GNRs. Theoretical calculations suggest that the nitrogen doping introduces electron scattering and that is largely responsible for the semiconducting-like features observed in  $N_x$ -GNRs. Further theoretical calculations considering the effect of loop formation and the stacking of different layers in the graphitic nanoribbons are still under investigation in order to better understand these doped nanocarbons. These new types of doped GNRs add new and attractive properties to the ones already exhibited by undoped GNRs, such as high aspect ratio, reactivity and high surface-to-volume ratio, thus making this material attractive for the fabrication of electronic nanodevices, catalysis or other related applications.

## **Bibliography**

- [1] A. L. Elías, A. R. Botello-Méndez, D. Meneses-Rodríguez, V. Jehová González, D. Ramírez-González, L. Ci, E. Muñoz-Sandoval, P. M. Ajayan, H. Terrones, and M. Terrones, "Longitudinal Cutting of Pure and Doped Carbon Nanotubes to Form Graphitic Nanoribbons Using Metal Clusters as Nanoscalpels," *Nano Letters*, vol. 10, no. 2, pp. 366–372, 2009.
- [2] L. Xie, H. Wang, C. Jin, X. Wang, L. Jiao, K. Suenaga, and H. Dai, "Graphene Nanoribbons from Unzipped Carbon Nanotubes: Atomic Structures, Raman Spectroscopy, and Electrical Properties," *Journal of the American Chemical Society*, vol. 133, no. 27, pp. 10394–10397, 2011.
- [3] A. G. Cano-Márquez, F. J. Rodríguez-Macías, J. Campos-Delgado, C. G. Espinosa-González, F. Tristán-López, D. Ramírez-González, D. A. Cullen, D. J. Smith, M. Terrones, Y. I. Vega-Cantú, and A. G. Cano-Márquez, "Ex-MWNTs: Graphene Sheets and Ribbons Produced by Lithium Intercalation and Exfoliation of Carbon Nanotubes," *Nano Letters*, vol. 9, no. 4, pp. 1527–1533, 2009.
- [4] I.-S. Byun, D. Yoon, J. S. Choi, I. Hwang, D. H. Lee, M. J. Lee, T. Kawai, Y.-W. Son, Q. Jia, H. Cheong, and B. H. Park, "Nanoscale lithography on monolayer graphene using hydrogenation and oxidation.," *ACS Nano*, vol. 5, no. 8, pp. 6417–24, 2011.

- [5] J. Cai, P. Ruffieux, R. Jaafar, M. Bieri, T. Braun, S. Blankenburg, M. Muoth, A. P. Seitsonen, M. Saleh, X. Feng, K. Mullen, and R. Fasel, "Atomically precise bottom-up fabrication of graphene nanoribbons", *Nature*, vol. 466, no. 7305, pp. 470–473, 2010.
- [6] J. Campos-Delgado and J. Romo-Herrera, "Bulk production of a new form of sp<sup>2</sup> carbon: Crystalline graphene nanoribbons," *Nano Letters*, vol. 8, pp. 2773–2778, 2008.
- [7] J. Ortiz-Medina, M. L. García-Betancourt, X. Jia, R. Martínez-Gordillo, M. A. Pelagio-Flores, D. Swanson, A. L. Elías, H. R. Gutiérrez, E. Gracia-Espino, V. Meunier, J. Owens, B. G. Sumpter, E. Cruz-Silva, F. J. Rodríguez-Macías, F. López-Urías, E. Muñoz-Sandoval, M. S. Dresselhaus, H. Terrones, and M. Terrones, "Nitrogen-Doped Graphitic Nanoribbons: Synthesis, Characterization, and Transport," *Advanced Functional Materials*, vol. 23, no. 30, pp. 3755–3762, 2013.
- [8] J. Campos-Delgado, Y. A. Kim, T. Hayashi, A. Morelos-Gómez, M. Hofmann, H. Muramatsu, M. Endo, H. Terrones, R. D. Shull, M. S. Dresselhaus, and M. Terrones, "Thermal stability studies of CVD-grown graphene nanoribbons: Defect annealing and loop formation," *Chemical Physics Letters*, vol. 469, no. 1–3, pp. 177–182, 2009.
- [9] A. Nevidomskyy, G. Csányi, and M. Payne, "Chemically Active Substitutional Nitrogen Impurity in Carbon Nanotubes," *Physical Review Letters*, vol. 91, no. 10, p. 105502, 2003.
- [10] B. Wang and S. T. Pantelides, "Controllable healing of defects and nitrogen doping of graphene by CO and NO molecules," *Physical Review B*, vol. 83, no. 24, p. 245403, 2011.
- [11] M. Terrones, P. M. Ajayan, F. Banhart, X. Blase, D. L. Carroll, J. C. Charlier, R. Czerw, B. Foley, N. Grobert, R. Kamalakaran, P. Kohler-Redlich, M. Rühle, T. Seeger, and H. Terrones, "N-doping and coalescence of carbon nanotubes: synthesis and electronic properties," *Applied Physics A: Materials Science & Processing*, vol. 74, no. 3, pp. 355–361, 2002.
- [12] R. Czerw, M. Terrones, J.-C. Charlier, X. Blase, B. Foley, R. Kamalakaran, N. Grobert, H. Terrones, D. Tekleab, P. M. Ajayan, W. Blau, M. Rühle, and D. L. Carroll, "Identification of Electron Donor States in N-Doped Carbon Nanotubes," *Nano Letters*, vol. 1, no. 9, pp. 457–460, 2001.
- [13] D. Wei, Y. Liu, Y. Wang, H. Zhang, L. Huang, and G. Yu, "Synthesis of N-Doped Graphene by Chemical Vapor Deposition and Its Electrical Properties," *Nano Letters*, vol. 9, no. 5, pp. 1752–1758, 2009.

- [14] L. Qu, Y. Liu, J.-B. Baek, and L. Dai, "Nitrogen-doped graphene as efficient metal-free electrocatalyst for oxygen reduction in fuel cells.," *ACS Nano*, vol. 4, no. 3, pp. 1321–1326, 2010.
- [15] A. L. Elias, P. Ayala, A. Zamudio, M. Grobosch, E. Cruz-Silva, J. M. Romo-Herrera, J. Campos-Delgado, H. Terrones, T. Pichler, and M. Terrones, "Spectroscopic Characterization of N-Doped Single-Walled Carbon Nanotube Strands: An X-ray Photoelectron Spectroscopy and Raman Study," *Journal of Nanoscience and Nanotechnology*, vol. 10, no. 6, pp. 3959–3964, 2010.
- [16] E. R. Alvizo-Paez, J. M. Romo-Herrera, H. Terrones, M. Terrones, J. Ruiz-Garcia, and J. L. Hernandez-Lopez, "Soft purification of N-doped and undoped multi-wall carbon nanotubes," *Nanotechnology*, vol. 19, no. 15, p. 155701, 2008.
- [17] J. C. Carrero-Sanchez, A. L. Elías, R. Mancilla, G. Arrellín, H. Terrones, J. P. Laclette, and M. Terrones, "Biocompatibility and toxicological studies of carbon nanotubes doped with nitrogen.," *Nano Letters*, vol. 6, no. 8, pp. 1609–16, 2006.
- [18] H. J. Burch, S. A. Contera, M. R. R. de Planque, N. Grobert, and J. F. Ryan, "Doping of carbon nanotubes with nitrogen improves protein coverage whilst retaining correct conformation.," *Nanotechnology*, vol. 19, no. 38, p. 384001, 2008.
- [19] J. M. Soler, E. Artacho, J. D. Gale, A. García, J. Junquera, P. Ordejón, and D. Sánchez-Portal, "The SIESTA method for ab initio order- N materials simulation," *Journal of Physics: Condensed Matter*, vol. 14, no. 11, p. 2745, 2002.
- [20] J. P. Perdew, K. Burke, and M. Ernzerhof, "Generalized Gradient Approximation Made Simple," *Physical Review Letters*, vol. 77, no. 18, pp. 3865–3868, 1996.
- [21] V. Barone, O. Hod, and G. E. Scuseria, "Electronic Structure and Stability of Semiconducting Graphene Nanoribbons," *Nano Letters*, vol. 6, no. 12, pp. 2748–2754, 2006.
- [22] S. Datta, *Quantum Transport: Atom To Transistor*. Cambridge University Press, 2005.
- [23] A. R. Botello-Méndez, E. Cruz-Silva, F. López-Urías, B. G. Sumpter, V. Meunier, M. Terrones, and H. Terrones, "Spin polarized conductance in hybrid graphene nanoribbons using 5-7 defects.," *ACS Nano*, vol. 3, no. 11, pp. 3606–3612, 2009.
- [24] V. Meunier, M. B. Nardelli, J. Bernholc, T. Zacharia, and J. C. Charlier, "Intrinsic electron transport properties of carbon nanotube Y-junctions," *Applied Physics Letters*, vol. 81, no. 27, pp. 5234–5236, 2002.
- [25] J. M. Romo-Herrera, M. Terrones, H. Terrones, and V. Meunier, "Electron transport

- properties of ordered networks using carbon nanotubes,” *Nanotechnology*, vol. 19, no. 31, p. 315704, 2008.
- [26] L. Pisani, J. Chan, B. Montanari, and N. Harrison, “Electronic structure and magnetic properties of graphitic ribbons,” *Physical Review B*, vol. 75, no. 6, 2007.
- [27] M. Brandbyge, J.-L. Mozos, P. Ordejón, J. Taylor, and K. Stokbro, “Density-functional method for nonequilibrium electron transport,” *Physical Review B*, vol. 65, no. 16, 2002.
- [28] S. S. Yu, W. T. Zheng, Q. B. Wen, and Q. Jiang, “First principle calculations of the electronic properties of nitrogen-doped carbon nanoribbons with zigzag edges,” *Carbon*, vol. 46, no. 3, pp. 537–543, 2008.
- [29] E. Cruz-Silva, Z. M. Barnett, B. G. Sumpter, and V. Meunier, “Structural, magnetic, and transport properties of substitutionally doped graphene nanoribbons from first principles,” *Physical Review B*, vol. 83, p. 155445, 2011.
- [30] J.-C. Charlier, P. Eklund, J. Zhu, and A. Ferrari, “Carbon Nanotubes” in *Topics in Applied Physics*, Editors: A. Jorio, G. Dresselhaus and M. S. Dresselhaus, Springer Berlin Heidelberg, vol. 111, pp. 673–709, 2008.

# Chapter 4

## Theoretical study on nanomaterials and biomolecules interactions: graphene and dopamine

### 4.1 Introduction to theoretical analysis of biosystems

A considerable part of the carbon nanotechnology boom was started from the theoretical predictions of the extraordinary physical properties they possess, with important contributions to the knowledge of graphite-based electronic structures dating as early as the 1950s [1, 2]. Since then, extensive advances in computing capacity have fueled an increasing complexity in theoretical analysis, which can now describe interactions of carbon and other nanostructured materials, from the electronic level for systems from several atoms (e.g., semiconducting crystals, metallic clusters, carbon nanotubes and graphene) to electrostatic and van der Waals interactions for systems with thousands of atoms, which is commonly the case for biosystems (e.g., peptides, proteins, DNA chains and phospholipid bilayers). The use of these theoretical approaches represent a crucial advantage for the development of specific biotechnological applications, since they allow to predict and analyze properties that otherwise would require extensive amounts of

experimental trials. For example, theoretical approaches for the assessment of an anticancer drug (docetaxel) solubility mediated by different types of excipient molecules has been reported (see [figure 4.1](#)). In this study, the results showed that the interactions between the drug and the corresponding excipient, specifically hydrogen bonds, are the most relevant for drug design in terms of solubility [3], providing a significant advantage for the experimental phase of the drug development. Other type of theoretical approaches allow studying interactions between potential drugs or biomolecules with specific sites of proteins, including the active sites of enzymes, which is important as well for drug development. For instance, in [figure 4.2](#) are shown molecular models for experimentally ([figure 4.2a](#) and [b](#)) and theoretically ([figure 4.2c](#) and [d](#)) resolved interaction sites between a human immunodeficiency virus (HIV) enzyme (integrase) and an inhibitor (5-CITEP) and a potential drug (Raltegravir) [4]. In this case, the theoretical models helped to explore additional binding sites for retroviral agents, which eventually could lead to new and effective drugs.

Within the variety of tools that have been built for analyzing biosystems theoretically, there are abundant modeling of well-established molecular parameters for all of the most important building blocks of proteins and nucleic acids. For the former the twenty aminoacids, that are the basis of all human proteins, for the latter the five nucleotides of DNA and RNA. This kind of parametrization allows to use simplifying approaches to speed up calculations with respect to *ab initio* techniques. A popular approach is molecular dynamics (MD), in which the simplifying assumptions are related with typical spatial

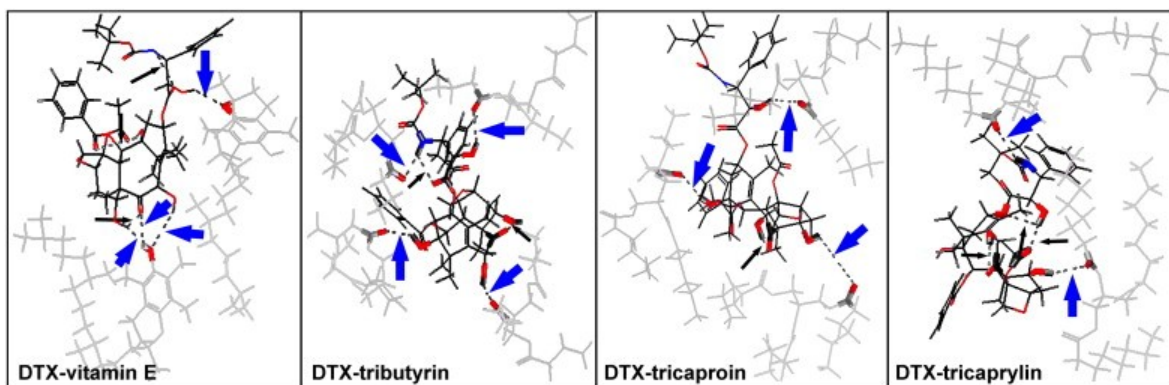


**Figure 4.1.** Anticancer drug docetaxel (DXT) simulated with different excipient molecules by MD simulations, in order to assess the solubility “index” and drug loading capacity of each excipient (figure taken from [\[3\]](#)).

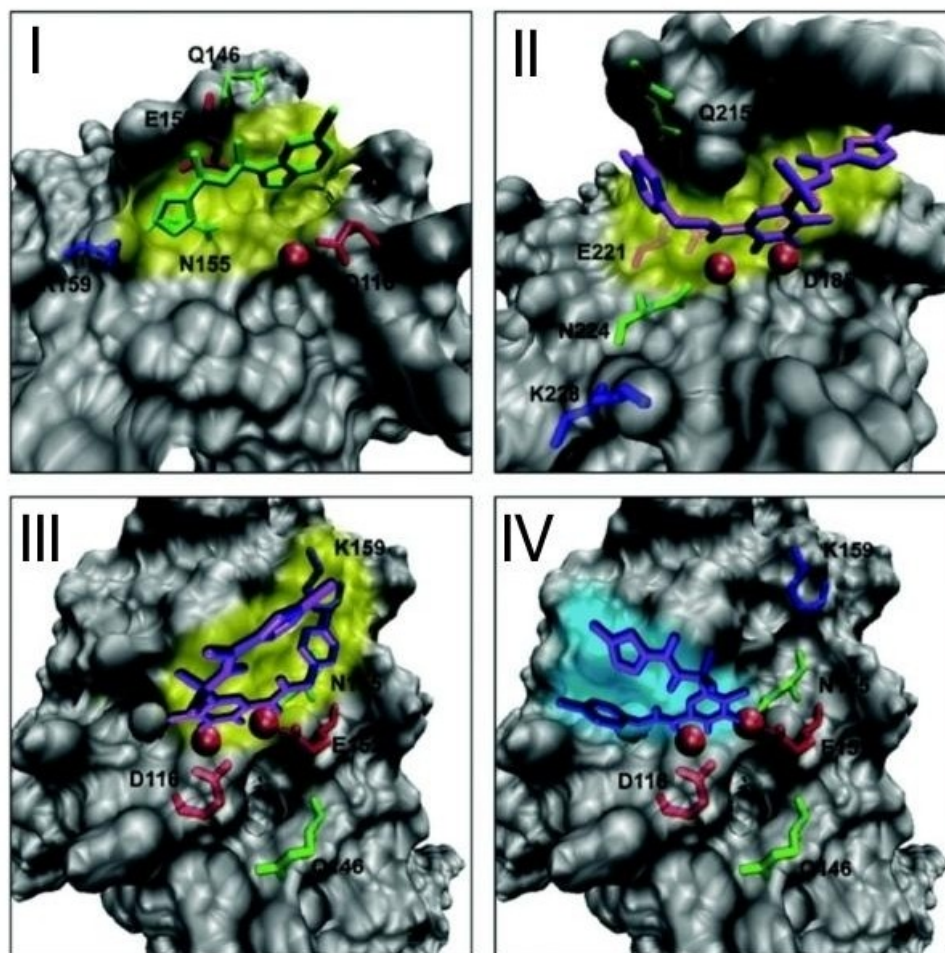


**Figure 4.2.** Comparison of drug/inhibitor-binding pockets to HIV integrase as solved experimentally and as predicted by theoretical modeling. (I-II) Experimental and (III-IV) calculated binding sites where the inhibitor 5-CITEP (green) and the drug Raltegravir (purple) bind to the viral enzyme (figure taken from [4]).

conformations of general building blocks, such as aminoacids or common organic functional groups, and with their mechanical interactions modeled by Newton's laws of motion. These kind of models require a considerable degree of parametrization in order to properly describe their interactions in function of time. An example of the use of MD for modeling of a biomolecule (bacteriophage lysozyme T4L) is shown in [figure 4.3a](#), depicting three snapshots of a MD study to understand the dynamics of this enzyme under biological conditions [5]. A different approach is coarse-grained simulations (CG). An example of CG simulation of a DNA section is shown in [figure 4.3b](#) with the atomistic and



CG models for a DNA section, illustrating the simplification process which “converts” portions of a molecule, in this case the individual nucleotide bases, into simpler units which interact in an identical way but are easier to analyze computationally [6].

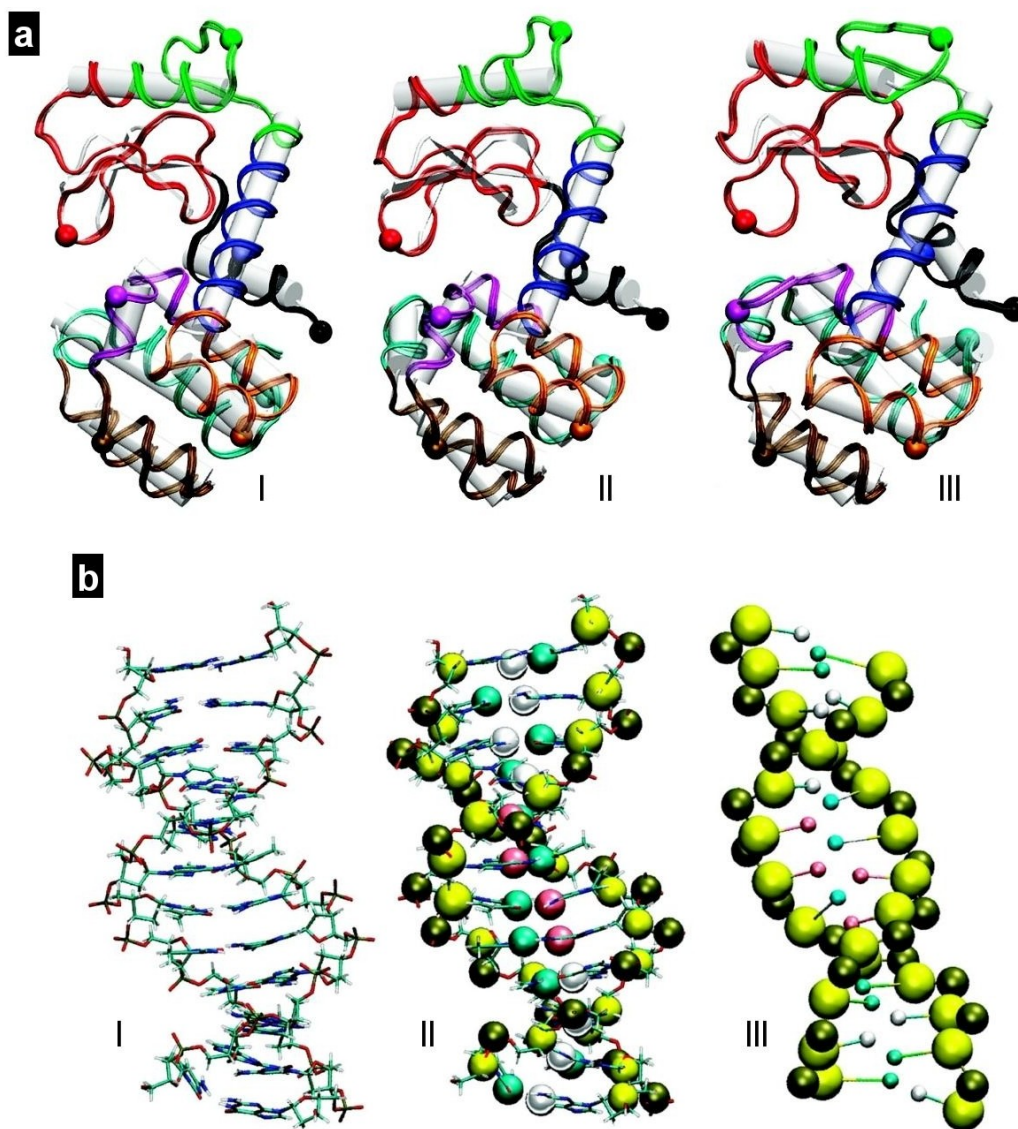


**Figure 4.3** (a) Molecular dynamics simulation of a bacteriophage lysozyme T4L, showing different stages of structure variations in function of time (I = 0 ns, II = 4 ns, III = 8.25 ns, figure taken from [5]). (b) Representation of a DNA fragment in its atomistic model (I), which has been simplified to the 3SPN-CG model and superimposed (II). (III) Shows the 3SPN-CG model utilized for simulation in [6].

It is important to highlight that this type of methodologies are currently being used even for the study of interactions between complex biosystems, such as a phospholipid bilayer membrane, and a carbon nanotube (see [figure 4.4](#)), leading to a deeper understanding on processes such as potential CNT cytotoxicity [7], a very relevant topic in the interaction of carbon nanostructures and living organisms.

In addition to these simplified approximations for simulating large biosystems, an increasing number of works study the interactions between biomolecules and nanostructures such as CNTs, graphene and other periodic systems, which are normally studied under more detailed frameworks. *Ab initio* calculations, for instance, allow to describe characteristics arising from quantum phenomena, such as the electronic properties of systems composed by several atoms up to few hundreds of them, since the methodologies used (such as density functional theory or DFT) are much more computationally demanding. [Figure 4.5](#) shows a DFT analysis of the interactions between

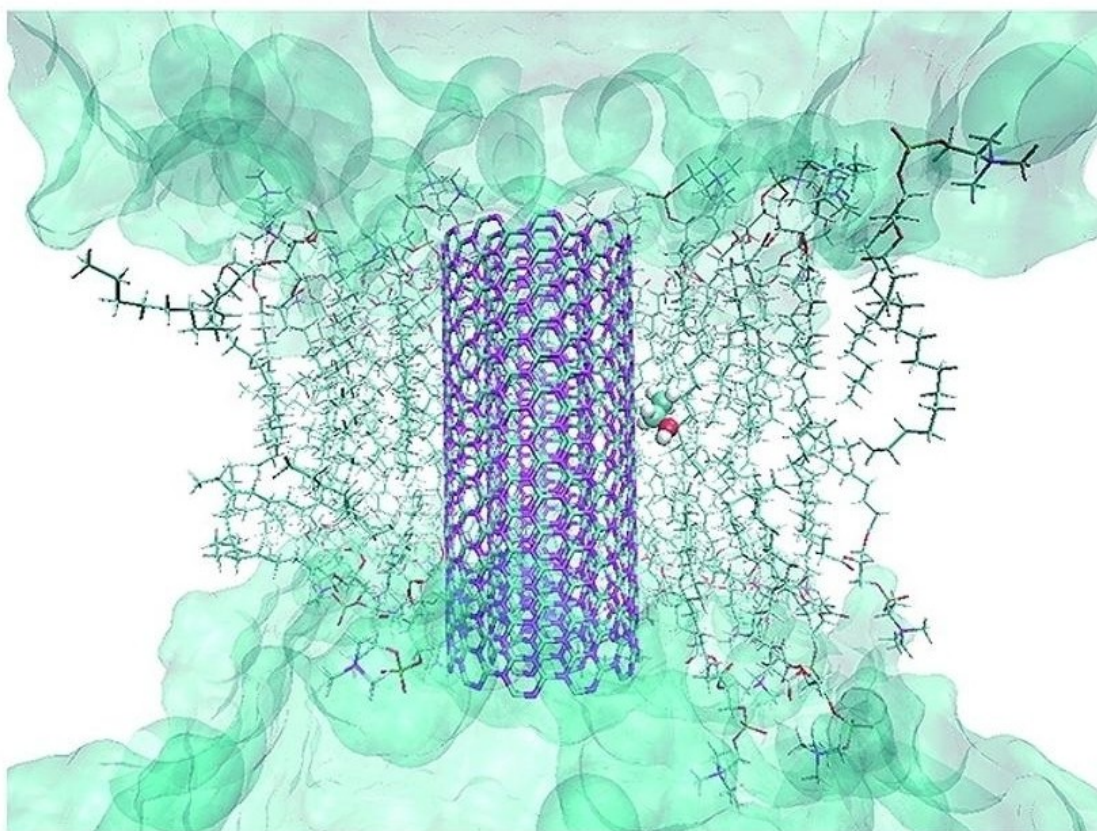


**Figure 4.4** CG simulation of a N-doped double-wall CNT embedded into a phospholipid bilayer (image taken from [\[7\]](#)).

pure and B-doped CNTs with the aminoacid glycine [8]. DFT shows that for the B-doped CNT the highest occupied molecular orbital (HOMO, which corresponds to the valence band of the system) is shared between the CNT and glycine, which could result in charge transfer, and thus be the basis for a biosensing device. The sensitivity of *ab-initio* methods to specific atomic interactions is also seen here by comparing how the change of the geometry changes the interactions of the glycine and the CNT.

In summary, the new capabilities in computing power in conjunction with the theoretical tools developed for the analysis of molecular systems at different scales, are allowing nanoscientists to explore complex interactions between nanostructured materials and biosystems, thus leading to important advancements in the development of nanobiotechnology.

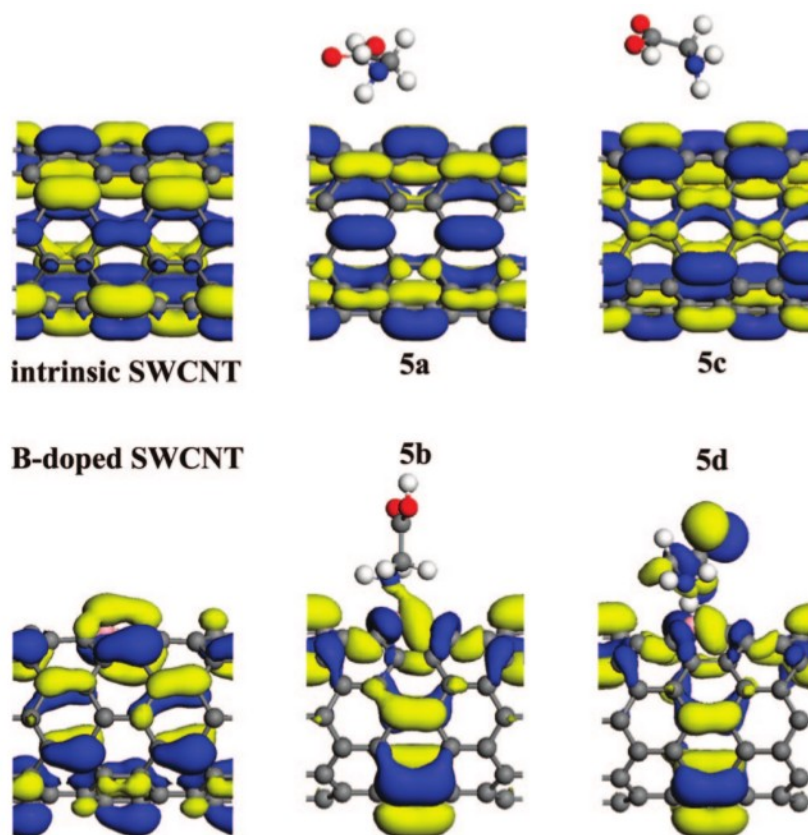


**Figure 4.5.** Isosurface plots calculated by DFT methods, depicting the highest occupied molecular orbital (HOMO) for pure (intrinsic) and B-doped SWNT, interacting with a glycine molecule, in two different spatial arrangements (figure taken from [8]).

## **4.2 Studying graphene and dopamine interaction**

Graphene based devices have several potential advantages for detection of specific molecules. Several theoretical [9-11] and experimental [12-17] reports have explored the possibility of graphene based field-effect transistors (FET) for nanodevices, in which electrostatic interactions between the analyte and the graphene channel provide sensing capabilities [18-20]. Graphene is a promising nanomaterial for fast sensor with high-sensitivity do to its properties: high electrical conductivity, quantum Hall effect, and a band gap tunable by chemical and physical means, including the application of external electric fields. For instance, Schedin et al. [21] demonstrated experimentally graphene based sensors capable of detecting individual gas molecules. This extremely high sensitivity has been attributed to conventional charge transfer phenomena occurring at the graphene surface, combined with the large changes in carriers density due to the addition of electrons or holes. Alternate explanations of the sensitivity of graphene consider chemical doping processes driven by electrostatic interactions between the graphene surface and charged sections of the adsorbed molecules. For example, Nistor et al. [22] refer to the 2D surface-induced electronegativity equalization produced by the conductive nature of graphene and special alignments between the adsorbate-graphene highest-occupied and lowest-unoccupied molecular orbitals (HOMO-LUMO).

The doping of graphene and other carbon nanomaterials has been explored as well as a practical way to tailor some of their properties [23]; it can alter the available charge density by the incorporation of non carbon atoms with excess electrons (e.g. nitrogen, for n-type doping) or electron-deficient (e.g. boron, for p-type doping) [14, 24-26]. Doping of nanocarbon materials increases reactivity near the doping sites due to localization of electronic states and reduced charge mobility due to electron scattering, which can be useful in FET devices for highly sensitive detectors [27, 28]. Moreover, the presence of lattice defects within the graphene structure can lead to changes in its electronic properties [29, 30]. For example, vacancy defects in graphene lattices induce strong localization of electronic states close to the Dirac point [31], thus enhancing chemical reactivity. In addition, theoretically show that pure graphene sections joined through 5-7 defects boundaries (i.e. consecutive pentagon-heptagon pairs fitted into graphene hexagonal lattices instead of two hexagons,) can present different electronic, magnetic and spin dependent conductance properties, depending on the orientation of these boundaries [32].

A deep understanding of the interactions between these graphene doping or defect

points and potential analytes is crucial for further advancements on graphene-based sensors development. It could be argued that, since changes on the electronic properties are different depending upon the doping or defect type, the interactions with external molecules would produce contrasting effects on the graphene electronic properties. This in turn could be advantageous in detection of biomolecules, since such chemical species are more complex than molecules detected by pure graphene-based gas sensors, for instance. There are some reports that have addressed the interactions between graphene or carbon nanotubes with important biomolecules such as aminoacids [8, 33], neurotransmitters [34, 35] and drugs [36, 37], demonstrating the feasibility of biosensors based on carbon nanomaterials.

In this study, we investigate the interactions between dopamine (DA) and pure (undoped), boron- and nitrogen-doped, and vacancy and Stone-Wales (SW) defected graphene (structures shown below in Figure 4.6), in order to determine differential effects on the graphene sheet in function of the doping or defect type present. We chose DA since it is an important biomolecule which has strong regulation effects on a wide range of biological processes, including neural processes as important as cognition; it also is representative of catecholamines, fundamental biomolecules with structures based on a benzene ring with two hydroxyl groups and a side-chain amine. We systematically assess how the graphene-DA interactions occur as a consequence of different doping and defect types, and in response to an electric field applied perpendicularly to the graphene's plane. This is, to the best of our knowledge, the first study to explore the combination of perpendicular E-fields with doped/defective graphene for biomolecule interaction studies, and therefore contributes a new approach to further develop carbon based biosensing applications.

### **4.3 Research contribution: theoretical model**

The electronic calculations were performed using density functional theory (DFT, see Appendix B for a description of this method) [38, 39] in the framework of the general gradient approximation (GGA) within the Perdew-Burke-Ernzerhof (PBE) approach [40] with a basis of linear combination of atomic orbitals (LCAO) as implemented in the SIESTA code [41, 42]. We used a double- $\zeta$  basis set plus polarization orbitals (DZP), the real-space grid used for charge and potential integration is equivalent to a plane wave cut-

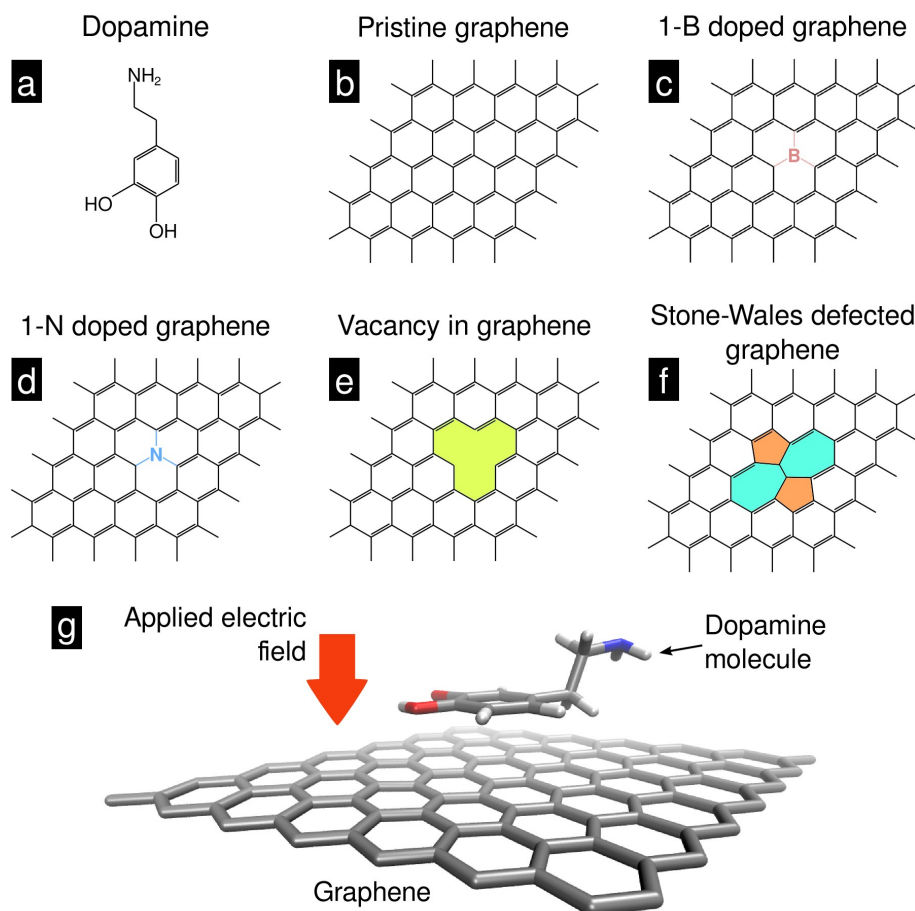


**Figure 4.6.** (a) Dopamine molecule. (b-f) Unit cell representations for pristine (undoped) graphene, boron- and nitrogen-doped graphene, and vacancy and SW defected graphene, respectively. (g) Molecular model of the calculated graphene systems, with the adsorbed dopamine molecule and the applied electric field.

off energy of 250 Rydbergs (Ry) and the pseudo-potentials (pp) were built from 1, 3, 4, 5, and 6 valence electrons for the hydrogen (H:  $1s^1$ ), boron (B:  $2s^2 2p^1$ ), carbon (C:  $2s^2 2p^2$ ), nitrogen (N:  $2s^2 2p^3$ ), and oxygen (O:  $2s^2 2p^4$ ) atoms respectively. The systems were constructed using a graphene supercell made of 98 atoms (97 for the vacancy case) plus the 22 atoms of DA for interaction calculations, with periodicity in two dimensions. The boron (nitrogen) doping were configured by substitutionally placing a B (N) atom into the graphene lattice, a carbon atom was removed for the vacancy and SW defects were achieved by rotating  $90^\circ$  one of the graphene's carbon-carbon bonds (see [figure 4.6b-f](#)). The vertical cell dimension was kept to a minimum of 40 Å in order to avoid graphene

layers interactions. For the calculations under E-field, we applied an external field of  $0.1 \text{ V \AA}^{-1}$ , perpendicular to the graphene plane and directed from the DA side to the graphene side (see [figure 4.6g](#)). All the calculations were performed using a Monkhorst-Pack grid of  $1 \times 25 \times 25$   $k$ -points, and relaxed by conjugate gradient minimization until the maximum forces were lower than  $0.06 \text{ eV \AA}^{-1}$ .

#### 4.4 Results and discussions

We analyzed the electronic structure of dopamine (molecular formula:  $\text{C}_8\text{H}_{11}\text{NO}_2$ , structural formula shown in [figure 4.6a](#)), which is formed by a benzene aromatic ring with two *meta*-(1,2) positioned hydroxyl groups and an ethyl amine side chain ( $-\text{C}_2\text{H}_4-\text{NH}_2$ ) in the 4-position. The calculated density of states (DOS) and wave functions around the Fermi level ( $E_F$ ) for DA are shown in [figure 4.7](#). The highest-occupied molecular orbital (HOMO, the molecule's valence orbital) is located at  $-2.815 \text{ eV}$  below  $E_F$ , whereas the lowest-unoccupied molecular orbital (LUMO) is localized  $1.219 \text{ eV}$  above  $E_F$ . Wave function isosurface plots corresponding to the HOMO-1, HOMO, LUMO, and LUMO+1 energy levels can be also seen in [figure 4.7](#), where the main difference between the occupied and unoccupied levels are the existence of electronic states for the  $\text{NH}_2$  tail only in the occupied levels. The benzene ring has states in both occupied and unoccupied levels, which are related to the  $\pi$  and  $\pi^*$  states arising from its aromatic nature.

In order to characterize the stability of the interactions between DA and the different doped/defective graphenes, the systems were relaxed using a conjugated gradient algorithm. After geometry optimization, the total energy and the different electronic properties were calculated. The cohesion energy ( $E_c$ ) was calculated by the following equation:

$$E_c = E_{\text{GNR-DA}} - E_{\text{DA}} - E_{\text{GNR}} \quad (\text{Eq. 1})$$

where the energy terms are, in succession:  $E_{\text{GNR-DA}}$  for the complex system (GNRs and dopamine),  $E_{\text{DA}}$  for the single dopamine molecule, and  $E_{\text{GNR}}$  the undoped or doped graphene nanoribbon used in the calculations. The counterpoise correction for the basis set superposition error was applied for all the systems and considered in the energy calculations. The cohesion energy results for each particular system, shown in [figure 4.8](#),

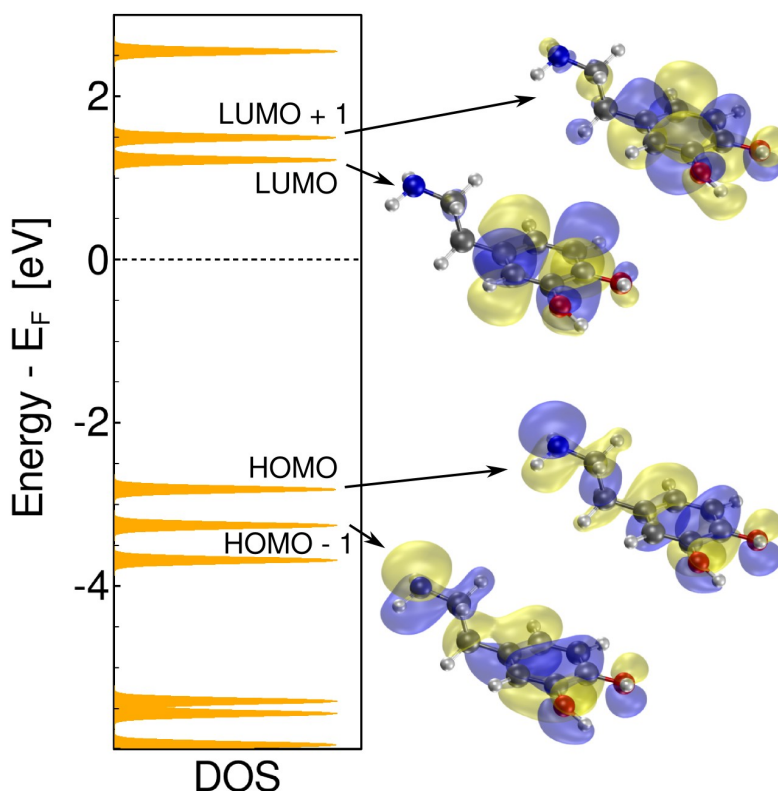


**Figure 4.7.** Electronic states energy distribution for an isolated DA molecule. The correspondent orbitals for the most relevant levels (i.e., HOMO-1, HOMO, LUMO and LUMO+1) are plotted as isosurfaces.

are in agreement with previous results on interactions between graphene and other molecules, which show for instance that for the L-leucine aminoacid, the adsorption energies can go from -170 to -310 meV, depending on the aminoacid geometry over the graphene sheet, whereas for other organic molecules such as tetracyanoquinodimethane (TCQN), these energies range from -151 to -635 meV [18, 19]. Also, the plot depicts the effects of an applied E-field on the stability. DA and B-doped graphene have the most energetically stable interactions (-436 meV), whereas less energetically favorable interactions occur between DA and defected graphene: SW (-111 meV) and vacancy defects (-55 meV). Interestingly, the presence of an external E-field produces significant changes in the DA-graphene interaction stability, specially for the pristine and B-doped cases, with changes around 140 meV, whereas for the N-doped, the difference is negligible (both systems are stabilized roughly at -190 meV). Both defective-graphene based systems also



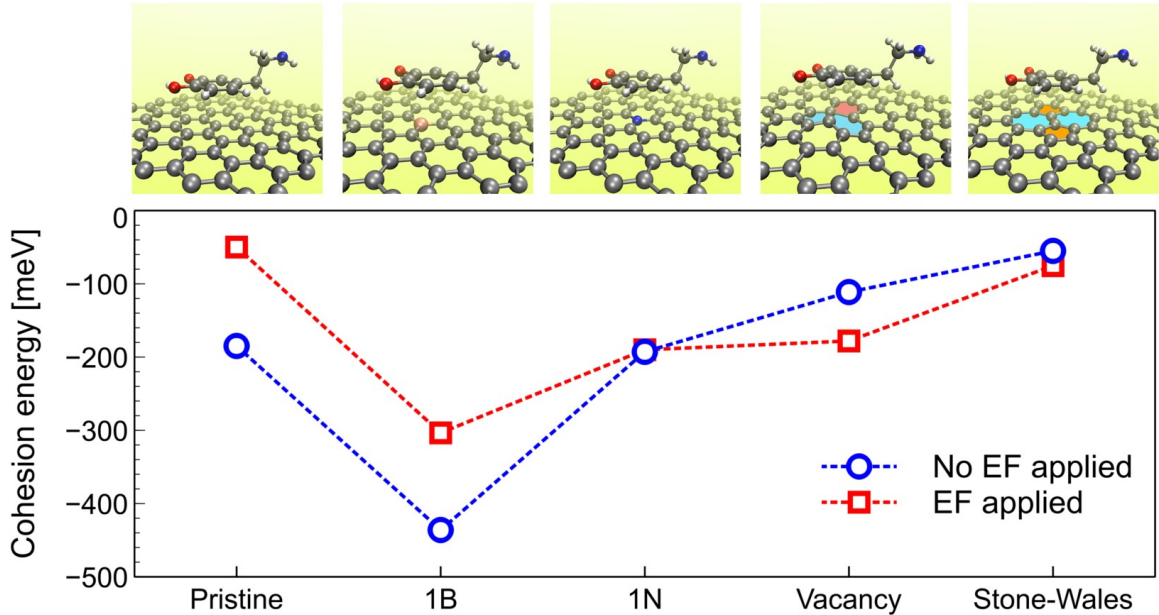


**Figure 4.8.** Energetic stability for all the systems calculated, in terms of DA-graphene cohesion energy. The molecular models on top represent the relaxed structure. The two plots show the stability changes induced by the application of an electric field ( $0.1 \text{ V \AA}^{-1}$ ) perpendicular to the graphene plane.

exhibit minimal changes in their interaction stability. These differences in stability can be attributed to alterations in the electronic local distribution at the doping/defective sites, which produce different configurations of occupied states with which the DA's valence orbitals can interact.

Figure 4.9 depicts the calculated band structures (fig. 4.9a-c), density of states (DOS, fig. 4.9d-f) and an isosurface plot for electronic states around the highest DA valence state (fig. 4.9g) for the system DA-pristine graphene. The band structures are plotted for pristine graphene (labeled pristine), graphene with an interacting DA molecule (pristine-DA), and graphene-DA with an applied perpendicular E-field (pristine-DA-field). As it can be observed, the DA states, which appear as flat bands in the plots, only are superimposed over graphene's valence energetic regions with a negligible effect on the graphene's electronic dispersion. The DOS plots confirm this from the well defined peaks arising only for DA states (orange/shaded peaks in fig. 4.9e and f). The effect of the applied E-field is clearly observed as an upshift of DA against graphene states, without noticeable effects on the electronic dispersion neither. The isosurface shown in fig. 4.9g represents the electronic

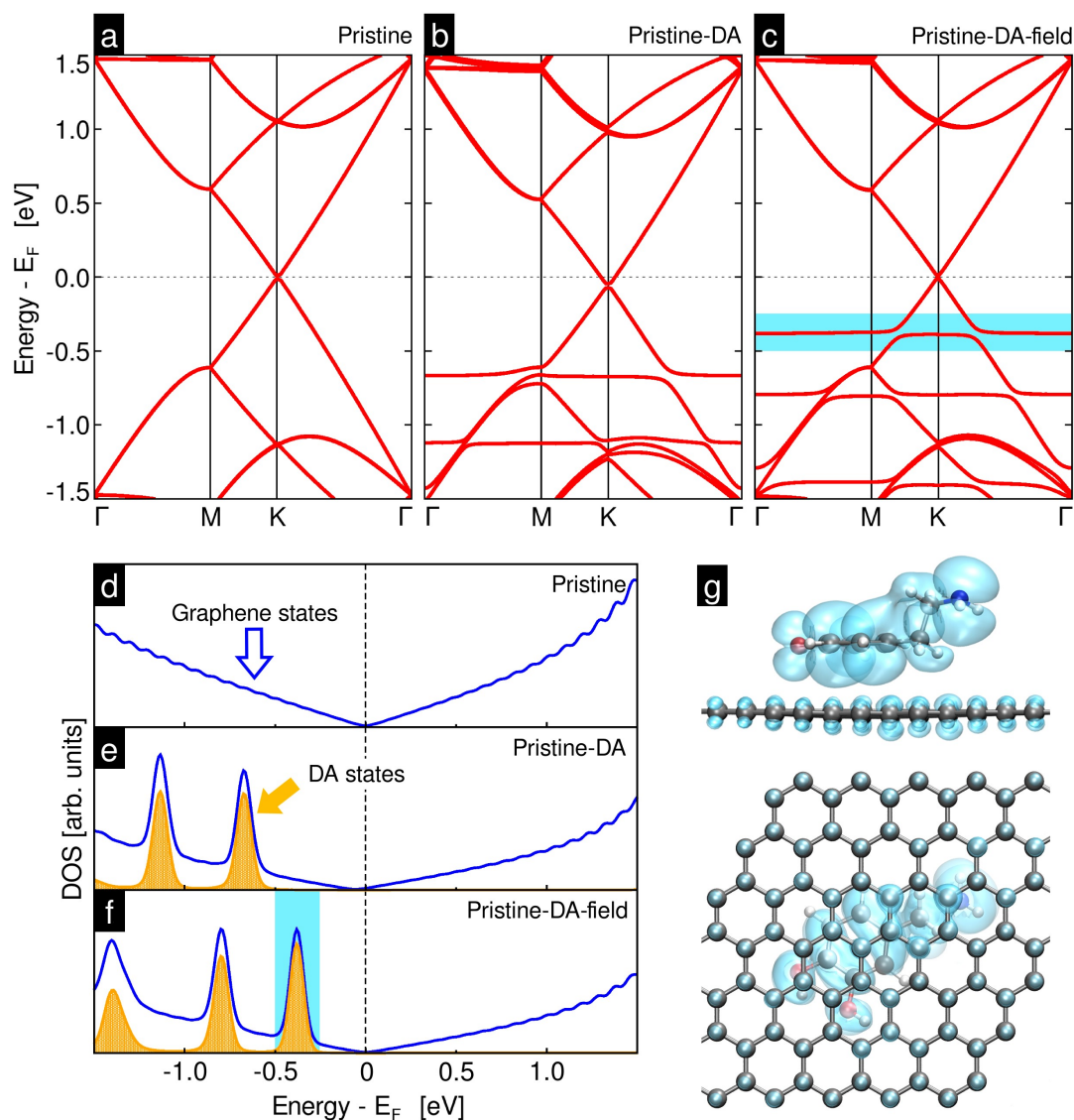


**figure 4.9.** (a) Band structure of pristine graphene, (b) interacting with an adsorbed DA molecule and (c) interacting with DA and under an applied E-field. (d-f) show the DOS, representing the states that belong to graphene (blue plots) and the ones introduced by DA (orange shaded peaks), for pure graphene, graphene-DA, and graphene-DA under applied E-field, respectively. (g) shows the bottom and side views of the electronic density isosurface plot ( $7 \text{ meV } \text{\AA}^{-1}$ ) of the system with the E-field applied. The isosurface was plotted for the electronic states around the highest DA valence state, highlighted in cyan shade in (c) and (f).

density within an energy window around the highest DA valence state (highlighted with a cyan shade in the band structure in [fig. 4.9c](#) and DOS peak in [fig. 4.9f](#)), which corresponds well with the orbitals shape observed for the DA's HOMO level (see [fig. 4.7](#)).

In [figure 4.10 and 4.11](#) are shown the band structures, DOS and electronic densities for both B- (labeled 1B-) and N-doped graphene (labeled 1N-) systems interacting with DA, with and without an applied E-field. In both cases, the band structure reveals the expected *p*-type (for 1B- systems) and *n*-type doping (for 1N- systems), and the corresponding effects of DA adsorption on the doped graphene. The DA valence states are introduced at different energetic levels within graphene's valence band, depending on the type of doping. It is noteworthy that the B-doping, which is the most energetically favored among the studied systems, allow DA states to exert significant changes in the electronic dispersion bands, evidenced by the broadening of DA peaks in the DOS plot (see [figs. 4.10e-f](#)). [Figure 4.10g](#) depicts the electronic density isosurface (bottom and side views) associated with the highest DA valence states (highlighted with a cyan shade in [figs. 4.10c and 4.10f](#)). In this case, the graphene and DA valence orbitals are considerably mixed, since the B-doping produces localized and highly reactive valence states around the doping sites that matches energetically with DA valence states. The effect of an applied E-field can be noted mainly at the intensity of the DA DOS peaks (see [fig. 4.10f](#)), which become stronger at highest energies with a consequent destabilization (see [fig. 4.8](#)). By contrasting, the same analysis for N-doped graphene reveals a much weaker interaction with DA, since the localized states are at graphene's conduction band, considerably far from the DA valence states (see [figs. 4.11b-c](#)). In this case, the DA states also undergo an upshifting when an E-field is applied, but no changes occur to the DA DOS peaks given the unlocalized nature of graphene's valence states ([figs. 4.11b-c and 4.11e-f](#)).

Similarly to the results for doped graphene, [figure 4.12 and 4.13](#) display the electronic structure for the defected (vacancy and SW) graphene interacting with DA, with and without an applied E-field. Neither vacancy nor SW defects induce significant changes towards *p*- or *n*-type semiconductor, nevertheless, strong electronic states localization can be observed for certain energetic levels. The vacancy-defected graphene exhibit a clear localized state just above  $E_F$ , which is associated to the C dangling bond produced by the vacancy (see [figs. 4.12a-c](#)), whereas for SW-defected graphene, there is as well a quasi-flat state in its conduction band, besides a small Dirac point shifting away from K (see [figs. 4.13a-c](#)). With respect to the interaction with DA, DOS plots reveal mixtures between graphene and DA electronic valence states (see [figs. 4.12e-f and 4.13e-f](#)), which are

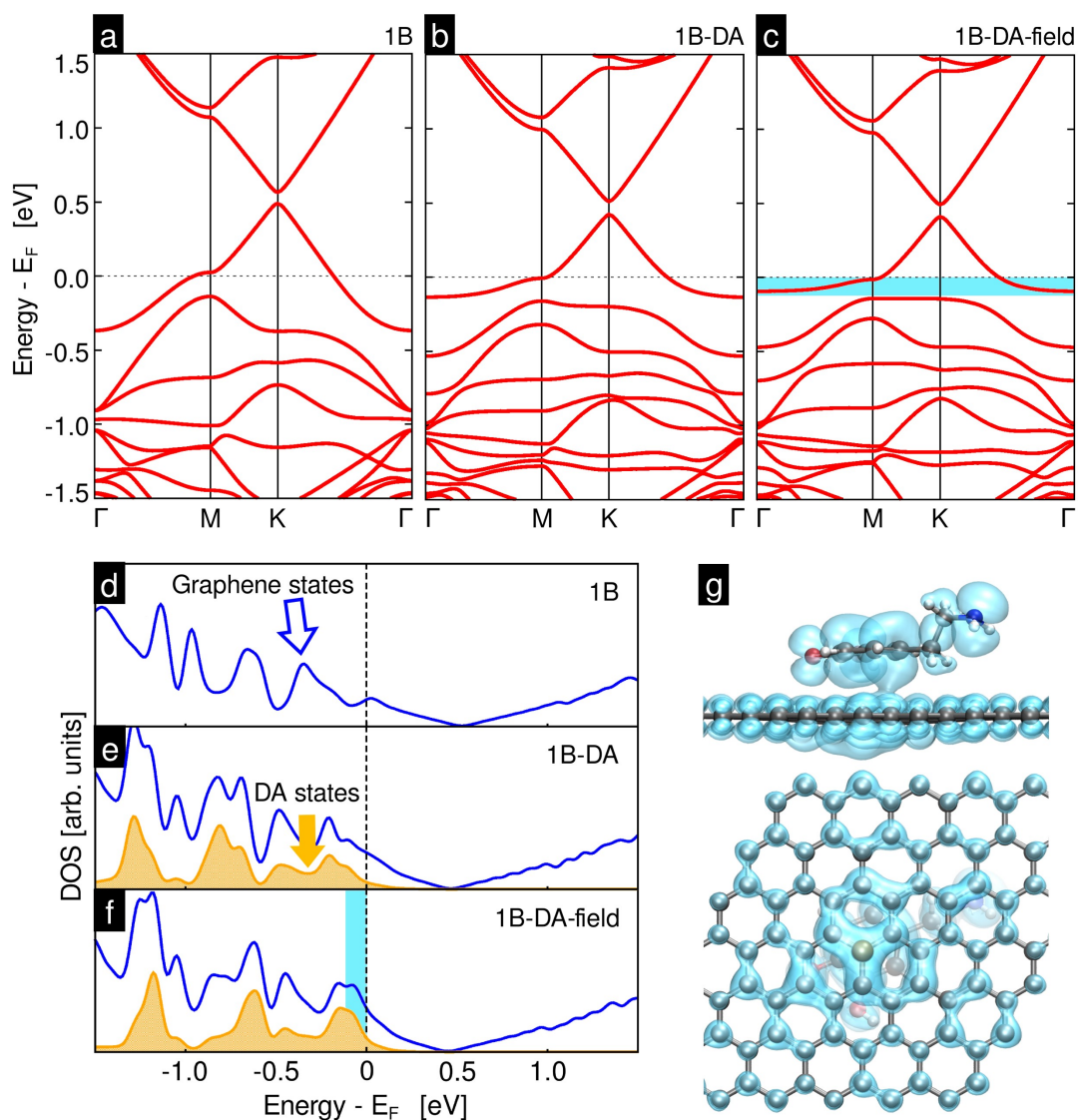


**Figure 4.10.** Band structure of (a) B-doped graphene, (b) B-doped graphene interacting with an adsorbed DA molecule and (c) interacting with DA and under an applied E-field. (d-f) show the DOS, representing the states that belong to graphene (blue plots) and the ones introduced by DA (orange shaded peaks), for pure B-doped graphene, B-doped graphene-DA, and B-doped graphene-DA under applied E-field, respectively. (g) shows the bottom and side views of the electronic density isosurface plot ( $7 \text{ meV } \text{\AA}^{-1}$ ) of the system with the E-field applied. The isosurface was plotted for the corresponding electronic states around the highest DA valence states, highlighted in blue shade in (c) and (f).

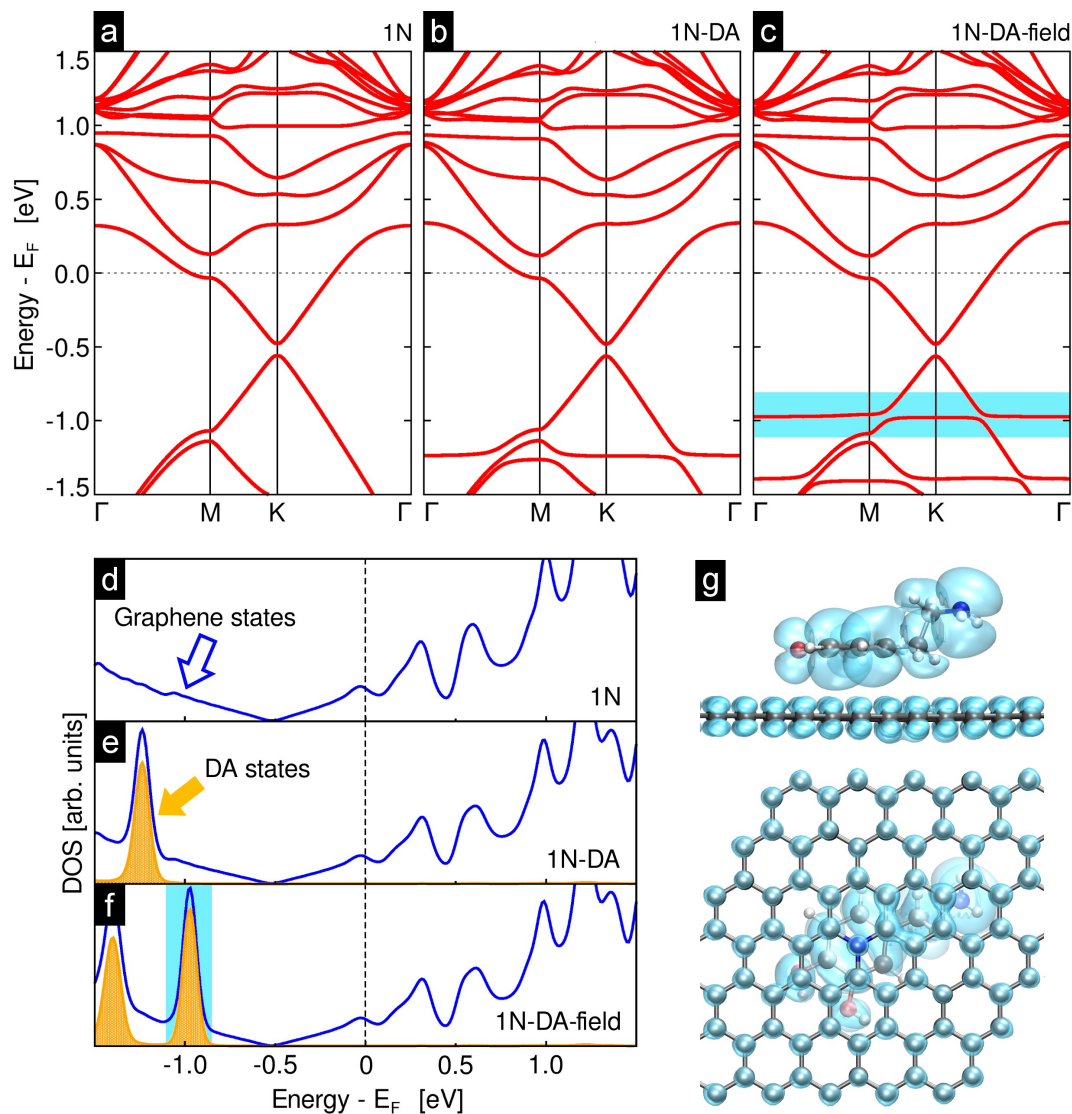


**Figure 4.11.** Band structure of **(a)** N-doped graphene, **(b)** N-doped graphene interacting with an adsorbed DA molecule and **(c)** interacting with DA and under an applied E-field. **(d-f)** show the DOS, representing the states that belong to graphene (blue plots) and the ones introduced by DA (orange shaded peaks), for pure N-doped graphene, N-doped graphene-DA, and N-doped graphene-DA under applied E-field, respectively. **(g)** shows the bottom and side views of the electronic density isosurface plot ( $7 \text{ meV } \text{\AA}^{-1}$ ) of the system with the E-field applied. The isosurface was plotted for the corresponding electronic states around the highest DA valence states, highlighted in blue shade in **(c)** and **(f)**.

sensitive in different extent to the application of an external E-field. As described for the doped graphene cases, the isosurfaces shown in [figs 4.12g](#) and [4.13g](#) represent the electronic density around the DA HOMO, where it is possible to observe that for the vacancy-defected graphene, the valence orbital mixing is dominated by DA states interacting with graphene's vacancy states. Also, they are closer to  $E_F$  when contrasted against SW-defected graphene. The applied E-field upshifts the DA states with respect to graphene, with an increase in the DOS peak intensity and sharpness related to rearrangements in orbital mixing, as occurred in doped graphene cases.

[Table 4.1](#) shows the changes induced on the DA orbital energies as a consequence of the applied E-field. The changes in DA energy gap ( $\Delta E_g$ ), i.e. the energetic difference between DA HOMO and LUMO, reveal that the B-doped and vacancy-defected graphene reduce  $E_g$  of adsorbed DA molecules, whereas pristine, N-doped and SW-defected graphene increases it when the perpendicular E-field is applied. The bigger magnitude changes are related to pristine, B- and N-doped graphene, with gap increasings/reductions up to 90 meV. Moreover, the DA HOMO upshiftings are also reported in [table 4.1](#) ( $\Delta E$  HOMO), where the largest changes induced by E-field are observed for pristine, N-doped and SW-defected graphene.

These results of DA adsorbed on graphene systems contrast significantly with previous studies where different type of organic molecules are placed in the surroundings of graphene sheets, given that the presence and effects of an applied electric field are considered. For instance, most of the related reports that address the changes occurring in graphene's electronic properties by electric fields are oriented to intrinsic pure or doped graphene, with one or two layers typically [\[10, 14\]](#). Moreover, some recent reports have appeared studying the effects of applied electric fields to doped graphene systems towards adsorption/desorption of simple molecules such as CO and H<sub>2</sub>, in hydrogen storage and high-sensitivity devices development [\[43-44\]](#). The studies addressing biomolecules adsorption in graphene are commonly limited to the analysis of the interaction energies and changes in graphene properties [\[45-47\]](#). This study agrees with most of the results presented in these reports; *i.e.* the energetic level of interactions between small biomolecules and graphene surface is between the range of 100 and 600 meV (in magnitude), and the presence of such biomolecules can produce charge transfer events in function of the molecule's electronic nature. In here we demonstrate that the use of electric fields, in combination of different type of doping or defect sites in graphene, can contribute to overcome some of the functional difficulties for graphene based devices development,

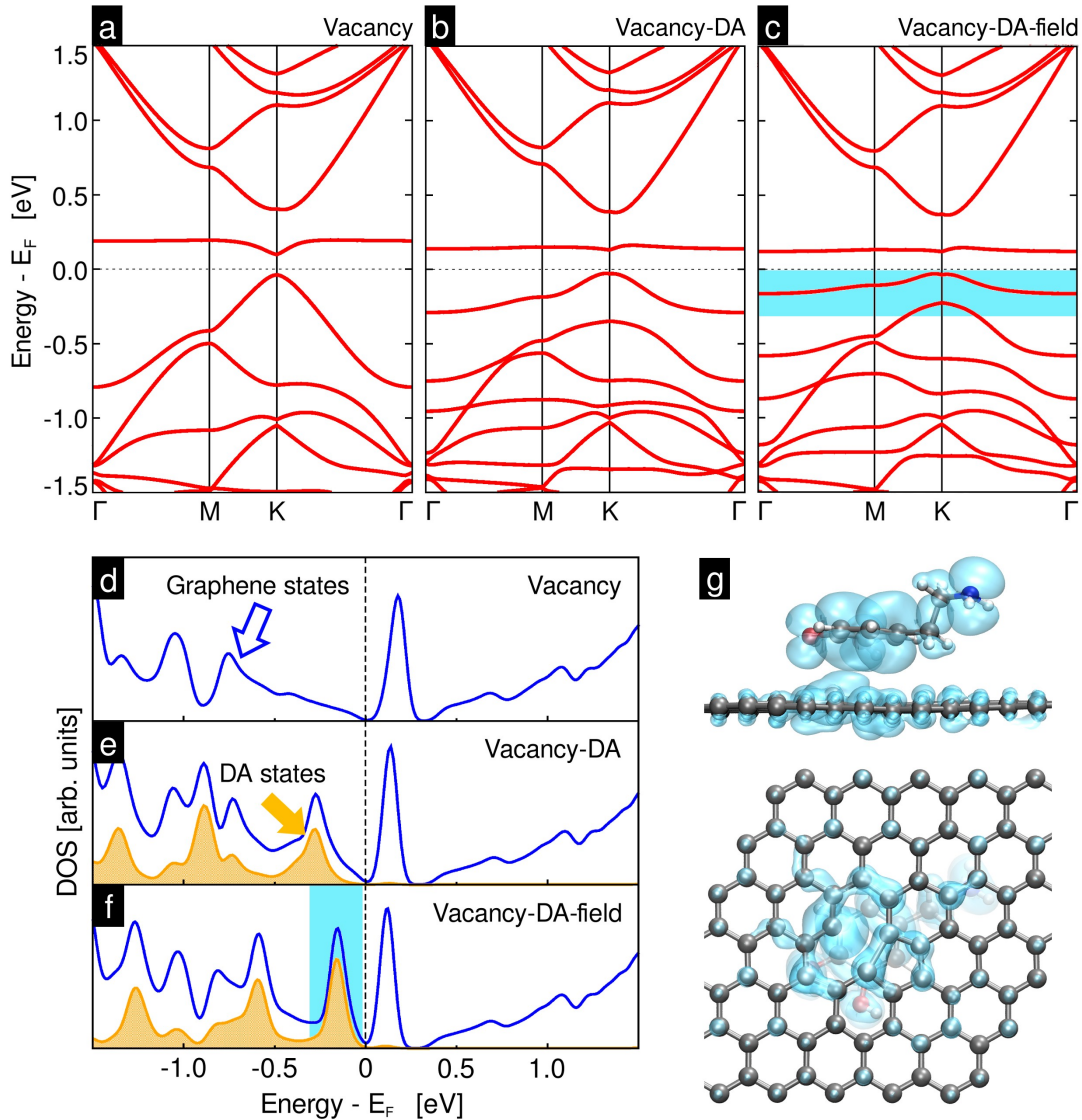


**Figure 4.12.** Band structure of (a) vacancy-defected graphene, (b) vacancy-graphene interacting with an adsorbed DA molecule and (c) interacting with DA and under an applied E-field. (d-f) show the DOS, representing the states that belong to graphene (blue plots) and the ones introduced by DA (orange shaded peaks), for pure vacancy-graphene, vacancy-graphene-DA, and vacancy-graphene-DA under applied E-field, respectively. (g) shows the bottom and side views of the electronic density isosurface plot ( $7 \text{ meV } \text{\AA}^{-1}$ ) of the system with the E-field applied. The isosurface was plotted for the corresponding electronic states around the highest DA valence states, highlighted in blue shade in (c) and (f).

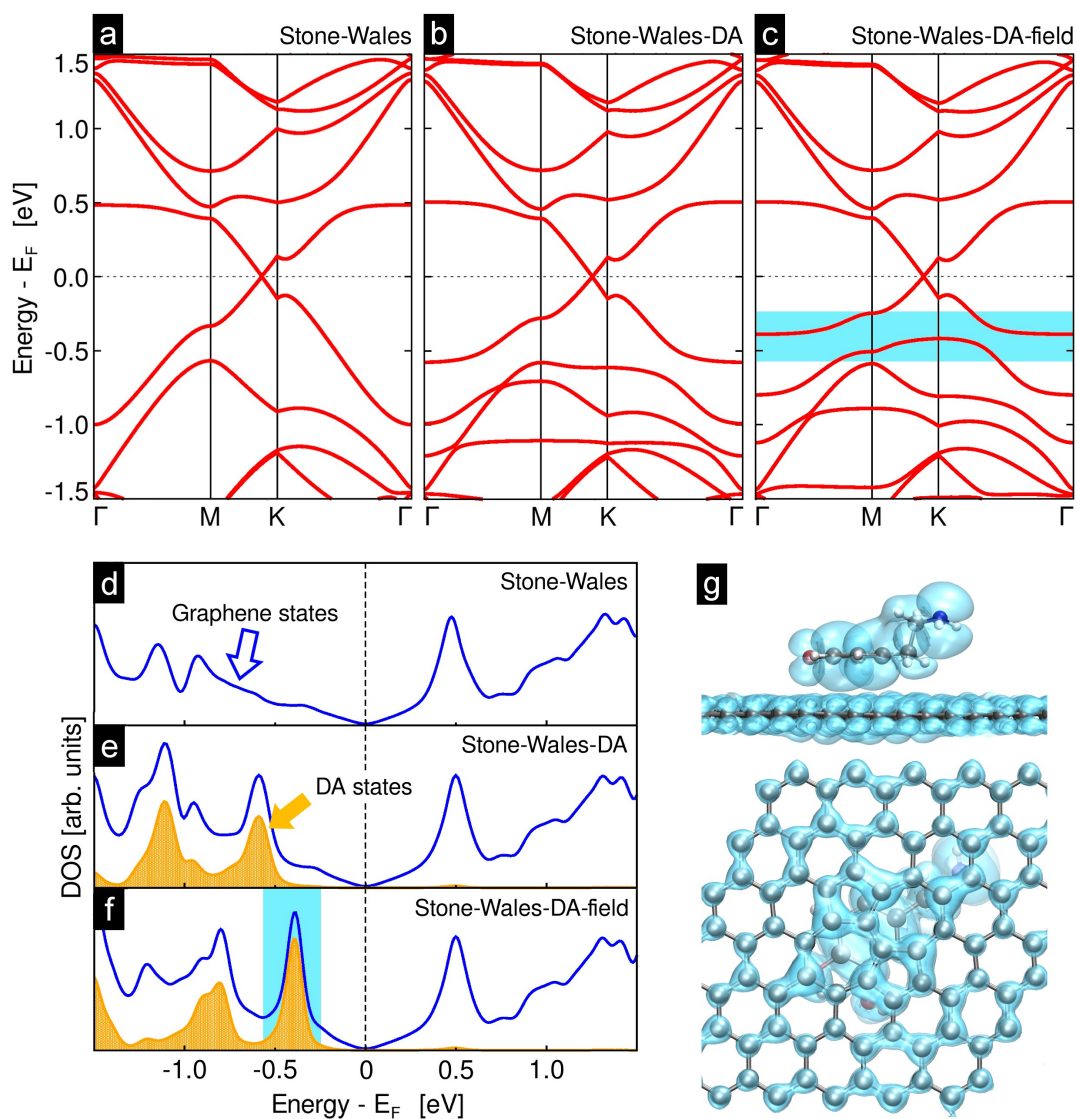


**Figure 4.13.** Band structure of (a) Stone Wales (SW)-defected graphene, (b) SW-graphene interacting with an adsorbed DA molecule and (c) interacting with DA and under an applied E-field. (d-f) show the DOS, representing the states that belong to graphene (blue plots) and the ones introduced by DA (orange shaded peaks), for pure SW-graphene, SW-graphene-DA, and SW-graphene-DA under applied E-field, respectively. (g) shows the bottom and side views of the electronic density isosurface plot ( $7 \text{ meV } \text{\AA}^{-1}$ ) of the system with the E-field applied. The isosurface was plotted for the corresponding electronic states around the highest DA valence states, highlighted in blue shade in (c) and (f).



such as easy control of the sensitivity for specific molecules, or the irreversible adsorption of species on the active sites, affecting the performance of high-sensitivity sensors.

## Conclusions

In summary, we investigated the electronic characteristics of the interaction between undoped, B- and N-doped graphene, vacancy- and SW-defected graphene with a DA molecule, and analyzed changes in function of a perpendicularly applied external E-field. Our DFT results revealed a physisorption mechanism for DA over the different graphene sheets, most likely due to relatively stable interactions between  $\pi$  electrons of the DA aromatic ring and the graphene's surface. Interestingly, the DA-graphene interaction can be controlled by means of external E-fields for pristine and B-doped graphene, whereas N-doped graphene-DA interactions are insensitive to them. Defects in graphene can also result in energetically stable adsorption of DA, with a smaller sensitivity to E-fields compared with doped ones. All this phenomena is related to the way DA valence levels mix with graphene's valence band, which is stronger when localized electronic states are available below graphene  $E_F$ . These results indicate the feasibility of using doped or defective graphene in biosensors for dopamine and related molecules.

**Table 4.1.** Changes in energy gap for DA ( $\Delta E_g$  DA) adsorbed on graphene, and upshiftings of DA HOMO energy ( $\Delta E$  DA) as a consequence of an applied E-field ( $0.1 \text{ V \AA}^{-1}$ ).

System	$\Delta E_g$ DA (meV)	$\Delta E$ DA HOMO (meV)
Pristine	63	291
1B-doped	-60	30
1N-doped	90	270
Vacancy-defected	-15	120
SW-defected	24	20

## **Bibliography**

- [1] C. A. Coulson and R. Taylor, "Studies in Graphite and Related Compounds I: Electronic Band Structure in Graphite" *Proceedings of the Physical Society. Section A*, vol. 65, no. 10, pp. 815–825, 1952.
- [2] M. S. Dresselhaus and J. G. Mavroides, "Fermi surface of graphite" *IBM Journal of Research and Development*, vol. 8, no. 3, p. 262, 1964.
- [3] L. Huynh, C. Neale, R. Pomès, and C. Allen, "Computational approaches to the rational design of nanoemulsions, polymeric micelles, and dendrimers for drug delivery.," *Nanomedicine : Nanotechnology, Biology, and Medicine*, vol. 8, no. 1, pp. 20–36, 2012.
- [4] T. Schlick, R. Collepardo-Guevara, L. A. Halvorsen, S. Jung, and X. Xiao, "Biomolecular modeling and simulation: a field coming of age," *Quarterly Reviews of Biophysics*, vol. 44, no. 02, pp. 191–228, 2011.
- [5] Z. Zhang and W. Wriggers, "Coarse-graining protein structures with local multivariate features from molecular dynamics" *Journal of Physical Chemistry B*, vol. 112, no. 44, pp. 14026–35, 2008.
- [6] R. C. DeMille, T. E. Cheatham, and V. Molinero, "A coarse-grained model of DNA with explicit solvation by water and ions" *Journal of Physical Chemistry B*, vol. 115, no. 1, pp. 132–42, 2011.
- [7] X. Li, Y. Shi, B. Miao, and Y. Zhao, "Effects of embedded carbon nanotube on properties of biomembrane" *Journal of Physical Chemistry B*, vol. 116, no. 18, pp. 5391–7, 2012.
- [8] W. Sun, Y. Bu, and Y. Wang, "Interaction between glycine/glycine radicals and intrinsic/boron-doped (8,0) single-walled carbon nanotubes: a density functional theory study" *Journal of Physical Chemistry B*, vol. 112, no. 48, pp. 15442–9, 2008.
- [9] A. H. Castro Neto, N. M. R. Peres, K. S. Novoselov, and A. K. Geim, "The electronic properties of graphene," *Reviews of Modern Physics*, vol. 81, no. 1, pp. 109–162, 2009.
- [10] J. G. Champlain, "A first principles theoretical examination of graphene-based field effect transistors," *Journal of Applied Physics*, vol. 109, no. 8, p. 084515, 2011.
- [11] L. Wang, J. Zheng, J. Zhou, R. Qin, H. Li, W.-N. Mei, S. Nagase, and J. Lu, "Tuning graphene nanoribbon field effect transistors via controlling doping level," *Theoretical Chemistry Accounts*, vol. 130, no. 2–3, pp. 483–489, 2011.

- [12] K. S. Novoselov, "Electric field effect in atomically thin carbon films," *Science*, vol. 306, pp. 666–669, 2004.
- [13] K. S. Novoselov, A. K. Geim, S. V. Morozov, S. V. Dubonos, Y. Zhang, and D. Jiang, "Room-temperature electric field effect and carrier-type inversion in graphene films", *Science*, vol. 306, no. 5696, pp. 660-662, 2004.
- [14] D. J. Late, A. Ghosh, K. S. Subrahmanyam, L. S. Panchakarla, S. B. Krupanidhi, and C. N. R. Rao, "Characteristics of field-effect transistors based on undoped and B- and N-doped few-layer graphenes," *Solid State Communications*, vol. 150, no. 15–16, pp. 734–738, 2010.
- [15] M.-W. Lin, C. Ling, Y. Zhang, H. J. Yoon, M. M.-C. Cheng, L. A. Agapito, N. Kioussis, N. Widjaja, and Z. Zhou, "Room-temperature high on/off ratio in suspended graphene nanoribbon field-effect transistors.," *Nanotechnology*, vol. 22, no. 26, p. 265201, 2011.
- [16] D. Reddy, L. F. Register, G. D. Carpenter, and S. K. Banerjee, "Graphene field-effect transistors," *Journal of Physics D-Applied Physics*, vol. 44, no. 31, p. 313001, 2011.
- [17] F. Schwierz, "Graphene transistors," *Nature Nanotechnology*, vol. 5, no. 7, pp. 487–496, 2010.
- [18] W. Qin, X. Li, W.-W. Bian, X.-J. Fan, and J.-Y. Qi, "Density functional theory calculations and molecular dynamics simulations of the adsorption of biomolecules on graphene surfaces," *Biomaterials*, vol. 31, no. 5, pp. 1007–1016, 2010.
- [19] M. Chi and Y.-P. Zhao, "First principle study of the interaction and charge transfer between graphene and organic molecules," *Computational Materials Science*, vol. 56, no. 0, pp. 79–84, 2012.
- [20] H. Jiang, "Chemical Preparation of Graphene-Based Nanomaterials and Their Applications in Chemical and Biological Sensors," *Small*, vol. 7, no. 17, pp. 2413–2427, 2011.
- [21] F. Schedin, A. K. Geim, S. V. Morozov, E. W. Hill, P. Blake, M. I. Katsnelson, and K. S. Novoselov, "Detection of individual gas molecules adsorbed on graphene," *Nature Materials*, vol. 6, no. 9, pp. 652–655, 2007.
- [22] R. A. Nistor, D. M. Newns, and G. J. Martyna, "The role of chemistry in graphene doping for carbon-based electronics.," *ACS Nano*, vol. 5, no. 4, pp. 3096–103, 2011.

- [23] R. Lv, Q. Li, A. R. Botello-Méndez, T. Hayashi, B. Wang, A. Berkdemir, Q. Hao, A. L. Elías, R. Cruz-Silva, H. R. Gutiérrez, Y. A. Kim, H. Muramatsu, J. Zhu, M. Endo, H. Terrones, J.-C. Charlier, M. Pan, and M. Terrones, "Nitrogen-doped graphene: beyond single substitution and enhanced molecular sensing.," *Scientific Reports*, vol. 2, p. 586, 2012.
- [24] T. Martins, R. Miwa, A. da Silva, and A. Fazio, "Electronic and Transport Properties of Boron-Doped Graphene Nanoribbons," *Physical Review Letters*, vol. 98, no. 19, 2007.
- [25] D. Wei, Y. Liu, Y. Wang, H. Zhang, L. Huang, and G. Yu, "Synthesis of N-Doped Graphene by Chemical Vapor Deposition and Its Electrical Properties," *Nano Letters*, vol. 9, no. 5, pp. 1752–1758, 2009.
- [26] S. S. Yu, W. T. Zheng, and Q. Jiang, "Electronic Properties of Nitrogen-/Boron-Doped Graphene Nanoribbons With Armchair Edges," *Nanotechnology, IEEE Transactions on*, vol. 9, no. 1, pp. 78–81, 2010.
- [27] E. Cruz-Silva, Z. M. Barnett, B. G. Sumpter, and V. Meunier, "Structural, magnetic, and transport properties of substitutionally doped graphene nanoribbons from first principles," *Physical Review B*, vol. 83, p. 155445, 2011.
- [28] X.-L. Wei, Y.-P. Chen, W.-L. Liu, and J.-X. Zhong, "Enhanced gas sensor based on nitrogen-vacancy graphene nanoribbons," *Physics Letters A*, vol. 376, no. 4, pp. 559–562, 2012.
- [29] H. Terrones, R. Lv, M. Terrones, and M. S. Dresselhaus, "The role of defects and doping in 2D graphene sheets and 1D nanoribbons.," *Reports on Progress in Physics*, vol. 75, no. 6, p. 062501, 2012.
- [30] P. T. Araujo, M. Terrones, and M. S. Dresselhaus, "Defects and impurities in graphene- like materials," *Materials Today*, vol. 15, no. 3, pp. 98–109, 2012.
- [31] J. Palacios, J. Fernández-Rossier, and L. Brey, "Vacancy-induced magnetism in graphene and graphene ribbons," *Physical Review B*, vol. 77, no. 19, 2008.
- [32] A. R. Botello-Méndez, E. Cruz-Silva, F. López-Urías, B. G. Sumpter, V. Meunier, M. Terrones, and H. Terrones, "Spin polarized conductance in hybrid graphene nanoribbons using 5-7 defects.," *ACS Nano*, vol. 3, no. 11, pp. 3606–12, 2009.
- [33] S. Wu, X. Q. Lan, F. F. Huang, Z. Z. Luo, H. X. Ju, C. G. Meng, and C. Y. Duan, "Selective electrochemical detection of cysteine in complex serum by graphene nanoribbon," *Biosensors & Bioelectronics*, vol. 32, no. 1, pp. 293–296, 2012.
- [34] S. Alwarappan, A. Erdem, C. Liu, and C.-Z. Li, "Probing the Electrochemical

- Properties of Graphene Nanosheets for Biosensing Applications,” *Journal of Physical Chemistry C*, vol. 113, no. 20, pp. 8853–8857, 2009.
- [35] Y. Zhang, R. Yuan, Y. Chai, W. Li, X. Zhong, and H. Zhong, “Simultaneous voltammetric determination for DA, AA and NO(2)(-) based on graphene/poly-cyclodextrin/MWCNTs nanocomposite platform.,” *Biosensors & Bioelectronics*, vol. 26, no. 9, pp. 3980–3977, 2011.
- [36] B. Ghalandari, M. Monajjemi, and F. Mollaamin, “Theoretical Investigation of Carbon Nanotube Binding to DNA in View of Drug Delivery,” *Journal of Computational and Theoretical Nanoscience*, vol. 8, no. 7, pp. 1212–1219, 2011.
- [37] V. V Chaban and O. V Prezhdo, “Water Boiling Inside Carbon Nanotubes: Toward Efficient Drug Release,” *ACS Nano*, vol. 5, no. 7, pp. 5647–5655, 2011.
- [38] P. Hohenberg, “Inhomogeneous Electron Gas,” *Physical Review*, vol. 136, no. 3B, pp. B864–B871, 1964.
- [39] W. Kohn and L. J. Sham, “Self-Consistent Equations Including Exchange and Correlation Effects,” *Physical Review*, vol. 140, no. 4A, pp. A1133–A1138, 1965.
- [40] J. P. Perdew, “Generalized Gradient Approximation Made Simple” *Physical Review Letters*, vol. 78, no. 7, p. 1396, 1997.
- [41] J. Junquera, O. Paz, D. Sánchez-Portal, and E. Artacho, “Numerical atomic orbitals for linear-scaling calculations,” *Physical Review B*, vol. 64, p. 235111, 2001.
- [42] J. M. Soler, E. Artacho, J. D. Gale, A. García, J. Junquera, P. Ordejón, and D. Sánchez-Portal, “The SIESTA method for ab initio order- N materials simulation,” *Journal of Physics: Condensed Matter*, vol. 14, no. 11, p. 2745, 2002.
- [43] Z. M. Ao, S. Li, and Q. Jiang, “Correlation of the applied electrical field and CO adsorption/desorption behavior on Al-doped graphene,” *Solid State Communications*, vol. 150, no. 13–14, pp. 680–683, 2010.
- [44] Z. M. Ao and F. M. Peeters, “Electric Field Activated Hydrogen Dissociative Adsorption to Nitrogen-Doped Graphene,” *Journal of Physical Chemistry C*, vol. 114, no. 34, pp. 14503–14509, 2010.
- [45] F. Ma, Z. Zhang, H. Jia, X. Liu, Y. Hao, and B. Xu, “Adsorption of cysteine molecule on intrinsic and Pt-doped graphene: A first-principle study,” *Journal of Molecular Structure: THEOCHEM*, vol. 955, no. 1–3, pp. 134–139, 2010.
- [46] C. Cazorla, “Ab initio study of the binding of collagen amino acids to graphene and A-doped (A=H, Ca) graphene,” *Thin Solid Films*, vol. 518, no. 23, pp. 6951–6961, 2010.

- [47] L. Ou, Y. Luo, and G. Wei, "Atomic-level study of adsorption, conformational change, and dimerization of an  $\alpha$ -helical peptide at graphene surface" *Journal of Physical Chemistry. B*, vol. 115, no. 32, pp. 9813–22, 2011.



# Chapter 5

## Biosensing properties of nanomaterials based devices

### 5.1 Introduction to biosensing devices

The advancements in microelectronics and materials research have allowed important improvements in biosensing devices, a clear multidisciplinary application example of both fields. The definition of biosensor we will follow here is: an electronic device that employs biological elements —such as anti-bodies, enzymes, receptor proteins, lectins, nucleic acids, cells, or tissue sections— as the analyte sensor and couples such biological element to a transducer (see [figure 2.13](#) as an example, in [Chapter 2](#)). Specific interactions between the target analyte and the biorecognition element produce a physicochemical change, which is detected and measured by the transducer. The transducer then converts the biochemical signal into an electronic signal that is processed into an analog or digital format. The amount of signal generated is directly proportional to the concentration of the analyte, allowing for both quantitative and qualitative measurements in real time.

Recent advancements in biochemistry, molecular biology and immunochemistry have expanded the range of biorecognition elements, improving assay selectivity and sensitivity, while the advent of new electronic and optoelectronic systems have enabled the



development of small, inexpensive biosensors. In addition, developments in fiber optics and micro-electronics have produced smaller and durable signal transducers, with improved signal/noise ratios and reduced manufacturing costs. Moreover, as mentioned in [Section 2.1.1](#), the introduction of nanomaterials into bioengineering has made easier some conventional approaches for biosensing and even for biostimulation applications. [Figure 5.1a](#) shows a scale comparison between common nanomaterials, and several biological systems and structures, the latter being the target for study or detection with the former. Exemplar 1D nanomaterials (CNTs, Si nanowires and inorganic nanobelts), are shown in [figure 5.1b-g](#) with two application models for biosensing [\[1\]](#).

Progress in nanomaterials represents tremendous opportunities for improving current bioelectronic sensing systems, since the materials currently used exhibit significant drawbacks. For instance, [figure 5.2a-b](#) shows a common model of neural electrodes intended to be inserted into nervous tissue to record electric activity and stimulate surrounding tissue with electric signals as well. The arrays of needle-like Si electrodes of such biosensors produce inflammation and immune response due to the traumatic insertion of the solid electrodes in the soft tissue, chemical and mechanical incompatibility of the electrode material and the tissue, and generation of toxic by-products at the electrode-electrolyte interface during electrical stimulation, which cannot be tolerated by the physiological medium [\[2\]](#). Additionally due to prolonged stimulation there is induced neuronal activity, which changes the ionic concentrations of both intracellular and extracellular fluids [\[3, 4\]](#).

An alternative design for recording cellular electric activity is shown in [figure 5.3](#): a semi-flat array of small and patterned electrodes which can interact directly with individual electrogenic cells such as neurons or cardiomyocytes. This kind of biosensing devices is built from deposition of metallic islands, which can be connected independently by conventional microelectronic technology. An oxide layer coating isolates the conductive parts, enabling operation in biological environments. Electrical contact is achieved when cells engulf the micronail tips, allowing recording of electrical activity as well as stimulation of individual cells [\[5\]](#). Even if this design presents several advantages in comparison to the needle-like Si electrodes, these biosensors still present complications associated with their electrical operation and natural immune response, such as degradation of metallic parts provoked by electrochemical reactions [\[4\]](#), cytotoxicity [\[6\]](#), charge transfer reduction from the electrode covering with extracellular proteins [\[7\]](#).

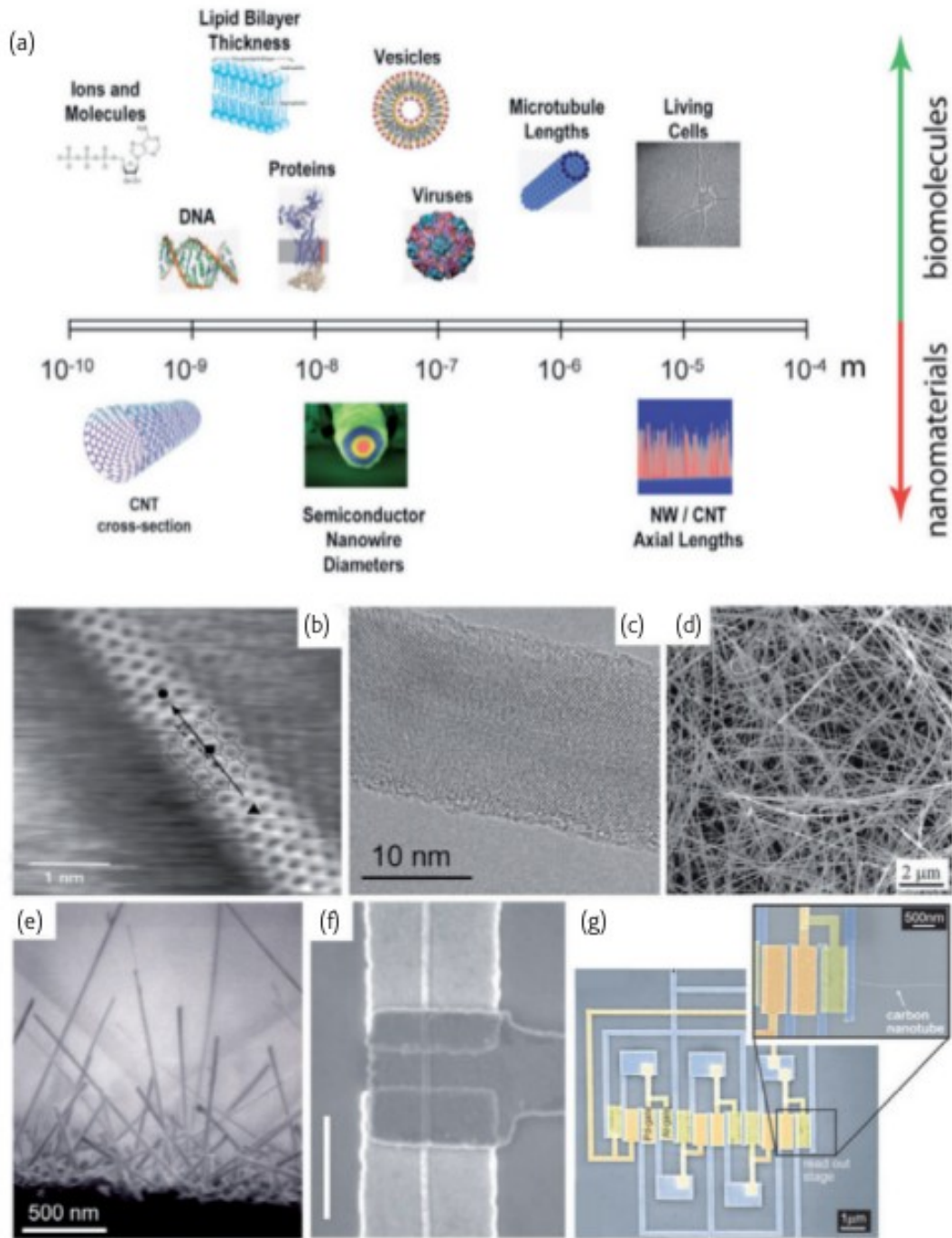


**Figure 5.1.** 1D nanomaterials and devices. (a) Comparative size of some key biological structures and nanomaterials. (b) STM image of a SWNT. (c) High-resolution TEM of a Si nanowire. (d) SEM image of  $\text{In}_2\text{O}_3$  nanobelts. (e) SEM image of Si nanowires. (f) SEM image of Ge/Si core/shell nanowire device. The Au top gate overlaps with the Ni source/drain electrodes (scale bar 500 nm). (g) SEM image of SWNT ring oscillator circuit. Image taken from [1].

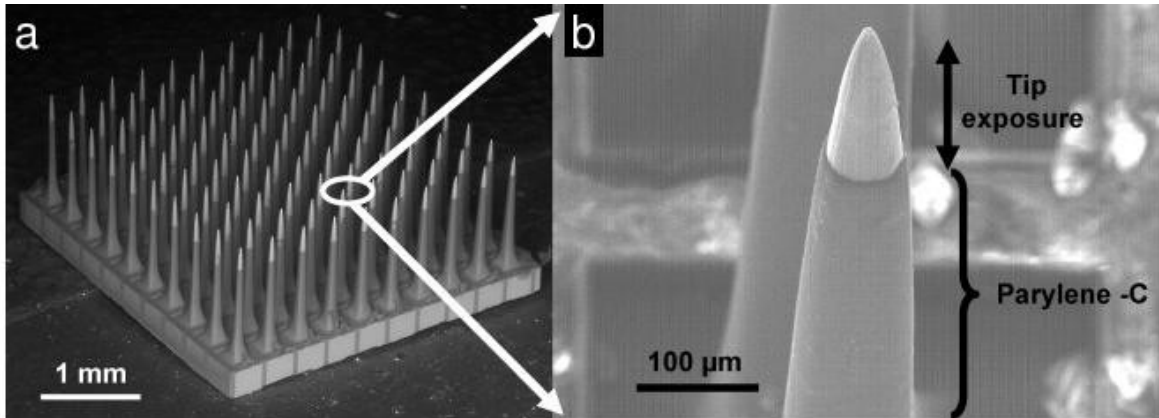


**Figure 5.2.** Common approaches for neural interface electrodes: **(a)** Scanning electron micrograph of the Utah electrode array (UEA) and **(b)** a higher magnification image of one electrode depicting tip exposure. The UEA is encapsulated by an insulating Parylene-C layer, with the exception of the tip ( $\sim 100 \mu\text{m}$ ) of the electrode which forms the active site for stimulation and/or recording of neural signals (images taken from [4]).

Given the novel characteristics of new nanomaterials, it is expected that advances in bionanotechnology research will be of great benefit to the development of new and efficient biosensing and biostimulating electronic devices. As presented above in [Section 2.1.1](#), metallic nanoparticles, nanowires, CNTs and other layered materials such as graphene, are being successfully explored for specific biosensing and other bioapplications. Yet, there is still potential for many further improvements in the exploitation of the electronic and optical properties of nanomaterials in biosensing.

### 5.1.1 Carbon nanomaterial based bioelectronics

Among carbon nanostructures, CNTs and graphene are object of the most intensive research, including their exploration for bioengineering applications. This is because, as reviewed in [Chapter 1](#), their characteristics rival or even outperform those of conventional materials. Their mechanical, chemical and electronic properties make them an ideal candidate for bionanoelectronic devices, from simply substituting conventional semiconductor materials in FET biosensors, through their use in conjunction with existing technologies in order to improve electrical and mechanical properties, to totally new designs of bioengineered devices [8].

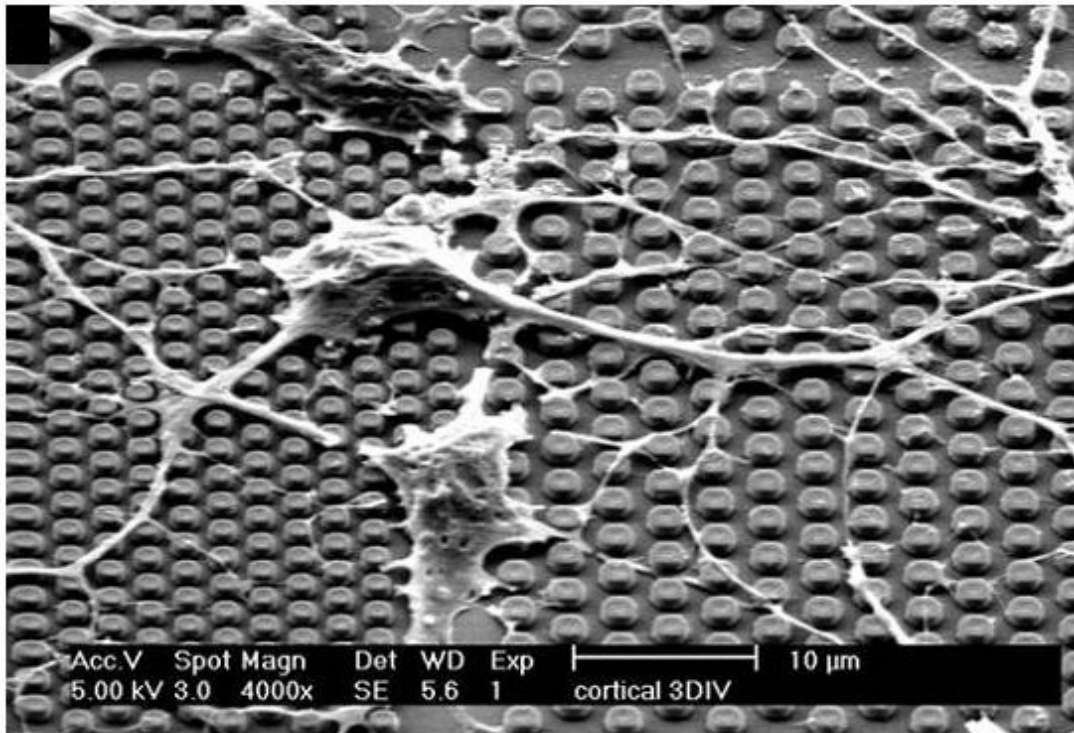


**Figure 5.3** Cortical neurons engulfing microscopic nail structures on the surface of IMEC's © micronail chip (3-day in vitro culture, image taken from [5]).

Figure 2.22a shows an example of CNTs being used as coating for conventional tungsten electrode, which results in an important impedance reduction and improvement in signal-to-noise ratio when used for neuronal recordings [9]. Figure 2.22g, h also shows the combination of conventional electronic circuitry with CNTs grown in specific sites, where the device is intended to interact with living electrogenic cells. The presence of CNT improved the quality of the cell activity recording performed, and even allows a better interaction for electric stimulation of individual cells, which is useful for neuronal networks research [10].

Carbon nanostructures and graphene are being explored intensively for new biosensing applications, where they are substituting conventional materials such as silicon or metallic oxides with results indicating superior sensitivities and design flexibilities. Additionally, the functionalization of CNTs and graphene for FET based biosensing has been demonstrated [11] (see, figure 5.4 for example). This approach is specially convenient for bioengineering applications, given their chemical and electronic properties: they can be functionalized with

an enormous variety of biomolecules, ranging from small aminoacids to peptides, big proteins and DNA or RNA chains, which confers them specificity by interactions such as ligand-receptor or nucleic acid matching (see [Section 2.1.2](#)). Moreover, the diverse functionalization reactions allow different linkage possibilities between nanomaterials and biosystems, which could be used to modulate the effect on the electronic behavior of the CNT or graphene FET channel [\[12\]](#).

### 5.1.2 Using doped carbon nanomaterials for bioelectronic devices

The study and synthesis of doped carbon nanomaterials is one of many considerable advancements in carbon nanotechnology; however, most of the applications that have been reported or are being explored currently are related to pure carbon nanostructures. This can be attributed to the relatively easier synthesis of undoped nanocarbons, or to the fact that

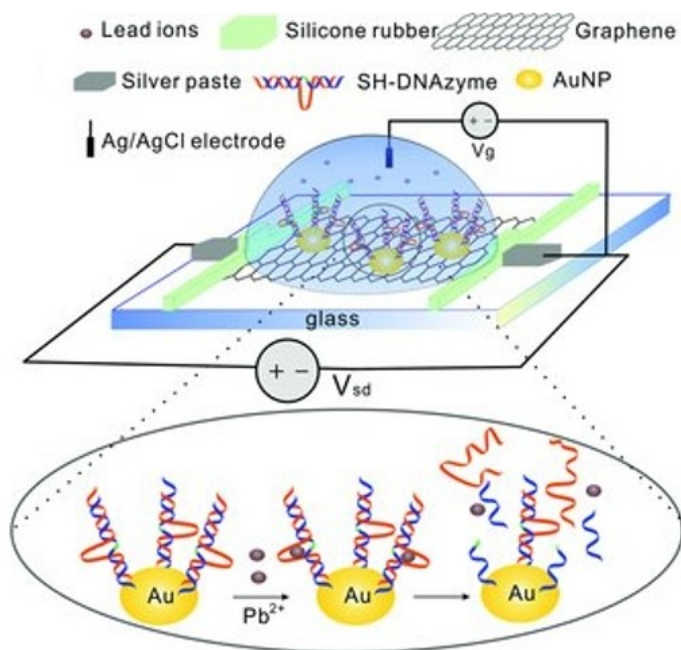


**Figure 5.4.** Nanomaterials for improving existing technologies: Nanostructures such as graphene are being explored for complete substitution of conventional semiconductors in FET biosensors (taken from [\[11\]](#)). See also the examples shown in [figure 2.22](#).

they are better known, as well as commercially available, than doped nanocarbons. In any case, the use of doped nanostructures, such as N-doped CNTs and graphene, can be advantageous from several perspectives that have been scarcely addressed and that have a great potential for improving the performance of nanomaterials based biodevices. Consider, for instance, the properties of N-doped CNTs, graphene and graphitic nanoribbons, described in [sections 1.3.2](#), [1.4.2](#) and [1.5.2](#), their substantial differences in chemical and electrical behavior can be utilized for more efficient chemical reactions, catalysis, and improved sensitivities in gas sensing applications, among other applications.

From the bioengineering point of view, doped carbon nanostructures are very appealing because they appear to be less toxic than their pure-carbon counterparts (see [section 2.1.3](#)). For example, N-doped CNTs can be administered through several ways, such as nasal,

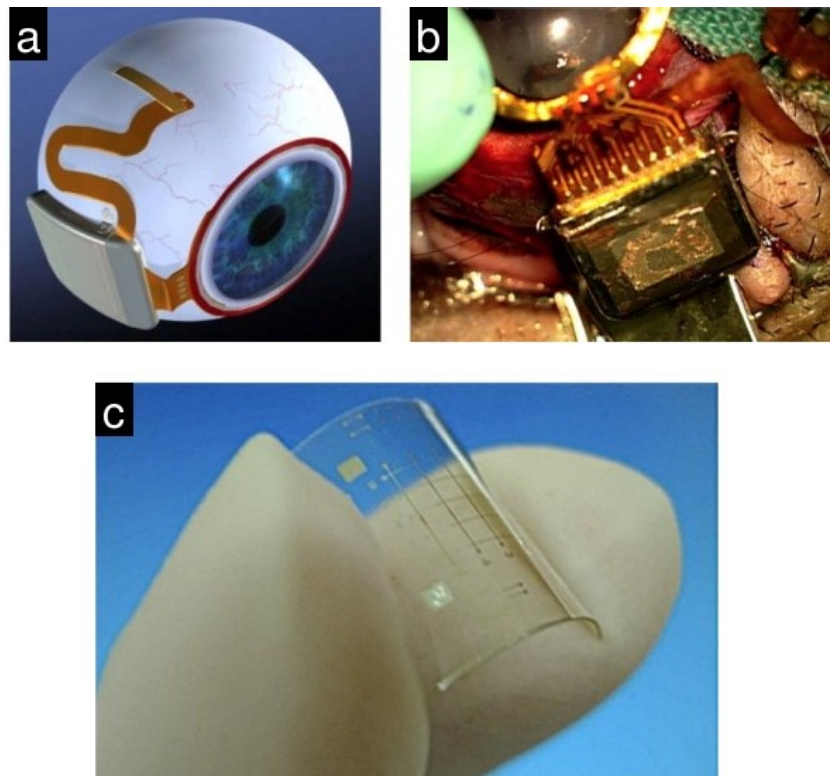


**Figure 5.5.** (a-b) Depiction and image of bioelectronic optical implants, intended for restoring vision (figure extracted from [\[17\]](#)). (c) The flexibility and biocompatibility of graphene based electronics present great promises for implantable and wearable electronics (image taken from [\[18\]](#)).

intraperitoneal or intravenous administration, to living organisms (mice in reference [13]) without producing significant immunologic responses. This is important since a considerable part of the expected advances in bionanoelectronics are related to implantable biosensors and other bioelectronics [14-16]. Such implantable devices are required to operate under biological conditions, tolerating humidity, ionic fluids, protein encapsulation, all without causing tissue inflammation. Some examples of devices based in conventional electronics (optical sensors for vision restoring [17], are shown in figure 5.5a-b. Doped carbon nanomaterials can contribute to reduce these and other potential undesirable immunological effects, while keeping their flexibility and electrical properties (see figure 5.5c).

Besides potential advantages in biocompatibility, the increased chemical activity of doped nanocarbons increases the possibility of interactions with biomolecules or other biosystems [19-21] which makes them suitable for biosensing applications. We have already seen in Chapter 4 that theoretical calculations show that nitrogen and boron doping of graphene changes the valence electronic states, and thus the way the graphene interacts with biomolecules (with dopamine used as a case study for the original results presented).

In addition to the results in Chapter 4 calculations made during this thesis (see figure 5.6 below) show that the inclusion of boron atoms into the graphene lattice produces a

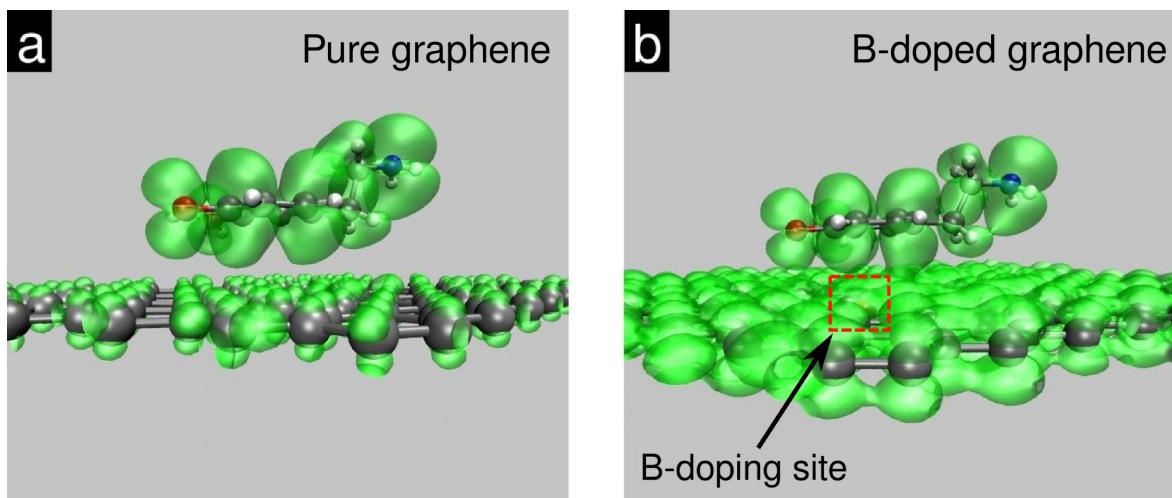


**Figure 5.6.** Dopamine (upper) molecule interacting with (a) pure and (b) B-doped graphene. The interaction is depicted by the electron density isosurfaces plotted in green, where a considerable increase of valence orbitals mixing is observed for B-doped graphene and dopamine (see [22]).

significant increase in orbitals mixing between dopamine and graphene, evident from the shared electron density near the B-doping site in electron density isosurface plots of dopamine (upper molecule) and pure and B-doped graphene [22].

It should be noted that doping also modifies the sensitivity of the graphene device to electric fields, an effect that is the operational base for FET devices. Doping can also alter the strength of interactions, allowing better control in adsorption/desorption processes at the device surface, which could reduce problems such as undesirable protein adsorptions). The possibility of tailoring electronic and chemical properties in graphene and CNTs is a key factor that should be addressed in the design of new nanobiotechnological devices, and needs to be explored for the implementation of bioelectronic systems.

## **5.2 Experimental Studies of Biosensors of N-doped CNT films**

In order to assess the differences in electrical performance between devices based on undoped and doped nanostructures when operated under biological environments, substrates with conductive networks of deposited CNTs were prepared by filtration of undoped MWNTs (CO<sub>x</sub>) and N-doped MWNTs (CN<sub>x</sub>). The undoped nanotubes used for this study were synthesized with ethanol in the precursor solution, which increase their crystallinity, but also introduces carbon-oxygen groups in the surface, which is why they are called CO<sub>x</sub>-MWNTs [23]. We selected CO<sub>x</sub> for comparison as they are naturally more hydrophilic than regular AA-CVD MWNTs and easier to disperse in alcohols, and to compare effects of simply having surface functionalized MWNTs vs. doping of CN<sub>x</sub>-MWNTs. The nanotubes were purified following the protocol reported in reference [24] before their use in the experiments described here.

Both types of nanotubes were dispersed in different solutions; pure isopropyl alcohol (IPA), aqueous solution of Triton X-100 (TX-100) and aqueous solution of chitosan (see figure 5.7). TX-100, a surfactant, and chitosan, a polysaccharide, are commonly used for biotechnology research purposes, but also as dispersant agents for CNTs and other nanostructures. The CNTs dispersions in IPA were prepared by ultrasonic bath of 3 mg CNT powders (90 minutes) in pure alcohol (400 mL), and in aqueous TX-100 solution (at 0.1% volume in 400 mL of deionized water) and chitosan solution (at 0.025% weight in 400 mL of 1% of HCl dissolution). All the dispersions were prepared at a concentration of 7.5 μg mL<sup>-1</sup> of nanomaterials. Finally, the dispersions were vacuum filtered, rinsed and



dried over a polytetrafluoroethylene filter (Sun Sri Titan PTFE membrane disc filter, 47 mm diameter, 0.45  $\mu\text{m}$  porosity), using a micro filtration device (VWR, vacuum filtration system, 9.6  $\text{cm}^2$  of filtration area) resulting in CNT thin film densities of  $\sim 310.2 \mu\text{g cm}^{-2}$ . [Figure 5.8](#) shows two SEM images of the conductive networks, for substrates made from filtration of  $\text{CO}_x$ - and  $\text{CN}_x$ -IPA dispersions.

The substrates were then cut into strips of 2.5 x 0.3 cm, and connected as depicted in [figure 5.7a](#). The next step was to measure the DC resistivity by the application of a sweeping DC current (from 0 to 200  $\mu\text{A}$ ), and measuring the corresponding voltage at the edges of the substrates. The measurements were made with over three different specimens

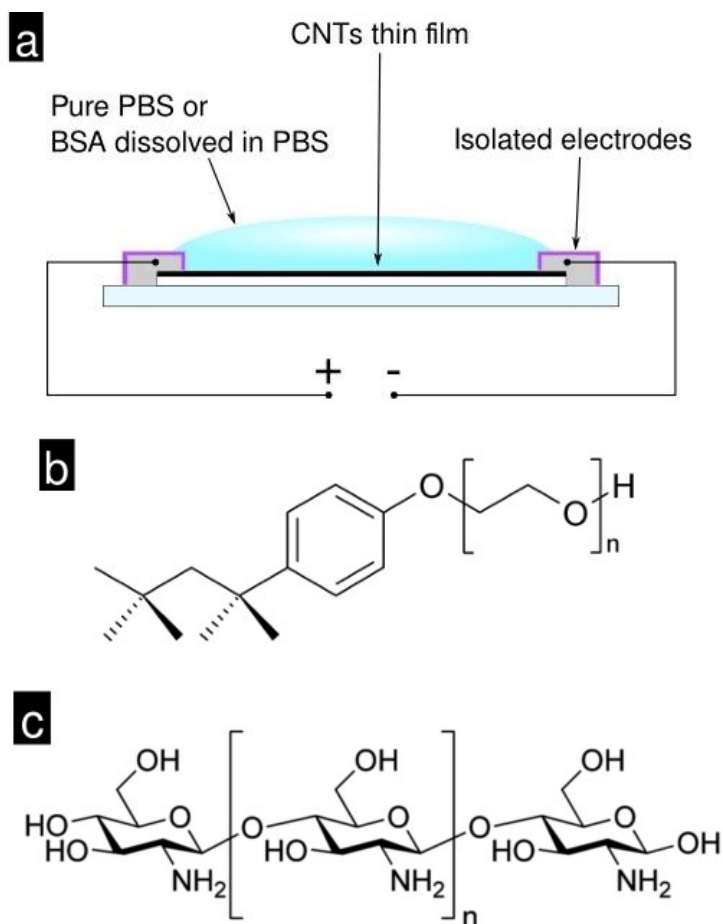


**Figure 5.7.** (a) Setup scheme for experimental measurements of substrates made with undoped and N-doped CNTs, in order to assess changes in their electric conductivity in the presence of model biofluids. The model biofluids were prepared using pure PBS, aqueous solutions of (b) TX-100 (the number of repeating units,  $n$ , is around 9-10) and (c) chitosan.

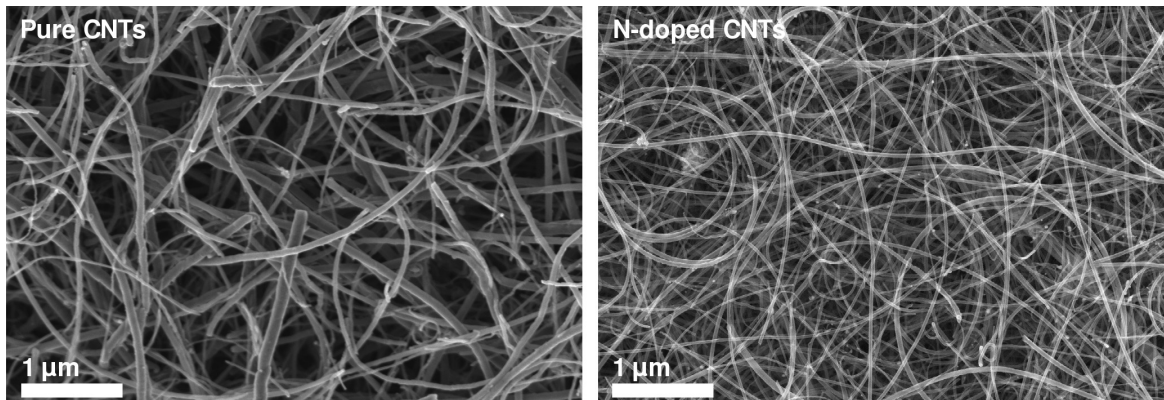


**Figure 5.8.** Scanning electron (SEM) micrographs of pure and N-doped CNTs ( $\text{CO}_x$  and  $\text{CN}_x$ , respectively) conductive networks, as deposited over the substrates for conductivity measurements.

of each type of substrate (pure, with adsorbed TX-100 and with adsorbed chitosan), for both types of CNTs. Finally, a set of measurements with constant voltage (1 V DC) were performed, in order to characterize the degree of change produced by the contact of substrates with two model biofluids. A phosphate buffered saline solution (PBS, 0.1M, pH 7.4) was used as a model of exposure to a saline environment, this solution is widely used in biological research and cell cultures as it is isotonic (having the same ionic concentrations and osmolarity) with the human body. The other solution was a model of a protein solution (potentially an analyte) in a biological fluid, a solution of bovine serum albumin (BSA) in PBS, at a concentration of  $40 \text{ mg mL}^{-1}$ .

The substrates were exposed to the solutions by placing them in an inclined surface (approximately  $45^\circ$ ) and applying consecutive fluxes of the different solutions and deionized water (DI) as flushing agent. A manual micro pipette was used to apply  $200 \mu\text{L}$  of each solution. The electrodes were protected by a non conductive resin to prevent contact with the liquids. The resistivity (current measurement, with a 1 V DC voltage applied) was measured continuously for consecutive periods of 30 seconds in which the model biofluid was applied and then flushed for another 30 seconds with DI still measuring the resistivity. The controlled timed exposure/flushing cycles of 1 minute were then repeated a few times.

## 5.2.1 Results

Figure 5.9 shows the resulting I-V curves from the initial substrates measurements made to evaluate any effect of the dispersants on the resistivity the CNT film. The curves correspond to  $\text{CO}_x$  (figure 5.9a), and  $\text{CN}_x$  (figure 5.9b); untreated, TX-100 dispersed and chitosan dispersed (gray, red and green plots respectively). As can be observed the pure  $\text{CO}_x$ -MWNTs present the lowest resistivity value ( $860 \Omega$ ), as the CNTs can interconnect freely in the film (see figure 5.8), forming a dense percolating network. Pure  $\text{CN}_x$  films have a similar percolating network, but the scattering of electrons due to doping and structural irregularities (see section 1.3.2.2) makes their resistance slightly higher ( $1.0 \text{ k}\Omega$ ).

Exposure of  $\text{CO}_x$  to TX-100 surfactant increases resistivity to  $1.3 \text{ k}\Omega$ , and to  $5.7 \text{ k}\Omega$  for chitosan. This could be explained by adhesion of the surfactant molecules to the CNT surfaces, preventing direct contact and limiting the passage of electric current. For  $\text{CN}_x$  the relative increases in resistivity, while measurable, are smaller. Films from TX-100 dispersions of  $\text{CO}_x$ , had 1.5 times the resistance of the untreated (isopropanol dispersion), whereas  $\text{CN}_x$  films exhibited a slight increase of 1.23 times. The difference is even more significant for chitosan treated CNTs, with a resistivity increase of 6.6 times for  $\text{CO}_x$  substrates versus 1.16 times for  $\text{CN}_x$  ones

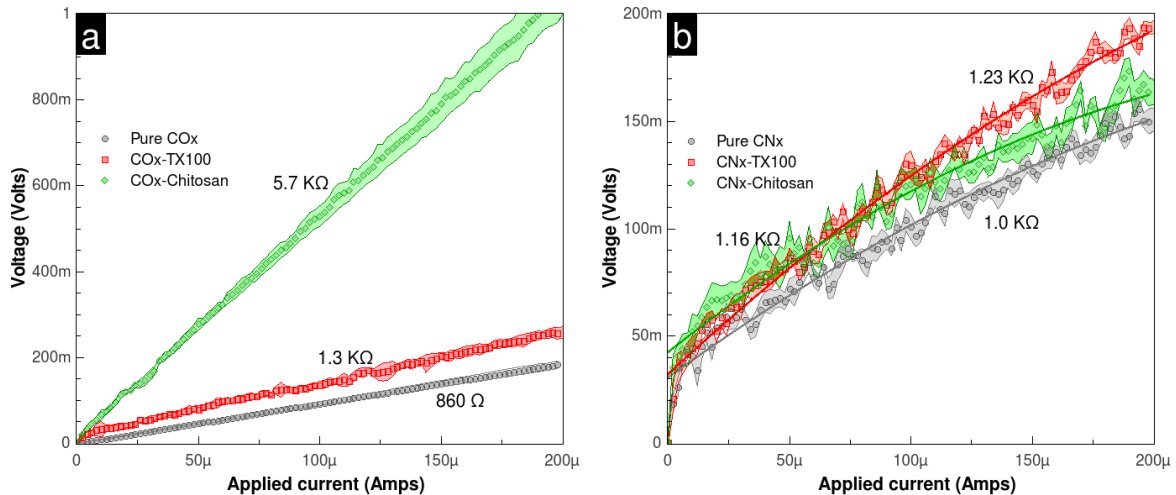


**Figure 5.9.** Current-voltage (I-V) curves from measurements on CNTs thin films substrates. **(a)** Curves for undoped CNTs ( $\text{CO}_x$ ) and for **(b)** N-doped CNTs ( $\text{CN}_x$ ). The marks represent the measurements average, and the correspondent shaded area depicts the standard deviation.

Doping could explain this differences, it has been proposed that doping with boron atoms can promote intertube electron hopping due to the introduction of electron states near the Fermi level, which can increase electron transport in percolating networks of carbon nanostructures [25]. In these  $CN_x$  substrates a similar effect could be enhancing conductivity even in the presence of adsorbed molecules, since N-doping produce localized states close to CNTs' Fermi level, with localized charges around doping sites. An additional explanation may be the difference in surface chemistry between  $CN_x$  and  $CO_x$  with the latter having oxygen sites it may have more affinity for a polysaccharide.

The results of the resistivity change (normalized with respect to initial resistivity) in the presence of PBS and BSA as model biofluids are shown in [figures 5.10](#) and [5.11](#) respectively. The use of PBS and BSA/PBS are intended to simulate the device operation under biological conditions, where fluids with abundant mineral salts, proteins and other biomolecules would be constantly interacting with bioelectronic systems. These results show that dispersion in TX-100 or chitosan the influence the electrical response of  $CO_x$  and  $CN_x$  substrates to PBS. For the untreated CNT substrates exposed to PBS ([figure 5.10a](#)) both nanotube types show an increasing resistivity as function of time, and that flushing with DI water, does not recover the initial conductivity. Both substrates show a spike in resistivity when PBS is added, followed by a plateauing behavior.  $CO_x$  present a clearer difference in resistivity for PBS and DI water (average ratio ca. 0.01).  $CN_x$  exhibit a noisier response, which can be attributed to interactions, even adsorption, of the PBS ions with the reactive sites on the  $CN_x$  surface. CNTs treated with TX-100 ([figure 5.10b](#)) and chitosan ([figure 5.10c](#)) show different results, starting with a change in magnitude (notice that the scale in [figure 5.10a](#) is one order of magnitude smaller), in  $CO_x$  substrates the resistivity increases in time, whereas for  $CN_x$  it trends downward. Moreover, substrates with  $CN_x$  show a relatively constant sensitivity, and noticeable spikes when changing between PBS and DI water when contrasted with  $CO_x$  ones. This could be due to the differences in reactivity between nitrogen doped and undoped nanotubes. With chitosan dispersions both types of CNT show more similar behaviors, with the main difference in the slope of the resistivity over time. Interestingly, the TX-100 and chitosan treatments appear to attenuate the noise effect produced by strong ionic interactions between  $CN_x$  surface and PBS, while keeping the high reactivity associated with doping. This results confirm the notion that surfactant residue should remain over the CNT, affecting their electrical properties, The surfactants having polar sites can also represent sites for ion adsorption, which could be an explanation for why resistivity spikes change over cycles of exposure to PBS and PBS-BSA.

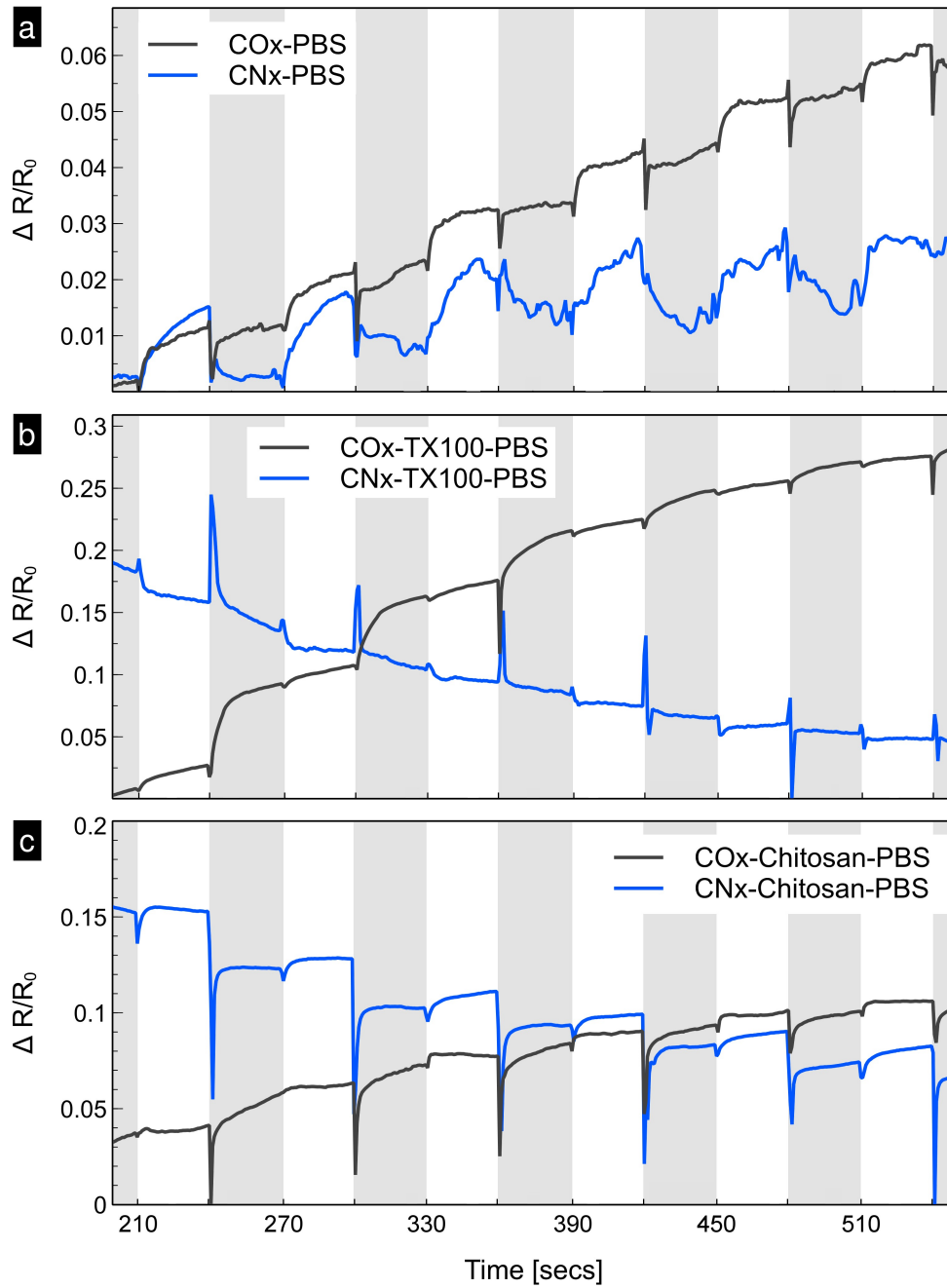


**Figure 5.10.** Comparison of changes in resistivity ( $\Delta R/R_0$ ) of  $\text{CO}_x$  (black curves) and  $\text{CN}_x$  (blue curves) untreated (a), TX-100 treated (b) and chitosan treated (c). The results were plotted as a time sequence of PBS (biofluid, shaded areas) and DI (flushing, white areas), with 30 seconds per step.

The measurements of resistivity changes with exposure to the protein solution of BSA in PBS buffer (figure 5.11) show a significant resistivity increase for surfactant-free CO<sub>x</sub> substrates, while for CN<sub>x</sub> spikes in resistivity upon exposure to BSA followed by plateauing to an almost constant level are seen (see figure 5.11a). BSA adsorption over the CNTs' surfaces could be reducing intertube contact and thus affecting the overall conductivity. CN<sub>x</sub> films in this case appear to be more tolerant to BSA adsorption, or maybe the absorption over CO<sub>x</sub> is not as reversible as for CN<sub>x</sub>. When the films are made with the surfactants TX-100 and chitosan treated CNTs (see figures 5.11b and 5.11c, respectively), resistivity changes are higher in magnitude, but with a more stable trend over time. Notably CN<sub>x</sub> substrates again showed a more consistent sensitivity for biofluid/DI water flushing pulses when contrasted with their CO<sub>x</sub> counterparts. The effect is specially noticeable for chitosan treated tubes (figure 5.11c), where the CO<sub>x</sub> substrates show little sensitivity to exposure to BSA after flushing steps and increasing resistivity after several cycles of both solutions.

It is important to mention that despite the differences in resistivity change trends, the strong peaks observed for measurements on CN<sub>x</sub> based substrates could be attributed to instant ionic fluxes produced by PBS, which strongly influence CN<sub>x</sub> networks because the high reactivity points at the doping sites. Moreover, the treatment of CNTs with surfactant as TX-100 or biopolymers as chitosan, which is relatively a common procedure for carbon nanomaterials use for bioengineering applications, appears to affect CO<sub>x</sub> conductive networks in more extent than to CN<sub>x</sub> ones. This would be an important factor when using carbon nanostructures for new and effective electronic biosystems intended to operate under biological conditions, where the tolerance to biofluids could be a decisive factor.

These results show that films of nitrogen doped nanotubes could be more robust sensors than undoped nanotubes, even when they present surface functionalization as CO<sub>x</sub> do. They also show clearly the importance of considering interactions with processing aids, while many literature reports seem to assume that surfactant dispersed CNTs behave as pure CNTs we show that this is not the case. The effect of minute differences in surface chemistry due to surfactants also reinforces the case that directed absorption biomolecules (e.g. by functional groups or antibodies that react with a specific analyte) is a very efficient sensing mechanism when using nanocarbon materials.

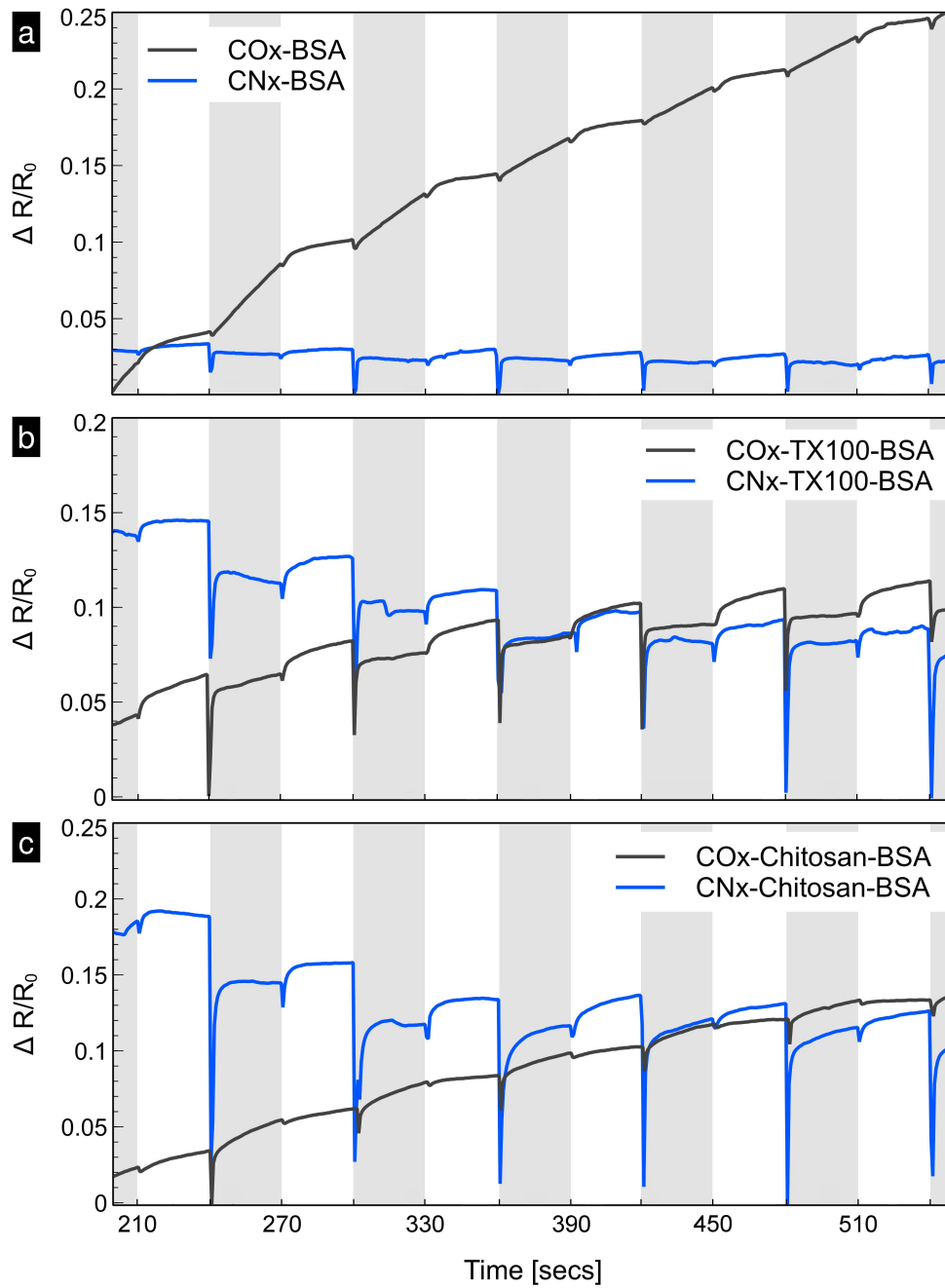


**Figure 5.11.** Comparison of changes in resistivity ( $\Delta R/R_0$ ) of  $CO_x$  (gray curves) and  $CN_x$  (blue curves) untreated (a), TX-100 treated (b) and chitosan treated (c). The results were plotted as a time sequence of BSA (biofluid, shaded areas) and DI (flushing, white areas), with 30 seconds per step.

## **Conclusions and Perspectives**

Real world applications of carbon nanotechnology are starting to become possible. Nevertheless, some difficulties still need to be overcome. For example, bioengineered systems tailored for exploiting the exceptional characteristics of nanomaterials such as graphene or CNTs are facing some of the classical problems associated with biodevices; bio-incompatibilities producing immune responses, or performance degradation caused by protein accumulation over implanted electrodes. Regarding this, the research of doped carbon nanomaterials for bioapplications present promises that can tackle effectively some of these issues. Here we showed that the use of nitrogen-doped CNTs can be advantageous for bioengineered devices, given the good biocompatibility exhibited when contrasted with undoped ones. Moreover, the results from electrical measurements shown here also suggest a functional advantage for bioelectronic devices based in N-doped CNTs, since their electrical properties appear to be more tolerant to interactions with biofluids, which are typically rich in ions and biomolecules capable to strongly interfere with normal electronic systems. The films produced in this work, even if simple in design, are feasible to be used for sensing, with further research to functionalize them with specific moieties, designed to guarantee specific interactions with analytes of interest.

## **Bibliography**

- [1] A. Noy, A. B. Artyukhin, and N. Misra, "Bionanoelectronics with 1D materials," *Materials Today*, vol. 12, no. 9, pp. 22–31, 2009.
- [2] S. L. Morton, "The Role of Oxygen Reduction in Electrical Stimulation of Neural Tissue," *Journal of the Electrochemical Society*, vol. 141, no. 1, p. 122, 1994.
- [3] K. W. Horch and G. S. Dhillon, *Neuroprosthetics: Theory and Practice*. Singapore, Singapore: World Scientific, 2004.
- [4] S. Negi, R. Bhandari, L. Rieth, R. Van Wagenen, and F. Solzbacher, "Neural electrode degradation from continuous electrical stimulation: comparison of sputtered and activated iridium oxide.," *Journal of Neuroscience Methods*, vol. 186, no. 1, pp. 8–17, 2010.
- [5] "Cell interface platforms-IMEC" [Online]. Available: [http://www2.imec.be/be\\_en/research/human-biomedical-electronics/cell-interface-](http://www2.imec.be/be_en/research/human-biomedical-electronics/cell-interface-)



- platforms.html. [Accessed: 22-Sep-2013].
- [6] R. A. Green, J. S. Ordonez, M. Schuettler, L. A. Poole-Warren, N. H. Lovell, and G. J. Suaning, "Cytotoxicity of implantable microelectrode arrays produced by laser micromachining.," *Biomaterials*, vol. 31, no. 5, pp. 886–93, 2010.
- [7] V. S. Polikov, P. A. Tresco, and W. M. Reichert, "Response of brain tissue to chronically implanted neural electrodes.," *Journal of Neuroscience Methods*, vol. 148, no. 1, pp. 1–18, 2005.
- [8] M. D. Angione, R. Pilolli, S. Cotrone, M. Magliulo, A. Mallardi, G. Palazzo, L. Sabbatini, D. Fine, A. Dodabalapur, N. Cioffi, and L. Torsi, "Carbon based materials for electronic bio-sensing," *Materials Today*, vol. 14, no. 9, pp. 424–433, 2011.
- [9] E. W. Keefer, B. R. Botterman, M. I. Romero, A. F. Rossi, and G. W. Gross, "Carbon nanotube coating improves neuronal recordings.," *Nature Nanotechnology*, vol. 3, no. 7, pp. 434–9, 2008.
- [10] E. Ben-Jacob and Y. Hanein, "Carbon nanotube micro-electrodes for neuronal interfacing," *Journal of Materials Chemistry*, vol. 18, no. 43, pp. 5181–5186, 2008.
- [11] Y. Wen, F. Y. Li, X. Dong, J. Zhang, Q. Xiong, and P. Chen, "The Electrical Detection of Lead Ions Using Gold-Nanoparticle- and DNAzyme-Functionalized Graphene Device.," *Advanced Healthcare Materials*, 2012.
- [12] J. Ortiz-Medina, M. L. García-Betancourt, X. Jia, R. Martínez-Gordillo, M. A. Pelagio-Flores, D. Swanson, A. L. Elías, H. R. Gutiérrez, E. Gracia-Espino, V. Meunier, J. Owens, B. G. Sumpter, E. Cruz-Silva, F. J. Rodríguez-Macías, F. López-Urías, E. Muñoz-Sandoval, M. S. Dresselhaus, H. Terrones, and M. Terrones, "Nitrogen-Doped Graphitic Nanoribbons: Synthesis, Characterization, and Transport," *Advanced Functional Materials*, vol. 23, no. 30, pp. 3755–3762, 2013.
- [13] J. C. Carrero-Sanchez, A. L. Elías, R. Mancilla, G. Arrellín, H. Terrones, J. P. Laclette, and M. Terrones, "Biocompatibility and toxicological studies of carbon nanotubes doped with nitrogen.," *Nano Letters*, vol. 6, no. 8, pp. 1609–16, 2006.
- [14] N. W. S. Kam, E. Jan, and N. A. Kotov, "Electrical Stimulation of Neural Stem Cells Mediated by Humanized Carbon Nanotube Composite Made with Extracellular Matrix Protein," *Nano Letters*, vol. 9, no. 1, pp. 273–278, 2009.
- [15] T. Kuila, S. Bose, P. Khanra, A. K. Mishra, N. H. Kim, and J. H. Lee, "Recent advances in graphene-based biosensors.," *Biosensors & Bioelectronics*, vol. 26, no. 12, pp. 4637–48, 2011.
- [16] A. Fabbro, G. Cellot, M. Prato, and L. Ballerini, "Interfacing neurons with carbon

- nanotubes: (re)engineering neuronal signaling.,” *Progress in Brain Research*, vol. 194, pp. 241–52, 2011.
- [17] E. E. O’Brien, U. Greferath, K. A. Vessey, A. I. Jobling, and E. L. Fletcher, “Electronic restoration of vision in those with photoreceptor degenerations.,” *Clinical & Experimental Optometry : Journal of the Australian Optometrical Association*, vol. 95, no. 5, pp. 473–83, 2012.
- [18] “Flexible graphene memristors - Printed Electronics World.” [Online]. Available: <http://www.printedelectronicsworld.com/articles/flexible-graphene-memristors-00002730.asp?sessionid=1>. [Accessed: 27-Jan-2013].
- [19] X. Chen, J. Chen, C. Deng, C. Xiao, Y. Yang, Z. Nie, and S. Yao, “Amperometric glucose biosensor based on boron-doped carbon nanotubes modified electrode,” *Talanta*, vol. 76, no. 4, pp. 763–767, 2008.
- [20] Z.-H. Sheng, X.-Q. Zheng, J.-Y. Xu, W.-J. Bao, F.-B. Wang, and X.-H. Xia, “Electrochemical sensor based on nitrogen doped graphene: simultaneous determination of ascorbic acid, dopamine and uric acid.,” *Biosensors & Bioelectronics*, vol. 34, no. 1, pp. 125–31, 2012.
- [21] R. Lv, Q. Li, A. R. Botello-Méndez, T. Hayashi, B. Wang, A. Berkdemir, Q. Hao, A. L. Elías, R. Cruz-Silva, H. R. Gutiérrez, Y. A. Kim, H. Muramatsu, J. Zhu, M. Endo, H. Terrones, J.-C. Charlier, M. Pan, and M. Terrones, “Nitrogen-doped graphene: beyond single substitution and enhanced molecular sensing.,” *Scientific Reports*, vol. 2, p. 586, 2012.
- [22] J. Ortiz-Medina, F. López-Urías, F. J. Rodríguez-Macías, H. Terrones, and M. Terrones, “Theoretical study on the interactions between dopamine and doped/defective graphene under electric fields” (*Manuscript in preparation*), 2013.
- [23] A. Botello-Méndez, J. Campos-Delgado, A. Morelos-Gómez, J. M. Romo-Herrera, Á. G. Rodríguez, H. Navarro, M. A. Vidal, H. Terrones, and M. Terrones, “Controlling the dimensions, reactivity and crystallinity of multiwalled carbon nanotubes using low ethanol concentrations,” *Chemical Physics Letters*, vol. 453, no. 1–3, pp. 55–61, 2008.
- [24] E. R. Alvizo-Paez, J. M. Romo-Herrera, H. Terrones, M. Terrones, J. Ruiz-Garcia, and J. L. Hernandez-Lopez, “Soft purification of N-doped and undoped multi-wall carbon nanotubes,” *Nanotechnology*, vol. 19, no. 15, p. 155701, 2008.
- [25] Y. Fukunaga, M. Harada, S. Bandow, and S. Iijima, “Variable range hopping conduction and percolation networks in the pellets formed from pristine and boron-doped carbon nanohorn particles,” *Applied Physics A*, vol. 94, no. 1, pp. 5–9, 2008.



# Conclusions and perspectives

During this research work, some of the key advancements that carbon nanotechnology has experimented were addressed. Nowadays nanostructures such as CNTs and, in much more extent, graphene, are being introduced into novel and promising prototypes for electronic and other devices which could outperform current microtechnologies. These advances from nanoscience to applied nanotechnology are direct consequence of the exceptional characteristics that carbon and other nanostructures exhibit, and the knowledge about how to exploit them for useful applications. The extraordinary mechanical, chemical and electrical properties that have been studied and reported for nanomaterials are being adapted to existing technologies and helping to develop new ones. Nevertheless, the full potential of nanostructured materials is still under intense research, since new nanostructures are being studied using theoretical approaches, and synthesized by the developed experimental expertise.

Within this framework, the present research work contributed with two concrete research results: first, a novel nitrogen doped carbon nanostructure; *i.e.* N-doped graphitic nanoribbons, were synthesized and characterized, demonstrating several characteristics which make them a promising nanomaterial for sensing, catalysis and other electronic potential applications, given its chemical and electrical properties. The characterization included common experimental routines utilized for carbon nanomaterials, such as electron microscopy, Raman and X-ray photoelectron spectroscopy, thermogravimetric analysis and electrical measurements, as well as calculations using theoretical models for comparison

---

and understanding of the observed characteristics. Second, the study of doping over CNTs and graphene, and its effects on electrical and biosensing properties. Specifically, changes in electronic properties of boron-, nitrogen-doped and defective graphene was analyzed under a theoretical approach, by means of the Density Functional Theory (DFT), which allowed to assess each different types of doping and defects on graphene, in conjunction with an applied electric field (as an conceptualization for simulating the operation of graphene based FETs) and an adsorbed biomolecule. The obtained results suggest that doping could be an important factor for improving current biosensors development.

Finally, within the same study of carbon nanostructures doping, experimental measurements were carried out using nitrogen-doped CNTs (CN<sub>x</sub>). Preliminary results of electrical characterization demonstrated that CN<sub>x</sub>, contrasted with undoped CNTs (CO<sub>x</sub>), are more tolerant to chemical treatments which modify their surface, in terms of electrical conductivity of percolating networks at least. This is important specially for nanomaterials based biosensing and bioelectronics, since these type of materials are commonly chemically treated (e.g. by functionalization with specific molecules, or dispersed using surfactants of biopolymers) for their compatibility with biological systems. Consequently, doped carbon nanomaterials would be a more adequate basis for the development of new generation bioelectronic devices, highly biocompatible and operationally stable under conditions which affect common microelectronic devices being used currently.

The perspectives for carbon and other nanomaterials for bioapplications are extremely promising, from the advancements that nanotechnology has experimented in the last years. For instance, graphene is currently being successfully used for flexible electronics, which would be easily translated to wearable and even implantable bioelectronics, with the proper research for assuring biocompatibility and efficiency. Moreover, and given that doped carbon nanomaterials are not commonly found for this type of research, further investigations on doping effects over biocompatibility and sensitivity should be carried out, from the promising results shown here and in other previous works (see [Chapter 2.1.3](#), for example). Summarizing, and based on the present research results, the perspectives for nanotechnology developments based on doped carbon nanomaterials can be stated as follows:

- The presumed superior *in vivo* biocompatibility of doped carbon nanomaterials should be extensively assessed, given that the available research addressing the

topic is still limited. In fact, according with the explored reports throughout this work, only nitrogen-doped CNTs (among untreated doped carbon nanostructures) have been experimentally evaluated *in vivo* for toxicity tests.

- The results of theoretical analyses on graphene indicating improved characteristics for biomolecules detection should be experimentally evaluated, since the obtained outcomes could have a significant impact in graphene based FETs devices, specially for bioelectronic applications.
- The observed enhanced tolerance of electrical operation to biological conditions of devices based on  $CN_x$  contrasted with  $CO_x$  needs further characterization, since even the acquired information is relevant for observing the phenomena, additional results could help to confirm and understand the underlying mechanism producing it. The results would be extremely useful for new bioelectronic devices development based in doped carbon nanomaterials.



# Appendix A

## Brief description of some nanomaterials characterization techniques

### A.1 Scanning Electron Microscopy (SEM)

Electron microscopy routines are widely used in materials research as basic characterization. SEM is commonly part of the first explorations when analyzing new materials, and it can be used for a variety of samples, including biological ones. SEM is the most common microscopy techniques for superficial morphology study, and it is capable to resolve sample's features close to 1 nm for modern high-resolution SEM systems. The operational principles of SEM rely on the use of an focused electron beam instead of light, which is accelerated through the microscope by electromagnetic means towards the sample, extracting electrons from the its surface and detecting them for image formation. As can be seen in [figure A.1](#), a SEM microscope is composed by an electron gun plus a set of electromagnetic lenses, which function as the electron beam condenser and controller. A set of scanning coils are in charge of deviating the electron beam for making a scan over the sample, in a similar way the cathodic tubes based TVs work. The impact of the electrons over the sample surface produce ejected particles (such as primary backscattered, secondary and auger electrons) and radiation (X-rays). All this emissions can be detected and used for



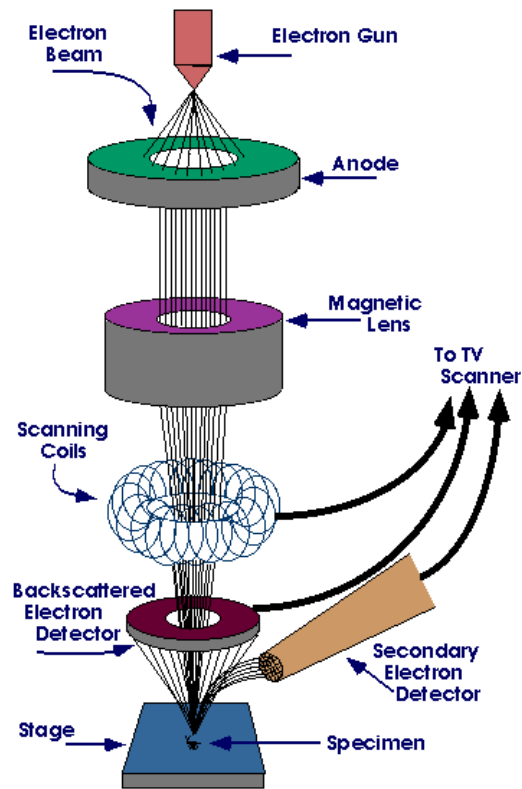


**Figure A.1.** Scheme of a SEM microscope, where its basic parts are represented. The image is obtained from the sample's extracted electrons (figure taken from [1]).

characterization, but for imaging purposes, mainly secondary electrons are used.

Because the SEM utilizes vacuum conditions and uses electrons to form an image, special preparations must be done to the sample. All water must be removed from the samples because the water would vaporize in the vacuum. All metals are conductive and require no preparation before being used. All non-metals need to be made conductive by covering the sample with a thin layer of conductive material, which can be done by metal sputtering or evaporation coating.

## A.2 Transmission Electron Microscopy (TEM)

TEM is also a recurrent technique in materials research characterization, due to the high-resolutions capabilities of most TEM systems. The operation principles are very similar to SEM, in the sense that TEM microscopes have an electron gun and electromagnetic lenses,

for generation and control of an electron beam. The difference is that the samples are located not at the end of the electron beam path, but somewhere in the middle. In this way, the focused beam is passed through the sample, magnified and projected in a visualization section, which can be a simple fluorescent screen or an electronic CCD detector (see [figure A.2](#)) [2].

An important point with TEM is that the samples to be analyzed should be prepared specifically for this type of analysis by making very thin sections of it. This is because the TEM relies on the electron beam passing through the sample, and in creating an image from the electrons which are absorbed, diffracted or scattered by it in their way to the imaging section.

TEM has a key advantage in terms of resolution, since it can resolve features in sub-nanometer range. Some of the most advanced systems can even image individual atoms. Another useful TEM feature is that it allows to obtain diffraction patterns from crystalline samples, which are useful for characterizing a wide variety of materials, including alloys, core-shell systems and even biomolecules such as complex proteins and DNA.

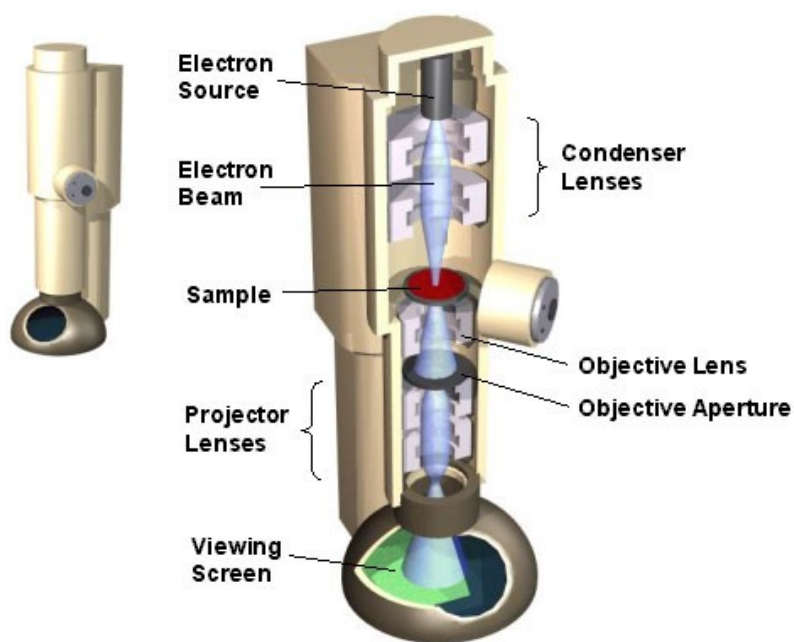


**Figure A.2.** Scheme of a TEM microscope, where its basic parts are represented. In this case, the sample is located in a central section of the electron beam path, and its magnified image is projected over a viewer screen (or CCD device) at the end of the path (figure taken from [2]).

### A.3 Scanning Probe Microscopy (SPM)

SPM is a characterization technique with many variants, being atomic force microscopy (AFM) and scanning tunneling microscopy (STM) two of the most used in materials characterization. The SPM underlying principle is the use of a micro-cantilever with a nanometer-sized probe, which is run over the sample's surface in a scanning-like mode. The probe-cantilever system responds mechanically to the topography, varying its height and orientation with respect to interaction with the sample. The transduction is optically achieved through a laser probe directed to the reflective cantilever tip, and a photodetector which measures laser position deviations occurring as consequence of cantilever's mechanical motion (see [figure A.3](#)) [3].

The flexibility of SPM characterization comes from the multiple variants on interactions between the nanosized probe and the sample. For instance, the probe can be functionalized with specific molecules, which can be used to map other molecules with high affinity over the sample's surface. Moreover, the system can be used for measuring electrical currents tunneling from the sample to the probe (as occurs in the STM case),

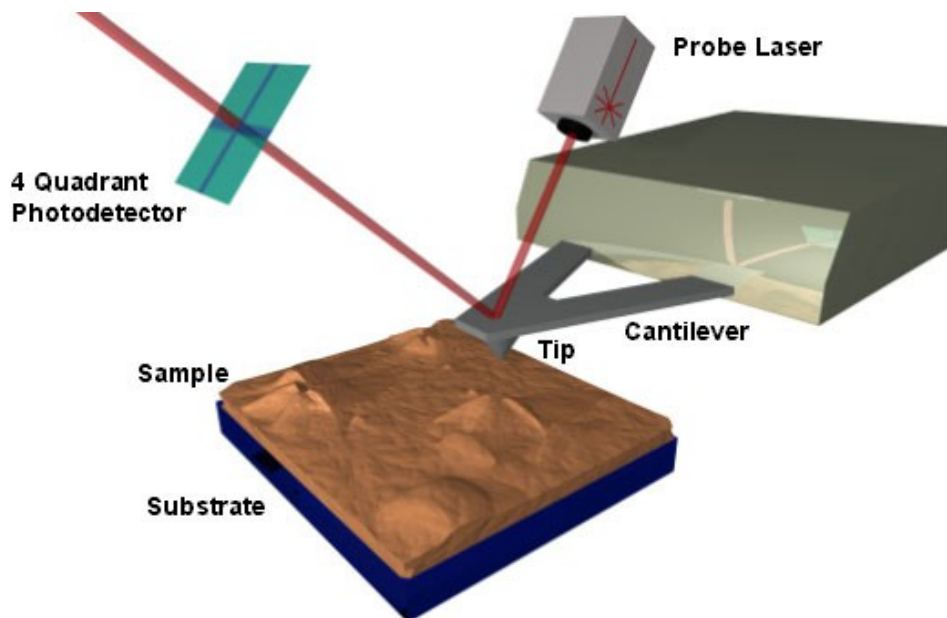


**Figure A.3.** Basic schematic of a SPM system. The nanometer-sized probe is run over the sample, with the micro-cantilever following the topographical surface's features. The changes in cantilever height and orientation are detected by a laser probe and a photodetector, which interpret the variations of the laser reflection to sample's features (figure taken from [2]).

revealing information about electronic properties (local density of states, for example) with an extremely high resolution, being capable of resolving the electron density of individual atoms.

## A.4 Raman Spectroscopy

Among spectroscopic characterization techniques, Raman spectroscopy is becoming increasingly popular for nanoscience research given its operational simplicity. Performing Raman measurements is as simple as illuminating the sample with monochromatic light, and measuring shifting in wavelength of scattered light. The physical principle of Raman spectroscopy is the Raman scattering effect, arising from interactions between light (photons) with molecular vibrations (phonons). In [figure A.4 \(left\)](#) are shown the common interactions between light and vibrational modes, where the transitions between “ground” vibrational energy states and virtual ones give rise to different type of photon scattering. All Raman scattering is inelastic, since the energy of the resulting mode is shifted with respect to the origin mode. Raman spectroscopy relies precisely on the detection of these shifted

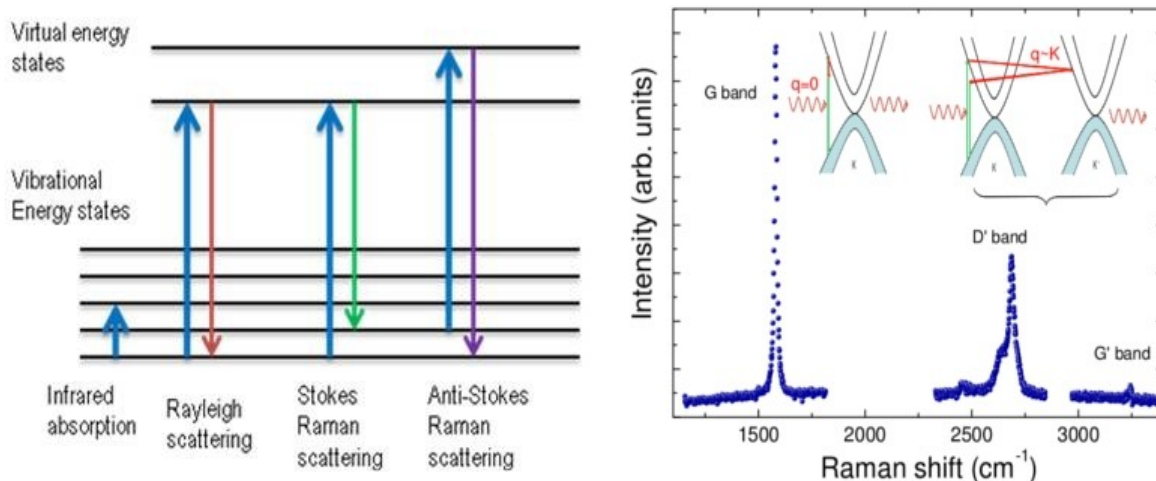


**Figure A.4. (Left)** Raman spectroscopy is based in the Raman effect, which is an inelastic photon scattering event occurring when light interacts with molecular vibrational modes (phonons). **(Right)** Example of Raman characterization of graphene samples, where the typical modes (G and D' bands) are shown, as well as a graphical explanations of the origin of such Raman modes, i.e., first order scattering (for G band), and second order scattering (for D' band). Figure taken from [\[4\]](#).

scattered photons, which can reveal important features regarding the vibrational, and thus, the electronic nature of a sample.

In [figure A.4 \(right\)](#) are depicted an example Raman spectrum for graphene and a graphical representation of its electronic origin in terms of electronic transitions [4]. Typical Raman modes for graphene (G and D' modes) are described as a first and second order scattering, respectively. These vibrational modes are related to C-C vibrations in a graphitic  $sp^2$  lattice (G mode), and to electronic dispersion paths (D'), sensitive to changes in electrons/holes ratio and thus, very useful for characterizing doped materials.

Raman spectroscopy exhibit high flexibility, from the many variants being used currently, such as Surface Enhanced Raman Spectroscopy (SERS) or Resonance Raman Spectroscopy (RRS). Additionally, mappings performed using Raman spectrometers can detect features on samples that would be difficult or expensive to resolve otherwise, like crystal lattice defects or doping sites.

## **A.5 X-ray Photoelectron Spectroscopy (XPS)**

XPS is a spectroscopic quantitative technique which allows to determine the elemental composition of the sample under study. XPS operational principle is based on the sample irradiation with X-rays, while simultaneously detecting the kinetic energy of photo-emitted electrons ejected from the sample's surface (between 1 to 10 nm depth) due to the X-ray radiation (see [figure A.5a](#)). The photo-emitted electrons possess a kinetic energy directly related with the orbital configuration of their origin atoms, and thus useful for elemental identification by comparison with the (known) energy of the emitted X-rays [5]. XPS detects the number of emitted electrons and measures their kinetic energies, resulting in plots like the one observed in [figure A.5b](#), where results are presented in counts/binding energy relation, with energetic regions associated with specific elements clearly identified.

XPS capabilities are not limited to detect the elemental composition of a sample, but also the empirical formula, chemical and electronic state of the elements present within a sample. This is because changes in atomic electronic configurations due to chemical activity produce slight binding energy shifts detectable in the photo-emitted electrons' kinetic energy. These characteristics make XPS a very useful technique for chemical analysis, being used extensively for carbon nanomaterials doping characterization, for example [6].

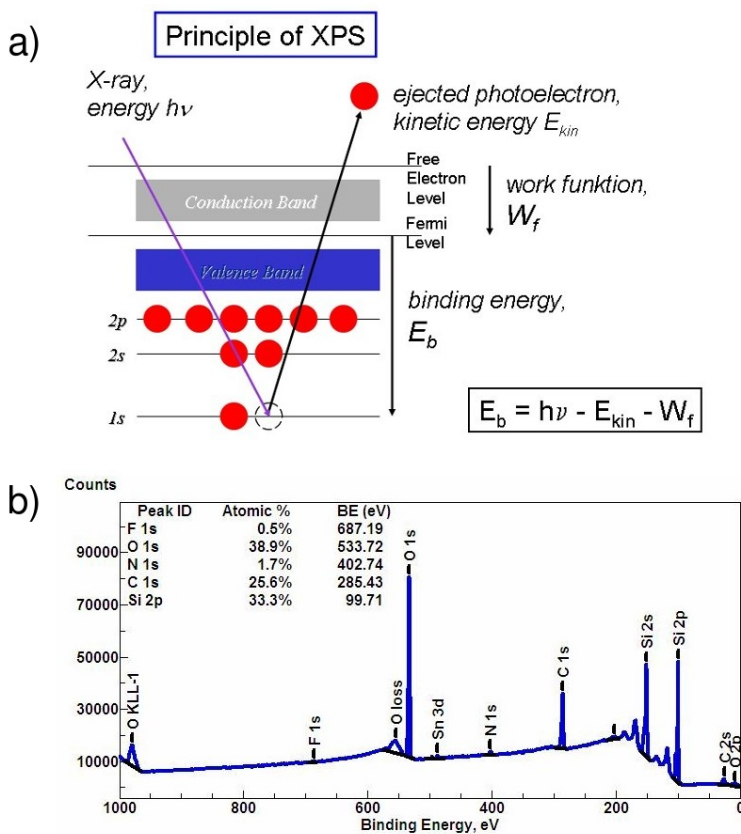


**Figure A.5.** (a) Physical principle of XPS. The sample's surface is irradiated with X-rays, producing photo-emitted electrons from the sample. The ejected electrons possess a kinetic energy directly related with the elemental orbital configuration where it was kicked off, which can be measured and quantified for sample's elemental composition representation (figure taken from [5]). (b) Typical XPS plot, where the quantification results are presented as a relation of counts and binding energy (image taken from [7]).

## A.6 InfraRed Spectroscopy (IR)

Another spectroscopic technique based on vibrational phenomena is IR spectroscopy. IR provides information about the presence of specific functional groups in the analyzed sample. The groups that can be identified by IR are common organic groups and bondings, such as N-H, O-H, C-H, C≡C, C≡N, C=O, C=N or C=C.

The operational principle of IR spectroscopy relies on the vibrational nature of covalent bonds, some of which can resonate when interacted with electromagnetic radiation in the

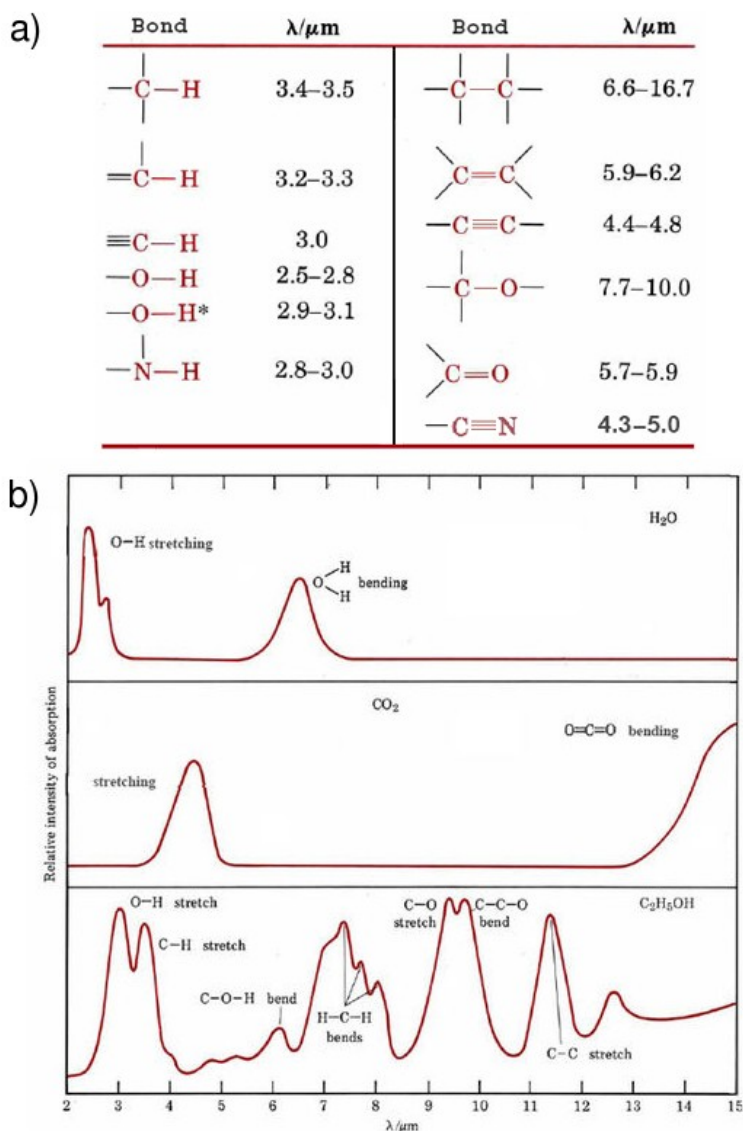


**Figure A.6.** (a) Relation between atomic bonds and corresponding wavelength for molecular vibration resonance. (b) Typical IR plots for water (top), carbon dioxide (center) and ethanol (bottom), where the characteristic vibrational modes are indicated (figures taken from [8]).

infrared range (wavelengths approximately in between 1 mm and 750 nm) absorbing part of the radiation in function of the bond nature [8]. In this way, an IR spectrometer irradiates the sample with an IR beam, which passes through the sample, and measures the amount of absorbed radiation at different wavelengths. In figure A.6a are shown the characteristic wavelengths of some chemical bonds, and in figure A.6b are depicted three example spectra for water, carbon dioxide and ethanol, with the respective groups labeled on the

correspondent spectra features.

IR is a very versatile technique, since it allows to analyze multiple types of samples, either in gaseous, liquid or solid state, with sample preparation relatively simple contrasted with other techniques. Also, a IR spectroscopy variant: Fourier Transform-InfraRed (FT-IR) spectroscopy, which takes advantage of signal processing methods, allows to perform fast and precise analysis, making FT-IR a very common characterization technique for materials research.

## A.7 Thermogravimetric Analysis (TGA)

TGA is a thermal characterization method which provides information about sample's physical and chemical properties, such as phase transitions, adsorptions, desorptions, decompositions, oxidation or reductions. It consists in a high precision weight micro-balance with an arm for the sample holder. For performing the analysis, the sample is put inside a high temperature furnace, in the presence of inert or oxidizing gas (see [figure A.7a](#)), and the system is heated either with controlled temperature ramp, or with constant temperature for thermal stability/time assessment. In [figure A.7b](#) is shown a typical TGA plot, consisting commonly of the TGA curve (sample's weight in function of temperature) and its first derivative, in order to clearly identify critical temperatures where changes in

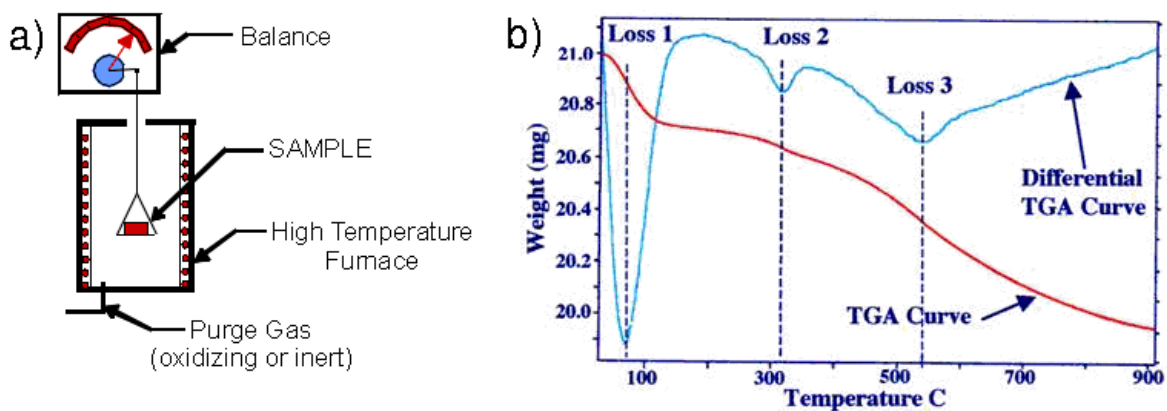


**Figure A.7.** (a) Schematic of basic TGA system. The sample is put in a suspended weight microbalance, inside a high temperature furnace which atmosphere can be controlled (either inert or oxidizing gas). (b) Example of a TGA run, performed by heating the furnace with a controlled rate, and recording the weight loss with the increasing temperature. Both curves (weight loss and its derivative) are commonly plotted (figure taken from [9]).



weight loss rates occur, normally indicative of phase changes or transitions, desorptions or degradations.

Given these characteristics, TGA is widely used for chemical processes characterization, including purification and functionalization, which are common treatments in nanomaterials research.

## Bibliography

- [1] "Scanning Electron Microscope." [Online]. Available: <http://www.purdue.edu/rem/rs/sem.htm>.
- [2] "BRG - A Brief Overview of Nanotechnology." [Online]. Available: <http://barrett-group.mcgill.ca/tutorials/nanotechnology/nano02.htm>.
- [3] M. A. Poggi, E. D. Gadsby, L. A. Bottomley, W. P. King, E. Oroudjev, and H. Hansma, "Scanning probe microscopy," *Analytical Chemistry*, vol. 76, no. 12, pp. 3429–43, Jun. 2004.
- [4] C. Faugeras, A. Nèrière, M. Potemski, A. Mahmood, E. Dujardin, C. Berger, and W. A. de Heer, "Few-layer graphene on SiC, pyrolytic graphite, and graphene: A Raman scattering study," *Applied Physics Letters*, vol. 92, no. 1, p. 011914, 2008.
- [5] "X-Ray Photoelectron Spectroscopy (XPS) — IFW Dresden." .
- [6] D. Wei, Y. Liu, Y. Wang, H. Zhang, L. Huang, and G. Yu, "Synthesis of N-Doped Graphene by Chemical Vapor Deposition and Its Electrical Properties," *Nano Letters*, vol. 9, no. 5, pp. 1752–1758, May 2009.
- [7] "X-ray photoelectron spectroscopy - Wikipedia, the free encyclopedia." [Online]. Available: [http://en.wikipedia.org/wiki/X-ray\\_photoelectron\\_spectroscopy](http://en.wikipedia.org/wiki/X-ray_photoelectron_spectroscopy).
- [8] "The Spectra of Molecules: Infrared | ChemPaths." [Online]. Available: [http://chempaths.chemeddl.org/services/chempaths/?q=book/General Chemistry Textbook/Spectra and Structure of Atoms and Molecules/1917/spectra-molecules-](http://chempaths.chemeddl.org/services/chempaths/?q=book/General%20Chemistry%20Textbook/Spectra%20and%20Structure%20of%20Atoms%20and%20Molecules/1917/spectra-molecules-).
- [9] "The Thermogravimetric Analysis of Silica Gel." [Online]. Available: [http://physicalchemistryresources.com/Book5\\_sections/TA\\_Thermogravimetric Analysis of Silica Ge1HTML\\_1.htm](http://physicalchemistryresources.com/Book5_sections/TA_Thermogravimetric%20Analysis%20of%20Silica%20Gel1HTML_1.htm).

# Appendix B

## Overview of Density Functional Theory as approach for carbon nanomaterials simulations

### B.1 Basics of Density Functional Theory

Among the theoretical approaches for the study of structures from the atomistic (and thus, quantum physics) perspective, Density Functional Theory, or DFT, has been one of the most used frameworks for modeling nanostructures, in order to calculate properties associated with calculable observables [1, 2]. DFT is an extremely successful approach for the description of ground state properties of metals, semiconductors, and insulators. Its success not only encompasses standard bulk materials but also complex materials such as proteins and carbon nanostructures.

The main idea of DFT is to describe an interacting system of fermions (*i.e.*, subatomic particles with a fractional spin, like electrons) via its density and not via its many-body wave function [1, 3, 4]. For  $N$  electrons in a solid, which obey the Pauli principle and repulse each other via the Coulomb potential, this means that the basic variable of the system depends only on three — the spatial coordinates  $x$ ,  $y$ , and  $z$  — rather than  $3*N$

degrees of freedom. Considering the classical Hamiltonian used for electronic structure determination,

$$\hat{H}\Psi = [\hat{T} + \hat{V} + \hat{U}] \Psi = \left[ \sum_i^N -\frac{\hbar^2}{2m_i} \nabla_i^2 + \sum_i^N V(\vec{r}_i) + \sum_{i<j}^N U(\vec{r}_i, \vec{r}_j) \right] \Psi = E\Psi$$

where, for the  $N$ -electron system,  $\hat{H}$  is the Hamiltonian,  $\hat{E}$  is the total energy,  $\hat{T}$  is the kinetic energy,  $\hat{V}$  is the potential energy from the external field due to positively charged nuclei, and  $\hat{U}$  is the electron-electron interaction energy. The operators  $\hat{T}$  and  $\hat{U}$  are called universal operators as they are the same for any  $N$ -electron system, while  $\hat{V}$  is system dependent. DFT allows to represent this complex expression by simpler approximations based on the electronic density, instead of all the subatomic entities. This eliminates the necessity of using the electron-electron interaction ( $\hat{U}$ ) explicitly, and expresses the potential energy ( $\hat{V}$ ) in terms of electron density ( $n(\vec{r})$ ), which is more easy and efficient to calculate computationally,

$$V_s(\vec{r}) = V(\vec{r}) + \int \frac{e^2 n_s(\vec{r}')}{|\vec{r} - \vec{r}'|} d^3r' + V_{XC}[n_s(\vec{r})]$$

Within DFT, there are several distinct approaches that introduce complementary terms (e.g., local density approximation or LDA, generalized gradient approximation or GGA, and even hybrid functionals, designed to better fit particles correlations) [5], in order to improve specific parameters, making it suitable for theoretical research and properties determination of a great variety of structures, such as carbon nanomaterials (CNTs [6] and graphene [7]), semiconductor crystals [8], biomolecules [9] and polymers [10].

Among the many features that can be calculated through theoretical approaches (DFT included), the most important ones are related with the *electronic band structure*, which graphically represents the energetic dispersion paths for charges (electrons and holes) along the crystalline units, providing information about the energetic distribution of orbitals and about the existence and position of electronic band gaps. Also, and strongly related with band structure is the *density of states* (DOS), which is a common representation of orbitals (or states) available at certain energies within the energetic range. These DOS plots are

commonly used, along with band structures, to shown the electrical nature of an analyzed material (isolator, semiconductor or metal). Moreover, theoretical models allow as well to calculate, within certain levels of error, the energetic stability, molecular geometry and reaction paths for molecular systems, which are used for analysis of interactions between systems towards sensing applications development, for instance.

It is necessary to mention nevertheless that DFT implementations are not suited for all kinds of systems. For instance, it has been established that some approximations (such LDA) tend to underestimate parameters such as band gap [4]. Moreover, when Van der Waals or long-range interactions are needed to be evaluated for example, additional corrections to erroneous calculation trends are required [5]. It is important to consider all these issues when dealing with modeling of systems and related properties determination.

## **B.2 DFT for carbon nanostructures electronic properties determination**

Much of the advancements that carbon nanotechnology has experimented was produced by theoretical predictions on nanostructures that had not been synthesized at the time their basic electronic properties had been determined. DFT had played, and still does, a crucial role in nanoscience, since it allows to explore theoretically on potential properties that would make a nanostructure worth of experimental research, and it can as well help to understand observed phenomena when characterizing nanomaterials, with the consequent benefits on the control of such properties.

Some examples of DFT theoretical results on carbon nanostructures can be cited in order to demonstrate its capabilities in electronic properties determination. For instance, the fundamental electronic characteristics associated with CNTs chirality have been abundantly reported and confirmed by DFT calculations, plus analysis of doping and defects affecting these properties [6, 11]. [Figure B.1](#) shows published results regarding the effects of boron- and nitrogen-doping over the electronic band structure and charge distribution, which in turn could be fundamental for understanding the basic electron behavior along the structure and thus, for developing real world applications [12, 13].

Graphene is probably the most popular carbon nanomaterial currently, and it is because of its exceptional electronic properties. A numerous amount of reports on DFT theoretical studies of graphene and graphene nanoribbons have fueled the interest for developing new electronics based in such material. These studies have confirmed that graphene is a zero-

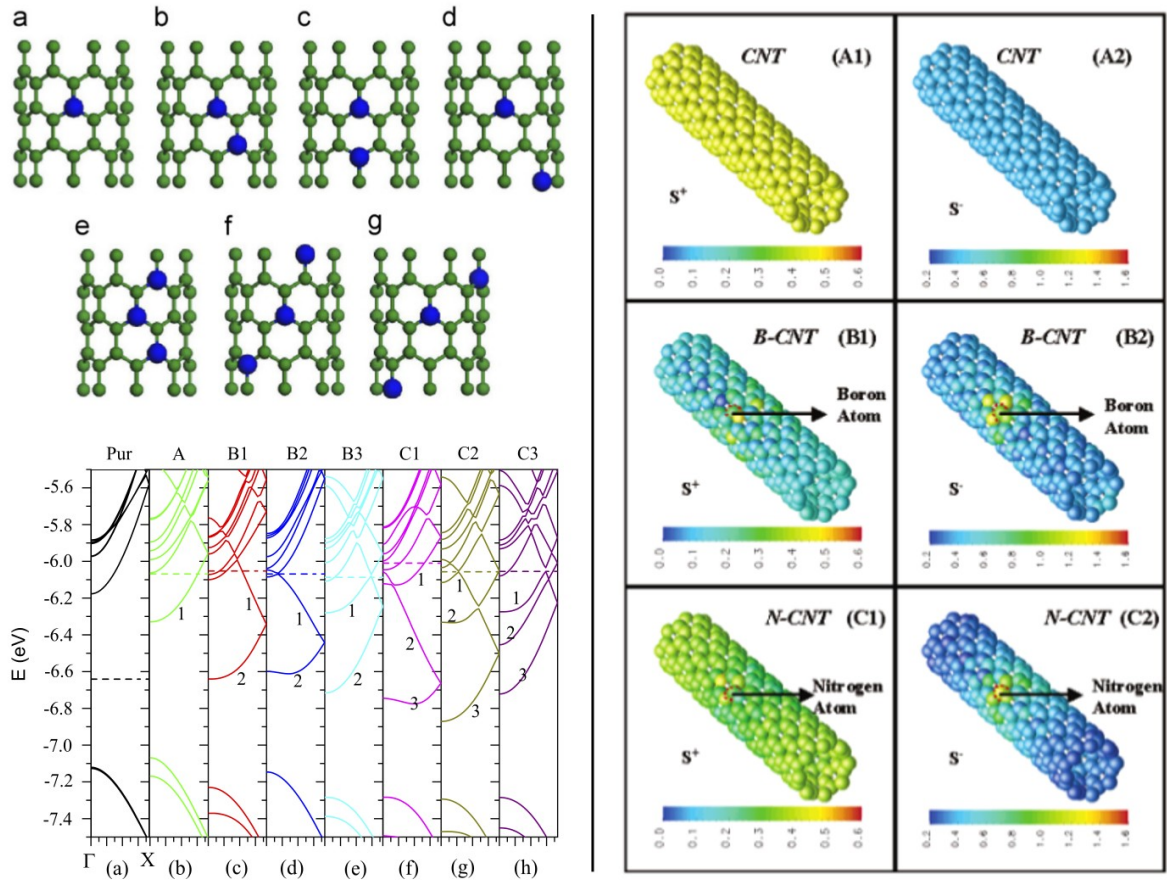


**Figure B.1. (Left panel)** Calculation of electronic properties for CNT with different degrees of N-doping, with the resultant electronic band structure (bottom, figures adapted from [12]). **(Right figure)** Effects of B-doping on the electric charge distribution along a CNT (image taken from [13]).

gap semiconductor, and that some of its properties are prone to be controlled by doping and interactions with electric and magnetic fields [7, 14]. In figure B.2 are shown example results from DFT calculations, performed for evaluating the effect of substitutional nitrogen doping on graphene nanoribbons. The panel displays graphs of band structure and DOS, comparing them with undoped ribbons. Moreover, quantum conductance is as well calculated and plotted, which can give an insight of potential useful properties for electronic devices development. Additionally, DFT, as well as many of theoretical models, can produce spatial renderings of calculated molecular orbitals and electronic charge densities, which are very revealing of physic-chemical interactions between the analyzed systems.

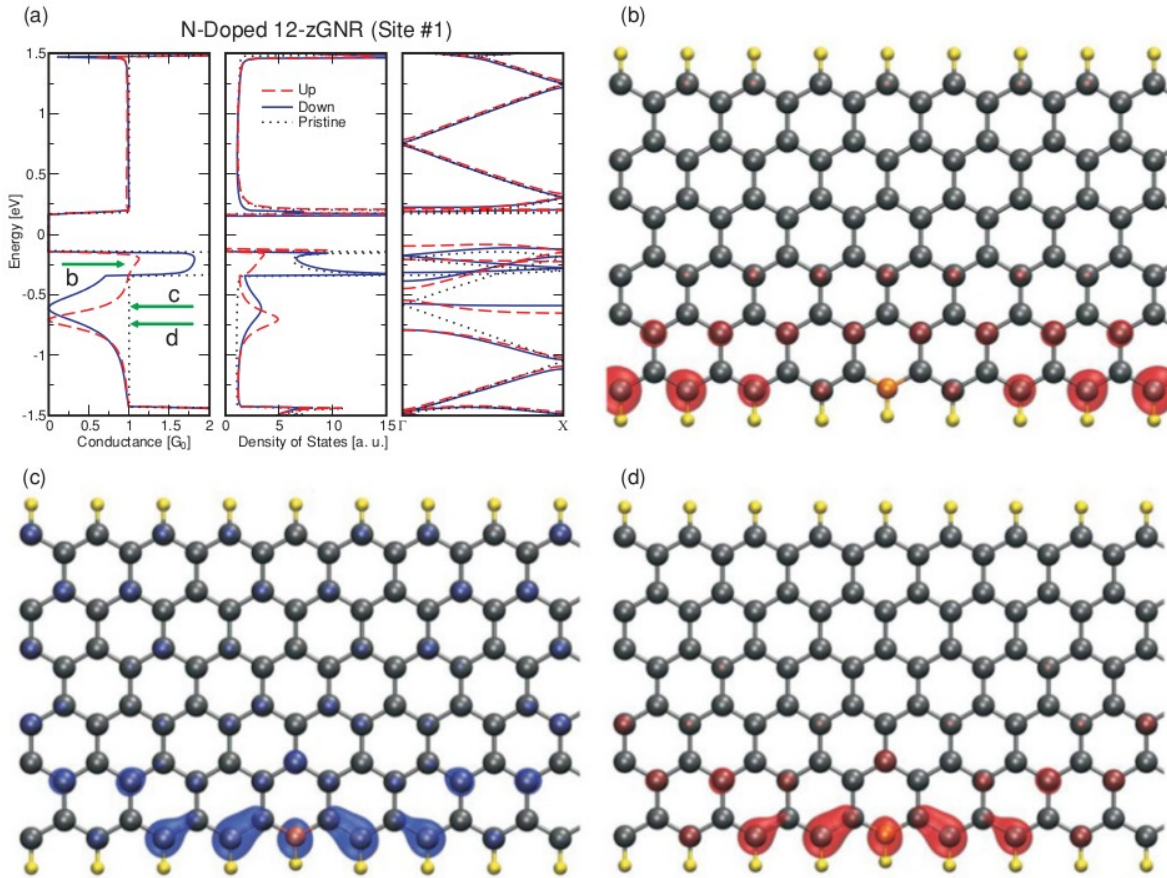


**Figure B.2.** Results of DFT calculations over graphene nanoribbons. The panel shows plots of calculated conductance, density of states and band structure **(a)**, and isosurface plots on molecular models, depicting electron density clouds **(b-d)**. Figure taken from [7].

In conclusion, DFT as a theoretical approach, can provide with information that would be impossible or very impractical to get by experimental methods. Nevertheless, it should be used within its limitations, since it is computationally demanding and relatively inaccurate under certain circumstances. However, DFT is still under evolution, with constant advancements in their formulations and implementations, which make it a more robust and popular approach for theoretical study of carbon and other nanostructures.

## Bibliography

- [1] W. Kohn and L. J. Sham, "Self-Consistent Equations Including Exchange and Correlation Effects," *Physical Review*, vol. 140, no. 4A, pp. A1133–A1138, 1965.
- [2] J. M. Soler, E. Artacho, J. D. Gale, A. García, J. Junquera, P. Ordejón, and D. Sánchez-Portal, "The SIESTA method for ab initio order- N materials simulation," *Journal of Physics: Condensed Matter*, vol. 14, no. 11, p. 2745, 2002.
- [3] P. Hohenberg, "Inhomogeneous Electron Gas," *Physical Review*, vol. 136, no. 3B, pp. B864–B871, Nov. 1964.
- [4] R. G. Parr and W. Yang, *Density-Functional Theory of Atoms and Molecules (Google eBook)*. Oxford University Press, 1989, p. 352.
- [5] S. Grimme, "Accurate description of van der Waals complexes by density functional theory including empirical corrections.," *Journal of Computational Chemistry*, vol. 25, no. 12, pp. 1463–73, Sep. 2004.
- [6] E. Gracia-Espino, F. Lopez-Urias, H. Terrones, and M. Terrones, "Doping (10, 0)-Semiconductor Nanotubes with Nitrogen and Vacancy Defects," *Materials Express*, vol. 1, no. 2, pp. 127–135, 2011.
- [7] E. Cruz-Silva, Z. M. Barnett, B. G. Sumpter, and V. Meunier, "Structural, magnetic, and transport properties of substitutionally doped graphene nanoribbons from first principles," *Physical Review B*, vol. 83, p. 155445, Apr. 2011.
- [8] C. Pouchan, D. Bégué, and D. Y. Zhang, "Between geometry, stability, and polarizability: density functional theory studies of silicon clusters  $Sin$  ( $n = 3-10$ ).," *The Journal of Chemical Physics*, vol. 121, no. 10, pp. 4628–34, Sep. 2004.
- [9] W. Qin, X. Li, W.-W. Bian, X.-J. Fan, and J.-Y. Qi, "Density functional theory calculations and molecular dynamics simulations of the adsorption of biomolecules on graphene surfaces," *Biomaterials*, vol. 31, no. 5, pp. 1007–1016, 2010.
- [10] P. Mori-Sánchez, Q. Wu, and W. Yang, "Accurate polymer polarizabilities with exact exchange density-functional theory," *The Journal of Chemical Physics*, vol. 119, no. 21, p. 11001, Dec. 2003.
- [11] J.-C. Charlier, M. Terrones, and M. Baxendale, "Enhanced electron field emission in B-doped carbon nanotubes," *Nano Letters*, vol. 2, no. 11, pp. 1191–1195, Nov. 2002.
- [12] J. Wei, H. Hu, H. Zeng, Z. Zhou, W. Yang, and P. Peng, "Effects of nitrogen substitutional doping on the electronic transport of carbon nanotube," *Physica E*:

*Low-dimensional Systems and Nanostructures*, vol. 40, no. 3, pp. 462–466, Jan. 2008.

- [13] S. Peng and K. Cho, “Ab Initio Study of Doped Carbon Nanotube Sensors,” *Nano Letters*, vol. 3, no. 4, pp. 513–517, Apr. 2003.
- [14] J. Ortiz-Medina, F. López-Urías, F. J. Rodríguez-Macías, H. Terrones, and M. Terrones, “Manuscript in preparation,” 2013.



# Nitrogen-Doped Graphitic Nanoribbons: Synthesis, Characterization, and Transport

Josue Ortiz-Medina, M. Luisa García-Betancourt, Xiaoting Jia, Rafael Martínez-Gordillo, Miguel A. Pelagio-Flores, David Swanson, Ana Laura Elías, Humberto R. Gutiérrez, Eduardo Gracia-Espino, Vincent Meunier, Jonathan Owens, Bobby G. Sumpter, Eduardo Cruz-Silva, Fernando J. Rodríguez-Macías, Florentino López-Urías, Emilio Muñoz-Sandoval, Mildred S. Dresselhaus, Humberto Terrones, and Mauricio Terrones\*

Nitrogen-doped graphitic nanoribbons ( $N_x$ -GNRs), synthesized by chemical vapor deposition (CVD) using pyrazine as a nitrogen precursor, are reported for the first time. Scanning electron microscopy (SEM) and high-resolution transmission electron microscopy (HRTEM) reveal that the synthesized materials are formed by multilayered corrugated GNRs, which in most cases exhibit the formation of curved graphene edges (loops). This suggests that during growth, nitrogen atoms promote loop formation; undoped GNRs do not form loops at their edges. Transport measurements on individual pure GNRs exhibit a linear  $I$ - $V$  (current-voltage) behavior, whereas  $N_x$ -GNRs show reduced current responses following a semiconducting-like behavior, which becomes more prominent for high nitrogen concentrations. To better understand the experimental findings, electron density of states (DOS), quantum conductance for nitrogen-doped zigzag and armchair single-layer GNRs are calculated for different N doping concentrations using density functional theory (DFT) and non-equilibrium Green functions. These calculations confirm the crucial role of nitrogen atoms in the transport properties, confirming that the nonlinear  $I$ - $V$  curves are due to the presence of nitrogen atoms within the  $N_x$ -GNRs lattice that act as scattering sites. These characteristic  $N_x$ -GNRs transport properties could be advantageous in the fabrication of electronic devices including sensors in which metal-like undoped GNRs are unsuitable.

## 1. Introduction

The rise of graphene, a unique one atom-thick carbon nanomaterial, has led to extensive efforts aimed at developing applications based on their exceptional electronic properties: zero-gap semiconducting band structure, a high charge carrier mobility and quantum Hall effect.<sup>[1,2]</sup> However, for finite graphene sheets, the electronic behavior becomes more complex due to the presence of edge effects. This becomes evident in semi-infinite sheets that extend continuously in one direction but are restricted to a finite width along the other, also known as graphene-nanoribbons (graphene-NRs). Fujita et al.<sup>[3]</sup> were the first using tight binding calculations to predict the electronic properties of graphene-NRs; more recently, detailed

J. Ortiz-Medina, M. L. García-Betancourt, Dr. E. García-Espino,  
Prof. F. J. Rodríguez-Macías, Prof. F. López-Urías,  
Prof. E. Muñoz-Sandoval  
Advanced Materials Department  
IPICYT, Camino a Presa San José 2055, Lomas 4a sección  
San Luis Potosí 78216, México

J. Ortiz-Medina, M. L. García-Betancourt, Dr. A. L. Elías,  
Dr. H. R. Gutiérrez, Prof. F. López-Urías, Prof. H. Terrones,  
Prof. M. Terrones  
Department of Physics, The Pennsylvania State University  
University Park, PA 16802, USA  
E-mail: mut11@psu.edu

Dr. X. Jia  
Department of Materials Science and Engineering  
Massachusetts Institute of Technology  
Cambridge, MA 02139, USA

R. Martínez-Gordillo  
Centre d'Investigació en Nanociència i Nanotecnologia (CSIC-ICN)  
Campus de la UAB, E-08193 Bellaterra, Spain

M. A. Pelagio-Flores, Prof. F. J. Rodríguez-Macías  
Departamento de Química Fundamental  
Universidade Federal de Pernambuco  
50740-540 Recife, PE, Brazil

DOI: 10.1002/adfm.201202947

D. Swanson  
Chemistry and Physics Departments  
Augustana College  
Sioux Falls, SD 57197, USA

Dr. V. Meunier, Dr. B. G. Sumpter, Dr. E. Cruz-Silva  
Oak Ridge National Laboratory  
Oak Ridge, TN 37831, USA

Dr. V. Meunier, J. Owens  
Department of Physics, Applied Physics and Astronomy  
Rensselaer Polytechnic Institute  
Troy, NY 12180-3590, USA

Prof. M. Dresselhaus  
Department of Electrical Engineering and Computer Science  
Massachusetts Institute of Technology  
Cambridge, MA 02139, USA

Prof. M. Dresselhaus  
Department of Physics  
Massachusetts Institute of Technology  
Cambridge, MA 02139, USA

Prof. M. Terrones  
Shinshu University, Research Center for Exotic Nanocarbons  
Nagano 3808553, Japan

